UNIVERSIDAD AUTÓNOMA DE MADRID

FACULTAD DE CIENCIAS

DEPARTAMENTO DE BIOLOGÍA

Bacillus subtilis RecD2 acts as an accessory helicase in DNA replication and balances RecA activities

DOCTORAL THESIS

CRISTINA RAMOS ANDRADES

Madrid, 2022

UNIVERSIDAD AUTÓNOMA DE MADRID

FACULTAD DE CIENCIAS

DEPARTAMENTO DE BIOLOGÍA

Bacillus subtilis RecD2 acts as an accessory helicase in DNA replication and balances RecA activities

Thesis presented by Cristina Ramos Andrades, who graduated in Biochemistry and Biomedical Sciences, to aim for the degree of Ph.D. in Microbiology with International Mention from the Universidad Autónoma de Madrid

Director:

Silvia Ayora Hirsch

Tutor:

Marta Martín Basanta

CENTRO NACIONAL DE BIOTECNOLOGÍA-CSIC

Madrid, 2022

The work presented in this thesis has been carried out in the Department of Microbial Biotechnology (Centro Nacional de Biotecnología, CNB), belonging to the Consejo Superior de Investigaciones Científicas (CSIC), under the direction of Dr. Silvia Ayora Hirsch.

Cristina Ramos Andrades has received the fellowship ‘‘Ayudas para contratos predoctorales para la formación de doctores (2017)’’ (reference: BES-2017-080504), belonging to the Subprograma Estatal de Formación del Ministerio de Economía, Industria y Competitividad (current Ministerio de Ciencia e Innovación).

Index

List of Tables

List of Figures

Abstract

DNA replication process can be halted in the presence of DNA lesions. If these lesions are not repaired, replication forks can arrest or collapse, situations that can compromise cell survival. Organisms have developed multiple mechanisms to repair DNA damages and reactivate DNA replication once the lesions are repaired. In this context, homologous recombination machinery is crucial. Several recombination proteins are recruited to active replication forks by their interaction with the single-stranded binding proteins. One of these recombination proteins is the bacterial RecD2 helicase, thought as equivalent to eukaryotic HELB helicase and present in bacteria that lack the RecBCD complex. RecD2 has been postulated as an accessory helicase during DNA replication, although its detailed action had been poorly analysed. In this work, the biochemical and functional activities of *Bacillus subtilis* RecD2 in the context of homologous recombination and DNA replication have been thoroughly explored.

The potential role of RecD2 in homologous recombination has been examined by different approaches. *In vivo* analysis has shown that RecD2 has a minor role during plasmid transformation and chromosomal transformation. However, in the absence of the nucleoid-associated factor Rok, RecD2 appears to be crucial for intra- and interspecies chromosomal transformation, as well as for the integration of micro-homologous sequences (~3-10 nt) into the bacterial chromosome. In addition, RecD2 is needed for the reconstitution of the SPP1 bacteriophage genome inside the bacterial cell. *In vitro* analysis has revealed that RecD2 has a dual role in homologous recombination, from one side, extending three-stranded recombination intermediates (D-loops) and favouring the recombination reaction, and, from other side, interacting with RecA and negatively regulating the RecA nucleoprotein filament.

The biochemical analysis of RecD2 has shown that this helicase preferentially binds and unwinds DNA without secondary structures. In addition to non-replicated fork structures, RecD2 efficiently unwinds stalled and regressed fork structures through its translocation along the parental or longer nascent lagging strands *in vitro*. It suggests a potential role of RecD2 in replication restart as an accessory helicase maybe supporting the unwinding activity of the replicative helicase DnaC in a 5’ to 3’ direction. *In vivo* single-molecule fluorescence microscopy has shown that RecD2 is a very dynamic protein whose association with the replication fork machinery may be transient. In addition, the interaction with SsbA, DnaE, DnaD and/or PolC may mediate the recruitment of RecD2 to the replisome. In an *in vitro* model of PriA-dependent replication, RecD2 contributes to replication restart via the removal of protein blocks, such as RecA. These findings contribute to understanding the potential role of RecD2 to overcome replicative stress and reactivate a stalled replication process.

Resumen

La replicación del ADN se puede detener en presencia de lesiones en el ADN. Si estas lesiones no se reparan, las horquillas de replicación pueden pararse o colapsar, situaciones que pueden comprometer la supervivencia celular. Los organismos han desarrollado múltiples mecanismos para reparar daños en el ADN y reactivar la replicación una vez las lesiones son reparadas. En este contexto, la maquinaria de recombinación homóloga es crucial. Varias proteínas de recombinación son reclutadas a horquillas de replicación activas a través de su interacción con las proteínas de unión a ADN de cadena sencilla. Una de estas proteínas de recombinación es la helicasa bacteriana RecD2, pensada como equivalente a la helicasa HELB de eucariotas y presente en bacterias que carecen del complejo RecBCD. RecD2 ha sido postulada como helicasa accesoria durante la replicación, aunque su acción detallada ha sido muy poco analizada. En este trabajo, se han explorado a fondo las actividades bioquímicas y funcionales de RecD2 de *Bacillus subtilis* en el contexto de la recombinación homóloga y la replicación del ADN.

El potencial papel de RecD2 en recombinación homóloga ha sido examinado a través de diferentes aproximaciones. El análisis *in vivo* ha mostrado que RecD2 tiene un papel menor en transformación plasmídica y cromosómica. Sin embargo, en ausencia del factor asociado al nucleoide Rok, RecD2 parece ser crucial en transformación cromosómica con ADN donadores de la misma o distintas especies, así como en la integración de secuencias micro-homólogas (~3-10 nt) en el cromosoma bacteriano. Además, RecD2 es necesaria para la reconstitución del genoma del bacteriófago SPP1 en el interior de la célula bacteriana. El análisis *in vitro* ha revelado que RecD2 tiene un papel dual en recombinación homóloga, por un lado, extendiendo intermediarios de recombinación de tres cadenas (D-loops) y favoreciendo la reacción de recombinación, y, por otro lado, interaccionado con RecA y regulando negativamente el filamento nucleoproteico de RecA.

El análisis bioquímico de RecD2 ha mostrado que preferentemente une y desenrolla ADN sin estructuras secundarias. Además de horquillas no replicadas, RecD2 desenrolla eficientemente horquillas de replicación bloqueadas y regresadas a través de su translocación a lo largo de las hebras retardadas parental o naciente alargada *in vitro*. Esto sugiere un potencial papel de RecD2 en el reinicio de la replicación como helicasa accesoria, quizás apoyando la actividad de la helicasa replicativa DnaC en dirección 5' a 3'. *In vivo*, la microscopía de fluorescencia *single-molecule* ha mostrado que RecD2 es una proteína muy dinámica cuya asociación con la horquilla de replicación puede ser transitoria. Además, la interacción con SsbA, DnaE, DnaD y/o PolC puede mediar el reclutamiento de RecD2 al replisoma. En un modelo *in vitro* de replicación dependiente de PriA, RecD2 contribuye al reinicio de la replicación al eliminar proteínas bloqueantes, como RecA. Estos hallazgos contribuyen a entender el potencial papel de RecD2 en la superación de estrés replicativo y la reactivación de un proceso de replicación bloqueado.

Abbreviations

4NQO 4-nitroquinoline 1-oxide
aa Amino acid
(d)ADP (Deoxy)adenosine monophosphate
ADR Alkylation damage repair
AP Apurinic/apyrimidinic
(d)ATP (Deoxy)adenosine triphosphate
ATPγS Adenosine 5′-[γ-thio]triphosphate
BER Base-excision repair
bp Base pair
BSA Bovine serum albumin
cds Circular double-stranded DNA
CFU Colony-forming units
CFP Cian fluorescent protein
Cm Chloranfenicol
css Circular single-stranded DNA
C-ter C-terminal domain
(d)CTP (Deoxy)cytidine triphosphate
D Apparent diffusion coefficient
DDR DNA damage response
D-loop Displacement-loop
DNA Deoxyribonucleic acid
DSB Double strand break
dsDNA Double-stranded DNA
DTT 1,4-dithiothreitol
EDTA Ethylenediaminetetraacetic acid
EMSA Electrophoretic mobility shift assay
(m)(µ)(n)g (Mili) (micro) (nano) gram
GM Minimal growth
(d)GTP (Deoxy)guanosine triphosphate
His Histidine
HJ Holliday junction
H_2O_2 Hydrogen peroxide
HPUra 6(p-hydroxyphenylazo)-uracil
HR Homologous recombination
IPTG Isopropyl β-D-1-thiogalactopyranoside
jm Joint molecule intermediate
k_{app} Apparent binding constant
k_{cat} Catalytic constant
kDa Kilodalton
K_m Michaelis Menten constant
(m)(µ)l (Mili) (micro) liter
LB Luria-Bertani
lds Linear double-stranded DNA
lss Linear single-stranded DNA
(m)(µ)(n)M (Mili) (micro) (nano) molar
MEPS Minumun efficient processing segment
MMC Mitomycin C
MMR Mismatch repair
MMS Methyl methanesulfonate
MOI Multiplicity of infection
NADH Nicotinamide adenine dinucleotide reduced
nc Nicked circular
NER Nucleotide-excision repair
NHEJ Non-homologous end joining
Nm Neomycin
nt Nucleotide
N-ter N-terminal domain
(d)(r)NTP (Deoxy)(ribo)nucleotides triphosphate
OD Optical density
PAGE Polyacrilamide gel electrophoresis
PBS Phosphate-buffered saline
PCR Polymerase chain reaction
PFU Plaque-forming unit
pmol Picomol
(p)ppGpp Guanosine (penta)tetraphosphate
Rif Rifampicin
RNA Ribonucleic acid
rpm Revolution per minute
s Second
SD Standard deviation
SDS Sodium dodecyl sulphate
SEM Standard error of the mean

Abbreviations

SF Superfamily

SHX Serine hydroxamate

Spect Spectinomycin

ssDNA Single-stranded DNA

TAE Tris-acetate-EDTA

TBE Tris-borate-EDTA

TE Tris-EDTA

TLS Translesion synthesis

(d)TTP (Deoxy)timidine triphosphate

UTP Uridine triphosphate

UV Ultraviolet

V_{max} Maximum velocity

wt Wild-type

Introduction

1. Introduction

1.1. DNA replication in *Bacillus subtilis*

DNA replication is a ubiquitous process in all organisms. Accurate chromosome duplication is fundamental for genome integrity and it is crucial for cell survival. All living cells have developed a complex machinery to duplicate their genome. This machinery is known as the replisome and it is composed by several number of proteins that are essential for life. These proteins work in concert forming a complex with the DNA and creating the replication fork structure. Due to the unique direction of replication and the different polarity of the DNA, each new strand is not replicated equally. Whereas one is synthetised continuously (leading strand), the other strand (lagging strand) is synthetised discontinuously in short fragments, known as Okazaki fragments.

The replisome that has been best characterised is from the Gram-negative bacterium *Escherichia coli*. On the other hand, for low G+C Gram-positive bacteria, the *Bacillus subtilis* replisome represents the most currently understood model. Both machineries are closely linked and share some conserved characteristics (**Figure 1**) (Sanders *et al.*, 2010; Beattie and Reyes-Lamothe, 2015).

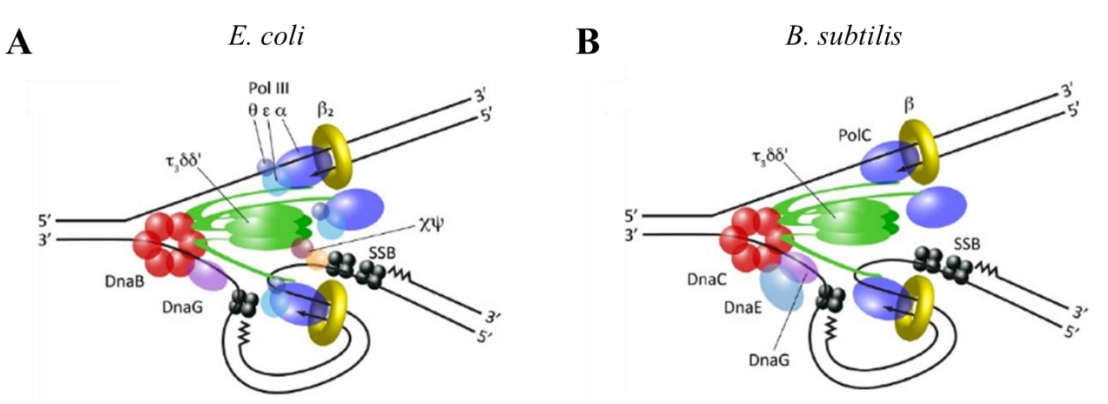

Figure 1. Schematic representation of *E. coli* and *B. subtilis* replisomes.
The architecture of the replisome in both (**A**) *E. coli* and (**B**) *B. subtilis* is very similar, but with some differences. PolIII is the replicative polymerase in *E. coli*, which has three subunits (α, ε and θ). In contrast, *B. subtilis* contains two replicative polymerases: PolC and DnaE. Both machineries have the hexameric replicative DNA helicase (DnaB in *E. coli* and DnaC in *B. subtilis*), the primase (DnaG), the clamp-loader ($\tau_3\delta\delta$'- χψ in *E. coli* and $\tau_3\delta\delta$' in *B. subtilis*), the β-clamp and SSB (also termed SsbA in *B. subtilis*). In addition to these proteins, replisome loaders are needed (not depicted here, see text). Figure from Beattie and Reyes-Lamothe, 2015.

Thirteen proteins have been identified as part of the *B. subtilis* replisome and are required for a properly DNA replication: DnaA (PriA), DnaB, DnaC, DnaD, DnaE, DnaG, DnaI, DnaN (β-clamp), DnaX (τ), HolA (δ), HolB (δ'), PolC and SsbA. A *B. subtilis* advancing replisome has been reconstituted *in vitro* (Sanders *et al.*, 2010). The chromosomal origin, known as *oriC* in both bacteria, is the site in which bacterial DNA replication starts. The initiation protein DnaA is an

AAA^+ ATPase that binds specifically to *oriC* and performs the melting in an AT rich region, known as DUE (DNA Unwinding Element), which is adjacent to *oriC*. This allows the binding of the rest of the replisome components (Smits *et al*., 2011). Alternatively, there is another initiation protein that is strictly needed for DNA replication restart in regions outside *oriC*, known as PriA. PriA is a 3' to 5' helicase that acts on stalled replication forks, remodeling the DNA structure and promoting the replisome reassembly for DNA replication progression (Gabbai and Marians, 2010). In *B. subtilis*, DnaA interacts with and performs the recruitment of DnaD first, and then of DnaB, to the origin of replication. These interactions contribute to activate the melting activity of DnaA in this region (Smits *et al*., 2011). DnaB is also involved in the attachment of the replication fork to the membrane through its C-terminal domain (Briggs *et al*., 2012). This scenario is simpler in *E. coli*, where there are not any functional proteins like DnaD and DnaB from *B. subtilis*, and just DnaA is required for the initiation of DNA replication (Beattie and Reyes-Lamothe, 2015).

The DnaA-DnaD-DnaB complex in *B. subtilis* mediates the assembly of the helicase loader DnaI (named DnaC in *E. coli*) and, subsequently, the replicative helicase DnaC (named DnaB in *E. coli*). DnaC forms a homohexameric ring onto one strand of the the melted DNA region that will correspond to the lagging strand, and unwinds the DNA in 5' to 3' direction. Single-stranded DNA binding protein, SSB (also known as SsbA in *B. subtilis*), binds to the ssDNA to prevent reannealing and protect it from degradation. DnaC also performs the recruitment of the primase DnaG, the clamp loader complex ($\tau_3\delta\delta'$) and the β-clamp (Jameson and Wilkinson, 2017; Beattie and Reyes-Lamothe, 2015). DnaG is involved in RNA primer synthesis into the lagging strand. The primase synthetises RNA oligonucleotides, around 16 nt, and its activity is stimulated by the interaction with DnaC (Rannou *et al*., 2013).

Differently to *E. coli*, which only has one replicative DNA polymerase, known as PolIII, *B. subtilis* harbours two: PolC and DnaE. PolC is the main replicative DNA polymerase. It interacts with DnaX (τ subunit of clamp loader) and the β-clamp exhibiting a high processivity. Moreover, PolC shows a high-fidelity extension, due to its 3' to 5' exonuclease proofreading action (Paschalis *et al*., 2017). Whereas PolC performs the leading and lagging strand synthesis, DnaE polymerase, structurally similar to *E. coli* PolIII, is responsible for the RNA primer extension synthetised by DnaG and the consequent Okazaki fragments generation in the lagging strand (Rannou *et al.*, 2013; Li *et al*., 2018). This limited action of DnaE as DNA polymerase is a consequence of its low processivity and error-prone activity (Rannou *et al.*, 2013; Paschalis *et al*., 2017). Replication rate by PolC is close to 500 nt/s, whereas DnaE elongation rate is around to 75 nt/s. However, a synergistic effect is observed with both polymerases, because PolC is not able to extend RNA primers, and higher levels of DNA synthesis are observed when both polymerases are present, suggesting that once DnaE initially adds some nucleotides to the RNA

primers, PolC elongates them (Sanders *et al.*, 2010). This is similar to eukaryotic DNA replication, where RNA primers are first extended by Polα and then, elongated by Polδ in the lagging strand, whereas Polε is devoted to the leading strand (Robinson *et al*., 2012).

Okazaki fragments need to be processed prior to their ligation by the DNA ligase. Okazaki fragment maturation, which involves the RNA removal and the subsequent DNA replacement, is carried out by PolA polymerase in *B. subtilis* (PolI in *E. coli*) in concert with RNase H enzymes (especially RNase HIII in *B. subtilis*) (Randall *et al*., 2019). PolI contains three functional domains: N-terminal domain with 5' to 3' exonuclease activity, a central domain with the proofreading 3' to 5' exonuclease action and the C-terminal domain involved in the polymerase activity. In contrast, PolA from *B. subtilis* lacks the proofreading 3' to 5' exonuclease activity. Additional 5' to 3' exonuclease protein is present in *B. subtilis*, known as YpcP (also named as ExoR), which exhibits highly preference to degrade RNA from the Okazaki fragments (Randall *et al*., 2019**)**. Whereas PolI is an essential protein in *E. coli*, the absence of PolA in *B. subtilis* is viable. However, the absence of both PolA and YpcP is lethal (Duigou *et al*., 2005).

DNA topoisomerases participate in DNA topology maintenance. They are crucial for the properly DNA replication because the replisome advance and the transcription process generate positive or negative supercoils that need to be processed. In Bacteria, two families of topoisomerases are present: type I and type II. The type I (Topo I and Topo III) are monomeric topoisomerases that cleave one DNA strand, whereas the type II (DNA gyrase and Topo IV) are heterotetramers that cleave both strands (Reuß *et al*., 2019). Whereas TopoI participates relaxing transcription-induced negative supercoiling, DNA gyrase contributes to introduce negative supercoiling and relax positive supercoils that form ahead of the replication and transcription complexes (McKie *et al*., 2021). DNA gyrase also controls the initiation of DNA replication by inhibiting DnaA-association to *oriC* (Samadpour and Merrikh, 2018). TopoIII and TopoIV are involved in the resolution of recombination intermediates and chromosome segregation (Reuß *et al*., 2019).

Replication termination is a not completely understood process. In bacteria with circular chromosomes, two replisomes are loaded in the *oriC* region and proceed clockwise and anticlockwise since they meet at the *Ter* region, located in the opposite side to *oriC*. Here, DNA replication finishes. The replication termination proteins, RTP in *B. subtilis* and Tus in *E. coli*, bind to different sites inside the *Ter* region and may promote the replisome disassembly (Jameson and Wilkinson, 2017).

1.2. DNA repair pathways: Homologous recombination in *B. subtilis*

The genetic material can suffer several types of damage that can affect the stability of the replication fork and promote the replisome stall or disassembly. DNA damaging agents can alter the DNA structure introducing breaks or nicks, or modify the sequence favouring the introduction of mis-incorporated bases. Environmental factors, such as ionizing radiation, and internal products of metabolic processes, such as free radicals or DNA replication errors, can induce DNA damage. Because DNA lesions can compromise cell survival and enhance the appearance of genetic diseases, all organisms have developed diverse DNA repair systems to overcome these lesions.

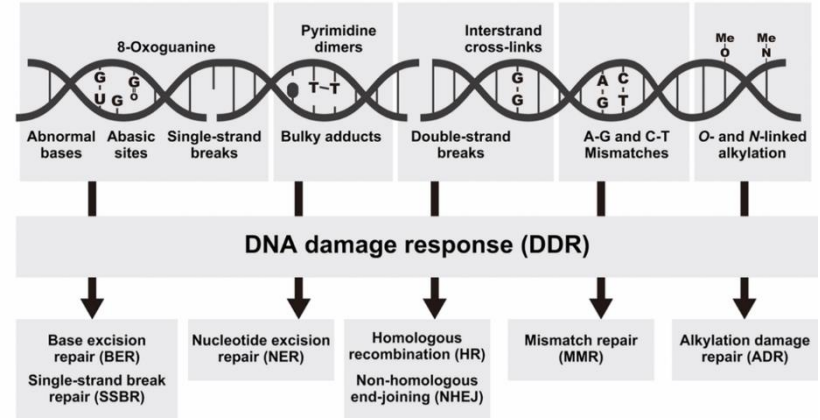

Figure 2. DNA repair pathways depending on the type of damage.
The presence of DNA lesions triggers the activation of DDR, which involves different DNA repair pathways that are specific for the type of damage that is produced. Figure from Tasaki *et al.,* 2018.

The DNA damage response (DDR) implies the activation of different DNA repair pathways depending on the type of lesion that is produced (**Figure 2**). Base-excision repair (BER) is the main pathway to resolve non-bulky lesions that do not significantly disturb the DNA helix, such as alkylation, methylation, oxidation, deamination or abasic sites. This process consists in the recognition of the damage by a glycosylase, which cleaves the N-glycosylic bond between the 2'-deoxyribose and the damaged base, creating an abasic site (AP site). The AP site has the risk of generate a ssDNA break that can endanger the genome integrity, so it needs to be processed by AP endonucleases and lyases, which produce a small gap that is then filled by a DNA polymerase and ligated (Dalhus *et al*., 2009; Lenhart *et al*., 2012; Chatterjee and Walker, 2017). On the other hand, a specific pathway, known as alkylation damage repair (ADR), can restore alkylation and methylation damage that can produce important DNA modifications. ADR involves the action of alkyl and methyl glycosylases and transferases to repair the alkylation damage (Lenhart *et al*., 2012). Nucleotide-excision repair (NER) is involved in the removal of bulky lesions, such as pyrimidine dimers, produced by UV radiation or chemical agents like mitomycin C. In *B. subtilis,* also in *E.coli*, this system implies the recruitment of the UvrA-UvrB-UvrC complex to the

damage. First, the UvrA-UvrB complex recognises the DNA lesion. Then, UvrA dissociates and UvrB recruits UvrC, which removes some nucleotides around the damage generating a single-stranded region that is subsequently filled (Truglio *et al*., 2006; Lenhart *et al*., 2012). Mismatch repair (MMR) acts on base mismatches produced during DNA replication. The two major players are MutS and MutL proteins. In *B. subtilis*, MutS interacts with the β-clamp and is recruited to the mismatch site. Later, MutS recruits MutL, which cleaves the nascent strand creating a nick that is processed and filled (Lenhart *et al*., 2012).

If the damage is not properly repaired by its specific DNA repair pathway, the DNA replication process could block or collapse, which implies the disassembly of the replication machinery. This situation promotes the accumulation of single-strand gaps and double strand breaks (DSBs) that need to be repaired. Homologous recombination (HR) becomes then essential to restore stalled or collapsed replication forks (Ayora *et al*., 2011; Wright *et al*., 2018). HR contributes to the repair of one-ended or two-ended DSBs, and implies several conserved steps among all organisms, although different proteins are involved (**Figure 3**) (Ayora *et al*., 2011; Lenhart *et al.,* 2012). In the presynaptic step, RecN, in concert with PNPase, recognises the ends of the DSB. PNPase performs an initial end processing from 3' to 5' (Cardenas *et al*., 2009). This is substrate for the end-resection machinery, which in *B. subtilis* is composed by the AddAB complex or by the concerted action of RecQ and RecS helicases, and RecJ exonuclease. AddAB (similar function to RecBCD from *E. coli*) is a protein complex with both helicase and nuclease activities involved in long end resection. The DNA resection continues until a specific site, known as Chi (χ), is found by the exonuclease. The χ sites in *B. subtilis* have a short sequence (5'-AGCGG-3') and are abundant and widely distributed in the chromosome. At the χ sites, DNA degradation stops (Chédin *et al.*, 2006; Lenhart *et al.,* 2012). Alternatively, the concerted action of RecQ/S and RecJ performs the end-resection. As a result, 3' ssDNA ends are created and SsbA binds to protect them from degradation.

In the synaptic step of HR, RecA is recruited to the 3' ends and polymerises forming a nucleoprotein filament. RecA is loaded onto the ssDNA by the RecFOR complex, specifically by RecO, which acts displacing SsbA molecules from de ssDNA that compete for the RecA binding (Ayora *et al*., 2011; Lenhart *et al*., 2012). In contrast to *E. coli*, where both RecBCD and RecFOR complexes can load RecA, in *B. subtilis* there is not any evidence that AddAB directly loads RecA onto the generated ssDNA, and RecO is required for that (Lenhart *et al*., 2014). The RecA nucleoprotein filament onto the ssDNA is a tightly regulated process. Some proteins can act as mediators or modulators of RecA, promoting its assembly or disassembly from the DNA (e.g. RecF, RecO, RecR, RecU, RecX) (Carrasco *et al*., 2005; Vlašić *et al.*, 2013). RecA bound to the ssDNA searches for homology in the chromosome and, if so, catalyses the strand exchange

invasion, creating first a three-strand recombination intermediate, known as the D-loop, with the aim to use the intact homologous DNA as a template to repair the break.

Finally, in the postsynaptic step, branch migration translocases, such as RecG, RuvAB or RadA/Sms, can migrate the D-loop generating a Holliday junction (HJ) structure, which is resolved by the RecU enzyme (Lenhart *et al*., 2012; Cañas *et al*., 2014; Torres *et al*., 2019). Depending on the orientation of the cleavage, the HR can trigger the formation of crossover or non-crossover DNA products. Several alternative pathways have been proposed highlighting the complexity of the process and the high number of proteins involved. For example, HJ structures could be also resolved by the action of TopoIII with RecQ or RecS helicases, generating non-crossover products (Ayora *et al*., 2011; Lenhart *et al*., 2012).

HR supposes an error-free mechanism for DSB repair. However, in *B. subtilis*, there is an alternative pathway to restore DSBs with low-fidelity, known as non-homologous end joining (NHEJ). This system consists in the joining of the two ends of the break without any homologous template. NHEJ involves two protein activities: Ku and LigD ligase. Ku protein recognises the ends of the break, preventing the action of nucleases, and recruits the ligase to join both ends. It has been proposed that NHEJ could act in prokaryotes during stationary phase or sporulation, because they suppose periods where only one copy of the chromosome is present (Weller *et al.,* 2002; Lenhart *et al*., 2012).

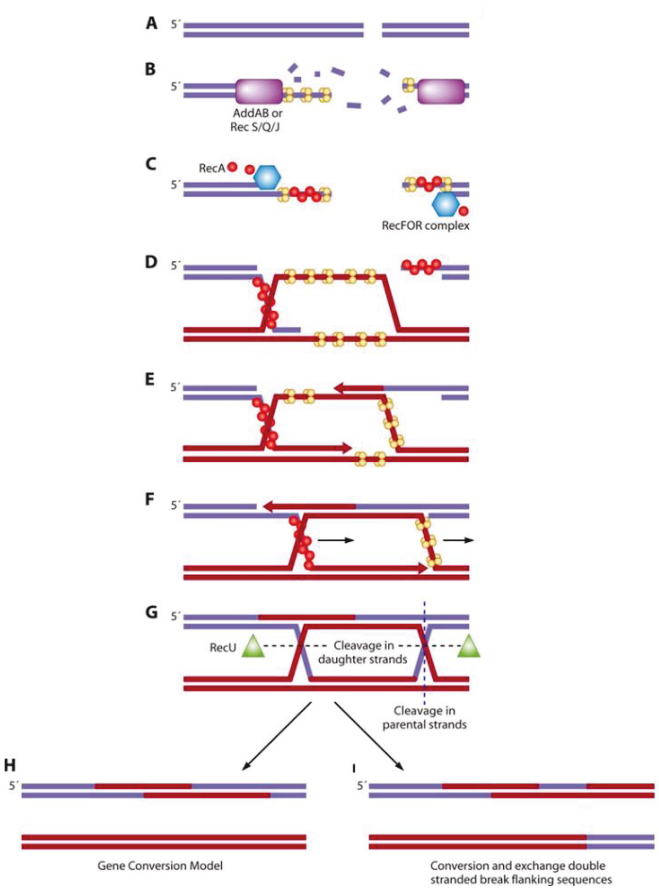

Figure 3. DSB repair via homologous recombination in *B. subtilis*.
(**A**) Certain DNA damaging agents could create a DSB. (**B**) RecN and PNPase recognise the DSB. AddAB or RecJ/RecQ/RecS perform the end resection of the DSB, creating 3' ssDNA ends that are protected from degradation by SsbA binding (*yellow circles*). (**C**) RecFOR complex removes SsbA and loads RecA onto the ssDNA. RecA forms a nucleoprotein filament. (**D**) and (**E**) The RecA nucleoprotein filament searches for homology and catalyses the strand exchange reaction, creating a D-loop. (**F**) Helicases like RecG and RuvAB branch migrate the D-loop forming a HJ. The DNA polymerase extends the 3' ends using the homologous DNA as a template. (**G**) The RecU endonuclease cleaves the HJ. (**H**) Depending on the orientation of the cleavage, crossover or non-crossover products are generated. Figure from Lenhart *et al*., 2012.

Additional roles for HR have been observed outside the context of DNA repair. In bacteria, recombination factors can act during natural transformation with the aim to facilitate the the integration of an exogenous DNA into the chromosome (**Figure 4**). Natural transformation supposes one mechanism of horizontal gene transfer that prokaryotic organisms have developed to acquire new genetic material. This process allows to the adaptation to the environment and is a source of bacterial evolution (Kidane *et al*., 2012). During natural transformation in *B. subtilis*, the DNA is internalised inside the cell by the DNA uptake apparatus, located at the cell membrane. Only one DNA strand is incorporated, whereas the other strand is degraded. This donor ssDNA is rapidly covered by single-stranded binding proteins (SsbA or the competence specific SsbB), and recognised by the RecA mediations, as DprA and RecO, that facilitates the RecA loading and the nucleoprotein filament formation. Then, if this ssDNA shares homology with a region of the chromosome, RecA catalyses the strand exchange invasion forming a D-loop, which is substrate for branch migration translocases. Similar to DSB repair, a HJ structure could be formed and finally processed by RecU. Alternatively, an unknown D-loop resolvase processes the heteroduplex. Consequently, the new incorporated DNA is integrated in the bacterial genome and this process is known as chromosomal transformation (Serrano *et al.,* 2018).

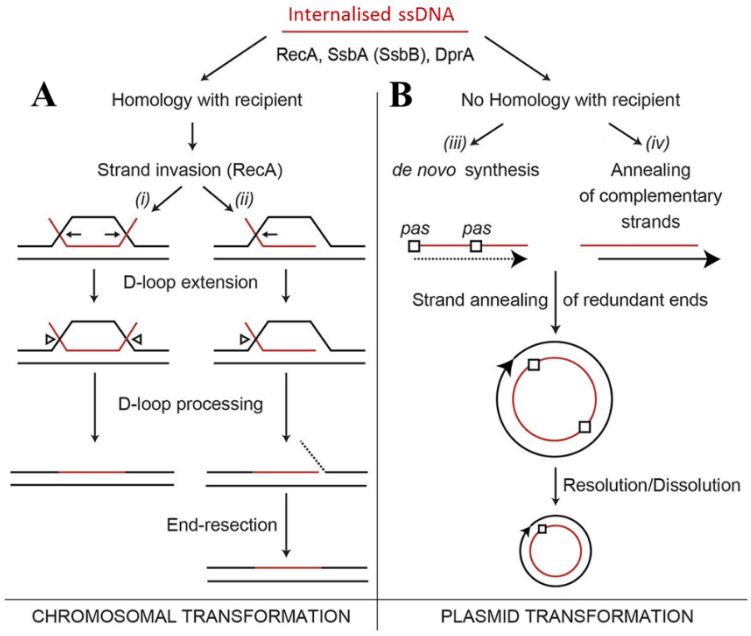

Figure 4. Model of chromosomal and plasmid transformation in *B. subtilis*.
During natural transformation, only one strand from the exogenous DNA is internalised inside the cell. Ssb proteins bind to the ssDNA and DprA mediator helps the RecA binding and filament formation. (**A**) In chromosomal transformation, the donor ssDNA shares enough homology with the chromosome. RecA performs the strand invasion using the bacterial genome as a template and the heteroduplex is resolved similarly to HR pathway. (**B**) In plasmid transformation, the donor ssDNA does not share enough homology to the chromosome. It could remain as an internal plasmid if the complementary strand is synthetised *de novo* (*iii*) or if the other strand is also internalised and both ssDNAs anneal (*iv*). Figure adapted from Serrano *et al*., 2018.

On the other hand, if the internalised ssDNA does not share enough homology to the chromosome, it could remain as an extrachromosomal element in a process that is known as plasmid transformation. Two models have been proposed for plasmid transformation. One possibility is that the other strand is not degraded and could be internalised as its complementary strand. Inside the cell, both complementary strands anneal and reconstitute a functional plasmid. Another possibility is that the internalised ssDNA is substrate for the replication machinery and the complementary strand is synthesised *de novo* (Kidane *et al*., 2012; Serrano *et al.,* 2018). Several, but not all, HR proteins are crucial for natural transformation. For instance, it has been observed that the deletion mutant strains Δ*recA*, Δ*recX* and Δ*radA* are defective in chromosomal transformation (Serrano *et al.,* 2018; Torres *et al*., 2019). Despite the fact that plasmid transformation is a RecA-independent process, other HR proteins may participate in this process. Deletion mutant strains Δ*recX* and Δ*recU* are impaired in plasmid transformation, probably because they contribute to RecA nucleoprotein filament disassembly from the ssDNA allowing other proteins to reconstitute the plasmid into the cell (Serrano *et al.,* 2018; Serrano *et al*., 2020).

1.3. DNA replication restart: Interplay with the homologous recombination machinery

HR and DNA replication are processes that are connected. The presence of DNA damage can promote the stalling of replication fork. In this context, the recruitment of HR machinery is crucial, because it can directly act on blocked forks to promote the restart of DNA replication. Several mechanisms have been proposed to restore a stalled replication fork (**Figure 5**) (Marians, 2018). If the DNA lesion is present into the leading strand, the leading strand synthesis stops, whereas lagging strand synthesis and template unwinding continue, which is known as replication uncoupling. This situation can promote the recruitment of specific polymerases that can bypass the DNA damage in a process known as translesion synthesis (TLS). In *B. subtilis*, TLS is mediated by PolY1 (possible counterpart of UmuC from *E. coli*) and PolY2 (possible counterpart of PolIV from *E. coli*) polymerases (Lenhart *et al*., 2012). On the other hand, lesion bypass can be performed by the replicative polymerase itself. Alternatively to TLS, replication can be reinitiated downstream of DNA lesion in a process known as lesion skipping. This process is mediated by the replisome itself and the resultant gap is repaired by either specific homology-directed gap repair or by TLS (Marians, 2018).

Template switching is another mechanism of DNA damage tolerance that implies the participation of HR proteins. In the presence of a DNA damage, RecA may anneal a nascent strand with the opposite nascent strand, using it as template, the lesion is repaired and consequently, DNA replication is restored (Marians, 2018). However, in an *in vitro* model of a blocked replication fork, RecA inhibited the resumption of DNA replication (Vlašić *et al.,* 2013).

Recombination intermediates formed at the replication fork need to be resolved to facilitate replication fork progression. Some branch migration translocases like *B. subtilis* RadA/Sms could contribute to that by unwinding recombination intermediates and thus promoting replication restart through its interaction with RecA (Torres and Alonso, 2021).

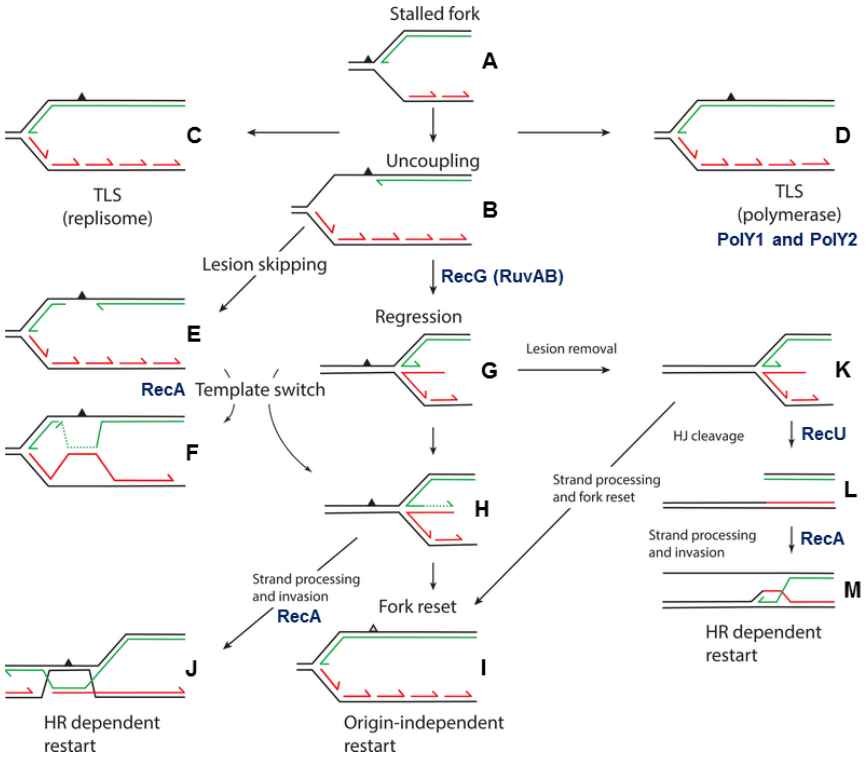

Figure 5. Mechanisms of DNA replication restart.
(**A**) The presence of a DNA lesion (*black triangle*) in the leading strand can promote the stall of DNA replication. (**B**) Whereas the synthesis of lagging strand continues, the leading strand synthesis stops (uncoupling). (**C**) TLS can bypass the damage by the replisome itself or (**D**) by the action of the TLS polymerases PolY1 and PolY2. (**E**) The lesion skipping occurs when the replication fork reinitiates downstream the damage. (**F**) The template switching by RecA can bypass the damage using the nascent lagging strand (*red lines*) as the template for the nascent leading strand (*green lines*). (**G**) RecG (and perhaps RuvAB) performs the fork regression and a HJ-like structure is created. (**H**) The DNA polymerase extends the nascent leading strand using the nascent lagging strand as a template. (**I**) Fork reset can occur when the replication reinitiates, although the damage has not been previously removed (*empty triangle*). (**J**) The HR machinery can remove the damage in a regressed fork and facilitates the replication restart. (**K**) Alternatively, a DNA lesion in a regressed fork can be removed by other DNA repair pathways like NER. (**L**) The regressed fork is processed by the cleavage of the HJ resolvase (RecU). (**M**) The cleavage of the replication fork generates substrates for the HR machinery, which restores the DNA replication. Figure adapted from Marians, 2018.

Fork regression (also termed fork reversal) is an alternative via that contributes to bypass replication stalling. This process is mediated by branch migration translocases, principally RecG, but also RuvAB, that catalyse the formation of a HJ-like structure, known as 'chicken foot structure', in a stalled replication fork, (Atkinson and McGlynn, 2009; Gupta *et al*., 2014; Torres *et al*., 2021). Therefore, the nascent leading and lagging strands anneal and the DNA polymerase uses the nascent leading strand as a template to extend the nascent lagging strand. In this context, the fork could be reset to the original configuration when DNA replication moves, leaving behind the damage (origin dependent restart) or the regressed fork is cleaved by the HJ resolvases, which

in *B. subtilis* is RecU (Cañas *et al*., 2014). After the cleavage, the HR recombination machinery promotes an HR-dependent PriA-dependent replication restart (Marians, 2018).

1.4. SsbA: A hub to link DNA replication, repair and homologous recombination

Several replisome proteins interact with and recruit DNA repair proteins to the replication fork to ensure replication progression. One of these proteins that links replication and repair is Ssb. *B. subtilis* harbours two Ssb proteins: SsbA and SsbB. Structurally, both are homotetrameric proteins, but SsbA contains a flexible C-terminal extension, absent in SsbB, which mediates the interaction with other proteins (Yadav *et al.*, 2012). Whereas SsbA is an essential and constitutively expressed protein, SsbB is not essential and its expression is regulated during the state of competence (Yadav *et al.*, 2012). Moreover, SsbA and SsbB perform different activities. SsbA forms part of the *B. subtilis* replisome and is important for DNA replication (Costes *et al.*, 2010). In contrast, SsbB colocalises with the cell pole and participates in the internalisation of the exogenous ssDNA during natural transformation (Kramer *et al*., 2007).

The interactome of SsbA at active replication forks has been characterised in both, *in vivo* and *in vitro*. By GFP fusions and tap-tag protein purification, it has been observed that SsbA interacts with many recombination and repair factors, such as PriA, RecQ, RecG, RecS, RarA, RecJ, RecO and RecD2 (also named as YrrC). The C-terminal domain of SsbA is crucial for these interactions, because *in vitro* experiments have shown that the SsbA C-ter deletion mutant is unable to form a protein complex with these proteins. Additionally, the SsbA C-ter deletion mutant strain is deficient in RecA loading onto the ssDNA (Lecointe *et al.,* 2007; Costes *et al.,* 2010). *E. coli* SSB, structurally similar to Ssb proteins from *B. subtilis*, also interacts with proteins that participates in DNA repair like RecQ, RecJ, RecG, RecO, PriA, PriB and ExoI (Shereda *et al*., 2008).

1.5. Accessory helicases in DNA replication

Helicases play central roles in diverse DNA metabolism pathways. They act unwinding the double strand DNA, or RNA-RNA/RNA-DNA duplexes, by using generally ATP hydrolysis energy. This type of enzymes is ubiquitous in all organisms due to its function in several processes, such as DNA replication, repair, transcription and translation (Singleton *et al*., 2007). Helicases have been classified in six different superfamilies in base to the number and the sequence of their motifs. Superfamilies 1 and 2 (SF1 and SF2) harbour the majority of recombination DNA repair helicases, with any of both polarities, 5' to 3' or 3' to 5'. SF1 is divided in two subgroups, A or B, depending on the polarity (SF1A, 3' to 5'; SF1B, 5' to 3'). Some examples of SF1A helicases in Bacteria are Rep, UvrD, RecB and PcrA; of SF1B are RecD and

RecD2; and of SF2 are RecQ, RecG, RuvB and PriA (Wu and Hickson, 2006; Singleton *et al*., 2007; Saikrishnan *et al*., 2009). Whereas some of them are crucial for a specific function (i.e. the replicative helicases DnaC in *B. subtilis* or DnaB in *E. coli*), many others participate as accessory factors during different processes. Particularly, there are accessory helicases that may contribute to replication fork progression and DNA repair.

In *E. coli*, replication restart mainly involves three distinct accessory helicases: PriA, Rep and UvrD. They are SF1A helicases that are able to remodel the replication fork structure in the presence of DNA damage and facilitate replisome loading (Heller and Marians, 2007). As mentioned, PriA interacts with SSB and travels with active replication forks (Shereda *et al*., 2008). PriA, in concert with PriB and DnaT, unwinds the nascent lagging strand and promotes the binding of DnaB helicase to the forked DNA (Heller and Marians, 2005). Rep performs a similar activity in concert with its activator factor PriC (Nguyen *et al.,* 2021). Rep also contributes to remove protein blocks that impede the progression of replication fork (Guy *et al.*, 2009). On the other hand, it has been proposed that UvrD acts removing recombination intermediates and facilitates the RecA disassembly from the ssDNA that can block the resumption of replication. Rep and UvrD are not essential for cell survival, but the absence of both proteins is lethal (Veaute *et al.*, 2005). In *B. subtilis*, PcrA helicase shows similarities in structure and function to Rep and UvrD from *E. coli* and it is an essential protein (Petit *et al*., 1998). PcrA unwinds preferentially RNA-DNA hybrids and, like UvrD, may participate in the backtracking of a stalled RNA polymerase (Epshtein *et al*., 2014; Moreno-del Álamo *et al.,* 2021).

PriA carries out the resumption of DNA replication in *B. subtilis*, with similar function to PriA from *E. coli* (Polard *et al.,* 2002). However, the resumption of DNA replication by this helicase in both organisms is different. Proteins like PriB or DnaT, which take part, in concert with PriA, in replication restart in *E. coli*, are absent in *B. subtilis*. Instead of that, PriA from *B. subtilis* interacts with the initiation proteins DnaD and DnaB to promote the replication restart. PriA in *B. subtilis* is an essential protein and *priA* mutants rapidly acquire suppressor mutations in *dnaD* or *dnaB* genes. Both DnaD and DnaB proteins are essential for initiation and re-initiation of DNA replication (Polard *et al.,* 2002; Gabbai and Marians, 2010).

RecG is another helicase that belongs to the SsbA interactome (Costes *et al*., 2010). This helicase participates as a branch migration translocase during the postsynaptic step of HR and contributes to restore the replication process via fork regression in the presence of a DNA lesion in the replication fork (see section 1.3). Another branch migration translocase that could act in the context of replication is RadA/Sms, although it is not part of the SsbA interactome. It has been observed that this helicase is able to process stalled or reversed forks by unwinding the nascent lagging strand (Torres and Alonso, 2021). RecQ and RecS are homologous helicases that may

participate in DNA end resection during HR in concert with RecJ exonuclease. RecQ is associated with the replication fork by its interaction with SsbA and, as PriA and RecG, may participate in replication restart (Lecointe *et al*., 2007). *E. coli* RecQ acts remodeling the replication fork structure by unwinding the nascent lagging strand (Hishida *et al*., 2004). *B. subtilis* RecQ recognises specifically replication forks structures *in vitro* (Qin *et al*., 2014), but it is a poorly characterised helicase.

1.6. RecD2 helicase

1.6.1. Biochemical activities of RecD2

Another helicase that belongs to the SsbA interactome is RecD2, which has been proposed as an accessory helicase in DNA replication and HR (Costes *et al*., 2010). This enzyme belongs to SF1B and unwinds DNA from 5' to 3', as the other members of this superfamily of helicases. RecD2 shows similarities in structure and sequence to RecD helicase from *E. coli* ($RecD_{Eco}$, also known as RecD1), but the first protein has an N-terminal extension with an unknown function and both proteins do not perform the same actions (Montague *et al*., 2009; Saikrishnan *et al*., 2009). RecD is part of the RecBCD complex and has been substantially studied in *E. coli*. RecBCD is involved in the long end resection of DSBs during the presynaptic step of HR, and it is absent in some Gram-positive bacteria like *B. subtilis*, where the helicase/nuclease AddAB complex plays a similar role in DSB repair (Chédin and Kowalczykowski, 2002; Lenhart *et al*., 2012). Usually, bacteria that contain RecD2 lack the RecBCD complex (Montague *et al*., 2009).

In contrast to RecD, RecD2 has been poorly studied and its role is not clearly known, although the published data suggest that this helicase may be involved in DNA replication and DNA repair. RecD2 from *Deinococcus radiodurans* ($RecD2_{Dra}$) represents the best structurally and biochemically characterised protein of this group of helicases. The crystal structure of $RecD2_{Dra}$ has been obtained with an N-terminal truncation (deletion of 150 amino acids that are missed in RecD proteins) with the aim to compare this helicase to its homologous $RecD_{Eco}$. The global structure of both proteins, $RecD_{Eco}$ and the N-terminal truncated RecD2 (Δ150-$RecD2_{Dra}$), is similar, and both are monomers (**Figure 6**) (Saikrishnan *et al*., 2008). RecD2 contains five domains: 1A, 1B, 2A, 2B and the N-terminal (Saikrishnan *et al*., 2008; Saikrishnan *et al*., 2009). Domains 1A and 2A have a RecA-like fold and form a channel that contacts with the ssDNA backbone, allowing the ssDNA crossing. 1B creates the pin or wedge region with its β-hairpin, which is crucial for the unwinding activity. 2B domain has a SH3 fold, not very common in prokaryotes, and is involved in ssDNA binding. Moreover, 2B may participate in the interaction with other proteins, because the SH3 fold is supposed to interact with peptides. The binding of ATP promotes a conformational change that results in that 1A and 2A domains get closer to the

nucleotide-binding site, creating a connection between the ssDNA binding and the ATPase site. It has been observed in the crystal structure that only eight bases from the ssDNA are in contact with the protein (Saikrishnan *et al*., 2009). RecD harbours similar domains, although 1B and 2B were disordered in the crystal structure (Saikrishnan *et al*., 2008).

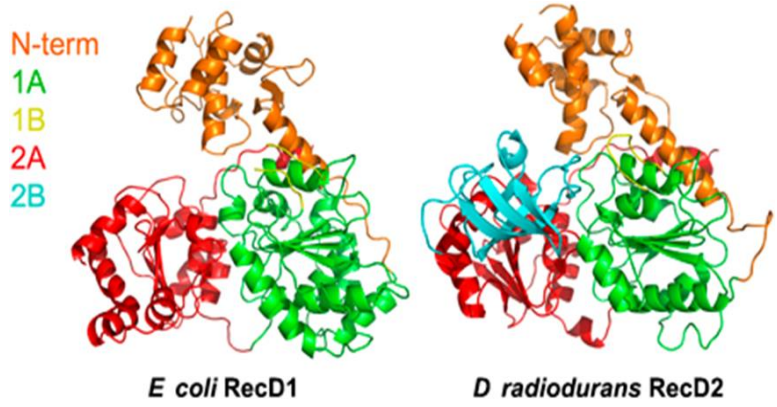

Figure 6. Crystal structure of *E. coli* RecD (RecD1) and *D. radiodurans* RecD2.
The crystal structure of *D. radiodurans* RecD2 has an N-terminal truncation with the deletion of 150 aa of this domain. Both proteins have similar structure and share the same domains, although 1B and 2B are disordered in *E. coli* RecD. Figure from Saikrishnan *et al*., 2008.

The biochemical activities of RecD2$_{Dra}$ have been explored. The ATPase activity of this helicase is highly stimulated by the presence of ssDNA, whereas its activity is considerably reduced using linear or circular dsDNA as effectors of the reaction (Wang and Julin, 2004). On the other hand, the ATP hydrolysis of the Δ150-RecD2$_{Dra}$ has been also characterised using polydTs with different lengths (20 to 60 nt). The catalytic constant (k_{cat}), which represents the velocity of ATP hydrolysis, for each polydT has shown a global $k_{cat} = 98 \pm 12$ s^{-1} for all of these DNA substrates (Saikrishnan *et al*., 2009). Additional experiments performed with the Δ150-RecD2$_{Dra}$ have shown a similar k_{cat} value (86.9 ± 1.5 s^{-1}) with a polydT$_{20}$ (Toseland and Webb, 2013). As a measure of protein affinity for ATP, the Michaelis-Menten constant (K_m) has been measured. K_m represents the concentration of a substrate needed to obtain the 50% of the maximum activity and it has been calculated using increasing concentrations of ATP, obtaining a K_m value of 30.3 ± 1.5 μM ATP for the Δ150-RecD2$_{Dra}$ (Toseland and Webb, 2013). The translocation rate along the ssDNA has been also characterised for the Δ150-RecD2$_{Dra}$, showing that the protein hydrolyses one ATP per base moved (Saikrishnan *et al*., 2009).

The DNA binding properties of RecD2$_{Dra}$ have been poorly explored. As the crystal structure and translocation assays have suggested, RecD2 binds and translocates along ssDNA (Saikrishnan *et al*., 2009). Electrophoretic mobility shift assays (EMSA) have shown that RecD2$_{Dra}$ binds efficiently to 5' ssDNA tails (Wang and Julin, 2004; Saikrishnan *et al*., 2008), obtaining an apparent binding constant, K_{app}, value of 2.5 ± 1.3 nM RecD2 for a substrate with a

12 nt 5' tail (Shadrick and Julin, 2010). Similar to K_m, K_{app} represents the protein concentration necessary to observe 50% of DNA binding and it is a measure of the affinity to the substrate.

The unwinding polarity of RecD2 has been also determined for the protein from both organisms, *D. radiodurans* and *B. subtilis*. As its equivalent partner RecD, RecD2 helicases unwind DNA from 5' to 3' (Wang and Julin, 2004; Walsh *et al*., 2014). The presence of a 5' ssDNA end is crucial for the unwinding, because $RecD2_{Dra}$ is not capable to unwind dsDNA with blunt ends (Wang and Julin, 2004). Not too many differences in unwinding efficiency have been observed in $RecD2_{Dra}$ between a substrate with 12 nt ssDNA 5' tail and a fork-like structure with two 12 nt ssDNA tails. In both cases, the duplex region had 20 bp and 100 nM $RecD2_{Dra}$ unwound approximately 80% of the substrate in a 30 min reaction (Shadrick and Julin, 2010). $RecD2_{Dra}$ appears to be not much efficient unwinding longer dsDNA regions with 52 or 76 bp, suggesting that this helicase has low processivity. The addition of SSB stimulates helicase activity of $RecD2_{Dra}$, maybe because it avoids DNA reannealing due to the excess of SSB in the reaction (ratio SSB:$RecD2_{Dra}$ of 80:1) (Wang and Julin, 2004). Moreover, it has been shown that $RecD2_{Dra}$ unwinds complex DNA structures like G-quadruplex (G4), which are typically formed in guanine-rich regions. The unwinding of G4 is crucial for genome stability (Xue *et al.,* 2020).

1.6.2. Genetic and functional analysis of RecD2

RecD2 has been postulated to participate in DNA repair, but its contribution remains unclear. The published genetic data show differences between species. For instance, the deletion of *recD2* gene in *D. radiodurans* confers sensitivity to different DNA damaging agents like UV irradiation, gamma irradiation and hydrogen peroxide (H_2O_2). However, this strain appears to be resistant to mitomycin C (MMC) and methyl methanesulfonate (MMS) (Servinsky and Julin, 2007). In *B. subtilis*, the absence of *recD2* gene (also termed *yrrC*) confers sensitivity to a wide variety of DNA damaging agents, such as MMS, MMC, UV irradiation, H_2O_2, phleomycin and 4-nitroquinoline 1-oxide (4NQO) (Walsh *et al*., 2014; Torres *et al*., 2017). These results indicate that RecD2 may have a role in several DNA repair pathways. On the other hand, *Bacillus anthracis recD2* mutant strain has a high accumulation of spontaneous mutations (~40-fold respect to the wild type strain, *wt*) with a similar mutation spectrum to when mismatch repair factors are defective, indicating a possible role of this helicase in MMR. However, no UV irradiation sensitivity has been observed in this strain compared to the *wt*. The N-terminal domain seems to be crucial, because mutations in this region affect the DNA repair activity of RecD2 (Yang *et al*., 2011). Nevertheless, the deletion of *recD2* in *B. subtilis* only moderately increases the spontaneous mutation rate (~3.6-fold respect to the *wt*) (Walsh *et al*., 2014). The observed differences in DNA damage sensitivity in the absence of *recD2* could be explained because RecD2 helicase is not the same protein between these organisms (**Figure 7**). In fact, whereas *B.*

subtilis RecD2 and *B. anthracis* RecD2 (798 aa and 778 aa, respectively) share 57% of amino acid identity (they belong to the same genus), *B. subtilis* and *D. radiodurans* RecD2 (715 aa) share 28% of amino acid identity (Walsh *et al*., 2014). Therefore, although *D. radiodurans* RecD2 is the most studied protein, it is difficult to directly extrapolate the results to other organisms.

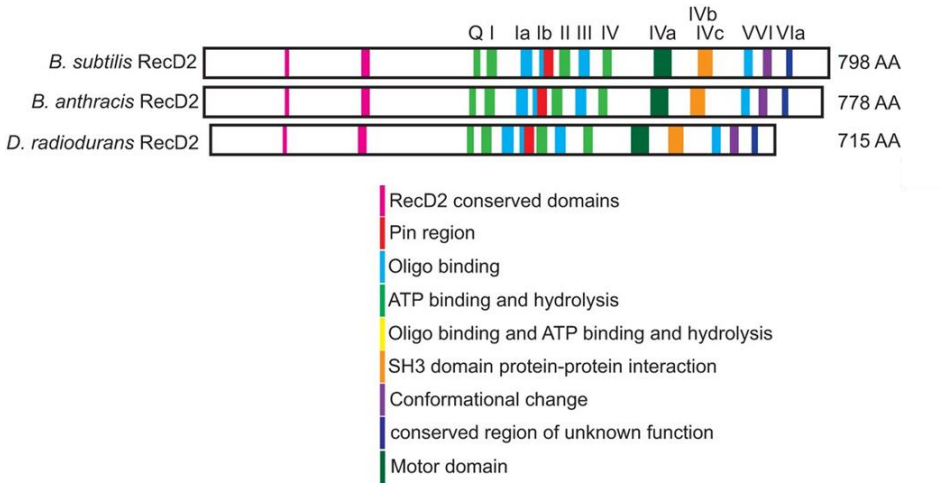

Figure 7. Comparison of functional motifs between *B. subtilis*, *B. anthracis* and *D. radiodurans* RecD2 proteins. These proteins share the same motifs that are present in helicases that belong to SF1B with an N-terminal region with conserved motifs, but with unknown function. *B. subtilis* RecD2 shares 57% of amino acid identity to *B. anthracis* RecD2 and *B. subtilis* RecD2 and *D. radiodurans* RecD2 share 28% of amino acid identity. Figure adapted from Walsh *et al*., 2014.

RecD2 has been considered as a recombination repair enzyme, although its role in HR pathway is poorly understood. The deletion of *recD2* has been combined with the absence of other recombination helicases in *B. subtilis* (Δ*recS*, Δ*recQ*, Δ*helD*, Δ*dinG*, Δ*addAB*, Δ*ruvAB* and Δ*recG*) with the aim to elucidate in which step of HR reaction this helicase could be acting. This analysis has shown that RecD2 is non-epistatic with AddAB, RecS, RecQ, DinG or HelD helicases, because the double mutants were more sensitive to DNA damaging agents (MMS and H_2O_2) than the single mutants. On the other hand, the double mutant strains Δ*recD2* Δ*ruvAB* and Δ*recD2* Δ*recG* were not viable (Torres *et al*., 2017). These results suggests that RecD2 may act as a branch migration translocase, as RecG or RuvAB, during the postsynaptic step of HR. However, more data is required to confirm that hypothesis.

RecD2 has been also postulated to be an accessory helicase in DNA replication. Previous authors have shown that the helicase from *B. subtilis* interacts *in vivo* and *in vitro* with Ssb, and both proteins colocalise in the absence of DNA damage, suggesting that RecD2 is normally associated to the replication fork (Costes *et al*., 2010; Walsh *et al.,* 2014). Furthermore, the absence of RecD2 leads to replication stress since there is more replication fork collapse in *recD2* deficient strain, and it promotes the accumulation of unsegregated chromosomes (Walsh *et al.,* 2014; Torres *et al.*, 2017). However, by using an *in vitro* heterologous model of a stalled replication fork with purified *E. coli* replisome proteins, it has been shown that $RecD2_{Dra}$ inhibited

the resumption of DNA replication. Nevertheless, this helicase did not affect elongating replisomes (Gupta *et al*., 2013). These negative results are not in agreement with the *in vivo* data that have shown that replisomes collapse more frequently in *recD2* mutants (Walsh *et al*., 2014), and this could be due because of the use of an heterologous system. Alternatively, these results suggest that RecD2 could participate in replication restart, preventing an anomalous initiation of replication when the replication fork is blocked and thus, leading time for the DNA repair machinery to act. Similar result has been observed with RarA from *B. subtilis*, which is an ATPase protein that has been proposed to modulate the replication restart (Carrasco *et al.*, 2018).

1.6.3. Eukaryotic HELB helicase

One interesting aspect of RecD2 is that this helicase is evolutionary conserved from prokaryotes to eukaryotes. RecD2 protein shows similarities in sequence to DNA helicase B (also termed HELB, HelB, DHB or HDHB), present in high eukaryotes. Murine HELB (1074 aa) shares 16.5% of amino acid identity with *B. subtilis* RecD2 and 11.1% to *E. coli* RecD. The three proteins contain seven conserved helicase motifs (I, Ia, II, III, IV, V and VI), which are 46.8% identical between murine HELB and *E. coli* RecD, and 42.7% identical between murine HELB and *B. subtilis* RecD2 (Tada *et al.*, 2001). As RecD2, HELB unwinds duplex DNA from 5' to 3' direction and its ATP hydrolysis activity is stimulated by the presence of ssDNA. HELB does not seem to be part of a complex or be associated to a nuclease (Taneja *et al.,* 2002; Hormeño *et al.*, 2022). Human HELB (1087 aa), with shares a strong homology with the murine protein (65% of amino acid identity), has three domains. The N-terminal extension has an unknown function. The central domain is RecD-like with helicase activity and also involved in DNA binding. The C-terminal domain is for the subcellular localisation of the protein, with a nuclear localisation sequence and a nuclear export sequence. The C-terminal domain has cyclin-dependent kinase phosphorylation sites that are phosphorylated during the late G1 phase. Consequently, the nuclear HELB is exported to the cytoplasm during S phase (Gu *et al.*, 2004; Hazeslip *et al.,* 2020).

As RecD2, HELB helicase has been also postulated as an accessory helicase in several processes, such as replication and recombination (**Figure 8**). The accumulation of HELB into the chromatin in response to DNA damage treatment suggests a role of this helicase in DNA repair (Hazeslip *et al*., 2020). HELB interacts with the single-stranded binding protein in eukaryotes, RPA, and this mediates the recruitment of HELB to the chromatin in the presence of DNA damage (Guler *et al*., 2012). Contrary to the published data from $RecD2_{Dra}$, RPA stimulates the ATPase and translocase activities of HELB, but it inhibits DNA unwinding. Furthermore, HELB removes RPA molecules from the ssDNA during translocation (Hormeño *et al.*, 2022). HELB also interacts with the DNA polymerase α-primase (pol-prim) and stimulates the synthesis of RNA primers in a dose-dependent manner. The presence of RPA inhibits the RNA synthesis by pol-prim, but

HELB overcomes this inhibition (Taneja *et al.*, 2002). It has been proposed that the HELB and pol-prim interaction could promote the loading of pol-prim into the leading strand in a stalled replication fork caused by the presence of DNA damage in this strand (Guler *et al.,* 2012; Hazeslip *et al*., 2020). An additional role of HELB has been discovered in the context of initiation of replication. Human HELB interacts via its N-terminal and helicase domains with TOPBP1 and Cdc45, which are two replication initiation proteins. The absence of HELB inhibits the initiation of DNA replication and reduces the accumulation of Cdc45 into the chromatin, suggesting that HELB may recruit replication initiation factors (Gerhardt *et al*., 2015). HELB could also facilitate the replisome progression via unwinding DNA secondary structures in fragile sites that could stall the replication fork (Guler *et al.*, 2018; Hazeslip *et al.*, 2020). On the other hand, it has been shown that HELB participates modulating the initiation of HR pathway. Particularly, HELB helicase inhibits EXO1 and BLM-DNA2, which are the nucleases involved in DNA end resection during the presynaptic step of HR necessary to repair DSBs. In this context, RPA is crucial because it recruits HELB to DSB sites (Tkáč *et al.,* 2016). HELB colocalises *in vivo* with the recombinase Rad51 (eukaryotic RecA). Moreover, this helicase stimulates *in vitro* the Rad51-mediated strand exchange reaction and the 5' to 3' D-loop extension in the presence of a dsDNA with a 3' ssDNA end (Liu *et al*., 2015).

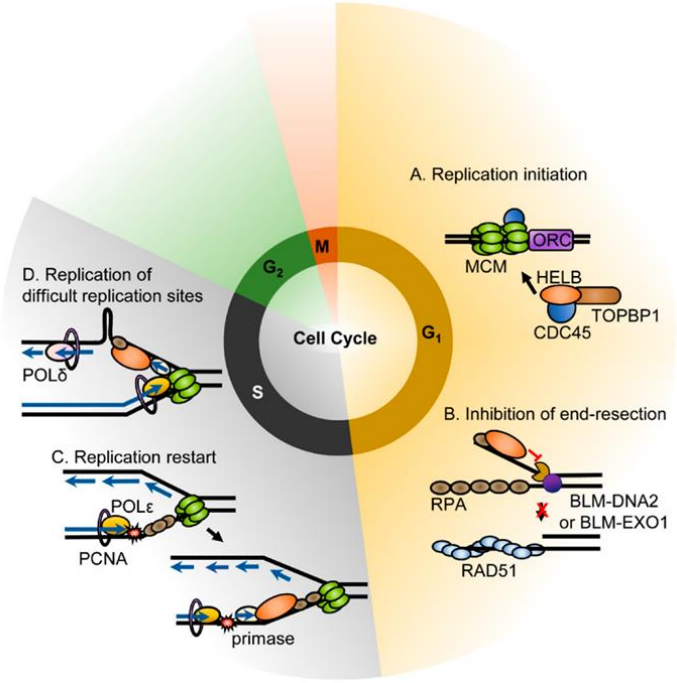

Figure 8. Roles of human HELB as accessory helicase in replication and recombination.
(**A**) HELB participates in replication initiation. This helicase interacts with and recruits the replication initiation factors Cdc45 and TOPBP1 to the origin of replication. (**B**) HELB reduces end-resection during HR pathway by inhibiting the nucleases EXO1 and BLM-DNA2. (**C**) HELB contributes to replication restart by its interaction with pol-prim. HELB is supposed to load pol-prim to the leading strand in a stalled replication fork. (**D**) HELB unwinds dsDNA structures in fragile sites promoting replication fork progression. Figure from Hazeslip *et al*., 2020.

Objectives

2. Objectives

The main objective of this thesis was the biochemical and functional characterisation of *B. subtilis* RecD2. The specific objectives were:

1. *In vivo* analysis of the contribution of RecD2 to natural transformation mechanisms: intra-and interspecies chromosomal transformation, plasmid transformation and viral transfection.

2. Biochemical characterisation of the RecD2 protein: DNA binding, translocation and unwinding.

3. Biochemical characterisation of RecD2 in concert with SsbA.

4. Quantification of the RecD2 protein levels present in *B. subtilis* cells.

5. Study of RecD2 in the context of DNA replication by *in vitro* DNA replication assays.

6. Analysis of the *in vivo* dynamics and the subcellular localisation of RecD2 by single-molecule fluorescence microscopy during unperturbed or perturbed DNA replication.

7. Analysis of the interplay between RecD2 and RecA in homologous recombination.

Materials and Methods

3. Materials and Methods

3.1. Materials

3.1.1. Bacterial strains

Table 1. *E. coli* strains.

Strain	Genotype	Description
XL1-Blue	*recA1 endA1 gyrA96 thi-1 hsdR17 supE44 relA1 lac [F proAB lacIqZΔM15 Tn10 (Tet^R)]*	Strain used for plasmid construction and isolation
BL21(DE3) [pLysS]	*F$^-$ dcm ompT hsdS (r_B^- m_B^-) gal λ (DE3) [pLysS Cat^R]*	Strain used for protein overexpression from pET plasmids by IPTG induction. pLysS plasmid expresses T7 lysozyme which suppresses basal expression of T7 RNA polymerase prior to induction

Table 2. *B. subtilis* strains.

Strain and genotype	Description
BG214, *trpCE metA5 amyE1 ytsJ1 rsbV37 xre1 xkdA1 att$^{SP\beta}$ att^{ICEBs1}*	*B. subtilis* 168 wild-type (*wt*, *rec*$^+$). Laboratory strain
BG190, + Δ*recA*	Mutation of *recA* gene. Cm^R (Ceglowski *et al*., 1990)
BG1455, + Δ*recD2*	Mutation of *recD2* (*yrrC*) gene. Cm^R (Torres *et al*., 2017)
BG1245, + Δ*radA/sms*	Mutation of *radA/sms* gene. Cm^R (Gándara and Alonso, 2015)
BG1635, + Δ*recD2* Δ*radA/sms*	Mutation of *recD2* and *radA/sms* genes. Cm^R. This work (Serrano *et al*., 2020)
BG1359, + Δ*rok*	Mutation of *rok* gene. Cm^R. (Carrasco *et al*., 2016)
BG1549, + Δ*rok* Δ*recD2*	Mutation of *rok* and *recD2* genes. Cm^R. This work (Serrano *et al*., 2021)
recD2$_{his6}$	*wt* expressing RecD2-6xHis from the original locus of *recD2* gene. Cm^R. This work (Ramos *et al*., 2022)
BG1329, *recD2-mVenus*	*wt* expressing fluorescent RecD2-mVenus from the original locus of *recD2* gene. Cm^R. (Romero, 2018)
dnaX-cfp recD2-mVenus	*wt* expressing fluorescent RecD2-mVenus from the original locus of *recD2* gene and DnaX-CFP in the *amyE* site from a xylose-inducible promoter (P_{xyl}). Cm^R and Spect^R. This work
dnaD23 recD2-mVenus	Thermosensitive mutation of *dnaD* gene and expression of RecD2-mVenus from the original locus of *recD2* gene. Cm^R. This work
dnaB37 recD2-mVenus	Thermosensitive mutation of *dnaB* gene and expression of RecD2-mVenus from the original locus of *recD2* gene. Cm^R. This work

3.1.2. Bacteriophages

Table 3. Bacteriophages.

Bacteriophage	Use
SPP1	Construction of *B. subtilis* strains by transduction. Used as donor DNA in viral transfection assays
Helper phage VCS	Production and isolation of sspGEM-3Zf (+) phagemid

3.1.3. Plasmids and phagemids

Table 4. Plasmids and phagemids.

Name	Description
pSG1164-C-ter-*recD2*-His	Integrative plasmid containing 500 bp of *recD2* fused to 6xHis. It allows expression of RecD2-6xHis from its natural promoter. This work (Ramos *et al*., 2022)
pET3b-*recD2*-His	pET3b derived plasmid. Used for the overexpression of RecD2-6xHis. This work (Ramos *et al*., 2022)
pET3b-*recD2*-K373A-His	pET3b derived plasmid. Used for the overexpression of RecD2 K373A-6xHis. This work (Ramos *et al*., 2022)
pUB110	Donor DNA used in plasmid transformation assays. Nm^R
pCB980	Donor DNA used in chromosomal transformation assays. The plasmid derived from the cloning of *rpoB* gene from *B. subtilis* 168 in pUC57 vector. The cloned *rpoB* contains a single mutation (C482T) that confers Rif^R. (Carrasco *et al*., 2016)
pCB981	Donor DNA used in chromosomal transformation assays. The plasmid derived from the cloning of *rpoB* gene from *B. subtilis* W23 in pUC57 vector. The cloned *rpoB* contains the mutation (C482T) that confers Rif^R. (Carrasco *et al*., 2016)
pCB982	Donor DNA used in chromosomal transformation assays. The plasmid derived from the cloning of *rpoB* gene from *B. atrophaeus* 1942 in pUC57 vector. The cloned *rpoB* contains the mutation (C482T) that confers Rif^R. (Carrasco *et al*., 2016)
pCB983	Donor DNA used in chromosomal transformation assays. The plasmid derived from the cloning of *rpoB* gene from *B. amyloliquefaciens* DSM7 in pUC57 vector. The cloned *rpoB* contains the mutation (C482T) that confers Rif^R. (Carrasco *et al*., 2016)
pCB984	Donor DNA used in chromosomal transformation assays. The plasmid derived from the cloning of *rpoB* gene from *B. licheniformis* DSM13 in pUC57 vector. The cloned *rpoB* contains the mutation (C482T) that confers Rif^R. (Carrasco *et al*., 2016)
pCB985	Donor DNA used in chromosomal transformation assays. The plasmid derived from the cloning of *rpoB* gene from *B. thuringiensis* MC28 in pUC57 vector. The cloned *rpoB* contains the mutation (C482T) that confers Rif^R. (Carrasco *et al*., 2016)
pCB1054	Donor DNA used in chromosomal transformation assays. The plasmid derived from the cloning of *rpoB* gene from *B. gobiensis* FJAT4402 in pUC57 vector. The cloned *rpoB* contains the mutation (C482T) that confers Rif^R. (Serrano *et al*., 2021)
pCB1056	Donor DNA used in chromosomal transformation assays. The plasmid derived from the cloning of *rpoB* gene from *B. smithii* DSM4216 in pUC57 vector. The cloned *rpoB* contains the mutation (C482T) that confers Rif^R. (Serrano *et al*., 2021)

Table 4. Plasmids and phagemids (continued).

Name	Description
pGEM-T Easy	Used as intermediary vector during plasmid construction (Promega)
pGEM-3Zf (+)	Phagemid used as the source of ssDNA and dsDNA in biochemical assays
Minicircular RC	Template used for *in vitro* DNA replication (rolling circle) assays (Sanders *et al*., 2010)

3.1.4. DNAs for biochemical assays

Table 5. Oligonucleotides.

Name	Sequence (5' to 3')
polydT$_{15}$	TTTTTTTTTTTTTTT
polydT$_{20}$	TTTTTTTTTTTTTTTTTTTT
polydT$_{30}$	TTTTTTTTTTTTTTTTTTTTTTTTTTTTTT
polydT$_{40}$	TTTTTTTTTTTTTTTTTTTTTTTTTTTTTTTTTTTTTTTT
polydT$_{60}$	TTTTTTTTTTTTTTTTTTTTTTTTTTTTTTTTTTTTTTTTTTTTTTTTTTTTTTTTTTT
polydT$_{70}$	TTTTTTTTTTTTTTTTTTTTTTTTTTTTTTTTTTTTTTTTTTTTTTTTTTTTTTTTTTTTTTTTTTT
polydT$_{80}$	TTTTTTTTTTTTTTTTTTTTTTTTTTTTTTTTTTTTTTTTTTTTTTTTTTTTTTTTTTTTTTTTTTTTTTTTTTT
polydA$_{80}$	AAAAAAAAAAAAAAAAAAAAAAAAAAAAAAAAAAAAAAAAAAAAAAAAAAAAAAAAAAAAAAAAAAAAAAA
dT$_{30}$-mer up	ACGGCCTAGATCGTGAACCTGCAGGTAAGGTTTTTTTTTTTTTTTTTTTTTTTTTTTT
dT$_{30}$-mer down	TTTTTTTTTTTTTTTTTTTTTTTTTTTTTCCTTACCTGCAGGTTCACGATCTAGGCCGT
16-M-90	GCTGGATATGGACGCTGCCGAATTCTACCAGTGCCTTGCTAGGACATCAGTCGTAGGATCCCTTACCTGCAGGTTCACGATCTAGGCCGT
17-M-46	ACGGCCTAGATCGTGAACCTGCAGGTAAGGGGCTGCTCATCGTAGG
17-M-60	ACGGCCTAGATCGTGAACCTGCAGGTAAGGGGCTGCTCATCGTAGGTTAGCGTAAATTAG
17-M-70	ACGGCCTAGAACGGCCTAGATCGTGAACCTGCAGGTAAGGGGCTGCTCATCGTAGGTTAGCGTAAATTAG
17-M-80	ACGGCCTAGAACGGCCTAGAACGGCCTAGATCGTGAACCTGCAGGTAAGGGGCTGCTCATCGTAGGTTAGCGTAAATTAG
17-M-90	ACGGCCTAGATCGTGAACCTGCAGGTAAGGGGCTGCTCATCGTAGGTTAGCGTAAATTAGTGGTAGAATTCGGCAGCGTCCATATCCAGC

Table 5. Oligonucleotides (continued).

Name	Sequence (5' to 3')
18-M-46	CATCAGTCGTAGGATACCTTACCTGCAGGTTCACGATCTAGGCCGT
18-M-60	GTGCCTTGCTAGGACATCAGTCGTAGGATACCTTACCTGCAGGTTCACGATCTAGGC CGT
18-M-70	GTGCCTTGCTAGGACATCAGTCGTAGGATACCTTACCTGCAGGTTCACGATCTAGGC CGTTCTAGGCCGT
18-M-80	GTGCCTTGCTAGGACATCAGTCGTAGGATACCTTACCTGCAGGTTCACGATCTAGGC CGTTCTAGGCCGTTCTAGGCCGT
19-M-60	GGCTGCTCATCGTAGGTTAGCGTAAATTAGGATCCTACGACTGATGTCCTAGCAAGG CAC
20-M-60NC	GATCCTACGACTGATGTCCTAGCAAGGCACGGCTGCTCATCGTAGGTTAGCGTAAAT TAG
21-M-30	TATCCTACGACTGATGTCCTAGCAAGGCAC
22-M-30	CTAATTTACGCTAACCTACGATGAGCAGCC
170	AGACGCTGCCGAATTCTGGCTTGGATCTGATGCTGTCTAGAGGCCTCCACTATGAAA TCG
171	CGATTTCATAGTGGAGGCCTCTAGACAGCA
172	TGCTGTCTAGAGACTATCGATCTATGAGCT
173	AGCTCATAGATCGATAGTCTCTAGACAGCATCAGATCCAAGCCAGAATTCGGCAGC GTCT
J3-1	CGCAAGCGACAGGAACCTCGAGAAGCTTCCGGTAGCAGCCTGAGCGGTGGTTGAAT TCCTCGAGGTTCCTGTCGCTTGCG
J3-2	CGCAAGCGACAGGAACCTCGAGGAATTCAACCACCGCTCAACTCAACTGCAGTCTA GACTCGAGGTTCCTGTCGCTTGCG
J3-2 comp	CGCAAGCGACAGGAACCTCGAGTCTAGACTGCAGTTGAGTTGAGCGGTGGTTGAAT TCCTCGAGGTTCCTGTCGCTTGCG
J3-2-110-5	AAGTCTTTCCGGCATCGATCGTAGCTATTTCGCAAGCGACAGGAACCTCGAGGAATT CAACCACCGCTCAACTCAACTGCAGTCTAGACTCGAGGTTCCTGTCGCTTGCG
J3-3	CGCAAGCGACAGGAACCTCGAGTCTAGACTGCAGTTGAGTCCTTGCTAGGACGGAT CCCTCGAGGTTCCTGTCGCTTGCG
J3-4	CGCAAGCGACAGGAACCTCGAGGGATCCGTCCTAGCAAGGGGCTGCTACCGGAAGC TTCTCGAGGTTCCTGTCGCTTGCG
Hind24	GCAGGCATGCAAGCTTGAGTATTC
BioT-45	GTACGTATTCAAGATACCTCGTACTCTGTACTGACTCGGATCC(biodT)A
F1-30-dA	AGAGGATCCCCGGGTACCGAGCTCGAATTCAAAAAAAAAAAAAAAAAAAAAAAAA AAAAA
F2-30-dA	AAAAAAAAAAAAAAAAAAAAAAAAAAAAAAAGAATTCGAGCTCGGTACCCGGGGAT CCTCT
KpnI-30	GTACCTCTAGAGTCGACCTGCAGGCATGCA

Table 5. Oligonucleotides (continued).

Name	Sequence (5' to 3')
KpnI-50	GTACCGCCAGTACTAAGCTTCGATTTCTAGAGTCGACCTGCAGGCATGCA
HindIII-35	AGCTTGCATGCCTGCAGGTCGACTCTAGAGGTACC
HindIII-55	AGCTTGCATGCCTGCAGGTCGACTCTAGAAATCGAAGCTTAGTACTGGCGGTACC
20-dT_{37}	AGCTGCTCATCGTAGGCTAGTTTTTTTTTTTTTTTTTTTTTTTTTTTTTTTTTTT
16-dT_{37}	TTTTTTTTTTTTTTTTTTTTTTTTTTTTTTTTTTTTTTCTAGCCTACGATGAGC

Table 6. DNA structures.

Name	Oligonucleotide composition	Structure
5'-tailed	17-M-60 + 22-M-30	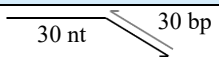
3'-tailed	18-M-60 + 21-M-30	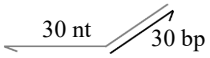
Blunt-ended dsDNA	J3-2 + J3-2 comp	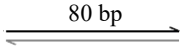
Fork 30-30	17-M-60 + 18-M-60	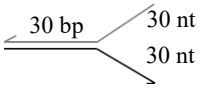
Fork 30-16	17-M-46 + 18-M-46	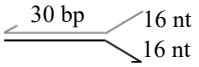
Fork 30-dT_{30}	dT_{30}-mer up + dT_{30}-mer down	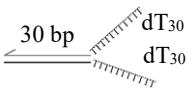
Fork 30-dA_{30}	F1-30-dA + F2-30-dA	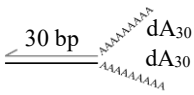
Fork 40-30	17-M-70 + 18-M-70	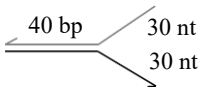
Fork 50-30	17-M-80 + 18-M-80	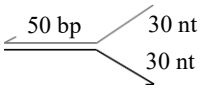
Fork 50-dT_{37}	KpnI-30 + HindIII-35 + 20-dT_{37} + 16-dT_{37}	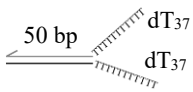
Fork 70-dT_{37}	KpnI-50 + HindIII-55 + 20-dT_{37} + 16-dT_{37}	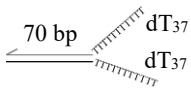
5'-forked	17-M-60 + 22-M-30 + 18-M-60	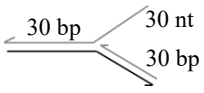
3'-forked	17-M-60 + 21-M-30 + 18-M-60	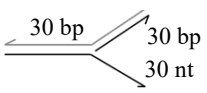

Table 6. DNA structures (continued).

Name	Oligonucleotide composition	Structure
5'-regressed fork	170 + 171 + 173	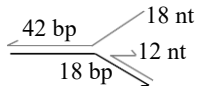
3'-regressed fork	170 + 172 + 173	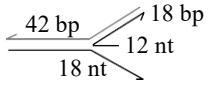
Holliday junction	J3-1 + J3-2 + J3-3 + J3-4	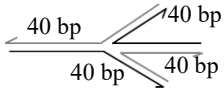
5'-tailed fully regressed fork	J3-1 + J3-2-110-5 + J3-3 + J3-4	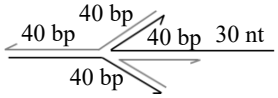
3'-invading D-loop	16-M-90 + 17-M-90 + 19-M-60	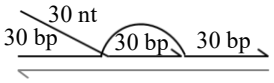
5'-invading D-loop	16-M-90 + 17-M-90 + 20-M-60NC	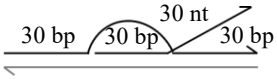
pGEM-Hind24	sspGEM-3Zf (+) + Hind24	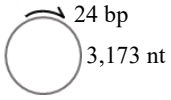

3.1.5. Reagents

Table 7. Reagents.

Antibodies	Manufacturer
6xHis monoclonal antibody	Takara-Clontech
Anti-mouse IgG conjugated with peroxidase	Cytiva
Membranes	**Manufacturer**
Nitrocellulose membrane 0.45 µm	Bio-Rad
Immobilon-P PVDF 0.45 µm	Merk (Millipore)
Antibiotics	**Manufacturer**
Ampicillin, chloramphenicol, kanamycin, neomycin, spectinomycin, tetracyclin	Merk
Rifampicin	Fluka
Enzymes	**Manufacturer**
Pfu DNA polymerase	Promega

Table 7. Reagents (continued).

Enzymes	**Manufacturer**
DNA polymerase I large Klenow, T4 DNA ligase, T4 polynucleotide kinase (PNK), restriction enzymes	New England Biolabs
Taq DNA polymerase	Biotools
NZYlong DNA polymerase	NZYtech
Proteinase K, Pyruvate kinase/Lactic dehydrogenase	Merk
Creatine kinase	Roche
General reagents	**Manufacturer**
Absolute ethanol, ammonium acetate, ammonium persulphate (APS), adenosine 5′-[γ-thio]triphosphate (ATPγS), biotin, boric acid, bovine serum albumin (BSA), 5-bromo-4-chloro-3-indolyl-β-D-galactopyranoside (X-Gal), bromophenol blue, calcium chloride ($CaCl_2$), casamino acids, chloroform, coomassie blue, deoxynucleotides triphosphate (dNTPs), disodium hydrogen phosphate (Na_2HPO_4),1,4-dithiothreitol (DTT), ethylenediaminetetraacetic acid (EDTA), ethidium bromide, glucose, glutamate, glutaraldehyde, glycine, hydrogen peroxide (H_2O_2), 6(p-hydroxyphenylazo)-uracil (HPUra), imidazole, iron (III) chloride ($FeCl_3$), isopropanol, lysozyme, magnesium acetate, magnesium chloride ($MgCl_2$), magnesium sulphate ($MgSO_4$), manganese chloride ($MnCl_2$), β-mercaptoethanol, methyl methanesulfonate (MMS), methanol, L-methionine, , mitomycin C (MMC), nucleotides triphosphate (NTPs), phenol, phosphoenolpyruvate, pluronic F68, polyethylene glycol 6000 (PEG 6000), polyethylene glycol 8000 (PEG 8000), potassium phosphate dibasic (K_2HPO_4), potassium glutamate, potassium phosphate monobasic (KH_2PO_4), DL-serine hydroxamate (SHX), sodium citrate, sodium dodecyl sulphate (SDS), sodium hydroxide, sodium phosphate monobasic (NaH_2PO_4), spermidine trihydrochloride, streptavidin, sucrose, thiamine-HCL, trichloroacetic acid (TCA), Triton X-100, D/L-tryptophan, xylose, zinc chloride ($ZnCl_2$), zinc sulphate ($ZnSO_4$)	Merk (Sigma-Aldrich)
Acetic acid, Tris, vaselin	PanReac AppliChem
Acrilamide, bisacrilamide	Serva
Ammonium sulphate, glycerol	MP Biomedicals
Sodium chloride	Carlo Erba
Hydroxyapatite, TEMED	Bio-Rad
Creatine phosphate, NADH	Roche
Agarose	Pronadisa
Bacteriological agar	Condalab
Bactoyeast extract	BD Biosciences
Casein hydrolysate acid	ICN Biomedicals
λ DNA-HindIII Digest	New England Biolabs
LB Broth	NZYtech
Bactotryptone	Gibco
Isopropyl β-D-1-thiogalactopyranoside (IPTG)	Calbiochem

Table 7. Reagents (continued).

General reagents	Manufacturer
Ni-Sepharose High Performance, Q-Sepharose Fast Flow, Sephadex G-50	GE Healthcare
1 kb Ladder marker	Thermo Fisher Scientific
Rainbow Marker-Full range	Cytiva
Hellmanex	Hellma
[γ-^{32}P]-ATP, [α-^{32}P]-dGTP, [α-^{32}P]-dCTP,	Perkin Elmer
Kits	**Manufacturer**
Plasmid Mini, Midi and Maxiprep	Qiagen
Speedtools PCR-Clean up	Biotools
Clarity^{TM} Western ECL Substrate	Bio-Rad
Quickchange site-directed mutagenesis	Stratagene
Other material	**Manufacturer**
Medical X-Ray films blue	Agfa
Phosphor Imager screens	Bio-Rad
Circular coverslips (5 mm and 2.5 mm)	Menzel

3.1.6. Media

Table 8. Media.

Media	Composition
LB (*E. coli*)	25 g/l LB Broth
LB-agar (*E. coli*)	25 g/l LB Broth, 12 g/l bacteriological agar
LB (*B. subtilis*)	10 g/l bactotryptone, 5 g/l bactoyeast extract, 5 g/l sodium chloride
LB-agar (*B. subtilis*)	10 g/l bactotryptone, 5 g/l bactoyeast extract, 5 g/l sodium chloride, 12 g/l bacteriological agar
F medium	14 g/l bactoyeast extract, 8 g/l bactotryptone, 12 g/l K_2HPO_4, 1.2 g/l KH_2PO_4, 1% glucose
GM1	1 X SBase (2 g/l ammonium sulphate, 14 g/l K_2HPO_4, 6 g/l KH_2PO_4, 1 g/l sodium citrate), 0.5% glucose, 0.1% bactoyeast extract, 0.04% casein hydrolysate acid, 0.8 mM $MgSO_4$, 25 µg/ml D/L-tryptophan, 50 µg/ml L-methionine
GM2	GM1, 3.3 mM $MgSO_4$, 0.5 mM $CaCl_2$
S750	104,7 g/l MOPS, 13.2 g/l ammonium sulphate, 6.8 g/l KH_2PO_4, 200 mM $MgCl_2$, 70 mM $CaCl_2$, 5 mM $MnCl_2$, 0.1 mM $ZnCl_2$, 2 mM HCl, 0.5 mM $FeCl_3$, 0.1 g/l thiamine-HCl, 1% glucose, 0.1% glutamate, 0.004% casamino acids

3.2. Methods

3.2.1. E. coli competent cells

Bacterial cells that have the ability to acquire DNA from their environment are competent cells. *E. coli* do not develop natural competence, so their membranes need to be permeabilised prior to the transformation with exogenous DNA. For preparation of competent cells, *E. coli* strains were plated first on LB-agar plates overnight at 37ºC with the properly antibiotic (tetracyclin, Tc, 10 µg/ml for XL1-Blue and chloranfenicol, Cm, 15 µg/ml for BL21 (DE3) [pLysS]). A CFU (Colony-Forming Unit) was selected from the plate and grown overnight in LB at 30ºC under agitation (250 rpm). The next day, the overnight culture was diluted in fresh LB to OD_{600} = 0.05 and grown at 37ºC under agitation until OD_{600} = 0.5 (exponential phase). Cells were collected by centrifugation for 15 min at 9,000 rpm and 4ºC, and then resuspended in cold 50 mM $CaCl_2$. After 1 h of incubation on ice, cells were centrifuged at the same conditions and resuspended in cold 50 mM $CaCl_2$ and 16% (v/v) glycerol. Finally, cells were aliquoted and stored at -80ºC.

3.2.2. B. subtilis competent cells

In contrast to *E. coli*, *B. subtilis* is a naturally competent bacterium under certain stress conditions, such as nutrient starvation. *B. subtilis* strains were plated first on LB-agar plates overnight at 37ºC with the appropriated antibiotic. A CFU was selected from the plate and grown overnight in GM1 minimal medium at 30ºC without agitation. The next day, the overnight culture was diluted in fresh GM1 to OD_{560} = 0.05 and grown at 37ºC under agitation. The OD_{560} was measured every hour until OD_{560} = 1 (point of inflexion between exponential phase and stationary phase). Afterwards, cells were incubated for 1 h at 37ºC with agitation (stationary phase). Glycerol was added to the culture to 20% (v/v) as final concentration and cells were aliquoted and stored at -80ºC.

3.2.3. Plasmid construction and isolation

Plasmids used in this work were isolated from *E. coli* XL1-Blue or *B. subtilis* by Mini, Midi or MaxiPrep (Qiagen). NanoDrop ND-1000 Spectrophotometer (Thermo Scientific) was used to obtain the DNA concentration measuring the absorbance at 260 nm. 0.8% (w/v) agarose gels were run using 1 kb ladder marker to check the plasmid size and DNA concentration.

The construction of the pSG1164-C-ter-*recD2*-His plasmid was designed to allow the expression in *B. subtilis* of the RecD2 protein fused to a linker (Gly-Pro-Gly-Leu-Ser) and a histidine tag (6xHis) at the C-terminal domain from its natural promoter on the *B. subtilis* chromosome. First, the C-ter region of the *recD2* gene (~500 bp) without the stop codon was

amplified by PCR with Pfu DNA polymerase using primers to obtain the region flanked with KpnI and SfiI restriction sites. The PCR product was ligated into the pGEM-T Easy vector and then digested with KpnI and SfiI. The digestion was run in a 0.8% (w/v) agarose gel in 1 X TAE. The C-ter of *recD2* was subsequently purified from the gel using the Speedtools PCR-Clean up kit and ligated into the integrative vector pSG1164-His (4,824 bp). The resultant pSG1164-C-ter-*recD2*-His plasmid was checked by DNA sequencing and then used to construct the *B. subtilis* $recD2_{his6}$ strain.

The pET3b-*recD2*-His plasmid was constructed for the overexpression and purification of RecD2 fused to 6xHis at the C-terminal domain from *E. coli* cells. First, the *recD2* gene with the stop codon (2,397 bp) was amplified by PCR with Pfu polymerase using primers to obtain the gene flanked with NdeI and BamHI restriction sites. The *recD2* gene was subsequently ligated into the pET3b vector (4,639 bp). The construction of pET3b-*recD2* plasmid was validated by DNA sequencing. This plasmid was initially used to overexpress and attempt to purify RecD2. However, the protein was poorly soluble and tended to aggregate, so after several attempts, RecD2 was fused to the His-tag to facilitate the purification. For that purpose, the pSG1164-C-ter-*recD2*-His plasmid was digested by BseRI and BamHI to obtain the C-terminal region of RecD2 fused to 6xHis. The C-terminal domain of RecD2 in pET3b-*recD2* was then replaced with the C-terminal of RecD2 fused to the linker and 6xHis by digestion and subsequent ligation. The resultant plasmid pET3b-*recD2*-His was validated by DNA sequencing and was used to transform *E. coli* XL1-Blue competent cells (for plasmid storage and isolation) and *E. coli* BL21 (DE3) [pLysS] competent cells (for overexpression of RecD2-His).

pET3b-*recD2* K373A-His was used to overexpress and purify a RecD2 variant with a mutation in the Walker A motif, which is involved in ATP binding and hydrolysis (Walsh *et al*., 2014). The plasmid was constructed by site-directed mutagenesis with the Quickchange kit (Stratagene). In RecD2, the Walker A motif involves a sequence of three amino acids (aa): Gly-Lys-Thr (GKT), located in 372-373-374 aa respectively. pET3b-*recD2*-His plasmid was used as DNA template for the PCR reaction. Two primers were designed to amplify the complete plasmid but replacing the Lys codon to Ala codon in 373 aa position (1,118 bp position in the gene sequence). The PCR product was subsequently treated with DpnI restriction enzyme for 2 h at 37ºC to remove the DNA template, which has been naturally methylated after its transformation in *E. coli* XL1-Blue. Afterwards, the resultant plasmid pET3b-*recD2* K373A-His was used to transform *E. coli* XL1-Blue and The construction was confirmed by DNA sequencing. Finally, the plasmid was introduced into *E. coli* BL21 (DE3) [pLysS] for protein overexpression.

The pCB980, pCB981, pCB982, pCB983, pCB984, pCB985, pCB1054 and pCB1056 plasmids were constructed previously (Carrasco *et al.,* 2016). All these plasmids contain the

house-keeping *rpoB* gene (2,997 bp) cloned into the pUC57 vector (2,710 bp). The *rpoB* gene in these plasmids encodes the essential β-subunit of RNA polymerase from different *Bacilli* species, so with different sequence divergence respect to the original *rpoB* from *B. subtilis* 168 *wt* strain. The plasmids share the single C to T transition mutation at codon 482 in the *rpoB* gene (named *rpoB*482 variant) that confers rifampicin (Rif) resistance. pCB980 contains only this single mutation in *rpoB* gene (**Table 9**).

Table 9. Percentage of sequence divergence in *rpoB*482 variants.

Plasmid	Bacilli origin strain	Number of mismatches	Percentage (%) of sequence divergence to *B. subtilis* 168 *rpoB* gene
pCB980	*B. subtilis* 168	1	0.03
pCB981	*B. subtilis* W23	74	2.47
pCB982	*B. atrophaeus* 1942	250	8.35
pCB983	*B. amyloliquefaciens* DSM7	303	10.12
pCB984	*B. licheniformis* DSM13	435	14.52
pCB1054	*B. gobiensis* FJAT4402	510	17
pCB985	*B. thuringiensis* MC28	624	20.83
pCB1056	*B. smithii* DSM4216	681	22.74

pGEM-3Zf (+) ssDNA (named as sspGEM-3Zf (+) in this work (3,197 nt) was obtained from the *E. coli* XL1-Blue strain containing the pGEM-3Zf (+) dsDNA phagemid as follows. First, this strain was plated on a LB-agar plate with ampicillin (Amp) 100 µg/ml and Tc 10 µg/ml overnight at 37ºC. A CFU was selected from the plate and grown overnight in LB with the antibiotics at 37ºC under agitation. This culture was then diluted in fresh LB to OD_{600} = 0.05 and grown to OD_{600} = 0.1. To produce ssDNA, the helper phage VCS was used to infect the cells using a multiplicity of infection (MOI) between 15-30 phages/cell. The infected culture was incubated for 1 h at 37ºC with agitation. The culture was then diluted 10 times in fresh LB with Amp, Tc and kanamycin (Kan) 50 µg/ml, to select the new forming phages, and grown overnight at 37ºC with agitation. Phages were recovered from the culture by centrifugation at 8,000 rpm for 10 min at 4ºC. Then, they were precipitated from supernatant with 0.5 M NaCl and 3.5% (v/v) PEG 6000 (final concentrations) for 2 h at 4ºC under agitation and then centrifuged at 14,000 rpm for 30 min at 4ºC. The resultant pellet was resuspended in 1 X TE and the pGEM-3Zf (+) ssDNA was extracted by phenol-chloroform and precipitated with absolute ethanol at -20ºC. For pGEM-3Zf (+) dsDNA preparation, the MiniPrep protocol was followed.

The minicircular RC template for DNA replication assays was kindly provided by the Dr. Charles S. McHenry's laboratory from the University of Colorado (USA). The plasmid (409 bp) has a ssDNA tail (396 nt) with a strong dG-dC strand bias (50:1) (Sanders *et al.*, 2010).

3.2.4. Transformation of E. coli competent cells

E. coli competent cells were transformed with plasmid DNA by heat shock. First, 100 ng of the plasmid were incubated with 100 µl of thawed competent cells for 15 min on ice. The same volume of cells without DNA was used as a negative control of transformation. The heat shock was performed incubating for 2 min at 42ºC. Cell were then placed on ice for 5 min. LB was added (400 µl) and cells were grown for 1 h at 37ºC with agitation. Afterwards, cells were collected by centrifugation for 5 min at 12,000 rpm, resuspended in fresh LB and plated on LB-agar plates with the properly antibiotic to select transformants. Plates were incubated overnight at 37ºC.

3.2.5. Construction of B. subtilis strains

The *B. subtilis* strains used in this work are listed in **Table 2** (see section 3.1.1., Materials) and are isogenic to the *wt* strain BG214. All the constructed strains were validated by PCR and DNA sequencing. The Δ*recD2* strain was constructed by transformation of BG214 competent cells with the *six-cat-six* cassete (SCS) flanked with homologous sequences to the *recD2* gene. The SCS is composed of two directly oriented β-recombinase sites (*six* sites) and the *cat* gene, which confers chloramphenicol resistance (Cm^R). Once the mutant Δ*recD2::scs* was confirmed, site-specific recombination by the β-recombinase provided with a pHP13 plasmid promoted recombination between the two directly oriented *six* sites and thereby the deletion of the cloranfenicol resistance gene yield the Cm sensitive Δ*recD2* strain. The Δ*recD2* Δ*radA/sms* strain was constructed transforming Δ*recD2* competent cells with a SCS cassete flanked with homologous sequences to *radA/sms* region. Consequently, *radA/sms* was deleted. The Δ*rok* strain was created by the SPP1 infection of WKS1038 cells, carrying the deletion of the *rok* gene, and the subsequent transduction of BG214 cells with Cm selection. The Δ*rok* Δ*recD2* strain was constructed by the SPP1 infection of Δ*rok* cells and the subsequent transduction of Δ*recD2* with Cm selection.

The $recD2_{his6}$ strain, which contains the *recD2* gene fused to a 6xHis-tag in C-terminal regulated by its own promoter, was constructed with the integration of the pSG1164-C-ter-*recD2*-His plasmid into the BG214 chromosome by transformation. The resultant construction was Cm^R.

The *recD2-mVenus* strain was used to construct the *dnaX-cfp recD2-mVenus*, *dnaD23 recD2-mVenus* and *dnaB37 recD2-mVenus* strains by the SPP1 infection of *recD2-mVenus* and the subsequent transduction of *dnaX-cfp*, *dnaD23* and *dnaB37* cells with Cm selection. *dnaX-cfp*

recD2-mVenus cells harbour the *dnaX-cfp* fusion integrated into the *amyE* site and regulated by a xylose promoter (P_{xyl}), so the expression of the fluorescent DnaX-CFP protein was ectopic. All of these strains were Cm^R, and also spectinomycin resistant ($Spect^R$) in the case of *dnaX-cfp recD2-mVenus* strain.

3.2.6. SPP1 transduction

SPP1 transduction was used to construct *B. subtilis* mutant strains as an alternative method to transformation. *B. subtilis* cells were grown in LB supplemented with 15 mM $MgCl_2$ at 37ºC and agitation. Once the OD_{560} reaches 0.4, cells were infected with SPP1 phages using a MOI of 10 phages/cell. The culture was incubated for 2 h at 37ºC with agitation and then centrifuged at 12,000 rpm for 5 min. The supernatant was filtered by 0.45 µm filters and stored at 4ºC. This supernatant contained SPP1 particles with random chromosomal sequences of the infected *B. subtilis* strain. In a second step, this transducing lysate was titrated to quantify the number of Plaque-Forming Units (PFUs) per ml and used to infect a second *B. subtilis* strain to construct the mutant. This second strain was grown in LB with 15 mM $MgCl_2$ at 37ºC and agitation until $OD_{560} = 0.4$. Then, the culture was infected with the transducing lysate using a MOI between 1-5 phages/cell and incubated for 5 min at room temperature to allow the entry of phages but preventing the cell lysis. Cells were collected by centrifugation at 14,000 rpm for 5 min. Later, cells were resuspended in LB and plated on LB-agar plates with the appropriate antibiotic. The strain construction was analysed checking the resultant CFUs by PCR and DNA sequencing.

3.2.7. Plasmid and chromosomal transformation of B. subtilis competent cells

Transformation assays of *B. subtilis* competent cells were performed for two purposes. One purpose was the construction of mutant strains. The second purpose was the analysis of plasmid and chromosomal transformation efficiencies in mutant strains of *B. subtilis* compared to the *wt*.

Plasmid transformation efficiency assays were performed in *wt*, Δ*recD2* and Δ*recD2* Δ*radA/sms* strains. EcoRI-digested and self-ligated pUB110 plasmid was used as donor DNA. This DNA does not share homology with the *B. subtilis* chromosome, so it remains as an extra-chromosomal element. 500 µl of thawed competent cells were grown in 5 ml of GM2 for 1.5 h at 37ºC and agitation. Later, 100 ng of pUB110 were incubated with 1 ml of the culture for 1 h at 37ºC and agitation. Appropriate dilutions were plated on LB-agar plates with neomycin (Nm) 5 µg/ml to select transformants. Competent cells without DNA were also used as negative control and were plated on LB-agar plates without antibiotic, to obtain the total number of CFUs/ml, and on plates with Nm 5 µg/ml, to obtain the rate of spontaneous mutants. Plates were incubated overnight at 37ºC. Transformation efficiencies were calculated dividing the number of

transformants per the total number of CFUs/ml. The obtained values for the mutant strains were compared considering the efficiency of the *wt* strain as the 100% (Alonso *et al*., 1988).

For chromosomal transformation efficiency assays, pCB980, pCB981, pCB982, pCB983, pCB984, pCB985, pCB1054 and pCB1056 were used as donor DNAs (**Table 9**, see section 3.2.3). A fraction of the *rpoB* gene present in these plasmids could be integrated by homologous recombination into the *B. subtilis* chromosome depending on the percentage of divergence shared with the original *rpoB* gene. The strains used were Δ*rok*, Δ*rok* Δ*recD2*, *wt* and Δ*recD2*. In these experiments, Δ*rok* was used as the *wt* and it contained the deletion of the *rok* gene in order to increase the proportion of cells that became competent (Carrasco *et al*., 2016). The experiments were carried out similarly to plasmid transformation. However, the amount of both competent cells and donor DNA were higher as the percentage of divergence present in these plasmids increased, in order to obtain countable number of CFUs. Cells were plated on LB-agar plates with Rif 8 μg/ml to select transformants. Cells without the addition of DNA were used as negative control to evaluate the number of spontaneous mutants. Transformation efficiencies were calculated as in plasmid transformation, considering the efficiency of the Δ*rok* strain as the 100%.

3.2.8. Analysis of the integration lengths in chromosomal transformation

Once chromosomal transformation efficiency assays were performed, the next step was to sequence the region of the *rpoB* gene into the chromosomes of the transformants, in order to map the integrated fragment lengths and the recombination end-points. Colony PCRs were carried out with the NZYlong DNA polymerase to amplify the *rpoB* region. The amplifications were checked in 0.8% (w/v) agarose gels and PCR products were purified by Speedtools PCR-Clean up kit and sequenced. The resultant sequences were aligned with the donor and the recipient *rpoB* sequences. The presence or the absence of mismatches between the donor and the recipient DNAs was used to determine the integration length (Serrano and Carrasco, 2019).

3.2.9. Viral transfection

The ability of a *B. subtilis* cell to reconstitute an infective bacteriophage particle was analysed by viral transfection assays (Rottländer and Trautner, 1970). This method is similar to transformation, but the donor DNA used was the complete SPP1 genome (~44 kb), isolated from viral particles by phenol-chloroform extraction. Viral transfection experiments were performed with the *wt*, Δ*recD2* and Δ*recD2* Δ*radA/sms* strains. 1 ml of thawed competent cells was grown in 10 ml of GM2 for 1.5 h at 37ºC and agitation. Later, 1 ml of the culture was treated with 100 ng of purified SPP1 DNA. The mixture was incubated for 1 h at 37ºC and agitation. Concurrently, a *wt* culture was grown in LB supplemented with 15 mM $MgCl_2$ at 37ºC with agitation until OD_{560} = 0.4. 100 μl of this culture were plated on LB-agar with 15 mM $MgCl_2$ plates to obtain a 'seed'

to detect the PFUs. Then, proper dilutions of the transfected cells were plated on the seeded plates. The plates were incubated overnight at 37ºC and the number of PFUs was counted. The transfection efficiencies were calculated by comparison of the number of PFUs/ml obtained for each transfected strain to those for the *wt*, and considering the efficiency of the *wt* strain as the 100%.

3.2.10. Viability assays

The *recD2*$_{his6}$ strain was used to test the functionality of the RecD2 protein fused to 6xHis-tag *in vivo*. *B. subtilis wt*, Δ*recD2* and *recD2*$_{his6}$ strains were plated on LB-agar plates with the properly antibiotic and incubated overnight at 37ºC. A CFU was grown in LB at 37ºC until OD_{560} = 0.5 and then, appropriate dilutions were spotted on LB-agar plates containing 1.5 mM MMS. The plates were incubated overnight at 37ºC and photographed.

3.2.11. Quantification of RecD2 molecules by Western blot

The amount of RecD2 molecules in the cell was quantified using the *recD2*$_{his6}$ strain, which expresses *B. subtilis* RecD2 fused to 6xHis from its natural promoter. This strain was plated on a LB-agar plate with Cm 5 µg/ml and incubated overnight at 37ºC. A CFU was grown overnight in LB with the antibiotic at 30ºC under agitation. Later, the culture was diluted in fresh LB with antibiotic (250 ml) and grown at 37ºC until OD_{560} = 0.7. Then, cells were harvested by centrifugation at 9,000 rpm for 15 min. The collected cells (0.2 g wet weight) were resuspended in 1 ml of buffer containing 50 mM Tris-HCl pH 7.5, 1 mM DTT, 500 mM NaCl and 10% (v/v) glycerol. Lysozyme was added at 0.2 mg/ml and the mixture was incubated for 1 h at 4ºC under agitation. Later, cells were sonicated five times with pulses of 15 s ON and 45 s OFF and power of 35 with the B Braun LabSonic U sonicator. Cells were centrifuged at 12,000 rpm for 30 min and 4ºC. The pellet was resuspended in the same volume of buffer and centrifuged at the same conditions. The resultant supernatant of both centrifugations was loaded onto a Ni-Sepharose previously equilibrated with the buffer. RecD2-His was eluted with two elutions of 100 µl of the buffer supplemented with 200 mM imidazole. 30 µl of each fraction were loaded in a 12.5% SDS-polyacrilamide gel (PAGE). Increasing amounts of purified RecD2-His (6 to 50 ng) were loaded in the same gel to obtain a standard curve of protein concentration.

Once the gel ran, Western blot was performed as follows. First, the gel was transferred to a pre-wetted PVDF 0.45 µm membrane using the TE 22 Mighty Small Tank Transfer Unit (Amersham Biosciences) for 1 h 40 min. The membrane was subsequently blocked overnight at 4ºC with blocking solution containing 1 X phosphate-buffered saline (PBS) and 5% (w/v) skim milk powder. After washing the membrane with washing solution (1 X PBS, 0.5% (w/v) skim milk powder and 0.1% (v/v) Triton X-100), the primary antibody anti-His (dilution 1:10,000) was

added to the membrane to detect RecD2-His. The membrane was then incubated for 1 h at 4ºC. Later, the membrane was washed and then incubated with the secondary antibody anti-mouse IgG conjugated with peroxidase for 1 h at room temperature. RecD2-His was visualised staining the membrane with the Clarity™ Western ECL Substrate kit (Bio-Rad). The images were obtained with the ChemiDoc Imaging System (Bio-Rad). The intensity of the bands was quantified with the Image Lab software (Bio-Rad) and compared to that of the standard curve to obtain the amount of RecD2-His present in each sample. The number of RecD2 molecules was calculated dividing the resultant amount of RecD2-His by the molecular mass (89 kDa) and multiplying the result with the Avogadro number (6,022 x 10^{23} mol^{-1}).

The number of *recD2*$_{his6}$ cells at OD_{560}=0.7 was obtained plating several dilutions of the culture on LB-agar plates. The number of CFUs per ml was counted and multiplied with the total volume of the culture (250 ml). Finally, the number of RecD2-His molecules was divided by the number of cells to calculate the amount of RecD2 molecules per cell.

3.2.12. Protein overexpression and purification

3.2.12.1. RecD2 and RecD2 K373A

For RecD2 protein overexpression, *E. coli* BL21 (DE3) [pLysS] cells were transformed with the overexpression plasmid pET3b-*recD2*-His. A CFU was selected from the plate and was grown in LB supplemented with Amp 100 µg/ml and Cm 15 µg/ml overnight at 30ºC and agitation. The culture was then diluted in fresh LB with the antibiotics to OD_{600} = 0.07 and grown at 30ºC with agitation. Once the OD_{600} reached 0.2, the culture was incubated at 18ºC and agitation. The overexpression of RecD2 was induced by the addition of 0.25 mM IPTG at OD_{600} = 0.4. Then, the culture was incubated overnight. Cells were collected by centrifugation at 9,000 rpm for 15 min at 4ºC. The overexpression yield was generally 3.5 g (wet weight) of cell mass per liter of culture. RecD2 K373A was overexpressed from *E. coli* BL21 (DE3) [pLysS] carrying the pET3b-*recD2* K373A-His plasmid and following the same protocol.

For RecD2 purification, the cell mass was resuspended in buffer with 50 mM Tris–HCl pH 7.5, 1 M NaCl, 1 mM DTT and 10% (v/v) glycerol, supplemented with 5 mM imidazole (five volumes of buffer per gram of cells). Cell lysis was performed sonicating four times for 40 s with pulses ON and OFF of 1 s and 25% amplitude with the Q500 Sonicator (Qsonica). Cells were then centrifuged at 18,000 rpm for 45 min and 4ºC. The pellet was resuspended in the same volume of buffer and centrifuged at the same conditions. The resultant supernatant of both centrifugations was loaded onto a Ni-Sepharose column equilibrated with the same buffer. Protein was eluted using a gradient of increasing concentrations of imidazole (5 to 100 mM) and analysed by 12.5% SDS-PAGE and Coomassie blue staining. Fractions containing RecD2 were precipitated with the addition of 70% ammonium sulphate for 30 min. The protein pellet was

recovered by centrifugation at 18,000 rpm for 30 min and 4ºC, and resuspended in buffer 50 mM Tris–HCl pH 7.5, 1 M NaCl, 1 mM DTT, 10% (v/v) glycerol, 1 mM EDTA and 10 mM sodium phosphate buffer pH 7.5. Then, it was loaded onto a hydroxyapatite column. Protein elution was carried out with a gradient of increasing concentrations of sodium phosphate (10 to 100 mM). Purified RecD2-His (89 kDa) was aliquoted and stored at -80ºC. RecD2 K373A-His was purified following the same protocol. Purified proteins were validated by MALDI-TOF spectrometry (Proteomics Facility, CNB). The concentration of RecD2 and RecD2 K373A was expressed as monomers.

3.2.12.2. Replisome proteins of B. subtilis

The purified proteins to reconstitute the *B. subtilis* replisome PriA (94.5 kDa), PolC (166 kDa), HolA (δ, 42.1 kDa), HolB (δ', 40.5 kDa), DnaX (τ, 62,7 kDa), DnaN (β, 42.1 kDa), DnaC (50 kDa), DnaG (68.8 kDa), DnaE (125 kDa), DnaB (54.9 kDa), DnaD (28.8 kDa) and SsbA (18.8 kDa) were kindly provided by the Dr. Charles S. McHenry's laboratory from the University of Colorado (USA). PriA, PolC, HolA, HolB, DnaG and DnaE were used as monomers; DnaN as a dimer; DnaX, DnaB, DnaD and SsbA as tetramers; and DnaC as a hexamer.

DnaI was purified as previously described in Sanders *et al.*, 2010. *E. coli* AP1.L1 cells bearing pA1-BS-*dnaI-dnaC* overexpression plasmid were grown in F medium supplemented with Amp 100 µg/ml at 37ºC until OD_{600} = 1. Protein overexpression was induced by the addition of 1 mM IPTG for 2 h at 37ºC and agitation. Cells were harvested by centrifugation at 9,000 rpm for 15 min at 4ºC. The overexpression yield was around 6.5 g (wet weight) of cell mass per liter of culture. The cell mass was resuspended in buffer 50 mM Tris-HCl pH 8, 100 mM NaCl, 1 mM EDTA, 6 mM DTT, 10 % (v/v) sucrose and 20 mM spermidine trihydrochloride. Cell lysis was performed by the addition of 0.2 mg/ml lysozyme. The mixture was first incubated for 1 h at 4ºC and then 4 min at 37ºC. Cells were centrifuged at 18,000 rpm for 1 h and 4ºC. The supernatant was treated with 32.5% ammonium sulphate for 30 min and then centrifuged at 18,000 rpm for 30 min and 4ºC. The pellet was washed two times with 20% ammonium sulphate solution (20 g ammonium sulphate in 100 ml of buffer 50 mM Tris-HCl pH 7.5, 20% (v/v) glycerol, 1 mM EDTA, 100 mM NaCl and 5 mM DTT) for 30 min at 4ºC and agitation. After the centrifugation at 18,000 rpm for 30 min at 4ºC, the pellet was resuspended in buffer 50 mM Tris-HCl pH 7.5, 20% (v/v) glycerol, 1 mM EDTA, 100 mM NaCl and 5 mM DTT and loaded onto a Q-sepharose, previously equilibrated with the same buffer. Protein elution was carried out by increasing concentrations of NaCl (75 to 400 mM). DnaC was eluted at 350 mM NaCl and DnaI at 100 mM NaCl. The fractions containing DnaI were loaded onto a hydroxyapatite. DnaI eluted at 20 mM sodium phosphate buffer pH 7.5, and was then loaded onto a new Q-sepharose to concentrate the

protein. Fractions containing DnaI (36.1 kDa) were aliquoted and stored at -80ºC. The concentration of DnaI was expressed as a hexamer.

3.2.12.3. Recombination proteins of B. subtilis

The recombinase RecA (38 kDa) and RecO (29.3 kDa) proteins were purified as previously described in Manfredi *et al*., 2008 by Dr. Begoña Carrasco from the Dr. Juan Carlos Alonso laboratory (CNB). RecA was expressed as a monomer and RecO as a dimer.

3.2.13. ATP hydrolysis assay

The ATP hydrolysis activities of RecD2 and RecD2 K373A were measured by ATP/NADH-coupled spectrophotometric assays using the Shimadzu CPS-20A dual-beam spectrophotometer equipped with a temperature controller. The ATPase activity was coupled to an ATP regeneration reaction in which phosphoenolpyruvate is converted to pyruvate by the pyruvate kinase enzyme. This reaction produces ATP as a product that is subsequently transformed to ADP by a protein with ATPase activity. Pyruvate is then converted to lactate by the lactate dehydrogenase enzyme in a process that consumes NADH. The consumption of NADH is monitored measuring the absorbance at 340 nm (A_{340}) along the time and it is inversely proportional to the accumulation of ADP.

Reactions (final volume of 60 µl) were performed in a buffer containing 50 mM Tris-HCl pH 7.5, 1 mM DTT, 50 µg/ml BSA, 50 mM NaCl, 5% (v/v) glycerol, 0.5 mM phosphoenolpyruvate, 0.3 mM NADH, 10 U/ml pyruvate kinase and 10 U/ml lactate dehydrogenase. Variable concentrations of $MgCl_2$ were assayed. The DNA substrates in the reaction (i.e. polydTs or pGEM-3Zf (+)) were used at 3 µM in nucleotide as final concentration. RecD2 or RecD2 K373A (5 nM) was added and the reactions were incubated for 5 min at 37ºC. Then, 0.2 mM ATP was added and the A_{340} was monitored at 37ºC for 5-10 min. ATPase activity of RecD2 was also performed in the presence of increasing concentrations of SsbA or SsbB, preincubating the proteins 5 min at 37ºC prior to ATP addition.

The data of the A_{340} were converted to ADP concentration that accumulated, following this equation: $(0- A_{340})/ (\varepsilon \times L)$, where ε is the extinction coefficient for NADH (6,220 $M^{-1}cm^{-1}$) and L is the path length (1 cm). The catalytic constants (k_{cat}) were calculated measuring the slopes.

3.2.14. DNA radiolabeling

Oligonucleotides were phosphorylated at 5' end with radiolabeled [γ-^{32}P]-ATP by the T4 polynucleotide kinase enzyme. In the reaction, 5 pmol of the oligonucleotide were incubated with 5 pmol of [γ-^{32}P]-ATP (3.3 pmol/ µl), 1 X T4 polynucleotide kinase buffer and 10 U of T4 polynucleotide kinase enzyme. The reactions were incubated at 30ºC for 30 min and then

at 65ºC for 20 min to inactivate the enzyme. To remove non-incorporated [γ-^{32}P]-ATP, the samples were filtered loading onto Sephadex G-50 mini-columns. The quantification of radiolabeled DNA (cpm/µl) was performed by liquid scintillation counting (Tri-Carb 4910 TR, Perkin Elmer).

As DNA marker of DNA replication products, the λ-DNA-HindIII Digest was radiolabeled with the DNA polymerase I large Klenow as follows. 500 ng of the λ-DNA-HindIII were incubated with a dNTPs mix containing dTTP, dATP and dGTP at 0.08 mM each as final concentration. Then, 10 pmol of [α-^{32}P]-dCTP (3.3 pmol/ µl) were added and the reaction was incubated for 30 min at 30ºC and for 20 min at 65ºC. Afterwards, non-incorporated [α-^{32}P]-dCTP were removed by Sephadex G-50 filtration and the radiolabeling was quantified by liquid scintillation counting.

3.2.15. Annealing and purification of radiolabeled DNA structures

The annealing of radiolabeled DNA substrates was carried out with the aim to construct different DNA structures, such as forks, HJ or D-loops. 0.5 pmol of a radiolabeled oligonucleotide were incubated with 1 pmol of non-radiolabeled complementary oligonucleotides in the presence of 100 mM sodium phosphate buffer pH 7.5. The mixture was incubated for 10 min at 100ºC in a thermoblock. Next, the thermoblock was turned off and the reaction was then allowed to cool overnight to facilitate the annealing of complementary oligonucleotides. The annealed DNA structures were confirmed running native 10% PAGE gels in 0.5 X TBE buffer at 200 V. The gels were exposed to phosphor imager screens and then analysed using the Personal Molecular Imager and the Image Lab software (Bio-Rad). The DNA structures used in this work are listed in **Table 6** (see section 3.1.4).

Sometimes the annealing was not complete and there were some free radiolabeled DNA in the mixture. In these cases, the structures were purified as follows. The total volume of the annealing reaction was run in a 10% PAGE gel in 0.5 X TBE buffer at 200 V to separate the annealed structure from the free DNA. The gel was autoradiographed to detect the position of the desired DNA structure. Then, the band was cut and incubated overnight with a buffer containing 0.5 M ammonium acetate, 1 mM EDTA and 0.1% (v/v) SDS. Later, the mixture was centrifuged and filtered to remove rest of the gel and the DNA structure was extracted by ethanol precipitation.

3.2.16. DNA helicase assay

DNA helicase assays were performed to test the DNA unwinding activity of RecD2 and RecD2 K373A. Increasing concentrations of each helicase were incubated for 10 min at 37ºC in a reaction containing 0.25 nM of radiolabeled DNA, 50 mM Tris-HCl pH 7.5, 50 mM NaCl, 1 mM DTT, 0.05 mg/ml BSA, 2 mM ATP, 2 or 10 mM $MgCl_2$ and 5% (v/v) glycerol. Reactions

were stopped with the addition of stop buffer with 20 mM EDTA pH 8 and 0.5% (v/v) SDS as final concentrations and the incubation for 15 min at 37ºC. In experiments in which SsbA and/or RecA were added in the reaction, the stop buffer contained also 0.5 mg/ml proteinase K for the properly deproteinization. The samples were run in 10-15% PAGE gels in 0.5 X TBE buffer at 200 V. Later, gels were exposed to phosphor imager screens and then analysed using the Personal Molecular Imager and the Image Lab software (Bio-Rad).

If pGEM-3Zf (+) ssDNA annealed with the Hind24 oligonucleotide was used as DNA substrate in helicase assays, the reactions were run in 1.2% (w/v) agarose gels in 1 X TAE buffer at 100 V. After electrophoresis, gels were treated with 7% (w/v) trichloroacetic acid for 30 min under agitation and dried. Later, gels were analysed similarly as described for the PAGE gels.

3.2.17. Electrophoretic mobility shift assay (EMSA)

The property of a protein to bind DNA was tested by EMSA. In these assays, increasing concentrations of RecD2 or RecD2 K373A were incubated for 15 min at 37ºC in a reaction buffer containing 0.25 nM of radiolabeled DNA, 50 mM Tris-HCl pH 7.5, 50 mM NaCl, 1 mM DTT, 0.05 mg/ml BSA, 2 or 10 mM $MgCl_2$ and 5% (v/v) glycerol. Instead of ATP, ATPγS (2 mM) was used, which is a non-hydrolysable ATP analogue, to study the dependence of ATP binding for the protein-DNA interactions. Glutaraldehyde was subsequently added (0.05% (v/v) as final concentration) to fix protein-DNA complexes. Reactions were incubated for 15 min at 37ºC and then were run in 8% PAGE in 0.5 X TBE buffer at 200 V. Gels were dried for 2 h at 80ºC using the Gel-dryer Model 583 (Bio-Rad) and exposed to phosphor imager screens. Gels were analysed using the Personal Molecular Imager (Bio-Rad). The apparent binding constant, k_{app}, was calculated as the concentration of the protein needed to obtain the 50% of DNA bound. The intensity of each band was quantified with the Image Lab software (Bio-Rad).

3.2.18. Protein-protein interaction by immuno dot-blot

Protein-protein interaction *in vitro* was studied by immuno dot-blot, as previously described (Walsh *et al*., 2012), using the Bio-Dot apparatus (Bio-Rad) connected to vacuum. This method allows to directly visualise the interaction between two proteins with antibodies. First, a pre-wetted nitrocellulose membrane with 1 X PBS was placed in the Bio-Dot apparatus. Increasing amounts of a protein (i.e. SsbA, RecA, RarA) were applied to the membrane. BSA was also applied as negative control of interaction. The membrane was then incubated overnight at 4ºC with blocking solution (1 X PBS and 5% (w/v) skim milk powder). Later, the membrane was incubated for 6 h at 4ºC with RecD2-His (200-300 ng/ml) in binding solution (1 X PBS, 0.5% (w/v) skim milk powder and 0.1% (v/v) Triton X-100). After three washes with binding solution, primary antibody anti-6xHis (1:6,000) was added to detect the RecD2-His retained in the

membrane because of interaction and the membrane was incubated overnight at 4ºC. The membrane was then washed three times with binding solution. The secondary antibody anti-IgG conjugated with peroxidase (1:5,000) was added and the membrane was incubated for 1 h at room temperature. The blots were visualised staining with the Clarity™ Western ECL Substrate kit (Bio-Rad). The images were obtained with the ChemiDoc Imaging System (Bio-Rad).

3.2.19. DNA replication assay

DNA replication assays were carried out using a PriA-rolling circle DNA replication system, as previously described (Sanders *et al*., 2010). The minicircular RC plasmid was used as template of the reaction. Due to the strong dG-dC strand bias (50:1) present in the DNA template, leading and lagging strand synthesis can be analysed separately, because radiolabeled [α-^{32}P]-dCTP is incorporated mostly into the leading strand, whereas [α-^{32}P]-dGTP is incorporated into the lagging strand.

First, an enzyme mix was done in 1 X BsRc buffer (40 mM Tris-acetate pH 7.8, 12 mM MgOAc, 200 mM potassium glutamate, 3 μM $ZnSO_4$, 1% (w/v) PEG 8000, 0.02% (v/v) Pluronic F68 and 1 mM DTT) containing the proteins needed to reconstitute the replisome of *B. subtilis in vitro*, except SsbA (20 nM PriA, 20 nM PolC, 25 nM HolA (δ), 25 nM HolB (δ'), 25 nM $DnaX_4$(τ), 25 nM $DnaN_2$ (β), 25 nM $DnaI_6$, 30 nM $DnaC_6$, 30 nM DnaG, 15 nM DnaE, 50 nM $DnaB_4$ and 50 nM $DnaD_4$). The replisome was preassembled incubating the enzyme mix for 5 min at 37ºC with a substrate mix containing 5 nM minicircular DNA template, 5 μM ATPγS and 100 μM rNTPs (CTP, GTP and UTP) in 1 X BsRc buffer. The substrate mix contained also 90 nM $SsbA_4$, 500 nM RecA, 50 nM $RecO_2$ and/or increasing amounts of RecD2 (5-40 nM). Then, the reactions were initiated by the addition of 1 mM ATP, 24 μM dNTPs and 0.02 μM [α-^{32}P]-dCTP or [α-^{32}P]-dGTP at 37ºC. The reactions were stopped at certain times by the addition of an equal volume of stop buffer (20 mM Tris-HCl pH 8, 0.2% (v/v) SDS, 50 mM EDTA pH 8 and 0.5 mg/ ml proteinase K as final concentrations) and the incubation for 20 min at 37ºC. Unincorporated dNTPs were removed loading the samples onto Sephadex G-50 mini-columns. DNA quantification synthesis was carried out by liquid scintillation counting (Tri-Carb 4910 TR, Perkin Elmer). Later, the samples were run in alkaline 0.8% (w/v) agarose gels (30 mM NaOH and 2 mM EDTA pH 8) mixing aliquots with loading dye buffer (30 mM NaOH, 2 mM EDTA pH 8, 5% (v/v) glycerol and 0.1% (v/v) bromophenol blue). Gels were fixed with 7% (w/v) trichloroacetic acid for 30 min and subsequently dried. To visualise the replication products, gels were exposed to phosphor imager screens and analysed with the Personal Molecular Imager (Bio-Rad).

3.2.20. Biotin-streptavidin displacement

To test the ability of RecD2 to displace a protein block from the ssDNA, biotin-streptavidin displacement assays were performed, as previously described (Bruning *et al*., 2016). 0.5 nM of radiolabeled oligo BioT-45, biotinylated at 3' end, was incubated with 2.5 nM streptavidin for 5 min at room temperature in a reaction buffer containing 50 mM Tris-HCl pH 7.5, 2 mM $MgCl_2$, 2 mM DTT, 50 mM NaCl, 0.05 mg/ml BSA and 2 mM ATP. An equal volume of a solution containing increasing concentrations of RecD2 and 50 nM biotin as a trap for the displaced streptavidin was added. The reactions were then incubated for 20 min at 37ºC and stopped with stop buffer (25 mM EDTA pH 8 and 0.5% (v/v) SDS as final concentrations) for 10 min at 37ºC. The samples were separated on 10% PAGE in 1 X TBE at 200 V. Gels were exposed to phosphor imager screens and analysed using the Personal Molecular Imager and the Image Lab software (Bio-Rad).

3.2.21. DNA strand exchange assays

DNA strand exchange reactions in the presence of RecD2 and RecD2 K373A were performed as described in Carrasco *et al*., 2015. The circular pGEM-3Zf (+) dsDNA (3,197 bp) was first linearised by the KpnI digestion for 2 h at 37ºC. Then, KpnI-linearised pGEM-3Zf (+) dsDNA (20 µM in nt, 3 nM in molecules) and its homologous circular pGEM-3Zf (+) ssDNA (10 µM in nt, 3 nM in molecules) were mixed in a reaction buffer (50 mM Tris–HCl pH 7.5, 10 mM $MgCl_2$, 50 mM NaCl, 1 mM DTT, 0.05 mg/ml BSA and 5% (v/v) glycerol) in the presence of RecA (1.5 µM), $RecO_2$ (200 nM) and $SsbA_4$ (300 nM). An ATP regeneration system was included in the reaction (8 mM creatine phosphate and 8 U/ml creatine kinase). Increasing concentrations of RecD2 or RecD2 K373A were added into the reaction at time 0 (before starting the reaction). The reactions were initiated adding 2 mM ATP and incubated 20 or 40 min at 37ºC. In other reactions, ATP was added to initiate strand exchange and after 20 min, RecD2 was added. Later, the samples were deproteinised with stop buffer (25 mM EDTA pH 8, 0.5% (v/v) SDS and 0.5 mg/ml proteinase K as final concentrations) for 20 min at 37ºC. DNA species were separated by 0.8% (w/v) agarose gel electrophoresis in 1 X TBE. Gels were stained with ethidium bromide and analysed using a GelDoc system (Bio-Rad). Densitometry analysis was performed with the Image Lab software (Bio-Rad) to quantify the percentage of the three-stranded recombination intermediates (joint molecules, *jm*) and the final exchanged products (nicked circular dsDNA, *nc*).

3.2.22. Single-molecule fluorescence microscopy

The *in vivo* dynamics of RecD2 at single-molecule level was assayed by single-molecule microscopy. These experiments were performed during the stay of three months at the Dr. Peter

Graumann's laboratory (Chemistry Department, University of Marburg, Germany), which is specialist in the study of diverse bacterial proteins with this method.

The *dnaX-cfp recD2-mVenus* strain was used to study the distance between the replisome and RecD2 using single-molecule fluorescence microscopy. This strain was plated overnight at 37ºC on a LB-agar plate with Cm 5 µg/ml. A CFU was selected from the plate and grown in LB supplemented with 0.2% (v/v) xylose at 30ºC under agitation until reach OD_{560} = 0.5. Then, replicative stress was induced by the treatment with 0.5 mM H_2O_2, 50 or 100 ng/ml MMC or 50 µg/ml HPUra for 1 h at 30ºC or 5 mg/ml serine hydroxamate (SHX) for 15 min at 30ºC. Later, 1 ml of the culture was collected by centrifugation for 3 min at 3,000 rpm. The cell pellet was resuspended in 500 µl of fresh LB to remove rest of the drug and 3 µl were deposited on a circular coverslip (5 mm, Menzel), previously sonicated for 30 min in 2 X Hellmanex and 30 min in H_2O Milli-Q. Then, a smaller circular coverslip (2.5 mm, Menzel), with 1% (w/v) agarose pad prepared in S750 minimal medium, was placed over the 3 µl of cells. The cells were visualised using the Olympus IX71 microscope with immersion oil, 100 X objective and 1.45 numerical aperture. First, a bright-field image was taken to obtain the cell shape. The DnaX-CFP foci were detected by excitation with a 418 nm laser and then, the dynamic of RecD2-mVenus was tracked by excitation with a 514 nm laser. A total of 2,500 images were acquired with an exposure time of 30 ms.

Time-lapse images were first processed with Image J software (National Institutes of Health, Bethesda, MD) to select the region in which the fluorescent intensity reaches a plateau (single-molecule level). The cell shape was selected with Oufti software (Jacobs-Wagner laboratory, Stanford University) using the bright-field images. The tracks of the RecD2-mVenus molecules were acquired with U-track (laboratory for Computational Cell Biology, Harvard Medical School), run in MATLAB. Finally, the collected data were globally analysed with the SMTracker software, developed by the Dr. Peter Graumann's laboratory (Rösch *et al*., 2018). This software allowed the visualisation of each RecD2-mVenus track and its subcellular localization. Moreover, SMTracker performed the statistical analysis of the data, following the Gaussian mixture model and calculating the apparent diffusion coefficient for each treatment (*D*), which represents the velocity of the RecD2-mVenus molecules. The distance between each track of RecD2-mVenus to the DnaX-CFP foci was also calculated for each treatment with SMTracker.

On the other hand, the thermosensitive strains *dnaD23 recD2-mVenus* and *dnaB37 recD2-mVenus* were used to study the dynamic of RecD2-mVenus when the replisome proteins DnaD or DnaB are inactive. Each strain was plated on LB-agar plates with Cm 5 µg/ml and grown overnight at 30ºC (permissive temperature). A CFU for each strain was grown in LB at 30ºC until OD_{560} = 0.5. Then, the culture was separated in two, and one was incubated for 1 h at 30ºC and

the other to 42ºC (non-permissive temperature) under agitation. Cells were prepared as described above and visualised by excitation with 514 nm laser for the RecD2-mVenus tracking. A temperature controller coupled to the microscope was also used to keep a constant temperature of 30 or 42ºC. A total of 2,500 images were taken with an exposure time of 30 ms and were processed with the softwares, as described above.

Results

4. Results

4.1. Chapter 1: Analysis of *B. subtilis* RecD2 in natural transformation

4.1.1. The absence of RecD2 slightly reduces chromosomal and plasmid transformation

During natural transformation in *B. subtilis*, the exogenous DNA is incorporated inside the cell by the uptake apparatus, which only internalises one DNA strand. This ssDNA is internalised independently of the sequence or the polarity (Kidane *et al*., 2012). Ssb proteins rapidly cover the incoming ssDNA and RecA mediators facilitate the loading of RecA into the ssDNA. In this context, HR proteins are needed for the genetic recombination between the incorporated ssDNA and the chromosome if both DNA sequences share enough homology (chromosomal transformation). Recombination activity is also needed to process the internalised ssDNA when it has not sufficient homology to the bacterial chromosome (plasmid transformation) (Kidane *et al*., 2012; Serrano *et al.,* 2018) (see section 1.2., Introduction).

Particularly, the contribution of *B. subtilis* RecD2 in natural transformation had not been explored. Previous authors observed that the chromosomal transformation efficiency of the *D. radiodurans recD2::kan* mutant was greater than the efficiency of the wild-type LS18 strain. Depending on the transformation method used, the efficiency of the *recD2::kan* mutant was 3 to 7-fold or even 30 to 100-fold higher than the wild-type (Servinsky and Julin, 2007).

To gain insight into the contribution of *B. subtilis* RecD2 in natural transformation, chromosomal and plasmid transformation assays were carried out in the Δ*recD2* strain using different donor DNAs. The *B. subtilis* wild-type BG214 (*rec*$^{+}$, *wt*) was also tested to compare the transformation efficiencies between both strains. Chromosomal transformation was performed with the pCB980 DNA, which harbours the house-keeping *rpoB* gene (2,997 bp) from the *B. subtilis* 168 *wt* strain with a single point mutation C482T (named as *rpoB*482 variant) that confers Rif^{R}. The Rif^{R} mutation was located approximately at the centre of the donor DNA (position 1,444 bp of the *rpoB* gene). For plasmid transformation, an oligomeric plasmid is required to reconstitute a circular plasmid inside the bacterial cell by intramolecular recombination. In fact, the transformation efficiency with an oligomeric plasmid is 1,000-fold higher than using a monomeric plasmid (Canosi *et al*., 1978; Serrano *et al*., 2018). For testing plasmid transformation, the pUB110 plasmid (4.5 kb) was digested with EcoRI and then self-ligated for the formation of concatemers. This plasmid was used as donor DNA, which confers Nm^{R}.

The results showed that Δ*recD2* competent cells had a reduced plasmid transformation efficiency respect to *wt* competent cells (~4.5-fold), whereas chromosomal transformation efficiency was only marginally affected (~2.6-fold) (**Table 10**). The data suggest that the

contribution of RecD2 to plasmid and chromosomal transformation is not crucial because these processes were not greatly impaired in the absence of this helicase (Serrano *et al*., 2020)

Table 10. Efficiencies of chromosomal and plasmid transformation in Δ*recD2*.

Strain	Relevant genotype	Chromosomal transformation efficiency (%)	Plasmid transformation efficiency (%)
BG214	*rec*$^+$ (*wt*)	100 (2.1×10^3)	100 (4.2×10^2)
BG1455	+ Δ*recD2*	38 ± 7.8	22 ± 5

Competent *B. subtilis* cells (1 ml) were transformed with 0.1 µg of the *rpoB*482 DNA or self-ligated pUB110 plasmid. The yield of chromosomal (Rif^R/ml) and plasmid (Nm^R/ml) transformation was normalised relative to that of the *rec*$^+$ strain, recorded as 100%. In parenthesis are represented the number of transformants per ml of competent cells. The results are shown as mean ± SEM of at least six independent experiments.

4.1.2. Chromosomal and plasmid transformation efficiencies in the absence of RecD2 and RadA/Sms

RecD2 has been postulated as a branch migration translocase during the postsynaptic step of HR, as RecG or RuvAB, because the double mutant Δ*recD2* Δ*recG* and Δ*recD2* Δ*ruvAB* strains are not viable in *B. subtilis* (Torres *et al*., 2017). Another helicase present in *B. subtilis* that facilitates branch migration is RadA/Sms. The Δ*radA/sms* strain is greatly impaired in chromosomal transformation respect to the *wt* (~140-fold), whereas it is not significantly affected in plasmid transformation (~1.6-fold) (**Table 11**) (Torres *et al*., 2019b).

Table 11. Efficiencies of chromosomal and plasmid transformation in Δ*recD2* Δ*radA/sms*.

Strain	Relevant genotype	Chromosomal transformation efficiency (%)	Plasmid transformation efficiency (%)
BG214	*rec*$^+$ (*wt*)	100 (2.1×10^3)	100 (4.2×10^2)
BG1455	+ Δ*recD2*	38 ± 7.8	22 ± 5
BG1245	+ Δ*radA/sms*	0.7 ± 0.2	66 ± 4.8
BG1635	+ Δ*recD2* Δ*radA/sms*	0.4 ± 0.2	4.5 ± 1.5

Competent *B. subtilis* cells (1 ml) were transformed with 0.1 µg of the *rpoB*482 DNA or self-ligated pUB110. The yield of chromosomal (Rif^R/ml) and plasmid (Nm^R/ml) transformation was normalised relative to that of the *rec*$^+$ strain, recorded as 100%. In parenthesis are represented the number of transformants per ml of competent cells. The results are shown as mean ± SEM of at least six independent experiments.

To analyse the putative contribution of RecD2 as a branch migration translocase, chromosomal and plasmid transformation were assayed in the double mutant Δ*recD2* Δ*radA/sms* strain. The simultaneous deletion of both genes *recD2* and *radA/sms* was viable. The results showed that the Δ*recD2* Δ*radA/sms* strain had a defect in chromosomal transformation, with a similar efficiency than the obtained in the absence of RadA/Sms alone, with just a marginal decrease (~1.75-fold reduction respect to the Δ*radA/sms* efficiency) (**Table 11**). This result supported that RadA/Sms is crucial for chromosomal transformation, whereas RecD2 may not have a substantial role in this process. On the other hand, a synergistic effect between RecD2 and

RadA/Sms was observed in plasmid transformation, because the transformation efficiency was highly reduced in the absence of both helicases (~22-fold) (Serrano *et al*., 2020).

4.1.3. Interspecies chromosomal transformation requires RecD2 in a Δrok background

B. subtilis, as other naturally competent bacteria, can integrate fully homologous DNA sequences (intraspecies chromosomal transformation) or partially homologous sequences with less efficiency (interspecies chromosomal transformation) during natural transformation (Fraser *et al*., 2007). The interspecies chromosomal transformation contributes to bacterial adaptation and evolution, as well as to the expansion of their pangenome by the integration of new genes flanked with homologous DNA sequences to the recipient chromosome (Kidane *et al*., 2012). In *B. subtilis*, the acquisition of divergent ssDNAs has been previously explored with the use of donor DNAs for transformation that contained the *rpoB*482 variant genes from different Bacilli with increasing degree of divergence respect to the *B. subtilis* 168 *rpoB* gene (**Table 9,** see section 3.2.3., Methods). The chromosomal transformation frequency of the *wt* strain decreases linearly as the sequence divergence increases (Carrasco *et al*., 2016). Beyond 8% sequence divergence, chromosomal transformation is highly reduced in the *wt* (Carrasco *et al*., 2016).

To increase the sensitivity of the system, the Δ*rok* mutant was used previously. Rok is a transcriptional factor that negatively regulates the expression of ComK, which is the master regulator of the state of competence. The deletion of *rok* increases the proportion of competent cells from 10% to 50% of the total number of cells (Maamar and Dubnau, 2005). Consistently, the chromosomal transformation frequency in *B. subtilis* is 20 to 50-fold higher in the Δ*rok* strain respect to the *wt*, and transformants are detectable with donor DNA of 20% sequence divergence (Carrasco *et al*., 2016). The Δ*rok* Δ*recD2* strain was constructed to test the chromosomal transformation efficiency in the absence of *recD2* in a Δ*rok* background.

Intraspecies chromosomal transformation was analysed in Δ*rok* Δ*recD2* competent cells and compared to Δ*rok* and *rec*$^+$ using the pCB980 (*B. subtilis* 168 *rpoB*482) as donor DNA, which only has a 0.034% sequence divergence. The results showed that the chromosomal transformation efficiency of the Δ*rok* Δ*recD2* cells was highly reduced compared to the Δ*rok*, *rec*$^+$ (~1,000-fold) (**Table 12**). This result was different from the observed for the Δ*recD2* strain in the *rok*$^+$ background, where chromosomal transformation was only ~2.6-fold decreased respect to the *wt* (see section 4.1.1). This unexpected behavior was also observed in some recombination mutants, like Δ*recJ,* Δ*recX,* Δ*dprA* and Δ*radA* (Serrano *et al*., 2021). For instance, the chromosomal transformation efficiency of Δ*rok* Δ*radA* was ~1,600-fold reduced in contrast to the ~140-fold reduction observed in Δ*radA, rok*$^+$ (see section 4.1.2). It has been postulated that Rok, which is a nucleoid-associated protein, plays a central role in the structural organization of the *B. subtilis* chromosome. Rok was found to mediate long-range chromosomal interactions leading to the

formation of anchored chromosomal loops (Dugar *et al*., 2022). The absence of *rok* could alter the nucleoid conformation and subsequently affect the action of some recombination mechanisms during chromosomal transformation (Serrano *et al*., 2021b).

Table 12. Efficiency of intraspecies chromosomal transformation in Δ*rok* Δ*recD2*.

Strain	Relevant genotype	Chromosomal transformation efficiency (%)
BG1359	Δ*rok, rec*$^+$	100 (3.3×10^4)
BG1549	+ Δ*recD2*	0.1 ± 0.05

Competent *B. subtilis* cells (1 ml) were transformed with 0.1 µg of the *rpoB*482 DNA. The yield of transformation (Rif^R/ml) was normalised relative to that of the Δ*rok*, *rec*$^+$ strain, recorded as 100%. In parenthesis are represented the number of transformants per ml of competent cells. The results are shown as mean ± SEM of at least six independent experiments.

The number of spontaneous Rif^R mutants that appeared in the absence of transforming DNA was remarkably higher in the absence of *recD2.* Whereas the spontaneous mutation frequencies in Δ*rok* and *rok*$^+$ (*wt*) competent cells were similar (~7 to 9 x 10^{-9}), in Δ*recD2* and Δ*rok* Δ*recD2* the spontaneous mutation frequency increased ~3-fold (~2 to 4 x 10^{-8}) (Serrano *et al*., 2021). This is consistent with previous data that described that the deletion of *recD2* in *B. subtilis* moderately increases the spontaneous mutation rate (~3.6-fold) respect to the *wt* (Walsh *et al*., 2014). These results suggest some contribution of RecD2 in DNA repair (maybe in MMR).

To elucidate the role of RecD2 during interspecies chromosomal transformation, Δ*rok* Δ*recD2* competent cells were transformed with different *rpoB* genes from natural origin, described in the **Table 9** (see section 3.2.3., Methods), harbouring the *rpoB*482 variant. These donor DNAs have increasing percentage of sequence divergence respect to the *wt rpoB* gene, and confer Rif^R resistance. The transformation frequency in Δ*rok*, *rec*$^+$ was normalised to give a value of 1 to the transformation rate obtained in the intraspecies chromosomal transformation (**Figure 9,** *black circles*). The transformation frequency in Δ*rok* Δ*recD2* was compared to that of the Δ*rok*, *rec*$^+$ competent cells (**Figure 9,** *white squares*). The results showed that chromosomal transformation frequency in the absence of *recD2* was greatly reduced as the sequence divergence increased. The frequency of spontaneous mutation was defined by the chromosomal transformation frequency in the absence of *recA*, which is essential in this process (**Figure 9,** *white triangles*). Furthermore, the transformation frequency in Δ*rok* Δ*recD2* cells was normalised to give a value of 1 to the transformation rate obtained in the intraspecies chromosomal transformation assay, as done in Δ*rok*, *rec*$^+$, to compare the decay in the transformation frequency depending on sequence divergence (**Figure 9,** *black squares*). The chromosomal transformation reached a plateau over 8% sequence divergence in Δ*rok* Δ*recD2*. These results suggest a crucial contribution of RecD2 during the interspecies chromosomal transformation (Serrano *et al*., 2021).

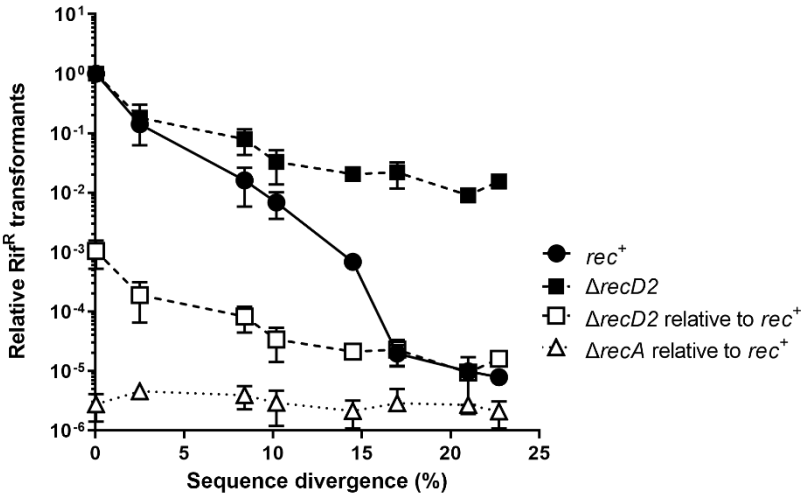

Figure 9. Chromosomal transformation frequencies as a function of increased sequence divergence in Δ*rok* Δ*recD2.*

Chromosomal transformation assays were performed using donor DNAs containing the *rpoB*482 variant, conferring Rif^R, with increasing percentage of sequence divergence respect to the *wt rpoB* gene: *B. subtilis* 168 (0.034% sequence divergence, homologous DNA), *B. subtilis* W23 (2.47%), *B. atrophaeus* 1942 (8.35%), *B. amyloliquefaciens* DSM7 (10.12%), *B. licheniformis* DSM13 (14.52%), *B. gobiensis* FJAT-4402 (17%), *B. thuringiensis* MC28 (20.83%) and *B. smithii* DSM4216 (22.74%). These DNAs were used to transform *B. subtilis* Δ*rok rec*$^+$, Δ*rok* Δ*recD2* and Δ*rok* Δ*recA* competent cells. The values are plotted relatives to *rec*$^+$, dividing the number of transformants/CFUs obtained in Δ*rok* Δ*recD2* (depicted here as Δ*recD2* relative to *rec*$^+$, *white squares*) and Δ*rok* Δ*recA* (depicted here as Δ*recA* relative to *rec*$^+$, *white triangles*) by the number of transformants/CFUs obtained in Δ*rok rec*$^+$, whose intraspecies transformation frequency was normalised to give a value of 1 (depicted here as *rec*$^+$, *black circles*). The intraspecies transformation frequency of Δ*rok* Δ*recD2* was also normalised to 1 (depicted here as Δ*recD2*, *black squares*). The transformation frequency of Δ*rok* Δ*recA* represents the frequency of spontaneous mutation. The results are plotted in log10 scale as the mean ± SD for at least three independent experiments.

4.1.4. RecD2 is needed for the integration of divergent sequences beyond ~15% during interspecies chromosomal transformation

For the integration of a sequence into a homologous or partially homologous (homeologous) chromosomal region, RecA needs a minimum efficient processing segment (MEPS) to initiate the DNA strand exchange. In *E. coli*, the length of the MEPS for RecA-mediated recombination is at least 40 nt (McIlwraith and West, 2001), whereas in *B. subtilis* is predicted to be between 25 to 30 nt (Majewski and Cohan, 1999). Furthermore, *in vitro*, a threshold of 9 nt of identity is required for a stable interaction and ~26 nt are needed for RecA to promote DNA strand exchange (Majewski and Cohan, 1999; Kidane *et al*., 2012). As the sequence divergence increases, the number of MEPS present in the donor DNA decreases, and this reduces the chromosomal transformation frequency and the integration length. Up to ~15% sequence divergence, homology-directed HR is involved in the integration. However, beyond this percentage of sequence divergence, homology-facilitated illegitimate recombination is predicted to occur, which can take place between non-allelic segments containing micro-homologous

regions and allows the integration of 3 to 10 nt (de Vries and Wackernagel, 2002; Prudhomme *et al*., 2002; Carrasco *et al*., 2019).

After interspecies chromosomal transformation, the length of the integrated sequence into the chromosome was analysed in Δ*rok* Δ*recD2* cells sequencing the *rpoB* gene and mapping the endpoints of recombination of 35 Rif^R clones, similarly as previously described for Δ*rok*, *rec*$^+$ (Carrasco *et al*., 2016; Serrano and Carrasco, 2019). At 0.034% sequence divergence, the length of the integrated sequence in the chromosome was practically the full *rpoB* gene in Δ*rok*, *rec*$^+$. Similar integration length was obtained at 2.47% sequence divergence (~2,000 bp). At 8.35% sequence divergence, ~1,000 bp were integrated in Δ*rok*, *rec*$^+$. Furthermore, at 10.12% and 14.52% sequence divergence, the integration length was reduced to ~400 bp and ~250 bp, respectively. However, beyond 15% sequence divergence, just micro-homologous regions were integrated (3 to 9 bp) in Δ*rok*, *rec*$^+$ (**Figure 10**, *black bars*) (Carrasco *et al*., 2016; Serrano *et al*., 2021). In Δ*rok* Δ*recD2* cells, the integration length was similar to that of the Δ*rok*, *rec*$^+$ below 10.12% sequence divergence. At 14.52% sequence divergence, only two of the 35 Rif^R clones sequenced were genuine transformants, with an integration length ~140 bp. Beyond ~15% sequence divergence, transformants were not detected in Δ*rok* Δ*recD2* and only spontaneous Rif^R mutants were obtained (**Figure 10**, *white bars*). These results imply that RecD2 is crucial for micro-homologous integration when the sequence divergence is larger than ~15% (Serrano *et al*., 2021).

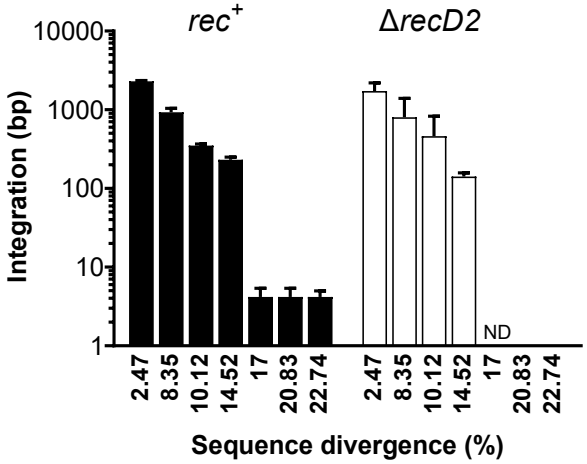

Figure 10. Integration length in Δ*rok* Δ*recD2* transformants for each divergent sequence used as donor DNA. After transformation with donor DNAs with increased sequence divergence, the length of the *rpoB*482 variants that were integrated into the Δ*rok, rec*$^+$ and Δ*rok* Δ*recD2* chromosomes was analysed by sequencing. Integration endpoints were defined as the average between the last single nucleotide polymorphism present and the next one absent in the sequence of transformants (integration endpoint). *Black bars*: integration length obtained for Δ*rok*, *rec*$^+$ (depicted as *rec*$^+$). *White bars*: integration length obtained for Δ*rok* Δ*recD2* (depicted as Δ*recD2*). ND: not detected genuine transformants (35 Rif^R clones). The results are represented in log10 scale as the mean ± SD for at least six sequenced clones.

In the absence of the nucleoid-associated Rok factor, the nucleoid topology could be altered because this protein could act as a bridge connecting further chromosomal regions (Dugar *et al*., 2022). In order to evaluate if the presence of Rok alters the integration length of dissimilar sequences, interspecies chromosomal transformation assays were also carried out in (*rok*$^+$) Δ*recD2* and *wt* cells. As previously described in Carrasco *et al*., 2016, the transformation frequency of the *wt* strain was approximately 1-log lower than Δ*rok*, probably because of the lower proportion of competent cells (**Figure 11**, *white circles*). The intraspecies chromosomal transformation in (*rok*$^+$) Δ*recD2* was similar to that obtained in *wt* competent cells, as previously observed in this work (**Table 10**, see section 4.1.1). At increased sequence divergence, the transformation frequency in (*rok*$^+$) Δ*recD2* decreased ~1-log respect to the results obtained for the *wt* cells (**Figure 11**, *white squares*). However, the absence of *recD2* in the Δ*rok* background conferred a great reduction in transformation frequency at less than ~8% sequence divergence (**Figure 11**, *black squares*), whereas no considerably differences were visualised compared to the *rok*$^+$ background at higher sequence divergence. These results suggest that the absence of Rok affects the transformation frequency in the absence of RecD2 at low sequence divergence (below 8%), perhaps because of topological changes in the nucleoid architecture that could affect the integration of larger DNA sequences (~2,000 bp).

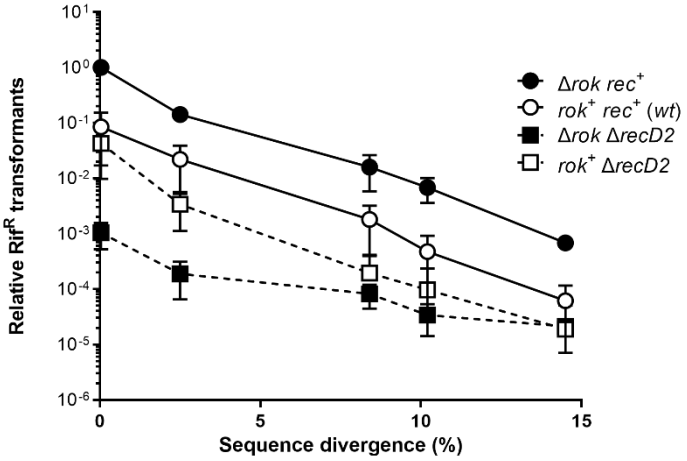

Figure 11. Chromosomal transformation frequencies as a function of increased sequence divergence in Δ*recD2*. Chromosomal transformation assays were performed using donor DNAs containing the *rpoB*482 variant, conferring Rif^R, with increasing percentage of sequence divergence respect to the *wt rpoB* gene: *B. subtilis* 168 (0.034% sequence divergence, homologous DNA), *B. subtilis* W23 (2.47%), *B. atrophaeus* 1942 (8.35%), *B. amyloliquefaciens* DSM7 (10.12%) and *B. licheniformis* DSM13 (14.52%). These DNAs were used to transform *B. subtilis* Δ*rok rec*$^+$ (*black circles*), *rok*$^+$ *rec*$^+$ (*wt*, *white circles*), Δ*rok* Δ*recD2* (*black squares*) and *rok*$^+$ Δ*recD2* (*white squares*) competent cells. The values are plotted relative to Δ*rok rec*$^+$ dividing the number of transformants/CFUs obtained in each condition by the number of transformants/CFUs obtained in Δ*rok rec*$^+$, whose intraspecies transformation frequency was normalised to give a value of 1. The results are plotted in log10 scale as the mean ± SD for at least three independent experiments.

35 Rif^R colonies were selected and sequenced to analyse the length of the integrated *rpoB*482 variant after chromosomal transformation in (*rok*$^+$) Δ*recD2* and compared to the data obtained for Δ*rok* Δ*recD2* cells (**Table 13**). No significant differences were observed in the

integration length in both strains at 2.47% and 8.35% sequence divergence. At 10.12% of divergence, only one of the total sequenced colonies was a genuine transformant, and no transformants were detected at 14.52% sequence divergence in the presence of Rok. In contrast, the deletion of *rok* allowed the detection of more genuine transformants, because at least six clones at 10.12% sequence divergence and two clones at 14.15% were obtained in Δ*rok* Δ*recD2*. As observed, the absence of *rok* increases the barrier for the detection of DNA acquisition from other Bacilli, and thus allows to understand the contribution of RecD2 during interspecies chromosomal transformation.

Table 13. Mean of the integration length in Δ*recD2* and Δ*rok* Δ*recD2*.

Source of donor DNA	Sequence divergence (%)	Integration length in *rok*$^+$ Δ*recD2* (bp)	Integration length in Δ*rok* Δ*recD2* (bp)
B. subtilis W23	2.47	2050 ± 617	1612 ± 528
B. atrophaeus 1942	8.35	1198 ± 564	908 ± 324
B. amyloliquefaciens DSM7	10.12	288[a]	462 ± 268
B. licheniformis DSM13	14.52	ND	145 ± 14[b]

The results are shown as mean ± SD for at least six different sequenced transformants. a: 35 Rif^R sequenced clones. Only one was a genuine transformant. b: 35 Rif^R sequenced clones. Only two were genuine transformants. ND: not detected genuine transformants (35 Rif^R sequenced clones).

4.1.5. Viral transfection is affected in the absence of RecD2

Bacterial competent cells can acquire ssDNA from the environment independently of the nature of the genetic material. One source of exogenous DNA can be proteolysed bacterial viruses (also known as bacteriophages or just phages). These broken DNA fragments from the bacteriophage can be incorporated inside the bacterial cell during natural transformation and reconstitute the viral genome leading to the formation of lytic phages that induce cell death. Commonly, DNA from bacteriophages does not share homology with the bacterial chromosome. As in plasmid transformation, this DNA could be reconstituted as a circular duplex molecule inside the competent cell in a mechanism known as viral transfection (Riva and Polsinelli, 1968; Spatz and Trautner, 1971). However, differently to plasmid transformation, there must be an intermolecular recombination between more than one DNA molecule to establish a viral particle. This is because the DNA uptake apparatus of *B. subtilis* is able to acquire ssDNA fragments below 16,000 nt (Dubnau and Cirigliano, 1972; Fornili and Fox, 1977), but usually the genomes of bacteriophages are longer. Due to the length of the SPP1 genome (44,016 bp), viral DNA is fragmented prior its incorporation inside the cytosol. Three or more DNA molecules need to be internalised inside the bacterial cell for the reconstitution of a viral particle (Trautner and Spatz, 1973; Humphreys and Trautner, 1981).

The lytic bacteriophage SPP1 infects specifically *B. subtilis* cells. This infection is used in the lab as a mechanism of horizontal gene transfer in which genetic material is transferred directly from one bacterium to another by transduction. Generalised transduction by SPP1 also transfers plasmids between bacteria. SPP1 encodes in their genome some viral recombination proteins required for transduction, such as the essential G35P, needed for the single-strand annealing, or the single-stranded binding protein G36P (Ayora *et al*., 2002; Lo Piano *et al*., 2011; Valero-Rello *et al*., 2017). On the other hand, exogenous SPP1 ssDNA can also be acquired by *B. subtilis* competent cells during viral transfection allowing the formation of infectious SPP1 particles inside the cell. Although viral transfection is a poorly understood process, it is supposed to be partially dependent of the bacterial HR machinery. During the early stages of viral transfection, ssDNA sequences from SPP1 are substrate for bacterial HR proteins prior the transcription and the subsequent production of viral proteins (Riva and Polsinelli, 1968; Spatz and Trautner, 1971).

The ability to reconstitute viral SPP1 bacteriophages was explored in the Δ*recD2* mutant with the aim to elucidate a possible role of RecD2 in this process. Viral transfection assays were carried out similarly to chromosomal or plasmid transformation, but using isolated genomic DNA from SPP1. In these experiments, the number of PFUs obtained in Δ*recD2* was compared to that of the *rec*$^+$ (*wt*) cells, which was considered as the 100%. Experiments were also carried out in Δ*recA* competent cells for comparison. The results showed that the absence of *recD2* highly reduced the viral transfection efficiency (~29-fold respect to the *wt*) (**Table 14**). The absence of *recA* also triggers a markedly reduction in viral transfection efficiency (~70-fold respect to the *wt*), because RecA is needed for the annealing of the different ssDNA sequences from the phage to reconstitute the viral particle. The data show an important role of RecD2 in the early stages of the reconstitution of a SPP1 infectious particle inside the *B. subtilis* cell (Serrano *et al*., 2020).

Table 14. Efficiency of viral transfection in Δ*recD2*.

Strain	Relevant genotype	Viral transfection efficiency (%)
BG214	*rec*$^+$(*wt*)	100 (1.9×10^3)
BG1455	+ Δ*recD2*	3.4 ± 3
BG190	+ Δ*recA*	1.4 ± 0.5

Competent *B. subtilis* cells were transformed with 0.1 μg of genomic SPP1 DNA. The yield of viral transfection (PFU/ml) was normalised relative to that of the *rec*$^+$ strain, recorded as 100%. In parenthesis are represented the number of PFUs per ml of competent cells. The results are shown as mean ± SEM of at least four independent experiments.

4.1.6. Viral transfection efficiency in the absence of RecD2 and RadA/Sms

Viral transfection assays were also performed in the double mutant Δ*recD2* Δ*radA/sms* with the aim to understand the contribution of these two helicases in the reconstitution of SPP1

bacteriophages. The absence of *radA*/*sms* marginally reduced the viral transfection efficiency (~3-fold respect to the *wt*), with no statistically significance. The absence of both helicases promoted a decrease in the efficiency (~20-fold reduction), similarly as obtained in the absence of *recD2* alone (~29-fold respect to the *wt*) (**Table 15**) (Serrano *et al*., 2020). These data support the crucial role of RecD2 during viral transfection, whereas RadA/Sms is mainly involved in the chromosomal transformation process.

Table 15. Efficiency of viral transfection in Δ*recD2* Δ*radA/sms*.

Strain	Relevant genotype	Viral transfection efficiency (%)
BG214	*rec*$^+$(*wt*)	100 (1.9×10^3)
BG1455	+ Δ*recD2*	3.4 ± 3
BG1245	+ Δ*radA/sms*	33 ± 4
BG1635	+ Δ*recD2* Δ*radA/sms*	5.2 ± 2

Competent *B. subtilis* cells were transformed with 0.1 μg of genomic SPP1 DNA. The yield of viral transfection (PFU/ml) was normalised relative to that of the *rec*$^+$ strain, recorded as 100%. In parenthesis are represented the number of PFUs per ml of competent cells. The results are shown as mean ± SEM of at least four independent experiments.

2. Chapter 2: Biochemical characterisation of *B. subtilis* RecD2

4.2.1. Purification of RecD2 and RecD2 K373A

B. subtilis RecD2 was purified with a 6xHis-tag placed in the C-terminal domain after several attempts of purification without the tag, because the protein had a reduced solubility and tended to aggregate. In fact, all published data about RecD2 have been obtained from a protein fused to a C-terminal 6xHis-tag (Saikrishnan *et al*., 2008; Shadrick and Julin, 2010; Walsh *et al*., 2014), but if the tag affects the activity of the protein *in vivo* was not yet tested. The functionality of the RecD2-His fusion *in vivo* was confirmed with the use of the *B. subtilis recD2$_{his6}$* strain that expresses the protein fused to 6xHis-tag from its natural promoter. This strain was plated on plates containing 1.5 mM MMS and the cells were as resistant as *wt*, whereas the Δ*recD2* mutant showed sensitivity to this DNA damaging agent (**Figure 12 A**), as previously described (Walsh *et al*., 2014; Torres *et al*., 2017). For that reason, it was concluded that the C-terminal 6xHis-tag did not affect the activity of RecD2, so the protein was purified with this tag. The Walker A motif mutant protein, RecD2 K373A, defective in ATP hydrolysis (Walsh *et al*., 2014), was also purified with the 6xHis-tag and following the same protocol of purification (**Figure 12 B**).

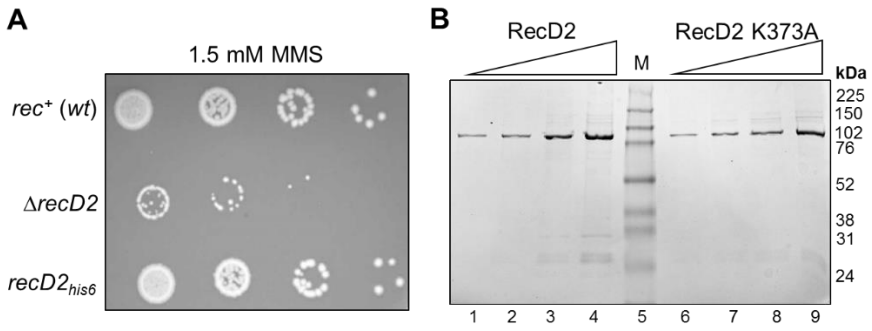

Figure 12. Assessment of RecD2-His.
(**A**) *rec*$^+$ (*wt*), Δ*recD2* and *recD2$_{his6}$* cells were grown until OD_{560} = 0.5. Then, several dilutions of each culture (10^{-3} to 10^{-6}) were spotted on LB-agar plates having 1.5 mM MMS. (**B**) Example of a 12.5% SDS-PAGE with increasing amounts (200 to 800 ng) of purified RecD2 (*lanes 1 to 4*) and RecD2 K373A (*lanes 6 to 9*) (89 kDa). Both proteins were purified with a 6xHis-tag fusion placed in the C-terminal domain. M: Rainbow molecular weight marker (kDa, *lane 5*).

4.2.2. ATP hydrolysis activities of RecD2

4.2.2.1. ATPase activity with different DNA substrates

Because of its nature as a helicase, RecD2 requires the energy of ATP hydrolysis for its translocation along the ssDNA. It was previously observed that the ATPase activity of RecD2$_{Dra}$ was greatly stimulated in the presence of ssDNA, but a reduced ATP hydrolysis was observed with linear or circular dsDNA (Wang and Julin, 2004). However, the ATPase activity of RecD2 from *B. subtilis* had not been explored so far. To gain insight into the ATP hydrolysis activities of RecD2, ATP/NADH-coupled spectrophotometric assays were carried out in the presence of an

ATP regeneration system and different DNAs as effectors. The pGEM-3Zf (+) DNA and the linearized KpnI-pGEM-3Zf (+) were used as circular and linear dsDNA substrates, respectively. As ssDNAs, sspGEM-3Zf (+), polydT$_{80}$ and polydA$_{80}$ were used in the reactions. The experiments were performed at 10 mM $MgCl_2$ and 0.2 mM ATP. As a measure of the ATP hydrolysis rate, the k_{cat} (s^{-1}) was calculated for each condition (**Table 16**), which represents the molecules of ATP hydrolysed per molecule of RecD2.

In the absence of DNA, ATPase activity of RecD2 was not observed (**Figure 13 A**, *black line*). Similar result was obtained for the RecD2 K373A with polydT$_{80}$, confirming the absence of hydrolysis activity of the mutant protein (**Figure 13 A**, *brown line*). The addition of circular or linear dsDNA did not substantially stimulate the activity of RecD2, with k_{cat} = 6.7 ± 2.2 s^{-1} and 11.3 ± 5.2 s^{-1}, respectively (**Figure 13 A**, *cian and red lines*). When sspGEM-3Zf (+), a ssDNA with secondary structures (i.e. regions of dsDNA), was added to the reaction, RecD2 hydrolysed ATP with more efficiency and the rate increased to 28.6 ± 5.9 s^{-1} (**Figure 13 A**, *orange line*). Moreover, the activity of RecD2 was also tested when ssDNAs without secondary structures were added. In the presence of polydA$_{80}$, the k_{cat} was similar to that obtained with sspGEM-3Zf (+) (20.9 ± 5.6 s^{-1}) (**Figure 13 A**, *green line*). In contrast, the ATPase activity of RecD2 was considerably elevated with polydT$_{80}$ (k_{cat} = 174.2 ± 15.3 s^{-1}), so RecD2 appears to have preference on pyrimidines rather than purines (**Figure 13 A**, *dark blue line*). The activity with sspGEM-3Zf (+) and polydT$_{80}$ was also assayed when ATP was replaced by dATP in the reactions. In this case, the activity was significantly lower than the observed with ATP, obtaining a k_{cat} = 32.2 ± 7.9 s^{-1} for polydT$_{80}$ and k_{cat} = 4.6 ± 1.1 s^{-1} for sspGEM-3Zf (+) (**Figure 13 A**, *grey and pink lines*). These results conclude that RecD2 might prefer the binding or translocation along ssDNA rather than dsDNA regions and the hydrolysis of ATP is crucial.

Due to the high activity observed with polydT$_{80}$, the ATP hydrolysis action of RecD2 was measured in the presence of polydTs with different lengths (15 to 80 nt) in order to analyse the minimal site size that RecD2 requires for a robust ATPase activity (**Figure 13 B**). Previous experiments done with the N-terminal truncated Δ150-RecD2$_{Dra}$ showed a k_{cat} = 86.9 ± 1.5 s^{-1} with a polydT$_{20}$ (Toseland and Webb, 2013). In addition, no differences in ATP hydrolysis rates were observed for Δ150-RecD2$_{Dra}$ between polydTs of 20, 30, 40, 50 and 60 nt, with a global k_{cat} = 98 ± 12 s^{-1} (Saikrishnan *et al*., 2009). ATPase experiments were performed as described above. The results showed a similar rate with polydT$_{70}$ (158.6 ± 10.4 s^{-1}) than the acquired with polydT$_{80}$ (174.2 ± 15.3 s^{-1}) (**Figure 13 B**, *dark blue and grey lines*). In the presence of polydT$_{60}$, the ATPase activity of RecD2 was moderately reduced (118 ± 7.7 s^{-1}) (**Figure 13 B**, *orange line*). No huge differences were shown between polydT$_{20}$ (90.1 ± 4.9 s^{-1}), polydT$_{30}$ (95.2 ± 3.3 s^{-1}) and polydT$_{40}$ (102.1 ± 9.7 s^{-1}) (**Figure 13 B**, *cian, green and pink lines*). However, the rate was significantly lower with polydT$_{15}$ (55.1 ± 7.2 s^{-1}) (**Figure 13 B**, *red line*). These data suggest that RecD2

essentially hydrolyses ATP during its translocation along the ssDNA, because the ATP hydrolysis rates decreases as the polydT length also declines. In addition, RecD2 might require a minimum ssDNA length of ~20 nt to show a robust ATPase activity, perhaps because of the binding of more than one protein molecule.

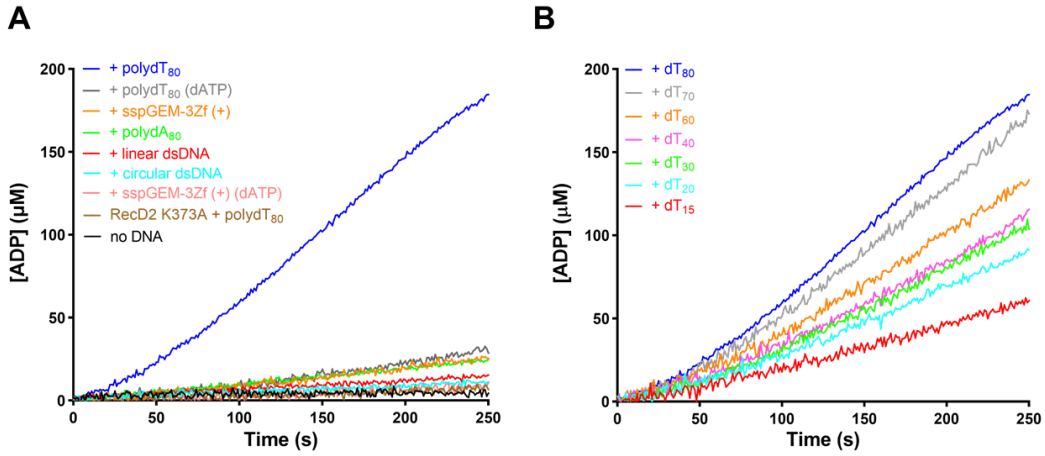

Figure 13. ATPase activity of RecD2 with different DNA substrates.
Representation of the ATPase activity of RecD2 as the concentration of ADP (µM) that accumulates along the time (s). RecD2 (5 nM) was incubated for 5 min at 37ºC with DNA (3 µM in nt) in a buffer containing 50 mM Tris-HCl pH 7.5, 10 mM $MgCl_2$, 1 mM DTT, 50 µg/ml BSA, 50 mM NaCl, 5% (v/v) glycerol, 0.5 mM phosphoenolpyruvate, 0.3 mM NADH, 10 U/ml pyruvate kinase and 10 U/ml lactate dehydrogenase. The reactions were started with the addition of 0.2 mM ATP and ATP hydrolysis was measured for 250 s at 37ºC. (**A**) Kinetic measurement of ATP hydrolysis with different DNAs: $polydT_{80}$ (*dark blue line*), sspGEM-3Zf (+) (*orange line*), $polydA_{80}$ (*green line*), pGEM-3Zf (+) dsDNA (*cian line*) and linearised KpnI-pGEM-3Zf (+) (*red line*). Reactions in the presence of dATP instead of ATP with $polydT_{80}$ (*grey line*) or sspGEM-3Zf (+) (*pink line*) are also shown. The *brown line* represents the activity of 25 nM RecD2 K373A with $polydT_{80}$. The reaction in the absence of DNA is shown in the *black line*. (**B**) ATPase activity of RecD2 when polydTs with increased length were added: $polydT_{15}$ (*red line*), $polydT_{20}$ (*cian line*), $polydT_{30}$ (*green line*), $polydT_{40}$ (*pink line*), $polydT_{60}$ (*orange line*), $polydT_{70}$ (*grey line*) and $polydT_{80}$ (*dark blue line*). The graphs represent the mean of at least three independent experiments for each condition.

Table 16. Kinetics of ATP hydrolysis of RecD2 with different DNAs.

	k_{cat} (s^{-1})
pGEM-3Zf (+)	6.7 ± 2.2
KpnI-pGEM-3Zf (+)	11.3 ± 5.2
sspGEM-3Zf (+)	28.6 ± 5.9
sspGEM-3Zf (+) (dATP)	4.6 ± 1.1
$polydT_{15}$	55.1 ± 7.2
$polydT_{20}$	90.1 ± 4.9
$polydT_{30}$	95.2 ± 3.3
$polydT_{40}$	102.1 ± 9.7
$polydT_{60}$	118 ± 7.7
$polydT_{70}$	158.6 ± 10.4
$polydT_{80}$	174.2 ± 15.3
$polydT_{80}$ (dATP)	32.2 ± 7.9
$polydA_{80}$	20.9 ± 5.6

The rates of the ATP hydrolysis, k_{cat} (s^{-1}), for each condition are shown as mean ± SD for at least three independent ATPase reactions.

4.2.2.2. Effect of the Mg^{2+} concentration on the ATPase activity

The concentration of magnesium present in the reactions is crucial for the optimal activity of a protein with ATPase activity. This cation is coordinated to specific amino acid residues and contributes to the activation of the catalytic reaction. The necessity of Mg^{2+} for the biochemical action of RecD2 was previously observed in Δ150-RecD2$_{Dra}$. In the absence of Mg^{2+}, the ATP hydrolysis activity of Δ150-RecD2$_{Dra}$ was not practically detected (<0.03 s^{-1}) (Toseland and Webb, 2013). The magnesium requirements of *B. subtilis* RecD2 during ATP hydrolysis were explored. Most of the published data about the biochemical activities of the protein were from experiments carried out at 10 mM $MgCl_2$, but other concentrations were not tested so far. To determine the optimal concentration of Mg^{2+} for RecD2, ATPase experiments were performed similarly as described in the section above, but increasing amounts of $MgCl_2$ (1 to 20 mM) were examined. The experiments were done with polydT$_{80}$ (no secondary structures) and sspGEM-3Zf (+) (ssDNA with secondary structures) as the effectors.

In the presence of a ssDNA without secondary structures, polydT$_{80}$, the k_{cat} was 123.9 ± 8.6 s^{-1} at 1 mM $MgCl_2$ (**Figure 14 A**, *cian line*), and greater rates were observed at 2 mM (183.1 ± 12.2 s^{-1}), 5 mM (176.7 ± 6.2 s^{-1}) and 10 mM (174.2 ± 15.3 s^{-1}) $MgCl_2$ (**Figure 14 A**, *dark blue, pink and green lines*). However, the ATPase action of RecD2 decreased at higher $MgCl_2$, obtaining k_{cat} values of 85 ± 0.8 s^{-1} at 15 mM $MgCl_2$ and 46.5 ± 9 s^{-1} at 20 mM $MgCl_2$ (**Figure 14 A**, *grey and red lines*). On the other hand, the rate of the hydrolysis was strongly increased at 1 and 2 mM $MgCl_2$ with a ssDNA containing secondary structures, sspGEM-3Zf (+), (k_{cat} = 209.5 ± 28 s^{-1} and k_{cat} = 147.2 ± 0.9 s^{-1}, respectively), compared with the results acquired at 10 mM $MgCl_2$ (k_{cat} = 28.6 ± 5.9 s^{-1}) (**Figure 14 B**, *cian, dark blue and green lines*). When reactions were done at 5 mM $MgCl_2$, the rate was ~1.5-fold higher than at 10 mM, with a k_{cat} = 40.5 ± 1.2 s^{-1} (**Figure 14 B**, *pink line*). At 15 mM $MgCl_2$, the activity of RecD2 was not practically stimulated (7 ± 2.4 s^{-1}) (**Figure 14 B**, *grey line*). Taking into account all these results, the concentration of Mg^{2+} is crucial for the activity of RecD2. Furthermore, the data showed differences in the ATPase activity depending on the ssDNA present in the reactions and this is probably because the concentration of Mg^{2+} also affects the conformation of the DNA. Whereas slight variations were observed between 2 or 10 mM $MgCl_2$ with polydT$_{80}$, drastic differences were obtained at these concentrations with a ssDNA that may have secondary structures, as sspGEM-3Zf (+) (**Figure 14 C**). Unlike polydT$_{80}$, which do not form secondary structures, the conformation of sspGEM-3Zf (+) is influenced by the amount of Mg^{2+} available in the reaction. At higher Mg^{2+}, the sspGEM-3Zf (+) structure is more compacted and dsDNA regions accumulate, hindering the binding or the translocation of RecD2.

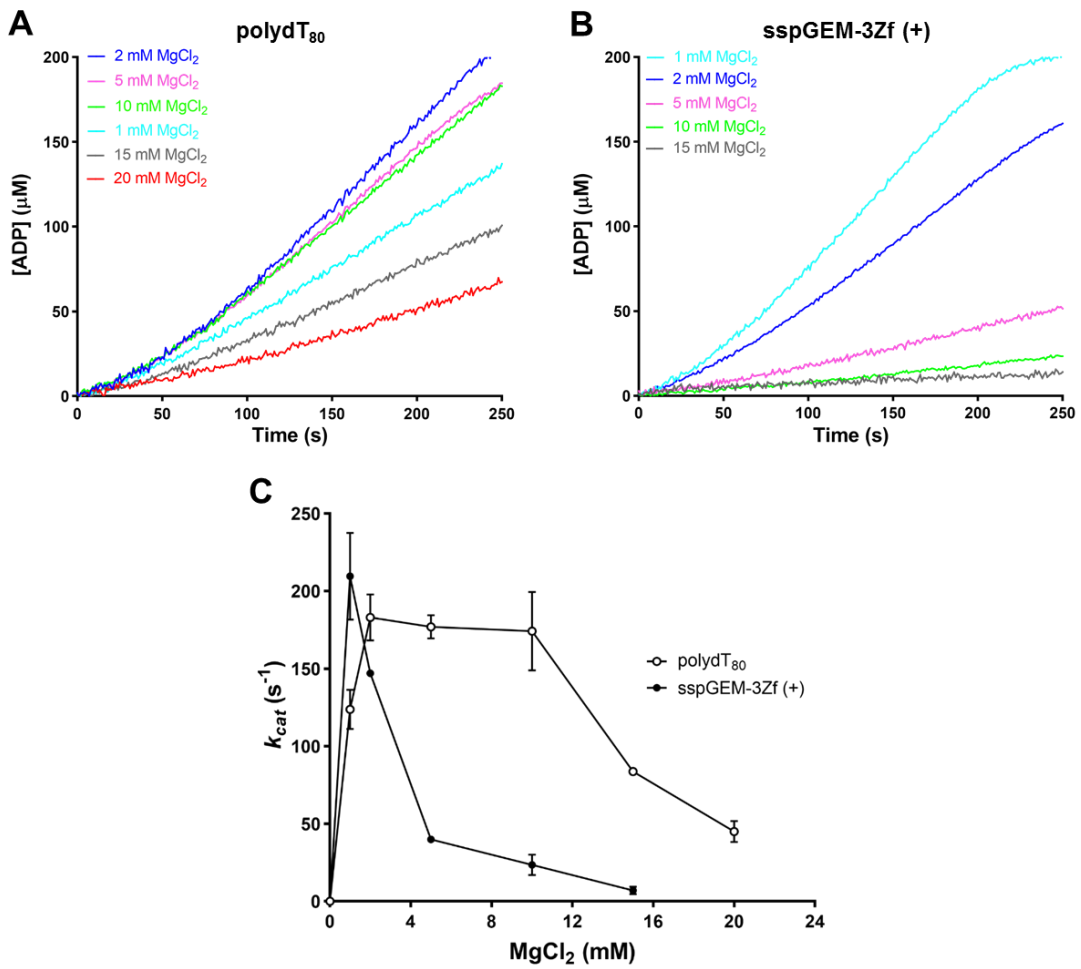

Figure 14. ATPase activity of RecD2 at increasing concentrations of $MgCl_2$.
RecD2 (5 nM) was incubated for 5 min at 37ºC with DNA (3 µM in nt) in a buffer containing 50 mM Tris-HCl pH 7.5, 1 mM DTT, 50 µg/ml BSA, 50 mM NaCl, 5% (v/v) glycerol, 0.5 mM phosphoenolpyruvate, 0.3 mM NADH, 10 U/ml pyruvate kinase, 10 U/ml lactate dehydrogenase and variable amounts of $MgCl_2$ (1-20 mM) The reactions were started with the addition of 0.2 mM ATP and ATP hydrolysis was measured for 250 s at 37ºC. Representation of the ATPase activity of RecD2 as the concentration of ADP (µM) that accumulates along the time (s) with (**A**) $polydT_{80}$ or (**B**) sspGEM-3Zf (+). Reactions at 1 mM (*cian lines*), 2 mM (*dark blue lines*), 5 mM (*pink lines*), 10 mM (*green lines*), 15 mM (*grey lines*) and 20 mM (*red line*) $MgCl_2$ are shown. (**C**) Rate of the ATP hydrolysis, k_{cat} (s^{-1}), as a function of the concentrations of $MgCl_2$ used (mM), plotted as mean ± SD. *White circles*: activity with $polydT_{80}$. *Black circles*: activity with sspGEM-3Zf (+). The graphs represent the mean of at least three independent experiments for each condition.

Due to the variations in ATPase activity observed depending on the $MgCl_2$ concentration, the affinity of RecD2 to ATP, represented as the K_m, was measured at 2 or 10 mM $MgCl_2$ with $polydT_{80}$ and sspGEM-3Zf (+). The experiments were done in the same way as described above, but increasing amounts of ATP (12.5 to 3,200 µM) were tested. Despite the maximum rate (V_{max}) was different for each condition, no huge differences in the affinity parameter were obtained (**Figure 15**). The kinetics acquired with $polydT_{80}$ gave K_m values of 104 ± 7.9 µM ATP at 2 mM $MgCl_2$ (V_{max} ~225 s^{-1}) and 122 ± 5.3 µM ATP at 10 mM $MgCl_2$ (V_{max} ~185 s^{-1}). The activity with sspGEM-3Zf (+) at 2 mM $MgCl_2$ was comparable to that with $polydT_{80}$, with a K_m = 128.3 ± 11.2 µM ATP (V_{max} ~200 s^{-1}). A slight decrease in the affinity was obtained with sspGEM-3Zf (+) at 10 mM $MgCl_2$ (K_m = 166.7 ± 5.8 µM ATP), although the V_{max} was strongly reduced (~55 s^{-1}).

These results conclude that the affinity of RecD2 for the ATP is not greatly affected neither by the concentration of Mg^{2+} nor by the nature of the ssDNA used in the reaction.

Figure 15. ATP affinity of RecD2 in the presence of different effectors.
RecD2 (5 nM) was incubated for 5 min at 37ºC with DNA (3 µM in nt) in a buffer having 50 mM Tris-HCl pH 7.5, 2 or 10 mM $MgCl_2$, 1 mM DTT, 50 µg/ml BSA, 50 mM NaCl, 5% (v/v) glycerol, 0.5 mM phosphoenolpyruvate, 0.3 mM NADH, 10 U/ml pyruvate kinase and 10 U/ml lactate dehydrogenase. The reactions were started with the addition of ATP (12.5 to 3,200 µM) and ATP hydrolysis was measured for 250 s at 37ºC. Representation of ATP hydrolysis rate (s^{-1}) as a function of the concentration of ATP (µM) with $polydT_{80}$ at 2 mM (*black circles*) or 10 mM $MgCl_2$ (*white circles*), or with sspGEM-3Zf (+) at 2 mM (*black squares*) or 10 mM $MgCl_2$ (*white squares*). The curves were used to obtain V_{max} and K_m parameters for each condition and represent the mean ± SD of three independent experiments.

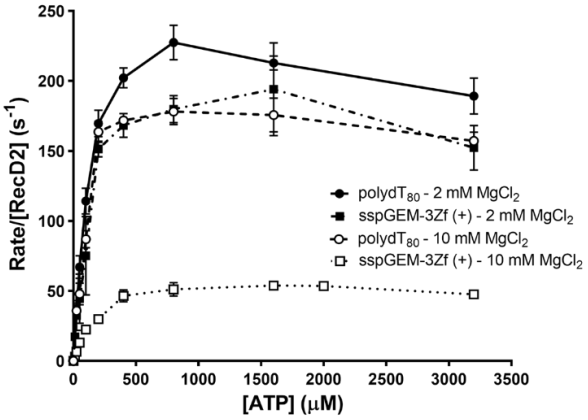

4.2.3. Helicase activities of RecD2

4.2.3.1. RecD2 is a 5' to 3' helicase that does not unwind blunt-ended dsDNA

Previous authors had already determined that the RecD2 helicases unwind DNA from 5' to 3' (Wang and Julin, 2004; Walsh *et al*., 2014). The polarity of the purified *B. subtilis* RecD2 used in this work was tested prior to perform further helicase experiments. For that purpose, the 5'-tailed and the 3'-tailed structures were used as DNA substrates, which contain a duplex region of 30 bp and 30 nt of 5' or 3' ssDNA end, respectively. Helicase activity of RecD2 was only observable on the 5'-tailed structure and at 6 nM RecD2, ~50% of the DNA duplex was unwound (**Figure 16 A**). In contrast, RecD2 could not unwind the 3'-tailed substrate even at a high protein concentration (100 nM), confirming the unwinding polarity 5' to 3' of the protein (**Figure 16 B**). As a control of the experiments, the Walker A motif mutant, RecD2 K373A, defective in ATP hydrolysis, was also included in the reactions. As expected, the helicase activity of RecD2 K373A was impaired (**Figure 16 A**, *lane 10,* and **B**, *lane 5*). On the other hand, it has been proposed that $RecD2_{Dra}$ might require a ssDNA end to translocate prior to perform the unwinding of a dsDNA region, because this protein is not capable to unwind dsDNA with blunt ends (Wang and Julin, 2004). Helicase assays were carried out using a dsDNA of 80 bp as substrate. The results showed that RecD2 was unable to unwind the blunt-ended dsDNA, suggesting that a ssDNA region is needed for the proper binding and translocation of the protein (**Figure 16 C**).

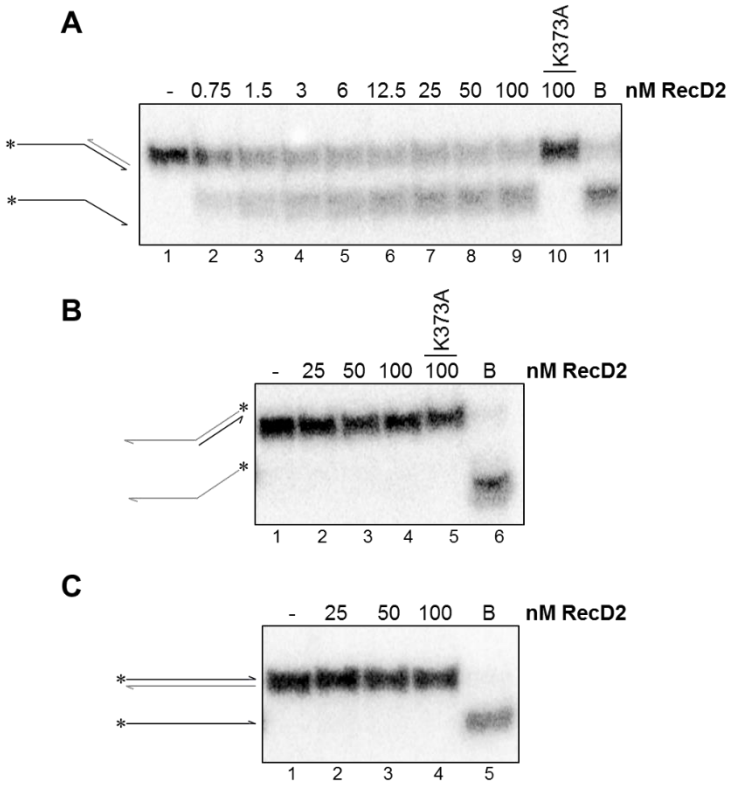

Figure 16. RecD2 is a 5' to 3' helicase that requires a 5' ssDNA end for the unwinding.
Increasing concentrations of RecD2 (nM) were incubated for 10 min at 37ºC with 0.25 nM in molecules of radiolabeled DNA in a reaction buffer containing 50 mM Tris-HCl pH 7.5, 50 mM NaCl, 1 mM DTT, 0.05 mg/ml BSA, 2 mM ATP, 2 mM $MgCl_2$ and 5% (v/v) glycerol. Then, reactions were stopped for 15 min at 37ºC adding stop buffer (20 mM EDTA pH 8 and 0.5% (v/v) SDS as final concentrations). DNA structures were separated on 15% PAGE in 0.5 X TBE buffer. (**A**) Unwinding activity of RecD2 on the 5'-tailed structure. (**B**) Helicase assay of RecD2 with the 3'-tailed structure. Reactions at 100 nM RecD2 K373A instead of RecD2 are also shown (**A**, *lane 10* and **B**, *lane 5*). (**C**) Helicase assay of RecD2 with the blunt-ended dsDNA (80 bp). B: boiled DNA at 100ºC, which represents the unwound product of the reaction. *: radiolabeled 5' end.

4.2.3.2. Unwinding of fork-like structures

As previously done in ATPase assays (see section 4.2.2.2), the Mg^{2+} requirements for the unwinding were explored prior to perform further helicase experiments. Published data about RecD2 activities were obtained at 8 or 10 mM magnesium for $RecD2_{Dra}$ (Wang and Julin, 2004; Shadrick and Julin, 2010) and at 4 mM magnesium for $RecD2_{Bsu}$ (Walsh *et al.*, 2014). To elucidate the optimal magnesium concentration needed for the helicase activity of RecD2, increasing amounts of the protein were incubated with the fork 30-30 (dsDNA of 30 bp and two ssDNA tails of 30 nt) in a reaction buffer containing variable $MgCl_2$ (1 to 15 mM as final concentrations). The unwinding of the fork was lower as the $MgCl_2$ increased (**Figure 17**), with a similar pattern than observed in ATPase assays with the sspGEM-3Zf (+) (**Figure 14 C**). Whereas at 1 mM $MgCl_2$, ~70% of the substrate was entirely unwound at 6 nM RecD2, only ~10% was at 10 mM $MgCl_2$ (**Figure 17 A**, *lanes 2 and 11*, and **B**). In addition, helicase activity was practically undetectable at 15 mM $MgCl_2$ at 6 nM RecD2 (**Figure 17 A**, *lane 14*, and **B**). Because no huge differences were observed between 1 and 2 mM $MgCl_2$ and the previous helicase assays had been done at 2 mM $MgCl_2$ (see section 4.2.3.1), the subsequent experiments were carried out at that $MgCl_2$ concentration.

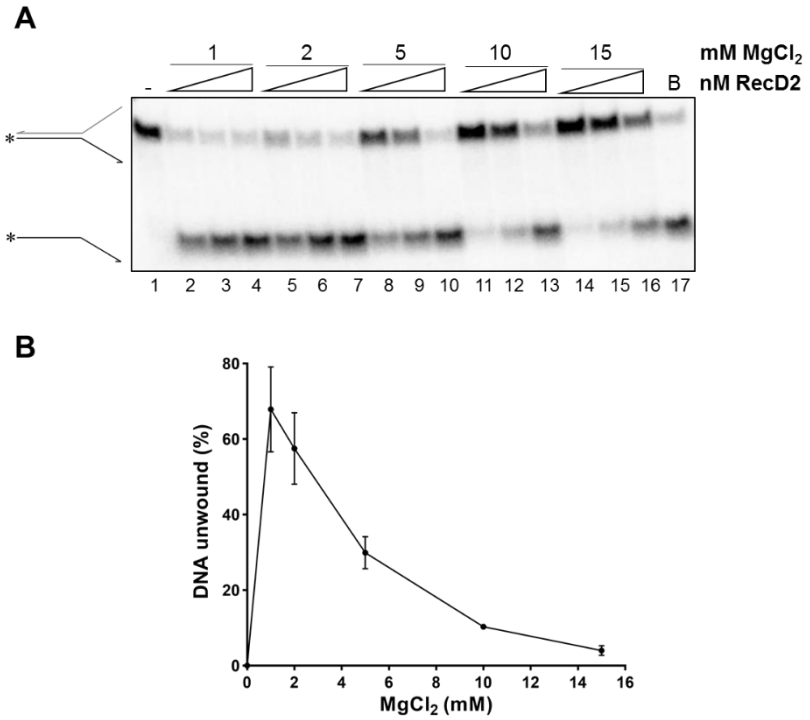

Figure 17. Effect of Mg^{2+} concentration on the helicase activity of RecD2.
(**A**) RecD2 (6 to 25 nM) was incubated for 10 min at 37ºC with 0.25 nM in molecules of the radiolabeled fork 30-30 (30 nt paired and two 30 nt tails of ssDNA) in a reaction buffer containing 50 mM Tris-HCl pH 7.5, 50 mM NaCl, 1 mM DTT, 0.05 mg/ml BSA, 2 mM ATP, variable amounts of $MgCl_2$ (1 to 15 mM) and 5% (v/v) glycerol. Then, reactions were stopped for 15 min at 37ºC adding stop buffer (20 mM EDTA pH 8 and 0.5% (v/v) SDS as final concentrations) and DNA structures were separated on 10% PAGE in 0.5 X TBE buffer. B: boiled DNA at 100ºC, which represents the unwound product of the reaction. *: radiolabeled 5' end. (**B**) Quantification of DNA unwound (%) as a function of the concentration of $MgCl_2$ (mM) at 6 nM RecD2. The graph represents the mean ± SD of three independent experiments.

The kinetics of DNA unwinding was measured in the presence of different non-replicated fork-like structures. It had been reported that $RecD2_{Dra}$ requires a minimum tail of 10 nt for a proper unwinding (Wang and Julin, 2004). In this work, the helicase activity of RecD2 was analysed on the fork 30-30 and the fork 30-16, which contains the same dsDNA region (30 bp), but two shorter ssDNA tails (16 nt). Whereas ~70% of the fork 30-30 was fully unwound at 12.5 nM RecD2, ~50% of the fork 30-16 was at the same protein concentration. In both cases, ~90% of the DNA was unwound at 100 nM RecD2 (**Figure 18**, *dark blue and red lines*). These results indicate that extended ssDNA regions favour helicase activity perhaps allowing the binding of several RecD2 molecules. On the other hand, due to the preference for pyrimidines rather than purines observed in ATPase assays (see section 4.2.2.1), the helicase action of the protein was also explored with the forks 30-dT_{30} and 30-dA_{30}, which harbour two polydT or polydA tails of 30 nt, respectively. The activity observed in the presence of the fork 30-dT_{30} was comparable to that acquired with the 30-30, whereas similar pattern to the fork 30-16 was obtained with the 30-dA_{30}. RecD2 efficiently unwound both structures at 100 nM. However, notable differences were obtained at lower concentrations of protein. At 6 nM RecD2, ~50% of the fork 30-dT_{30} was

unpaired, whilst ~30% of the 30-dA$_{30}$ was unwound (**Figure 18**, *green and pink lines*). These data support the hypothesis of the base preference of RecD2 for DNA binding and/or translocation.

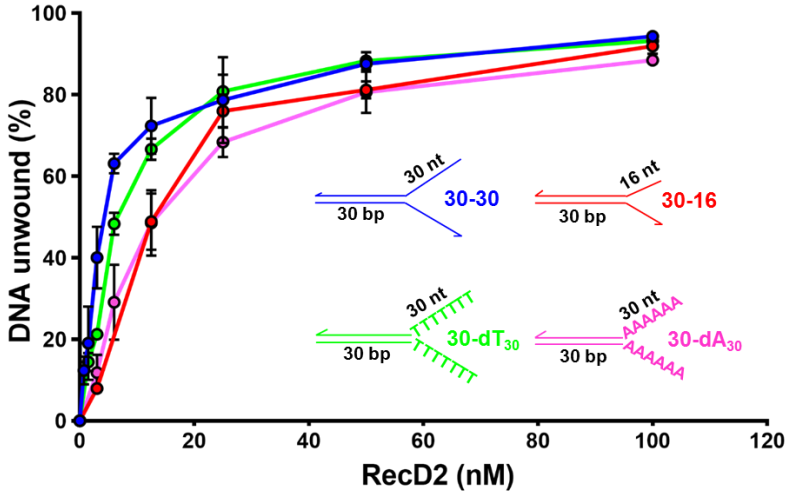

Figure 18. Helicase activity of RecD2 with different fork-like structures.
RecD2 (0.75 to 100 nM) was incubated for 10 min at 37ºC in a reaction buffer (50 mM Tris-HCl pH 7.5, 50 mM NaCl, 1 mM DTT, 0.05 mg/ml BSA, 2 mM ATP, 2 mM $MgCl_2$ and 5% (v/v) glycerol) with 0.25 nM in molecules of radiolabeled fork structures: 30-30 (*dark blue*), 30-16 (*red*), 30-dT$_{30}$ (*green*) or 30-dA$_{30}$ (*pink*). Then, reactions were stopped for 15 min at 37ºC adding stop buffer (20 mM EDTA pH 8 and 0.5% (v/v) SDS as final concentrations) and DNA structures were separated on 10% PAGE in 0.5 X TBE buffer. The percentage of DNA unwound (%) was quantified from the gels by ImageLab software and represented as a function of the concentration of RecD2 (nM). The graph represents the mean ± SD of at least three independent experiments for each condition.

4.2.3.3. Processivity of fork unwinding

It had been reported that RecD2$_{Dra}$ is not a high processive helicase, because its activity was considerably reduced on a substrate containing 52 bp dsDNA and 12 nt ssDNA and almost not detected on a longer dsDNA region (76 bp) (Wang and Julin, 2004). The processivity of RecD2 as helicase was explored using forked structures containing 30, 40, 50 or 70 bp, but, taking into account the previous data, a longer ssDNA region was present in all these structures. As observed for RecD2$_{Dra}$, the fraction of the total DNA unwound decreased as the length of the dsDNA region increased. For instance, ~80% of the fork 30-30 was completely unwound at 25 nM RecD2 (**Figure 19**, *dark blue line*). This ratio decreased to ~65% with the fork 40-30 (dsDNA region of 40 bp) or to ~25% in the case of the fork 50-30 (dsDNA region of 50 bp) (**Figure 19**, *red and green lines*). When the activity of RecD2 was tested on the fork 50-dT$_{37}$, having two polydT tails of 37 nt, the activity was greater (~45% unwound at 25 nM RecD2) to that observed with the fork 50-30 (**Figure 19**, *pink line*). Furthermore, similar kinetics of unwinding was observed with the fork 70-dT$_{37}$ compared to the fork 50-30, with ~25% of DNA unwound at 25 nM RecD2 (**Figure 19**, *black line*). These results show that the binding of RecD2 to the polydT is more efficient than to a random sequence of ssDNA and this facilitates DNA unwinding. Despite the helicase activity of the protein was reduced with larger dsDNA regions, all of the forked structures tested were practically unwound (~90%) at 100 nM RecD2 in 10 min of reaction.

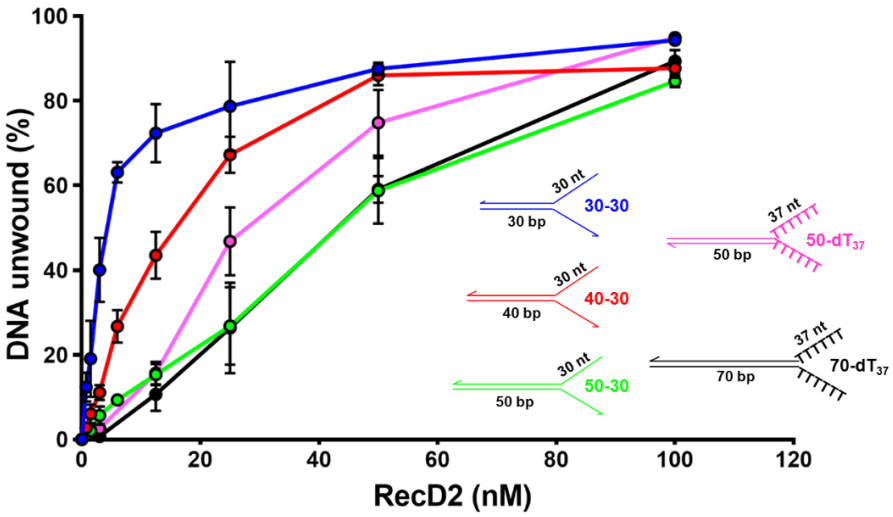

Figure 19. Unwinding activity of RecD2 with longer dsDNA regions.
RecD2 (0.75 to 100 nM) was incubated for 10 min at 37ºC in a reaction buffer (50 mM Tris-HCl pH 7.5, 50 mM NaCl, 1 mM DTT, 0.05 mg/ml BSA, 2 mM ATP, 2 mM $MgCl_2$ and 5% (v/v) glycerol) with 0.25 nM in molecules of radiolabeled fork structures: 30-30 (*blue*), 40-16 (*red*), 50-30 (*green*), 50-dT_{37} (*pink*) or 70-dT_{37} (*black*). Then, reactions were stopped for 15 min at 37ºC with the addition of stop buffer (20 mM EDTA pH 8 and 0.5% (v/v) SDS as final concentrations) and DNA structures were separated on 10% PAGE in 0.5 X TBE buffer. The percentage of DNA unwound (%) was quantified from the gels by ImageLab software and represented as a function of the concentration of RecD2 (nM). The graph represents the mean ± SD of at least three independent experiments for each condition.

4.2.3.4. RecD2 may regulate fork remodeling

During DNA replication, a DNA lesion supposes an obstacle for the progression of the replisome machinery and could lead to the stalling of the replication fork. If the lesion affects only one strand, DNA synthesis can continue in the other strand, a situation that promotes the replication uncoupling. Consequently, gaps in the leading or in the lagging strand are generated. The helicase action of RecD2 was explored on a 5'-forked structure (substrate with the entirely synthetised leading strand and a 5'-ssDNA flap of 30 nt that mimics a gap in the lagging strand) or a 3'-forked structure (substrate with the fully synthesised lagging strand and a 3'-ssDNA flap of 30 nt that simulates a gap in the leading strand) (**Table 6**, see section 3.1.4., Materials). Both structures contained a dsDNA region of 30 bp. RecD2 efficiently unwound the 5'-forked DNA through its binding to the 5'-ssDNA flap. At lower protein concentrations (0.2 to 3 nM), the 5'-tailed structure was generated due to the helicase activity (**Figure 20**, *lanes 2 to 6*). The final product of the unwinding started to be visible at 6 nM RecD2 (**Figure 20**, *lane 7*). As expected, no activity was observed on the 3'-forked due to the polarity 5' to 3' of the protein (**Figure 20**, *lanes 16 and 17*).

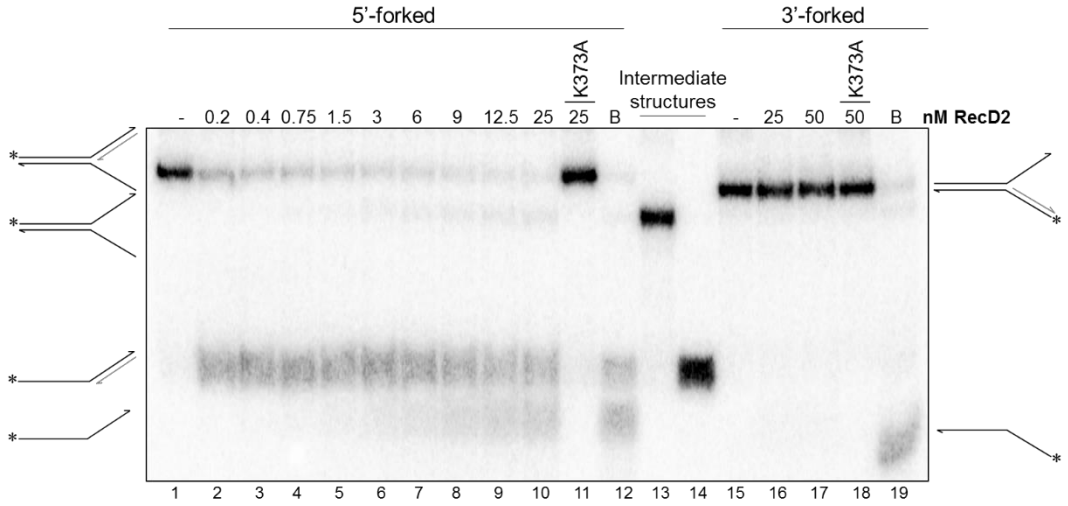

Figure 20. RecD2 unwinds a 5'-forked structure.
RecD2 was incubated for 10 min at 37ºC with 0.25 nM in molecules of radiolabeled 5'-forked (replicated fork with a gap in the lagging strand) (*lanes 1 to 10*) or 3'-forked (replicated fork with a gap in the leading strand) (*lanes 15 to 17*) in a reaction buffer containing 50 mM Tris-HCl pH 7.5, 50 mM NaCl, 1 mM DTT, 0.05 mg/ml BSA, 2 mM ATP, 2 mM $MgCl_2$ and 5% (v/v) glycerol. Then, reactions were stopped for 15 min at 37ºC with the addition of stop buffer (20 mM EDTA pH 8 and 0.5% (v/v) SDS as final concentrations) and DNA structures were separated on 15% PAGE in 0.5 X TBE buffer. Reactions in the presence of RecD2 K373A instead of RecD2 were tested (*lanes 11 and 18*). Intermediate structures of the unwinding were annealed and loaded into the gel as a control of the product migration (*lanes 13 and 14*). Parental strands are depicted in black colour and the new synthesised DNA in grey colour. B: boiled DNA at 100ºC, which represents the final unwound product of the reaction. *: radiolabeled 5' end.

As a mechanism of replication restart, a stalled replication fork can be remodel to a HJ-structure in a process known as fork regression, which can be catalysed by the branch migration translocases RecG or RuvAB. RecU enzyme can then resolve this HJ structure (Marians, 2018). Moreover, helicases can contribute to the processing of a regressed fork via facilitating the unwinding of the nascent strands, such as RadA/Sms (Torres and Alonso, 2021). The helicase action of RecD2 was first analysed on partially regressed fork structures. First, its activity was tested on a 5'-regressed fork (structure similar to the 5'-forked substrate, but the nascent leading strand contains a 3'-tail) or a 3'-regressed fork (similar to the 3'-forked, but the nascent lagging strand has a 5'-tail) (**Table 6**, see section 3.1.4., Materials). Depending on the spontaneous annealing of these structures, the length of the 3'-tail could be 12 nt or longer. RecD2 efficiently unwound the 5'-regressed fork through its translocation along the lagging strand, similarly as occurred with the 5'-forked substrate (**Figure 21 A**, *lanes 2 to 5*, and **D**). However, whereas RecD2 did not unwind the 3'-forked (**Figure 20**), the helicase was able to fully unwind the 3'-regressed fork, starting with the unwinding of the nascent lagging strand (**Figure 21 A**, *lanes 11 to 14*, and **D**). When the activity of RecD2 was tested on a fully regressed fork with blunt ends (HJ structure), no activity was detected, because its requirement of a 5' ssDNA to initiate the unwinding (**Figure 21 B**). However, RecD2 was able to unwind a fully regressed fork structure with a 5'-tail of 30 nt, although only at high concentrations (**Figure 21 C** and **D**). These substrate

would correspond to a regressed fork with a nascent lagging strand longer than the nascent leading strand. All these data conclude that RecD2 could contribute to unwind stalled or regressed forks.

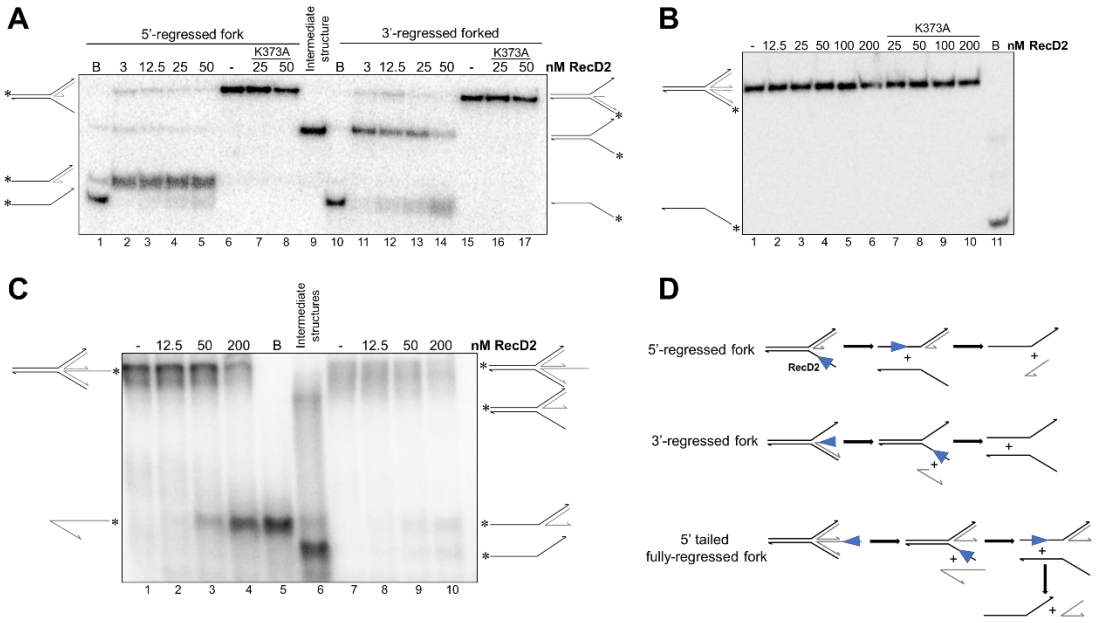

Figure 21. Unwinding activity of RecD2 on regressed fork structures.
Helicase activity of RecD2 was measured for 10 min at 37ºC with 0.25 nM in molecules of different radiolabeled regressed fork structures in a reaction buffer containing 50 mM Tris-HCl pH 7.5, 50 mM NaCl, 1 mM DTT, 0.05 mg/ml BSA, 2 mM ATP, 2 mM $MgCl_2$ and 5% (v/v) glycerol. Then, reactions were stopped for 15 min at 37ºC with the addition of stop buffer (20 mM EDTA pH 8 and 0.5% (v/v) SDS as final concentrations) and DNA structures were separated on 15% PAGE in 0.5 X TBE buffer. (**A**) Unwinding of the 5'-regressed fork (replicated fork with a partially regressed leading strand and a gap in the parental lagging strand) (*lanes 2 to 5*) or a 3'-regressed fork (replicated fork with a partially regressed lagging strand and a gap in the parental leading strand) (*lanes 11 to 14*). Reactions with RecD2 K373A instead of RecD2 were tested (*lanes 6 to 8 and 15 to 17*). An intermediate structure of the unwinding was annealed as a control of the product migration (*lane 9*). (**B**) Helicase activity with a fully regressed fork structure (HJ) in the presence of RecD2 (*lanes 2 to 6*) or RecD2 K373A (*lanes 7 to 10*). (**C**) Unwinding of a fully regressed fork with a 5'-tail (longer nascent lagging strand). The activity of RecD2 was tested radiolabeling two different strands in the structure: the regressed nascent lagging strand (*lanes 1 to 5*) or the leading strand (*lanes 7 to 10*). Intermediate structures were also annealed (*lane 6*). B: boiled DNA at 100ºC, which represents the final unwound product of the reaction. *: radiolabeled 5' end. (**D**) Schematic representation of the unwinding activities of RecD2 (*blue triangle*) on regressed forks. Parental strands are depicted in black colour and the new synthesised DNA in grey colour.

4.2.3.5. RecD2 unwinds 5' and 3'-invading D-loops

During HR, the end resection machinery processes the ends of the DSB, leading to the generation of 3' ssDNA ends. RecA binds to the 3' ends and promotes the strand exchange invasion of a homologous duplex region forming a 3'-invading D-loop. However, during natural chromosomal transformation, the end resection machinery is not acting, so it is possible that RecA could promote the strand invasion in both directions, 3' to 5' or 5' to 3', and a 5'-invading D-loop could be also created. To gain insight into the heteroduplex unwinding by RecD2, the two different D-loops were tested. These structures consist of a region of 30 nt paired to a duplex region displacing one strand, and 30 nt of a 5' or a 3'-tailed ssDNA (**Table 6**, see section 3.1.4.,

Materials). The fate of the displaced or the invading strands was analysed radiolabeling the corresponding strand.

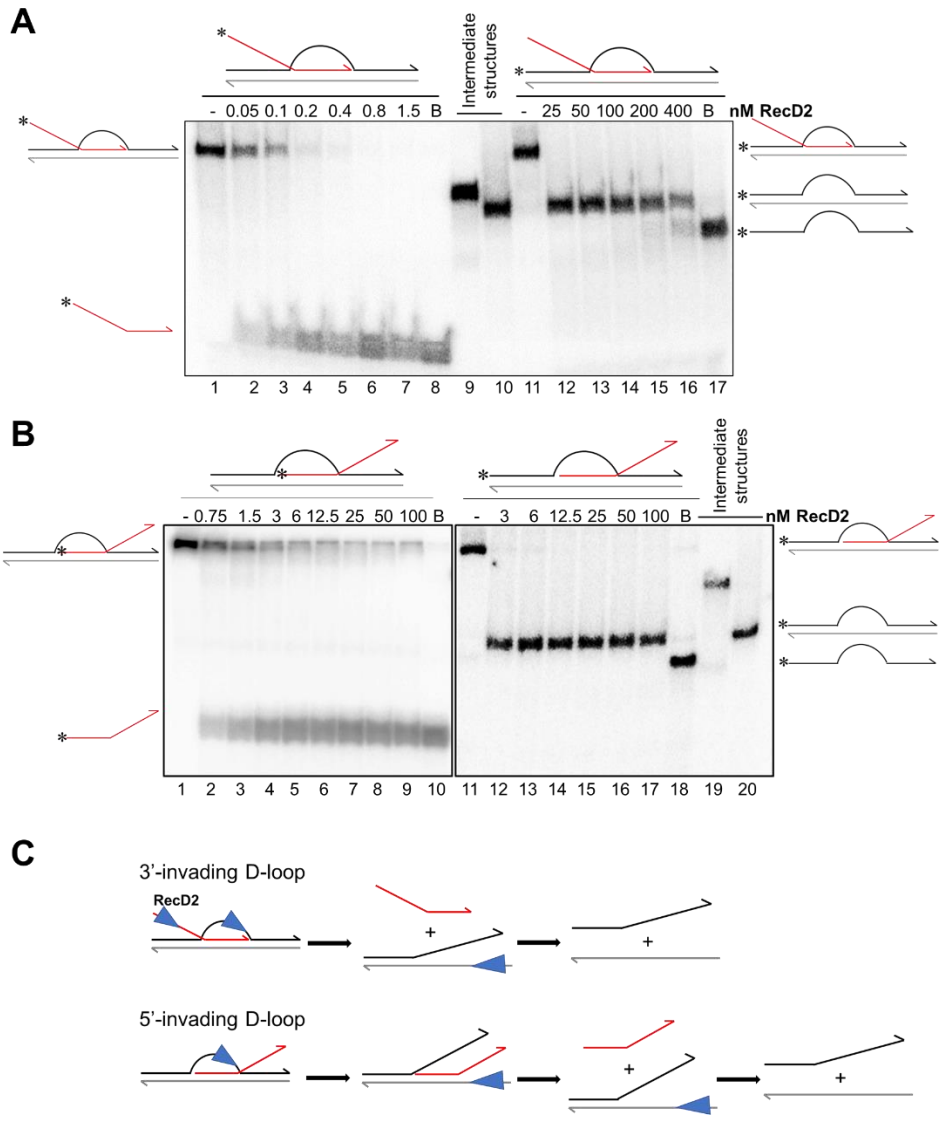

Figure 22. 3' or 5'-invading D-loops unwinding by RecD2.
Helicase activity was measured by the incubation of RecD2 for 10 min at 37ºC with 0.25 nM in molecules of radiolabeled DNA in a reaction buffer containing 50 mM Tris-HCl pH 7.5, 50 mM NaCl, 1 mM DTT, 0.05 mg/ml BSA, 2 mM ATP, 2 mM $MgCl_2$ and 5% (v/v) glycerol. Then, reactions were stopped for 15 min at 37ºC by the addition of stop buffer with 20 mM EDTA pH 8 and 0.5% (v/v) SDS as final concentrations and DNA structures were separated on 10% PAGE in 0.5 X TBE buffer. Unwinding activity of (**A**) 3'-invading D-loop or (**B**) 5'-invading D-loop. Intermediate structures of the unwinding were annealed and loaded into the gel as a control of the product migration (**A**, *lanes 9 and 10*, and **B**, *lanes 19 and 20*). B: boiled DNA at 100ºC, which represents the final unwound product of the reaction. *: radiolabeled 5' end. (**C**) Schematic representation of the unwinding activities of RecD2 (*blue triangle*) on the D-loops.

Helicase experiments showed that RecD2 protein separated the ssDNA that is invading the duplex in the 3'-invading D-loop structure at very low concentrations due to its 5' to 3' polarity (**Figure 22 A**, *lanes 2 to 8*, and **C**). On the other hand, when increasing amounts of RecD2 were incubated with the 5'-invading D-loop substrate, which contained a 3'-tail, the ssDNA that

invaded the duplex was also efficiently separated, but higher concentrations of the protein were needed (**Figure 22 B**, *lanes 2 to 9*, and **C**). For instance, whereas at 1.5 nM RecD2, the invading strand was entirely unwound in the 3'-invading D-loop, only ~50% was separated in the 5'-invading D-loop (**Figure 22 A**, *lane 7,* and **B**, *lane 3*). To fully unwind the complete structure, greater amounts of the protein (at least > 100 nM) were needed in both D-loops (**Figure 22 A**, *lanes 12 to 16,* and **B***, lanes 12 to 17*). According to the activity observed on the 5'-invading D-loop, RecD2 could bind the ssDNA region of the displaced strand and efficiently unwind the duplex, favouring the recombination reaction (**Figure 22 C**). However, an anti-recombinational activity of RecD2 was detected in the 3'-invading D-loop. These results suggest that RecD2 could act as a recombinational or anti-recombinational helicase during the strand exchange invasion, depending on the orientation of the strand (3' or 5') that is paired to the homologous dsDNA.

4.2.4. DNA binding activities of RecD2

4.2.4.1. RecD2 preferentially binds ssDNA without secondary structures

The affinities of RecD2 from *B. subtilis* to different DNA substrates had not been studied so far. Previous authors had observed that the N-terminal truncated $RecD2_{Dra}$ is able to bind ssDNA, such as a $polydT_{15}$ (Saikrishnan *et al*., 2008). In this work, the DNA binding activities were explored by EMSA assays. Prior to perform further experiments, the requirement of ATP in these assays was first analysed in the presence of a 60 nt ssDNA with random sequence (17-M-60 oligonucleotide). For that purpose, experiments were carried out in a reaction buffer containing or not 2 mM ATPγS, a non-hydrolysable ATP analogue. Glutaraldehyde was added to fix the interactions between the ssDNA and RecD2 molecules. The results showed that the ATP binding enhances the affinity to the ssDNA, obtaining the apparent binding constants, K_{app}, of 27.5 ± 3.5 nM and 13.5 ± 4.2 nM RecD2 in the absence or in the presence of ATPγS, respectively (**Figure 23**). For that reason, all the EMSA experiments were done at 2 mM ATPγS.

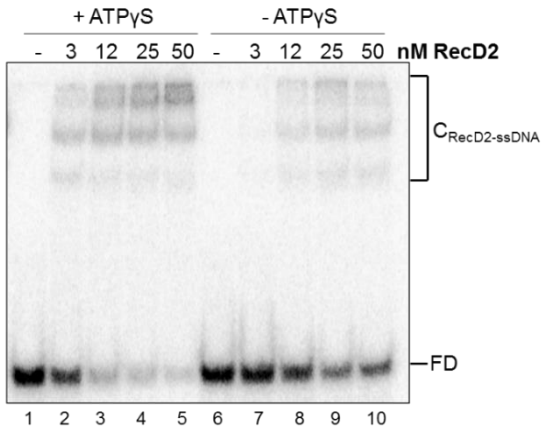

Figure 23. ATP binding increases the affinity of RecD2 to ssDNA.
Increasing amounts of RecD2 were incubated for 15 min at 37ºC with radiolabeled 60 nt ssDNA with random sequence (0.25 nM in molecules) in a reaction buffer containing 50 mM Tris-HCl pH 7.5, 50 mM NaCl, 1 mM DTT, 0.05 mg/ml BSA, 2 mM $MgCl_2$ and 5% (v/v) glycerol. Then, glutaraldehyde (0.05% (v/v) as final concentration) was added for another 15 min and the samples were separated on 8% PAGE run in 1 X TBE. *Lanes 1 to 5*: reactions with 2 mM ATPγS. *Lanes 6 to 10*: reactions without ATPγS. FD: free DNA. $C_{RecD2\text{-}ssDNA}$: complexes formed because of the binding of RecD2 molecules to the ssDNA.

Due to the differences observed in the ATPase activity of RecD2 between DNAs with or without secondary structures (see section 4.2.2), ssDNAs with random sequence or polydTs were

tested in the DNA binding assays and the K_{app} was calculated for each condition (**Table 17**). The binding affinity was very low in the case of a 30 nt ssDNA containing random sequence (22-M-30 oligonucleotide), with a K_{app} > 200 nM (**Figure 24 A**). However, the K_{app} was drastically lower when the length increased up to 60 nt (17-M-60 oligonucleotide) (K_{app} = 13.5 ± 4.2 nM) or 80 nt (17-M-80 oligonucleotide) (K_{app} = 11.1 ± 5.4 nM) (**Figure 24 B** and **C**). Similar experiments were performed with these substrates at 10 mM $MgCl_2$ instead of 2 mM $MgCl_2$. As observed in ATPase and helicase assays, DNA binding affinity was significantly lower at 10 mM $MgCl_2$ (**Table 17**).

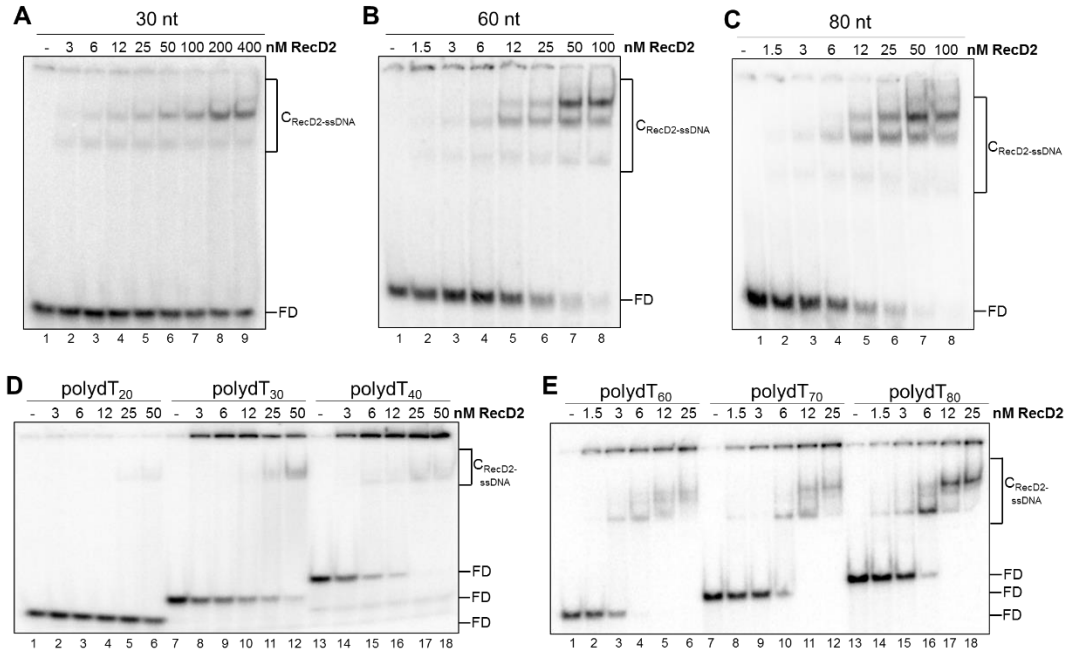

Figure 24. Binding of RecD2 to different ssDNAs.
Increasing amounts of RecD2 were incubated for 15 min at 37ºC with radiolabeled ssDNA (0.25 nM in molecules) in a reaction buffer containing 50 mM Tris-HCl pH 7.5, 50 mM NaCl, 1 mM DTT, 0.05 mg/ml BSA, 2 mM $MgCl_2$, 2 mM ATPγS and 5% (v/v) glycerol. Then, glutaraldehyde (0.05% (v/v) as final concentration) was added for another 15 min and the samples were separated on 8% PAGE run in 1 X TBE. Binding to ssDNA with random sequence of (**A**) 30 nt, (**B**) 60 nt and (**C**) 80 nt. (**D**) Binding to polydT$_{20}$ (*lanes 1 to 6*), polydT$_{30}$ (*lanes 7 to 12*) and polydT$_{40}$ (*lanes 13 to 18*). (**E**) Binding to polydT$_{60}$ (*lanes 1 to 6*), polydT$_{70}$ (*lanes 7 to 12*) and polydT$_{80}$ (*lanes 13 to 18*). FD: free DNA. $C_{RecD2\text{-}ssDNA}$: complexes formed due to the binding of RecD2 molecules to the ssDNA.

Binding of RecD2 to polydTs was substantially better than to ssDNA with random sequence, even with shorter lengths. Whereas the K_{app} for polydT$_{20}$ was > 50 nM, the affinity strongly increased with longer polydTs, observing a K_{app} value of 6 ± 2.8 nM for polydT$_{30}$ and 3.2 ± 0.5 nM for polydT$_{40}$ (**Figure 24 D**). Similar affinities were obtained between polydT$_{60}$, polydT$_{70}$ and polydT$_{80}$ (K_{app} values of 2.1 ± 0.8 nM, 2.9 ± 1 nM or 2.2 ± 1.1 nM, respectively) (**Figure 24 E**). These results suggests that RecD2 preferentially binds ssDNAs with no secondary structures. Moreover, whereas two different RecD2-ssDNAs complexes were observed with the 30 nt ssDNA containing random sequence, only one was appreciable with the polydT$_{30}$. At higher lengths, more than one RecD2-ssDNA complex were observed in the gels, indicating the binding of more than one helicase per ssDNA molecule. Taking into account all the results, the minimum

site size needed for the binding of one RecD2 monomer per molecule of ssDNA might be ~15-30 nt, which is consistent with the number of complexes formed.

Table 17. Summary of the RecD2-ssDNA binding affinities.

		K_{app} (nM)	
		2 mM $MgCl_2$	**10 mM $MgCl_2$**
ssDNA with random sequence	30 nt	212 ± 17.7	246 ± 20.2
	60 nt	13.5 ± 4.2	44.2 ± 14.1
	80 nt	11.1 ± 5.4	37.1 ± 15.4
polydTs	dT_{20}	50.3 ± 3.3	
	dT_{30}	6 ± 2.8	
	dT_{40}	3.2 ± 0.5	
	dT_{60}	2.1 ± 0.8	
	dT_{70}	2.9 ± 1	
	dT_{80}	2.2 ± 1.1	

The apparent binding constants K_{app} (nM), which represent the concentration of RecD2 that binds the 50% of ssDNA, are shown as mean ± SD for at least three independent experiments.

4.2.4.2. Binding affinities to fork-like structures

The affinity of RecD2 to fork-like structures was also analysed. Previous data obtained with $RecD2_{Dra}$ had shown that the protein is able to bind these structures through the 5' ssDNA tails (Wang and Julin, 2004; Saikrishnan *et al*., 2008). However, the binding to 3' ssDNA tailed structures had not been studied so far. Prior to investigate the affinity of RecD2 to fork-like structures, EMSA experiments were performed as done in the previous section with the 3' or 5'-tailed substrates.

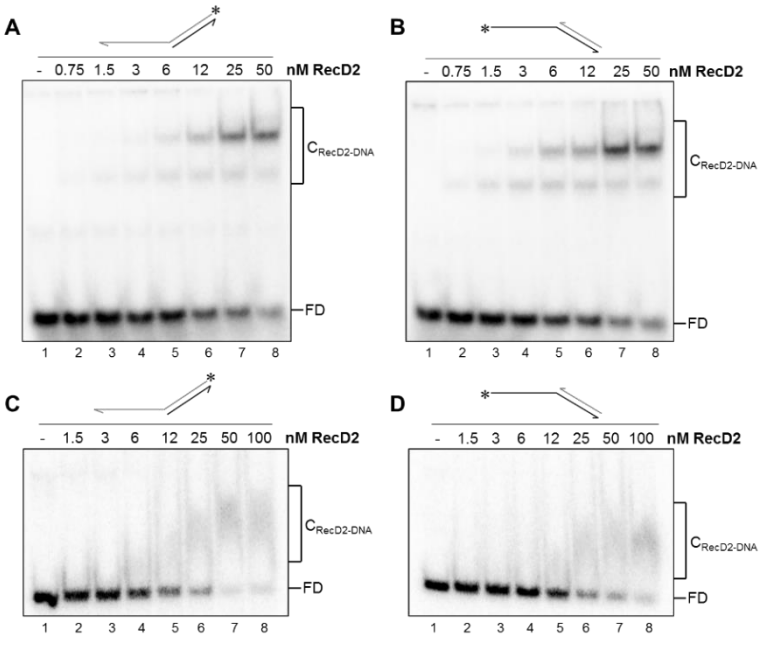

Figure 25. Affinity of RecD2 to the 3' or the 5'-tailed substrates. Increasing amounts of RecD2 were incubated for 15 min at 37ºC with radiolabeled DNA (0.25 nM in molecules) in a reaction buffer (50 mM Tris-HCl pH 7.5, 50 mM NaCl, 1 mM DTT, 0.05 mg/ml BSA, 2 mM $MgCl_2$, 2 mM ATPγS and 5% (v/v) glycerol). The samples were separated on 8% PAGE run in 1 X TBE. (**A**) and (**B**) Binding to the 3' or 5'-tailed structures, respectively, with the addition of glutaraldehyde (0.05% (v/v) as final concentration) for 15 min at 37ºC to fix the RecD2-DNA interactions. (**C**) and (**D**) Binding to the 3' or 5'-tailed structures, respectively, without glutaraldehyde. *: radiolabeled 5' end. FD: free DNA. $C_{RecD2\text{-}DNA}$: complexes formed due to binding of RecD2 molecules to the DNA.

The results showed that the binding affinity was similar in both structures, with K_{app} values of 15.5 ± 7.1 nM RecD2 for the 3'-tailed and 14.3 ± 5 nM for the 5'-tailed (**Figure 25 A** and **B**, and **Table 18**), concluding that RecD2 not necessarily requires a 5' ssDNA tail for the binding. Moreover, two different RecD2-ssDNA complexes were observed, which was consistent with the hypothesis of the requirement of a minimum length between 15-30 nt for the binding of one RecD2 monomer. Additionally, experiments without glutaraldehyde were also performed to check the stability of the RecD2-ssDNA complexes. In these cases, non-defined complexes were visualised, although the affinities were similar to that obtained in the presence of this cross-linking agent (K_{app} = 17 ± 3.5 nM for the 3'-tailed and K_{app} = 19 ± 2.6 nM for the 5'-tailed) (**Figure 25 C** and **D**, and **Table 18**).

Regarding the fork-like structures, the binding activity of RecD2 was first tested with the non-replicated fork 30-30. The affinity was very high, obtaining a K_{app} = 2.1 ± 0.7 nM, indicating the preference of RecD2 for this kind of structure (**Figure 26 A** and **Table 18**). Moreover, at least three different RecD2-ssDNA complexes were visualised in the gels. For comparison, the binding of the RecD2 K373A mutant to this substrate was also checked. In this case, the affinity was ~25-fold lower (K_{app} = 49.5 ± 0.5 nM) than the affinity of the wild-type protein (**Figure 26 B**). Because the Walker A mutant does not bind ATP, this result confirms that the ATP binding stimulates the binding to DNA. As done with the 3' and 5'-tailed structures, assays without the addition of glutaraldehyde were also evaluated, obtaining a similar affinity than in the presence of this agent in the reactions (K_{app} = 3 ± 1 nM), but poorly stable complexes (**Figure 26 C** and **Table 18**).

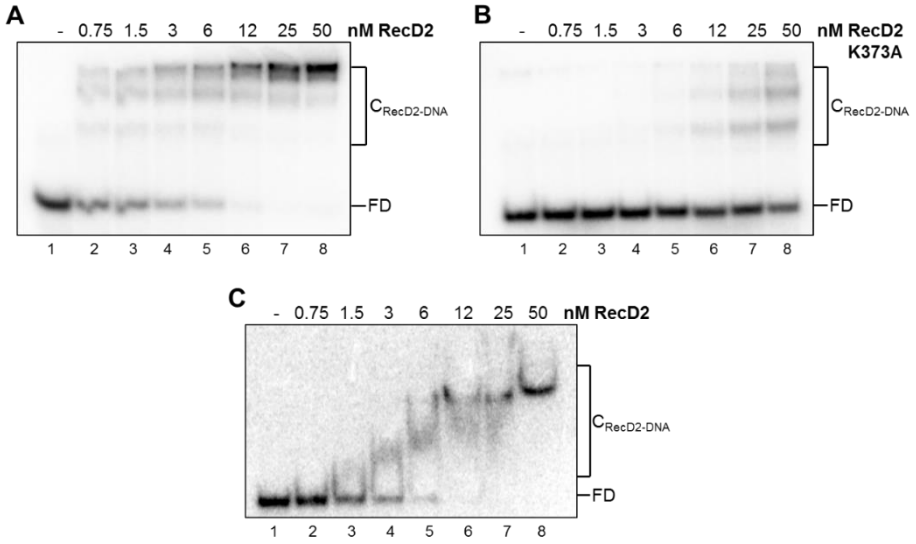

Figure 26. Binding of RecD2 to the non-replicated fork 30-30.
Increasing amounts of RecD2 were incubated for 15 min at 37ºC with the radiolabeled fork 30-30 (0.25 nM in molecules) in a reaction buffer containing 50 mM Tris-HCl pH 7.5, 50 mM NaCl, 1 mM DTT, 0.05 mg/ml BSA, 2 mM $MgCl_2$, 2 mM ATPγS and 5% (v/v) glycerol. The samples were separated on 8% PAGE run in 1 X TBE. (**A**) and (**B**) Binding of RecD2 or RecD2 K373A mutant, respectively, with the addition of glutaraldehyde (0.05% (v/v) as final concentration) for 15 min at 37ºC to fix the RecD2-DNA interactions. (**C**) Binding of RecD2 to the fork without glutaraldehyde. FD: free DNA. $C_{RecD2\text{-}DNA}$: complexes formed due to the binding of RecD2 molecules to the DNA.

On the other hand, EMSA experiments were also performed with partially replicated fork structures, such as the 5'-forked and the 3'-forked, described in the section 4.2.3.4. The results were comparable in both cases, with K_{app} values of 11.5 ± 2.6 nM for the 5'-forked and 13.3 ± 4.9 nM for the 3'-forked (**Figure 27 A** and **B**, and **Table 18**). In the absence of glutaraldehyde, non-defined complexes were visualised, as observed with the other substrates tested, and the affinities obtained were K_{app} = 9.3 ± 2.3 nM and K_{app} = 14 ± 4 nM for the 5' and the 3'-forked, respectively (**Figure 27 C** and **D**, and **Table 18**).

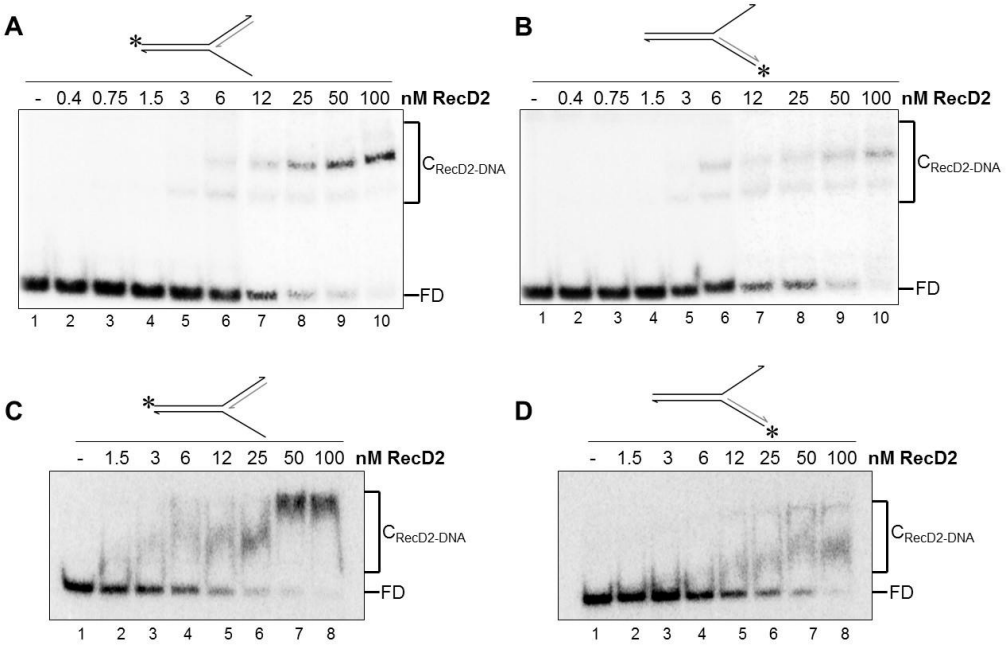

Figure 27. Affinity of RecD2 to the 5' or the 3'-forked substrates.
Increasing amounts of RecD2 were incubated for 15 min at 37ºC with radiolabeled DNA (0.25 nM in molecules) in a reaction buffer containing 50 mM Tris-HCl pH 7.5, 50 mM NaCl, 1 mM DTT, 0.05 mg/ml BSA, 2 mM $MgCl_2$, 2 mM ATPγS and 5% (v/v) glycerol. The samples were separated on 8% PAGE run in 1 X TBE. (**A**) and (**B**) Binding to the 5' or 3'-forked structures, respectively, with the addition of glutaraldehyde (0.05% (v/v) as final concentration) for 15 min at 37ºC to fix the RecD2-DNA interactions. (**C**) and (**D**) Binding to the 5' or 3'-forked structures, respectively, without glutaraldehyde. *: radiolabeled 5' end. FD: free DNA. $C_{RecD2\text{-}DNA}$: complexes formed due to the binding of RecD2 to the DNA.

Table 18. Summary of the binding affinities of RecD2 to fork-like structures.

		K_{app} (nM)	
		- Glutaraldehyde	**+ Glutaraldehyde**
3'-tailed	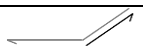	17 ± 3.5	15.5 ± 7.1
5'-tailed	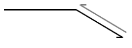	19 ± 2.6	14.3 ± 5
Non-replicated fork 30-30	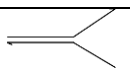	3 ± 1	2.1 ± 0.7
5'-forked	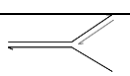	9.3 ± 2.3	11.5 ± 2.6
3'-forked	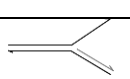	14 ± 4	13.3 ± 4.9

The apparent binding constant K_{app} (nM), which represents the concentration of RecD2 that binds the 50% of DNA, was calculated in the absence or in the presence of glutaraldehyde (0.05% (v/v) as final concentration) for each structure. The values are shown as mean ± SD for at least three independent experiments.

4.2.4.3. Binding affinities to recombination intermediates

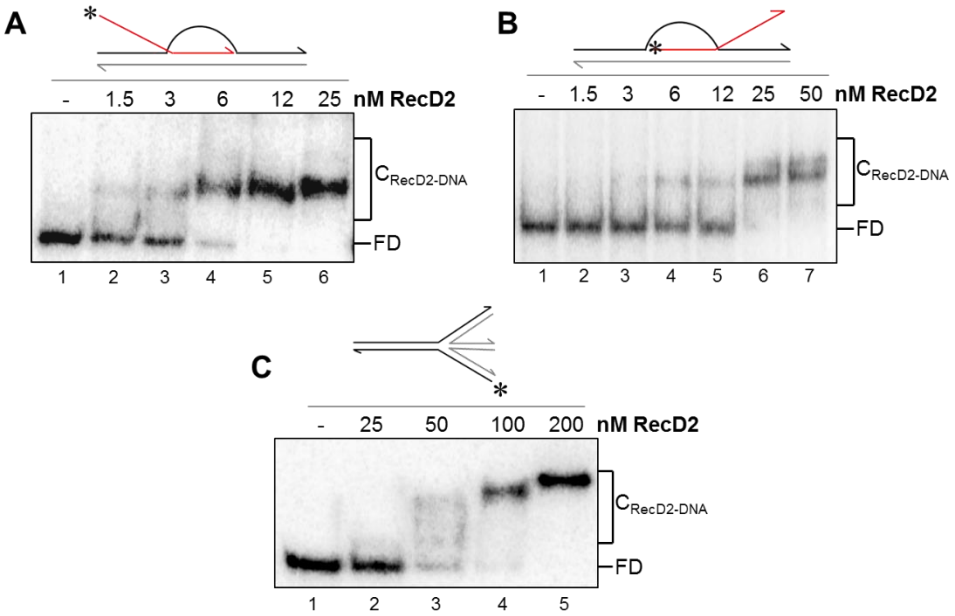

Figure 28. Affinity of RecD2 to recombination intermediates.
Increasing amounts of RecD2 were incubated for 15 min at 37ºC with radiolabeled DNA (0.25 nM in molecules) in a reaction buffer containing 50 mM Tris-HCl pH 7.5, 50 mM NaCl, 1 mM DTT, 0.05 mg/ml BSA, 2 mM $MgCl_2$, 2 mM ATPγS and 5% (v/v) glycerol. The samples were separated on 8% PAGE run in 1 X TBE. (**A**), (**B**) and (**C**) Binding to 3'-invading D-loop, 5'-invading D-loop or HJ structures, respectively. *: radiolabeled 5' end. FD: free DNA. $C_{RecD2\text{-}DNA}$: complexes formed due to the binding of RecD2 molecules to the DNA.

Because RecD2 may participate in HR, the affinity to recombination intermediates, such as the 3' or 5'-invading D-loops and the HJ, was studied. EMSA experiments were done similarly as described in the previous sections. The results showed that RecD2 efficiently bound the 3' and the 5'-invading D-loops, with K_{app} values of 3.6 ± 1.6 nM and 5.1 ± 1.8 nM, respectively (**Figure 28 A** and **B**). However, due to the absence of ssDNA regions, the binding of the HJ was much reduced (K_{app} = 45 ± 9.8 nM) (**Figure 28 C**), indicating that it is not a preferred structure recognised by RecD2, in addition to the fact that this protein especially binds and translocates along ssDNA.

4.3. Chapter 3: Functional interaction between *B. subtilis* RecD2 and SsbA

4.3.1. RecD2 interacts with SsbA, but not with SsbB

Previous authors had already described the interaction between *B. subtilis* RecD2 and SsbA, both *in vivo* and *in vitro* (Costes *et al*., 2010; Walsh *et al*., 2014). Particularly, these *in vitro* experiments showed that RecD2 and SsbA can directly interact and with independence to the presence of DNA (Walsh *et al*., 2014). To test if the purified RecD2-His was able to interact with SsbA, immuno dot-blot experiments were performed as previously described (Walsh *et al*., 2012; see section 3.2.18., Methods). The results confirmed the interaction between RecD2 and SsbA. Moreover, RecD2 could not interact with the competence specific SsbB protein, which lacks the extended C-terminal region present in SsbA-like proteins (**Figure 29**).

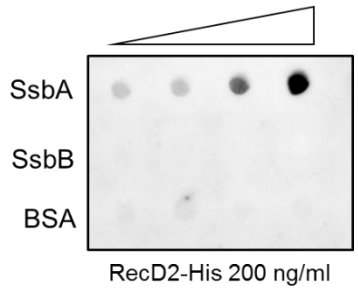

Figure 29. Interaction between RecD2 and Ssb proteins by immuno dot-blot.
Increasing amounts of SsbA, SsbB and BSA (25 to 200 ng) were applied to a nitrocellulose membrane. RecD2-His (200 ng/ml) was added into the binding solution. The membrane was first treated with the primary antibody anti-6xHis (1:6,000) to detect bound RecD2-His protein and then with the secondary antibody anti-IgG mouse conjugated with peroxidase (1:5,000). The experiment was performed four times to validate the result.

4.3.2. RecD2 and SsbA association with the ssDNA

Once the interaction between RecD2 and SsbA was confirmed, EMSA experiments were carried out in the presence of the two proteins to determine if a ternary complex RecD2-SsbA-ssDNA was formed. These assays were performed similarly as described in the section 4.2.4 (Chapter 2), but increasing amounts of SsbA were added to the reactions. To allow the simultaneous binding of both proteins, a ssDNA containing 90 nt was used, taking into account previous data from other authors that showed two binding modes for *E. coli* SSB, 35 or 65 nt (depending on Mg^{2+} and NaCl concentrations) (Roy *et al*., 2007), and our previous results that the affinity of RecD2 substantially increases with ssDNAs longer than 30 nt (see section 4.2.4.1., Chapter 2). Prior to the addition of SsbA together with RecD2, EMSA assays were done only with SsbA to determine the optimum range of the protein concentration to obtain less than the 50% of DNA bound. Similarly as observed by other authors with a ssDNA of 80 nt (Yadav *et al*., 2012), only one SsbA-ssDNA complex was visible, suggesting a binding mode of 65 nt rather than 35 nt (**Figure 30 A**).

A ternary complex between RecD2-SsbA-ssDNA was not visualised. The binding of RecD2 onto the ssDNA was observed separately from the binding of SsbA. Whereas three different complexes between RecD2 and the ssDNA were formed (**Figure 30 B**, *lanes 2 to 5*) only one was visualised between SsbA and the ssDNA (**Figure 30 B**, *lanes 6, 11 and 16*). Although

both proteins are capable to interact *in vitro*, they may not do it apparently on the ssDNA. Another possibility is that the ternary complex may not be stable enough over time to be observed in EMSA assays or perhaps the RecD2-SsbA-ssDNA complex could migrate at the same position than other RecD2-ssDNA complexes, obscuring the visualisation of the interaction.

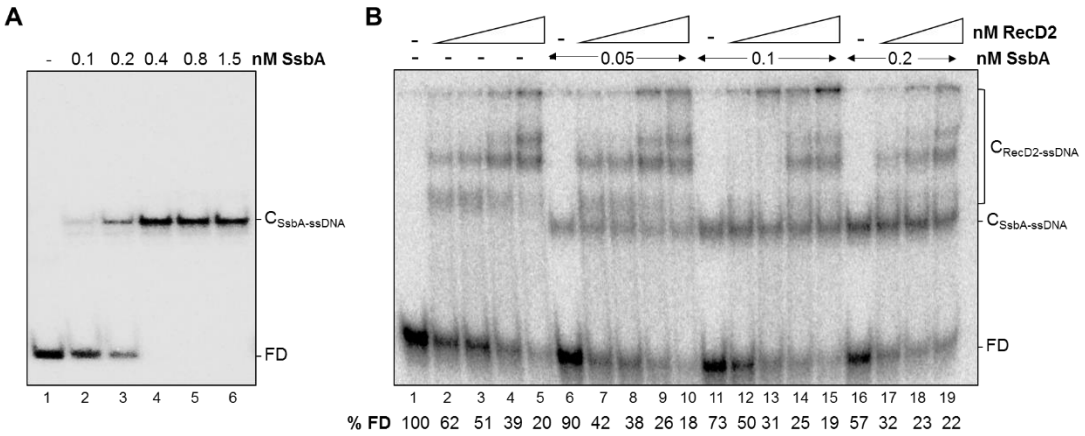

Figure 30. Binding of SsbA and RecD2 to ssDNA.
EMSA experiments were performed incubating the proteins for 15 min at 37ºC with radiolabeled ssDNA of 90 nt (0.25 nM in molecules) in a reaction buffer containing 50 mM Tris-HCl pH 7.5, 50 mM NaCl, 1 mM DTT, 0.05 mg/ml BSA, 2 mM $MgCl_2$, 2 mM ATPγS and 5% (v/v) glycerol. Then, glutaraldehyde (0.05% (v/v) as final concentration) was added for another 15 min and the samples were separated on 8% PAGE run in 1 X TBE. (**A**) DNA binding of SsbA (as tetramer). (**B**) DNA binding of RecD2 (3 to 25 nM) in the absence (*lanes 2 to 5*) or in the presence of 0.05 nM (*lanes 7 to 10*), 0.1 nM (*lanes 12 to 15*) and 0.2 nM SsbA (as tetramer) (*lanes 17 to 19*). *Lanes 6, 11* and *16* show the binding of SsbA without RecD2. *Lane 1* is the control reaction without any protein. The percentage of free DNA (FD) was quantified by ImageLab and a mean of three independent experiments is shown. $C_{RecD2\text{-}ssDNA}$: complexes formed between RecD2 molecules and the ssDNA. $C_{SsbA\text{-}ssDNA}$: complexes between SsbA and the ssDNA.

4.3.3. Effect of SsbA on the biochemical activities of RecD2

The functional interaction between RecD2 and SsbA had not been studied. A previous work with $RecD2_{Dra}$ suggested that SSB_{Dra} stimulated the helicase activity of the protein with a fork-like structure, however there was an excess of SSB in the reaction (ratio SSB_{Dra}:$RecD2_{Dra}$ of 80:1) (Wang and Julin, 2004). The activity of *B. subtilis* RecD2 in the presence of SsbA has not been explored so far. To gain insight into the interaction between RecD2 and SsbA, the biochemical activities of this helicase were analysed in the presence of SsbA to determine its influence on the RecD2 activity.

4.3.3.1. ATPase activity of RecD2 in the presence of SsbA and SsbB

The ATPase activity of RecD2 was studied similarly as described in the section 4.2.2 (Chapter 2), but with the addition of SsbA. The effect of SsbB, which did not interact with RecD2, was also tested. Although DNA binding domains are similar in both Ssb proteins, SsbB was found to bind ssDNA with more than 5-fold lower affinity than SsbA (Yadav *et al*., 2012). RecD2 was incubated with increasing concentrations of SsbA or SsbB in the presence of $polydT_{80}$ or sspGEM-3Zf (+) as ssDNA substrates. The results for $polydT_{80}$ showed that SsbA or SsbB

inhibited the ATPase activity of RecD2, but in a different manner. In both experimental conditions, the k_{cat} lowered as the amount of SsbA or SsbB increased (**Table 19**). However, the activity of RecD2 was not substantially affected with 5 nM SsbA (ratio RecD2:SsbA of 1:1) (**Figure 31 A**, *green line*). A slight decrease in the ATPase rate was observed in the presence of 10 nM SsbA (ratio RecD2:SsbA of 1:2) and 20 nM SsbA (ratio RecD2:SsbA of 1:4) (**Figure 31 A**, *red and brown lines*). At greater concentrations of SsbA, 40 nM and 60 nM, the k_{cat} decreased ~1.5-2-fold respect to that obtained with 5 nM RecD2 alone (**Figure 31 A**, *pink and cian lines*). On the other hand, the inhibition observed with SsbB was considerably higher than the acquired with SsbA. 5 nM SsbB diminished the k_{cat} ~1.4-fold (**Figure 31 B**, *green line*). Furthermore, in the presence of 10 nM and 20 nM SsbB, the ATPase rate was lowered ~1.9-fold and ~3.9-fold, respectively (**Figure 31 B**, *red and brown lines*), whereas at 40 nM SsbB, the activity of RecD2 was strongly inhibited (~12-fold) (**Figure 31 B**, *pink line*). These data suggest that Ssb proteins and RecD2 might compete for the binding to polydT$_{80}$.

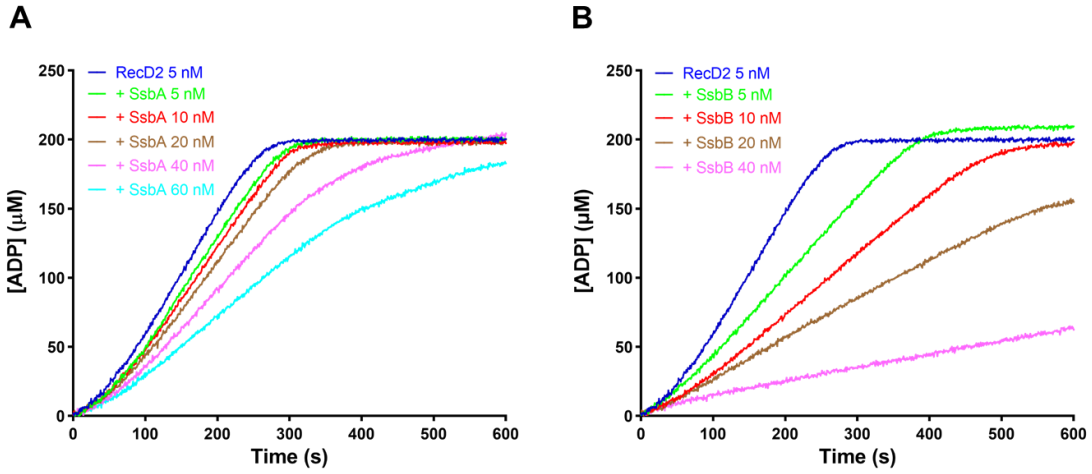

Figure 31. SsbA and SsbB differently reduce the ATPase activity of RecD2 with polydT$_{80}$.
Representation of the ATPase activity of RecD2 as the concentration of ADP (µM) that accumulates along the time (s). RecD2 (5 nM) was incubated for 5 min at 37ºC with polydT$_{80}$ (3 µM in nt) in a buffer containing 50 mM Tris-HCl pH 7.5, 10 mM $MgCl_2$, 1 mM DTT, 50 µg/ml BSA, 50 mM NaCl, 5% (v/v) glycerol, 0.5 mM phosphoenolpyruvate, 0.3 mM NADH, 10 U/ml pyruvate kinase and 10 U/ml lactate dehydrogenase. The reactions were started with the addition of 0.2 mM ATP and ATP hydrolysis was measured for 600 s at 37ºC. Reactions in the absence (*dark blue lines*) or in the presence of (**A**) SsbA or (**B**) SsbB as tetramers: 5 nM (*green lines*), 10 nM (*red lines*), 20 nM (*brown lines*), 40 nM (*pink lines*) or 60 nM (*cian line*). The graphs are plotted as the mean of at least three independent experiments for each condition.

As previously described in the section 4.2.2.2 (Chapter 2), the conformation of the DNA is affected by the concentration of Mg^{2+} and great differences were observed between 2 and 10 mM $MgCl_2$ in the ATPase activity of RecD2 with sspGEM-3Zf (+) as effector, due to conformational changes in the DNA structure. For that observation, ATP hydrolysis activity of RecD2 was monitored at both $MgCl_2$ concentrations in the presence of SsbA or SsbB with this ssDNA substrate. The results found that increasing concentrations of SsbB inhibited the activity of RecD2 at 2 and 10 mM $MgCl_2$. In spite of the ATPase rate was not significantly affected at 2

mM $MgCl_2$ with the addition of 5 nM, 10 nM or 20 nM SsbB, the k_{cat} was reduced ~4-fold at 40 nM SsbB respect to that obtained with RecD2 alone (**Figure 32 A** and **Table 19**). In contrast, SsbB strongly lowered the ATPase kinetics of RecD2 at 10 mM $MgCl_2$, even at low protein concentrations. At 40 nM SsbB, the activity of RecD2 was practically undetected (**Figure 32 B** and **Table 19**). These results conclude that, regardless of the type of ssDNA or the concentration of $MgCl_2$ used, SsbB and RecD2 compete for the binding to the ssDNA.

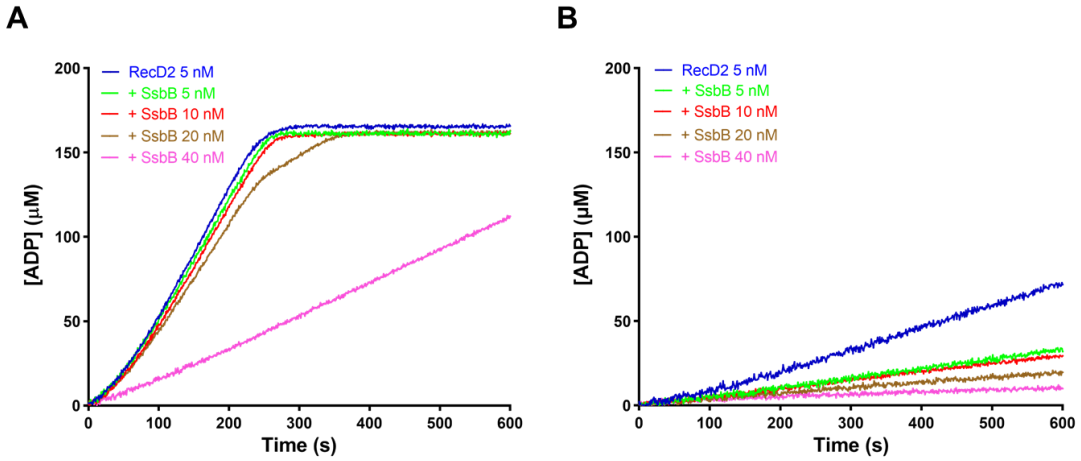

Figure 32. SsbB reduces the ATPase activity of RecD2 with sspGEM-3Zf (+) at 2 and 10 mM $MgCl_2$. Representation of the ATPase activity of RecD2 as the concentration of ADP (µM) that accumulates along the time (s). RecD2 (5 nM) was incubated for 5 min at 37ºC with sspGEM-3Zf (+) (3 µM in nt) in a buffer containing 50 mM Tris-HCl pH 7.5, 1 mM DTT, 50 µg/ml BSA, 50 mM NaCl, 5% (v/v) glycerol, 0.5 mM phosphoenolpyruvate, 0.3 mM NADH, 10 U/ml pyruvate kinase and 10 U/ml lactate dehydrogenase. The reactions were started with the addition of 0.2 mM ATP and ATP hydrolysis was measured for 600 s at 37ºC. Reactions in the absence (*dark blue lines*) or in the presence of SsbB are shown: 5 nM (*green lines*), 10 nM (*red lines*), 20 nM (*brown lines*) or 40 nM (*pink lines*) SsbB (as tetramer). (**A**) Reactions at 2 mM $MgCl_2$. (**B**) Reactions at 10 mM $MgCl_2$. The graphs are plotted as the mean of at least three independent experiments for each condition.

Similarly as observed with SsbB, the ATPase activity of RecD2 with sspGEM-3Zf (+) at 2 mM $MgCl_2$ was reduced as the concentration of SsbA increased (**Figure 33 A**). The presence of 5 nM, 10 nM and 20 nM SsbA decreased the k_{cat} ~1.2-fold, ~1.6-fold and ~1.8-fold, respectively, in comparison to the rate obtained with RecD2 alone, and the activity of RecD2 was greatly lowered at 60 nM SsbA (~3-fold) (**Table 19**). In contrast, ATP hydrolysis was stimulated with the addition of SsbA at 10 mM $MgCl_2$ (**Figure 33 B**). The k_{cat} increased ~1.2-fold at 5 nM SsbA, ~1.7-fold at 10 nM SsbA and ~2-fold at 20 nM SsbA. Moreover, the rate of ATP hydrolysis markedly increased at 40 nM SsbA (~2.5-fold) and at 60 nM SsbA (~2.7-fold) (**Table 19**). Due to the compacted conformation of the sspGEM-3Zf (+) and the stabilization of secondary structures at 10 mM $MgCl_2$, the obtained results suggest that SsbA stimulates the ATPase activity of RecD2 by reducing the presence of secondary structures in the ssDNA. The binding of SsbA onto the ssDNA prevents the annealing between complementary sequences and, thus, the amount of dsDNA regions diminishes. This situation may facilitate the binding and the translocation of RecD2 along the ssDNA. In addition, the interaction between RecD2 and SsbA may be crucial in

the stimulation of the ATPase activity, because SsbB, which does not interact with RecD2, inhibited the activity of RecD2 in all the conditions tested.

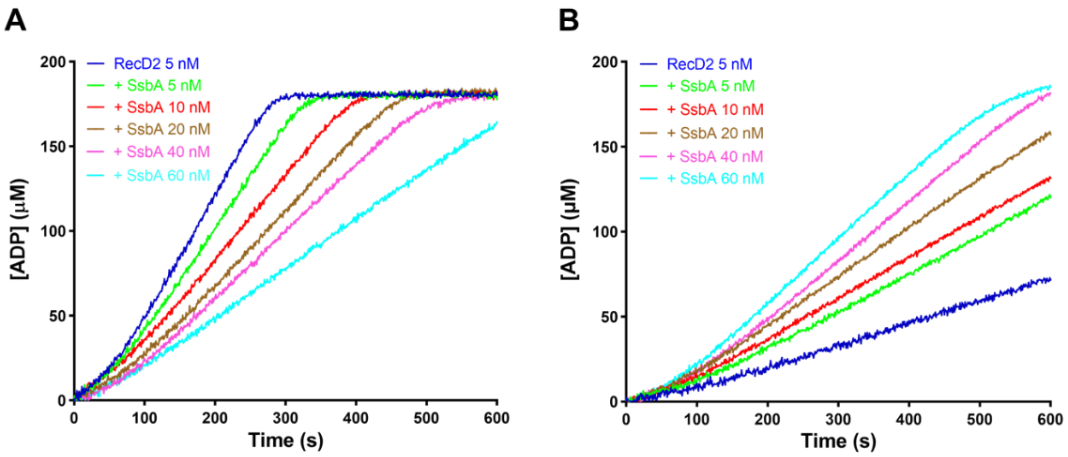

Figure 33. SsbA stimulates the ATPase activity of RecD2 with sspGEM-3Zf (+) at 10 mM $MgCl_2$.
Representation of the ATPase activity of RecD2 as the concentration of ADP (µM) that accumulates along the time (s). RecD2 (5 nM) was incubated for 5 min at 37ºC with sspGEM-3Zf (+) (3 µM in nt) in a buffer containing 50 mM Tris-HCl pH 7.5, 1 mM DTT, 50 µg/ml BSA, 50 mM NaCl, 5% (v/v) glycerol, 0.5 mM phosphoenolpyruvate, 0.3 mM NADH, 10 U/ml pyruvate kinase and 10 U/ml lactate dehydrogenase. The reactions were started with the addition of 0.2 mM ATP and ATP hydrolysis was measured for 600 s at 37ºC. Reactions in the absence (*dark blue lines*) or in the presence of SsbA are shown: 5 nM (*green lines*), 10 nM (*red lines*), 20 nM (*brown lines*), 40 nM (*pink lines*) or 60 nM (*cian line*) SsbA (as tetramer). (**A**) Reactions at 2 mM $MgCl_2$. (**B**) Reactions at 10 mM $MgCl_2$. The graphs are plotted as the mean of at least three independent experiments for each condition.

Table 19. Kinetics of the ATP hydrolysis of RecD2 in the presence of SsbA and SsbB.

	k_{cat} (s^{-1})		
	polydT$_{80}$	sspGEM-3Zf (+)	
		2 mM $MgCl_2$	10 mM $MgCl_2$
RecD2 5 nM	174.2 ± 15.3	148.3 ± 16.2	28.6 ± 5.9
+ SsbA 5 nM	163.2 ± 13.2	118.5 ± 3.9	43.4 ± 2.9
+ SsbA 10 nM	149.6 ± 13.7	91.1 ± 7.7	49 ± 3
+ SsbA 20 nM	132.5 ± 15.3	82.7 ± 6.7	57.6 ± 8.6
+ SsbA 40 nM	111.7 ± 17.9	72 ± 4.2	71.2 ± 5
+ SsbA 60 nM	77.6 ± 9.7	51.6 ± 10.5	76.5 ± 4.2
+ SsbB 5 nM	113.4 ± 4.1	140.1 ± 6.8	11.9 ± 1.5
+ SsbB 10 nM	89.5 ± 6.6	139 ± 5.9	9.7 ± 0.3
+ SsbB 20 nM	45.7 ± 6.1	97.1 ± 4	7 ± 0.6
+ SsbB 40 nM	14 ± 4.7	37.8 ± 8.9	2 ± 1

Rates of the ATPase activity of RecD2, k_{cat} (s^{-1}), in the absence or in the presence of SsbA and SsbB when polydT$_{80}$ or sspGEM-3Zf (+) were used as ssDNA substrates. The values are expressed as the mean ± SD for at least three independent experiments.

4.3.3.2. Helicase activity of RecD2 in the presence of SsbA

The helicase activity of RecD2 was explored in the presence of SsbA. These experiments were done as previously described in the section 4.2.3 (Chapter 2), but increasing amounts of SsbA were added to the reactions. Because of the differences observed between 2 and 10 mM $MgCl_2$ in ATP hydrolysis rates, the helicase assays were performed at both concentrations of $MgCl_2$, and the fork 30-30 was used as substrate. The results showed that SsbA inhibited the unwinding activity at 2 mM $MgCl_2$ (**Figure 34 A**). At 10 mM $MgCl_2$, the addition of SsbA did not significantly altered the helicase activity of RecD2, which was very low *per se* (**Figure 34 B**). Additional experiments with the 5'-tailed substrate at 2 and 10 mM $MgCl_2$ were tested, showing that SsbA inhibited the unwinding action of RecD2 at both $MgCl_2$ concentrations (**Figure 34 C** and **D**).

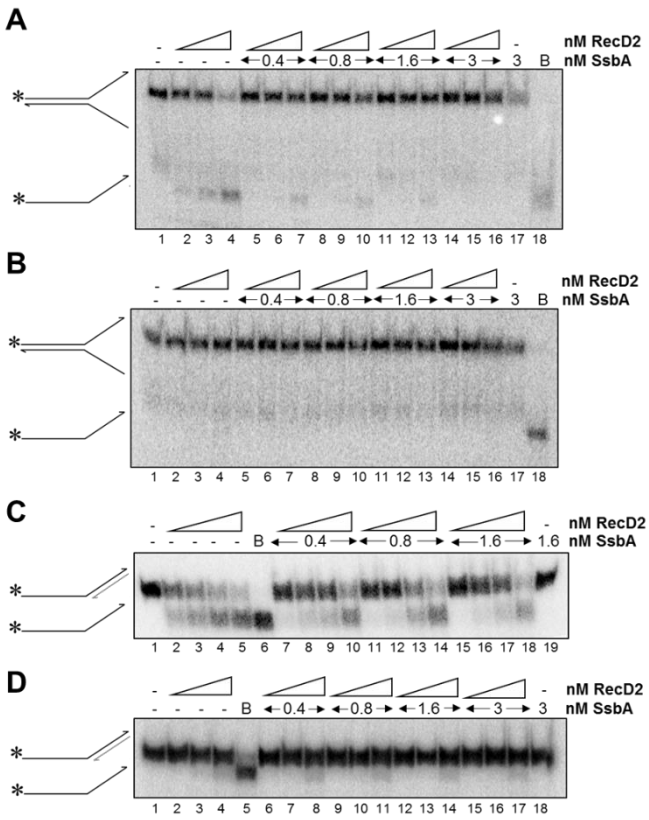

Figure 34. SsbA reduces the helicase activity of RecD2.
RecD2 was incubated for 5 min at 37ºC with SsbA in a reaction buffer containing 50 mM Tris-HCl pH 7.5, 2 mM DTT, 0.05 mg/ml BSA and 0.25 nM of radiolabeled DNA. ATP (2 mM) was added and reactions were incubated for 10 min at 37ºC. After stopping the reactions (20 mM EDTA pH 8, 0.5% (v/v) SDS and 0.5 mg/ml proteinase K), DNA structures were separated on 10% PAGE run in 1 X TBE. (**A**) Activity of RecD2 (3 to 12.5 nM) in the absence (*lanes 2 to 4*) or in the presence of SsbA (*lanes 5 to 17*) at 2 mM $MgCl_2$ with the fork 30-30. (**B**) Activity of RecD2 (25 to 100 nM) in the absence (*lanes 2 to 4*) or in the presence of SsbA (*lanes 5 to 17*) at 10 mM $MgCl_2$ with the fork 30-30. (**C**) Activity of RecD2 (6 to 50 nM) in the absence (*lanes 2 to 5*) or in the presence of SsbA (*lanes 7 to 19*) at 2 mM $MgCl_2$ with the 5'-tailed. (**D**) Activity of RecD2 (12.5 to 50 nM) in the absence (*lanes 2 to 4*) or in the presence of SsbA (*lanes 6 to 18*) at 10 mM $MgCl_2$ with the 5'-tailed. B: boiled DNA at 100ºC, which represents the unwound product of the reaction. *: radiolabeled 5' end.

The DNA structures tested had a very short ssDNA region to allow the simultaneous binding of both proteins. Because SsbA stimulated the ATPase activity of RecD2 at 10 mM $MgCl_2$ with sspGEM-3Zf (+) (see section 4.3.3.1), helicase experiments were performed using this large ssDNA annealed to a very short complementary oligonucleotide of 24 nt (pGEM-Hind24 substrate). Helicase assays were carried out with the addition of SsbA at 2 and 10 mM $MgCl_2$ as described above. In this case, SsbA stimulated the unwinding action of RecD2 at both

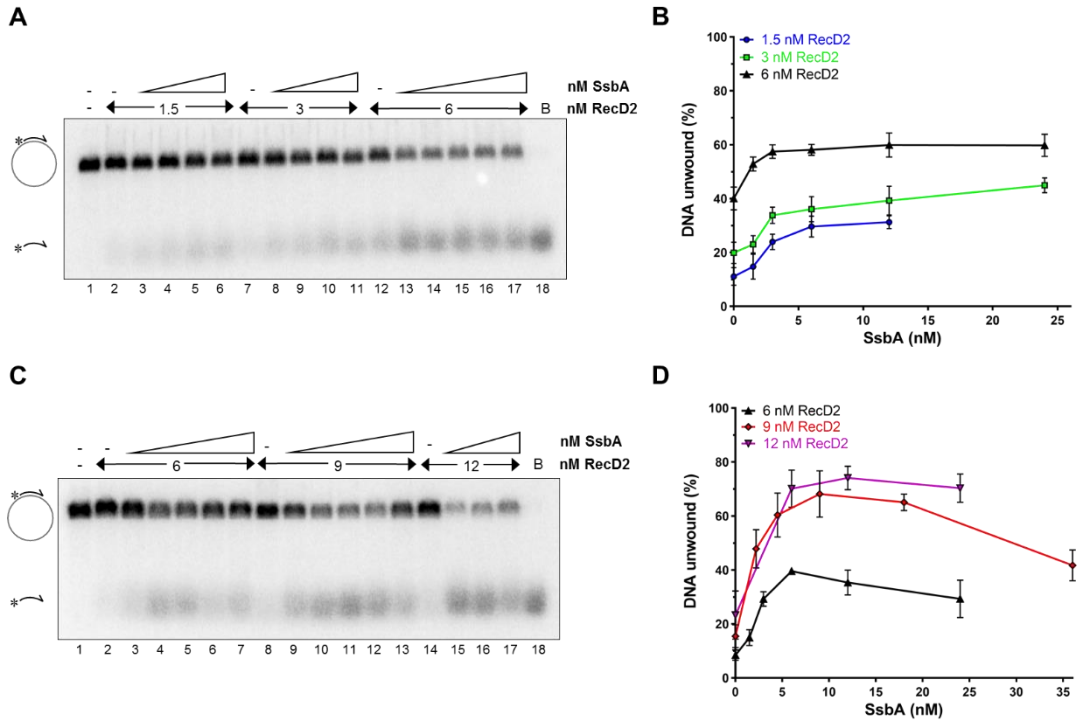

Figure 35. SsbA stimulates the helicase activity of RecD2 with pGEM-Hind24 structure.
RecD2 was incubated for 5 min at 37ºC with SsbA in a reaction buffer containing 50 mM Tris-HCl pH 7.5, 2 mM DTT, 0.05 mg/ml BSA and 0.25 nM of radiolabeled pGEM-Hind24. ATP (2 mM) was added and reactions were incubated for 10 min at 37ºC. After stopping the reactions (20 mM EDTA pH 8, 0.5% (v/v) SDS and 0.5 mg/ml proteinase K), DNA structures were separated on 1.2% (w/v) agarose gel electrophoresis run in 1 X TAE. (**A**) Activity of RecD2 at 2 mM $MgCl_2$ in the absence (*lanes 2, 7 and 12*) or in the presence of SsbA: 1.5 to 12 nM, (*lanes 3 to 6; lanes 8 to 11*) and 1.5 to 24 nM (*lanes 13 to 17*), as tetramer. (**B**) Quantification of the % DNA unwound at 2 mM $MgCl_2$ as a function of the concentration of SsbA (nM) at 1.5 nM (*dark blue circles*), 3 nM (*green squares*) and 6 nM (*black triangles*) RecD2. (**C**) Activity of RecD2 at 10 mM $MgCl_2$ in the absence (*lanes 2, 8 and 14*) or in the presence of SsbA: 1.5 to 24 nM, (*lanes 3 to 7*), 2 to 36 nM (*lanes 9 to 13*) and 6 to 24 nM (*lanes 15 to 17*), as tetramer. (**D**) Quantification of the % DNA unwound at 10 mM $MgCl_2$ as a function of the concentration of SsbA (nM) at 6 nM (*black triangles*), 9 nM (*red diamonds*) and 12 nM (*purple inverted triangles*) RecD2. B: boiled DNA at 100ºC, which represents the unwound product of the reaction. *: radiolabeled 5' end. (**B**) and (**D**) show a mean ± SD of three experiments.

concentrations of $MgCl_2$. Particularly, a constant stimulation on the helicase activity was observed at 2 mM $MgCl_2$ as the amount of SsbA increased (**Figure 35 A** and **B**). For instance, at 6 nM RecD2, ~40% pGEM-Hind24 structure was unwound, but the presence of 6 nM SsbA (ratio SsbA:RecD2 of 1), increased the fraction of DNA unwound to ~60%, and this proportion remained constant although the ratio SsbA:RecD2 was 2 or 4 (**Figure 35 A**, *lanes 12 to 17*, and **B**, *black triangles*). Nevertheless, the stimulation was more appreciable at 10 mM $MgCl_2$, in which the activity of RecD2 alone was lower than at 2 mM $MgCl_2$. The results showed that SsbA increased the unwound fractions especially when the ratio between SsbA:RecD2 was 1 (SsbA as tetramer and RecD2 as monomer) and the $MgCl_2$ concentration was 10 mM (**Figure 35 C** and **D**). As an example, at 6 nM RecD2 and 10 mM $MgCl_2$, ~10% DNA was unwound and this percentage increased up to ~40% with the addition of 6 nM SsbA (**Figure 35 C**, *lanes 2 to 7*, and **D**, *black triangles*). The amount of DNA unwound slightly decreased when the ratio SsbA:RecD2 was higher than 2 (**Figure 35 C**, *lanes 6, 7, 13 and 17*, and **D**, *black triangles*). These data suggest

that SsbA may enhance helicase activity in two different ways. From one side, at a protein ratio 1:1, there is a stimulation of the unwinding activity probably because protein:protein interaction. From the other side, the contribution of SsbA in the reduction of secondary structures from the ssDNA may facilitate the translocation and the helicase activity of RecD2. As observed in ATPase experiments, this effect is more visible at 10 mM $MgCl_2$, because this concentration of $MgCl_2$ stabilises dsDNA regions, so the action of SsbA is more noticeable.

4.4. Chapter 4: *B. subtilis* RecD2 in the context of DNA replication

4.4.1. RecD2 interacts with several replication proteins

It has been postulated that RecD2 might participate as an accessory helicase in DNA replication due to its interaction with SsbA, normally associated to the replication fork, in the absence of DNA damage (Costes *et al*., 2010; Walsh *et al*., 2014). *In vivo* experiments also showed that the *recD2* mutant in *B. subtilis* leaded to an increase in both replication fork collapse and unsegregated chromosomes (Walsh *et al.,* 2014; Torres *et al.*, 2017). However, the contribution of RecD2 to the DNA replication process remains unclear.

Further interacting partners of RecD2 in the context of DNA replication had not been previously described. In this work, the interaction between RecD2 and the replisome proteins was explored by the immuno dot-blot technique, similarly as done for the detection of RecD2-SsbA interaction (see section 4.3.1., Chapter 3). It has been observed that human HELB interacts with the DNA polymerase α-primase (pol-prim) (Taneja *et al*., 2002), equivalent complex to DnaE and DnaG proteins in *B. subtilis*. For that reason, the interaction between RecD2 and DnaE or DnaG was analysed. The results showed that RecD2 was able to interact *in vitro* with DnaE, but not with DnaG. On the other hand, human HELB is known to interact with some replication initiation proteins, such as Cdc45 and TOPBP1 (Gerhardt *et al*., 2015). Likewise, RecD2 was found to associate with DnaD, involved in the initiation of DNA replication in *B. subtilis*. Moreover, the PolC polymerase was also detected as interactant of RecD2, although this interaction seemed to be weaker. On the other hand, no interactions were observed with other components of the replisome, as all the subunits of the tau-complex (τ, δ and δ'), the β processivity factor, the replicative helicase (DnaC) and the other components of the helicase loading system (DnaI and DnaB) or the replication restart protein PriA, which also interacts with SsbA (Lecointe *et al*., 2007). A summary of the positive and negative interactions detected between RecD2 and the replisome components is shown in the **Figure 36**.

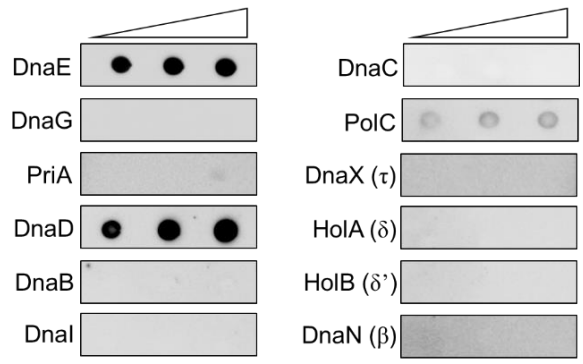

Figure 36. Interaction between RecD2 and replisome proteins.
Increasing amounts of the given replisome proteins (200 to 800 ng) were applied to a nitrocellulose membrane. RecD2-His (300 ng/ml) was added into the binding solution. The membrane was first treated with the primary antibody anti-6xHis (1:6,000) to detect the RecD2-His protein retained in the membrane by interaction, and then with the secondary antibody anti-IgG mouse conjugated with peroxidase (1:5,000). A representative membrane for each interaction is shown. The experiments were performed three times to validate the results.

4.4.2. RecD2 is a low abundant protein

Having observed connections between RecD2 and some replication proteins, before testing its putative effect in DNA replication with *in vitro* replication assays, the amount of RecD2 in the cell was quantified. Global transcriptome analysis had revealed that the levels of *recD2* transcripts were similar and comparable to the levels of replisome proteins transcripts, such as *priA*, *polC*, *dnaX*, *dnaC* or *dnaD* (Nicolas *et al*., 2012). However, the amount of protein had not been determined. Previous works about the analysis of the global proteome of *B. subtilis* did not detect the presence of RecD2, whereas other replisome proteins like SsbA were quantified (Muntel *et al*., 2014; Maaβ *et al*., 2014), implying that RecD2 may be a low abundant protein. According to this observation, the protein was not initially detected in cell extracts in this work. For that reason, RecD2-His was concentrated using a Ni-Sepharose column for the quantification of protein levels. *recD2$_{his6}$* cells, which express RecD2 fused to a 6xHis-tag from its natural promoter, were collected from a 250 ml culture grown until OD_{560} = 0.7 (~3.5 x 10^{10} cells). Then, the cells were lysed and centrifuged to separate the cell debris, and the soluble fraction was loaded onto a Ni-Sepharose column to concentrate the protein. The levels of RecD2 present in the elutions from the Ni-Sepharose were measured by a standard curve of increasing amounts of purified RecD2 protein (**Figure 37**). The results showed that the abundancy of RecD2 in the cell was low (~25 monomers/CFU) (Ramos *et al*., 2022).

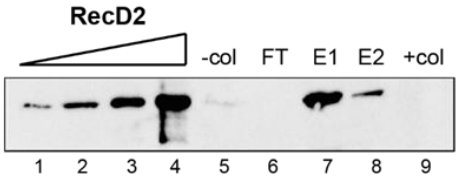

Figure 37. Measurement of RecD2 protein levels in the cell.
The *recD2$_{his6}$* cells were collected from a 250 ml culture grown until OD_{560} = 0.7. After the lysis, the cells were centrifuged and the supernatant (-col fraction, *lane 5*) was loaded onto a Ni-Sepharose column. The flow-through (FT, *lane 6*) represents the fraction with non-bound proteins to the Ni-Sepharose. RecD2 was eluted with two elutions of 100 µl of a buffer containing 200 mM imidazole (E1 and E2, *lanes 7 and 8*). The +col fraction (*lane 9*) shows the amount of protein retained into the Ni-Sepharose after the elutions. 30 µl of each fraction were separated on a 12.5% SDS-PAGE and Western blot analysis was performed for the detection of RecD2. The standard curve of RecD2 concentration was obtained loading increasing amounts of purified RecD2-His (6 to 50 ng) (*lanes 1 to 4*). The experiment was done three times to validate the result.

4.4.3. RecD2 may regulate replication restart

To elucidate the possible role of *B. subtilis* RecD2 in DNA replication, rolling circle assays were carried out as previously described in Sanders *et al*., 2010. This technique consists in an *in vitro* DNA replication reaction in which the used minicircular DNA template (409 bp) simulates a blocked or collapsed replication fork with a gap of 396 nt in the lagging strand (**Figure 38 A**). Furthermore, this DNA template contains a strong GC strand bias, so leading strand synthesis is visualised separately from the lagging strand synthesis, because radiolabeled dCTP

is incorporated mostly into the nascent leading strand, whereas radiolabeled dGTP is incorporated mainly into the nascent lagging strand (Sanders *et al*., 2010). In the *in vitro* DNA replication reactions, the DNA template was incubated with the proteins needed to reconstitute the *B. subtilis* replisome (the essential pre-primosomal PriA-DnaD-DnaB components, DnaI loader, DnaC helicase, PolC and DnaE polymerases, the clamp loader complex τδδ' (DnaX, HolA and HolB), the β-sliding clamp (DnaN) and DnaG primase), SsbA and increasing amounts of RecD2.

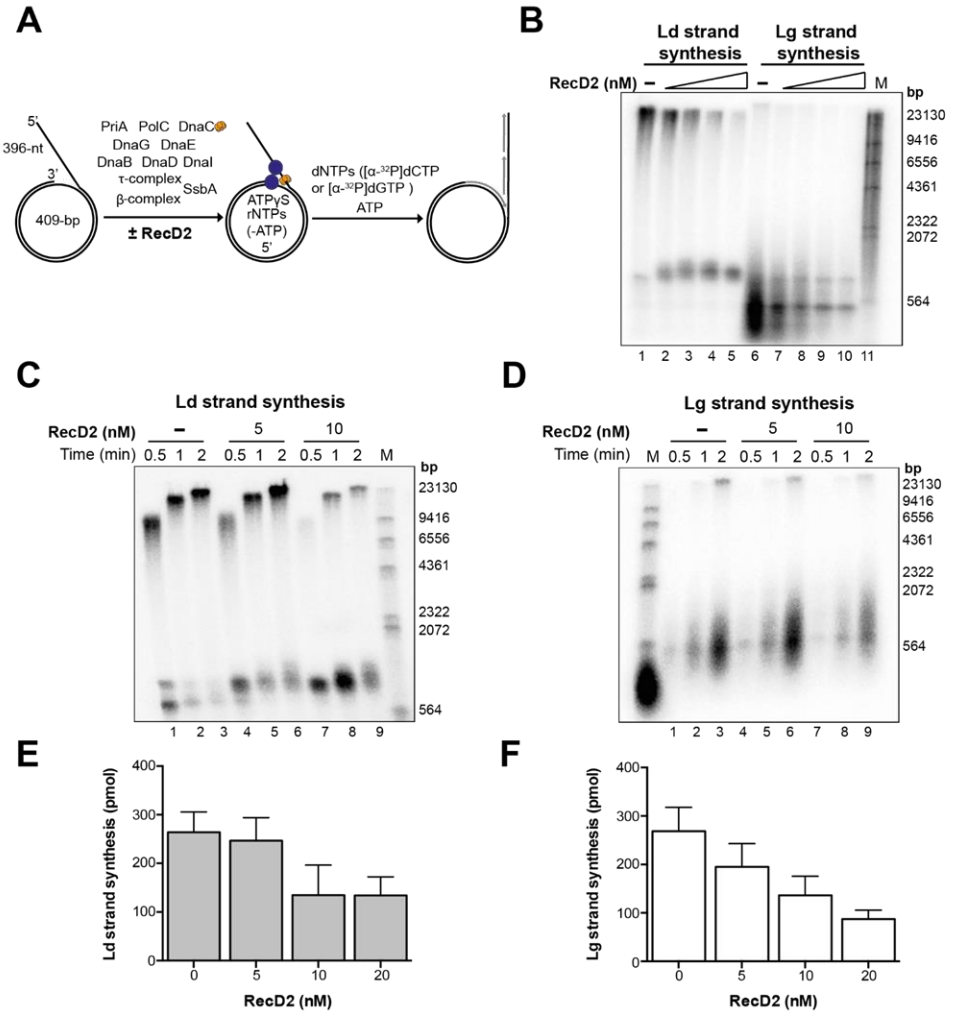

Figure 38. RecD2 modulates replication restart.
(**A**) Schematic representation of rolling circle DNA replication assay. The replisomes were assembled in the absence or in the presence of RecD2 onto the minicircular DNA template, which mimics a blocked replication fork with a gap in the lagging strand (396 nt), with the addition of 5 μM ATPγS. Reactions were initiated adding dNTPs and 1 mM ATP at 37ºC and stopped at certain times. Leading strand synthesis was visualised by the incorporation of radiolabeled dCTP, whereas lagging strand synthesis was visualised by the incorporation of radiolabeled dGTP. (**B**) Leading and lagging strand synthesis in the presence of increasing amounts of RecD2 (5 to 40 nM) after 2 min of reaction. (**C**) Leading strand synthesis at 5 and 10 nM RecD2 after 0.5, 1 and 2 min of reaction. (**D**) Lagging strand synthesis at 5 and 10 nM RecD2 after 0.5, 1 and 2 min of reaction. (**E**) Quantification of leading strand synthesis (pmol) obtained after 2 min of reaction in the absence or in the presence of 5 to 20 nM RecD2. (**F**) Quantification of lagging strand synthesis (pmol) obtained after 2 min of reaction in the absence or in the presence of 5 to 20 nM RecD2. Results are plotted as mean ± SD of five independent experiments. Ld: leading strand. Lg: lagging strand. M: radiolabeled λ-HindIII digested as molecular weight marker (bp).

The results showed that the presence of 5 nM RecD2 (ratio RecD2:DNA of 1) did not significantly affected the DNA synthesis, whereas increasing amounts (10 to 40 nM) highly reduced both, leading and lagging strand synthesis at 2 min of reaction in a dose-dependent manner (*p-values* < 0.01), suggesting that the inhibitory effect was dependent on protein concentrations. (**Figure 38 B**, **E** and **F**). The inhibition in DNA replication was also appreciable at shorter times of reaction (0.5 min and 1 min) (**Figure 38 C** and **D**). Taking into account these data, RecD2 could modulate replication restart on a blocked fork, probably preventing an aberrant initiation of DNA replication (Ramos *et al*., 2022).

As obtained in immuno dot-blot assays, RecD2 interacts with SsbA, PolC, DnaE and DnaD. PolC, DnaE and DnaD are essential proteins for DNA replication, because no DNA synthesis is obtained in the absence of any of them (Sanders *et al*., 2010). In contrast, SsbA is not essential for the *in vitro* DNA replication reaction, but DNA synthesis is substantially reduced without this protein (Seco and Ayora, 2017; Carrasco *et al*., 2018), as occurs in reactions lacking *E. coli* SSB (Antony *et al*., 2013). To test if the inhibitory effect observed in DNA replication assays with RecD2 was a consequence of some effect on SsbA or because of its interaction with other replisome proteins, *in vitro* DNA replication experiments were carried out without SsbA. According to previous works, DNA synthesis was less efficient when reactions contained all the replisome proteins except SsbA (**Figure 39**, compared to **Figure 38**). The results showed that in the absence of SsbA, RecD2 did not inhibit leading and lagging synthesis (**Figure 39 A**). Lagging strand synthesis was only reduced at 40 nM RecD2 after 2 min of reaction (**Figure 39 A**, *lane 10*). Non-significant effect was noticed at shorter times of incubation (0.5 min and 1 min) in both strands at 5 and 10 nM RecD2 (**Figure 39 B** and **C**). A slight increase in DNA synthesis was visualised in the presence of RecD2, but the observed differences were not statistically significant (*p-values* > 0.05) (**Figure 39 D** and **E**). These data suggest that the inhibitory effect of RecD2 on replication restart could be over the activity of SsbA, either promoting SsbA disassembly or preventing it to properly interact with other binding partners (Costes *et al*., 2010). To test the first hypothesis, *in vitro* DNA replication was assayed in the presence of RecD2 K373A, which has neither helicase nor translocase activity (see Chapter 2). In contrast to that observed with RecD2, increasing amounts of RecD2 K373A did not inhibit DNA replication in the presence of SsbA (**Figure 40**). Whereas at 40 nM RecD2 the DNA synthesis was strongly reduced in both leading and lagging strand, DNA replication was not affected at the same concentration of the mutant protein (**Figure 40**, *lanes 4, 7, 11 and 14*). This result supports the hypothesis that RecD2 disassembles SsbA molecules bound to the ssDNA via its translocation action along the ssDNA with the energy of ATP hydrolysis (Ramos *et al*., 2022).

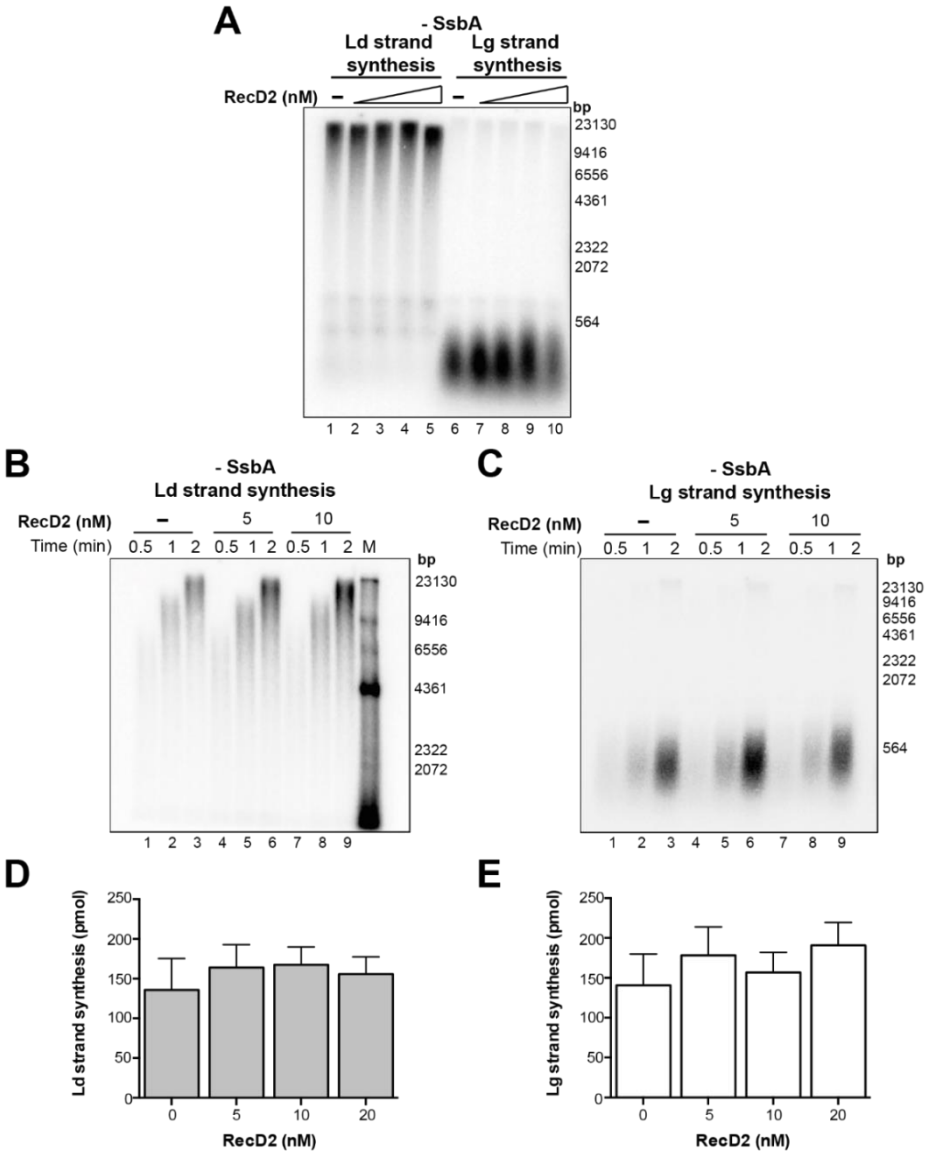

Figure 39. Action of RecD2 on replication restart in the absence of SsbA.
The replisomes without SsbA and in the presence of RecD2 were assembled onto the minicircular DNA template in a reaction buffer containing 5 µM ATPγS. Reactions were initiated by the addition of dNTPs and 1 mM ATP at 37ºC and stopped at certain times. Leading strand synthesis was visualised by the incorporation of radiolabeled dCTP, whereas lagging strand synthesis was visualised by the incorporation of radiolabeled dGTP. (**A**) Leading and lagging strand synthesis in the presence of increasing amounts of RecD2 (5 to 40 nM) after 2 min of reaction. (**B**) Leading strand synthesis at 5 and 10 nM RecD2 after 0.5, 1 and 2 min of reaction. (**C**) Lagging strand synthesis at 5 and 10 nM RecD2 after 0.5, 1 and 2 min of reaction. (**D**) Quantification of leading strand synthesis (pmol) obtained after 2 min of reaction in the absence or in the presence of 5 to 20 nM RecD2. (**E**) Quantification of lagging strand synthesis (pmol) obtained after 2 min of reaction in the absence or in the presence of 5 to 20 nM RecD2. Results are plotted as mean ± SD of three independent experiments. Ld: leading strand. Lg: lagging strand. M: radiolabeled λ-HindIII digested as molecular weight marker (bp).

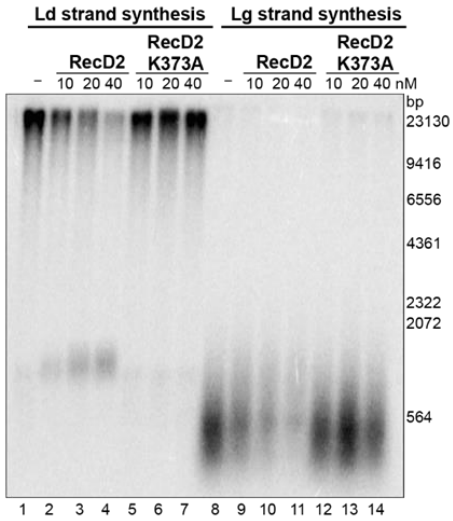

Figure 40. RecD2 K373A action on replication restart.
The replisomes containing SsbA were assembled with or without RecD2 or RecD2 K373A onto the minicircular DNA template in the presence of 5 μM ATPγS. Reactions were initiated by the addition of dNTPs and 1 mM ATP at 37ºC and stopped after 2 min of reaction. DNA replication was assayed in the absence (*lanes 1 and 8*) or in the presence of 10, 20 and 40 nM RecD2 (*lanes 2 to 4 and 9 to 11*) or RecD2 K373A (*lanes 5 to 7 and 12 to 14*). Ld: leading strand. Lg: lagging strand. Radiolabeled λ-HindIII digested was used as molecular weight marker (bp). The experiment was reproduced three times to validate the result.

4.4.4. Ongoing DNA replication in the presence of RecD2

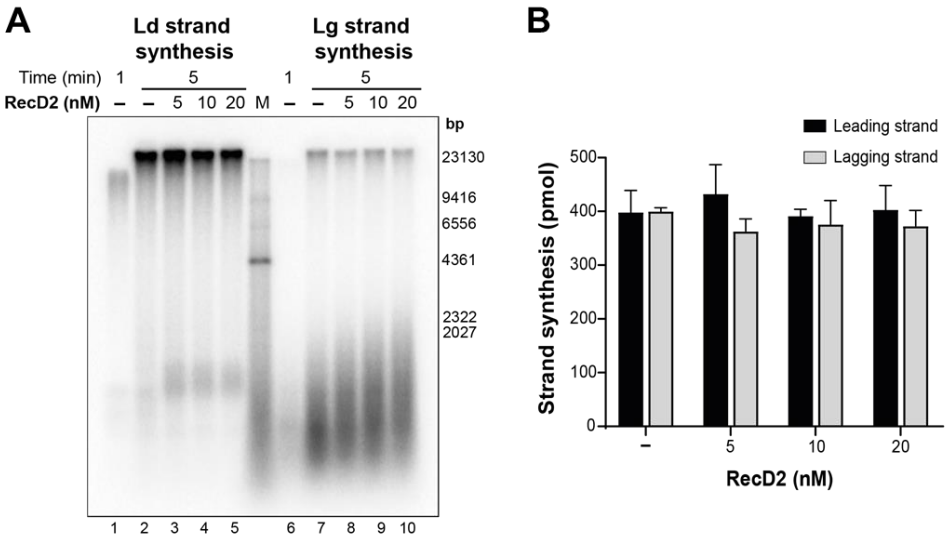

Figure 41. RecD2 does not affect ongoing DNA replication.
The replisomes were assembled onto the minicircular DNA template in the presence of 5 μM ATPγS. Reactions were initiated by the addition of dNTPs and 1 mM ATP at 37ºC. After 1 min, RecD2 was added and the reactions were stopped 5 min later. (**A**) Leading and lagging strand synthesis after 1 min (*lanes 1 and 6*) and 5 min of reaction in the absence (*lanes 2 and 7*) or in the presence of 5 to 20 nM RecD2 (*lanes 3 to 5 and 8 to 10*). (**B**) Quantification of DNA synthesis (pmol) plotted as mean ± SD of three independent experiments. Ld: leading strand. Lg: lagging strand. M: radiolabeled λ-HindIII digested as molecular weight marker (bp).

To explore the possible contribution in the course of the elongation step of DNA replication, the effect of RecD2 was tested during ongoing replication. Rolling circle assays were done as in the section above, but the complete replisome was first assembled on the DNA substrate and replication was allowed to start for 1 min. Then, increasing concentrations of RecD2 were added and DNA replication reactions continued for 5 min. The results showed that RecD2 did not affect the DNA synthesis, even at high protein concentrations, indicating that RecD2 might not

affect the progression of an unperturbed replication process (Ramos *et al*., 2022) (**Figure 41**). Nevertheless, increasing amounts of RecD2 promoted a slight increase in the length of the Okazaki fragments in the lagging strand (**Figure 41 A**, *lanes 8 to 10*).

4.4.5. RecD2 dynamics may be influenced by perturbations in DNA replication

In vitro replication assays showed that RecD2 might modulate replication restart on a blocked replication fork, preventing an aberrant initiation of DNA replication, and this inhibitory effect may be over SsbA (see section 4.4.3). It has been postulated that the interaction between RecD2 and SsbA may mediate the recruitment of RecD2 to the replication fork, also in the presence of DNA damage (Costes *et al*., 2010; Walsh *et al*., 2014). Similarly, human HELB localised *in vivo* to the chromatin through its interaction with RPA after the treatment of the cells with several DNA damaging agents (Guler *et al*., 2012). If RecD2 is constantly travelling with advancing replisomes or its dynamics is altered during perturbed DNA replication had not been explored.

The first experiments with a functional PolC-GFP fusion showed that rather than tracking along the DNA strands, the *B. subtilis* replisome is relatively stationary during replication and in cells with one replisome it is located at the midcell. Before cell division, two new replisome factories form (at 1/4 and 3/4 of the cell length) (Lemon and Grossman, 1998). However, single-molecule experiments have shown that there are movements that probably reflect the dynamics of a replisome in general. For example, the clamp loader protein DnaX engages in subtle motions confined within a small domain of ~100 nm (Liao *et al*., 2015). On the other hand, PolC is highly dynamic. This DNA polymerase is constantly recruited to and released from the centrally located replisome (Liao *et al*., 2016).

The dynamics of the RecD2 molecules under unperturbed replication and under different stress conditions was analysed by single-molecule microscopy with the use of the *recD2-mVenus* strain, which expresses RecD2 fused to mVenus fluorescent protein from its natural promoter in the *B. subtilis* chromosome (Romero, 2018). In this work, single-molecule tracking of RecD2-mVenus was performed to gain insight into its molecular diffusion pattern and its subcellular localisation in the absence of DNA damage and after the induction of replicative stress. The experimental conditions and the concentration of the drugs used were taken from previous single-molecule tracking experiments with other proteins from *B. subtilis* that showed effects in the localisation and the dynamics of the proteins, but not major effects in viability (Romero, 2018; Romero *et al*., 2019; Hernández-Tamayo *et al*., 2019; Hernández-Tamayo *et al*., 2021). We focused on treatments that had been use before in fluorescence microscopy experiments to perturb DNA replication: two DNA damaging agents (MMC and H_2O_2), the inhibition of replication by blocking PolC with the HPUra compound, and the inhibition of DnaG by (p)ppGpp after the

induction of the stringent response with serine hydroxamate (SHX) (Liao *et al*., 2016; Li *et al*., 2019; Romero *et al*., 2019; Hernández-Tamayo *et al*., 2019; Hernández-Tamayo *et al*., 2021).

Table 20. Summary of the total number of cells and RecD2-mVenus tracks analysed by single-molecule microscopy after the induction of DNA damage or replicative stress.

Condition	Number of cells	Number of cells with RecD2-mVenus tracks	Number of RecD2-mVenus tracks
No treatment	463	178	902
50 ng/ml MMC	317	96	810
100 ng/ml MMC	542	235	691
0.5 mM H_2O_2	521	191	465
50 µg/ml HPUra	410	148	500
5 mg/ml SHX	298	108	396

recD2-mVenus cells were grown until exponential phase and then treated with 50 or 100 ng/ml MMC, 0.5 mM H_2O_2 or 50 µg/ml HPUra for 1 h at 30ºC or with 5 mg/ml SHX for 15 min at 30ºC. Single-molecule microscopy was carried out for the detection of RecD2-mVenus tracks by excitation with a 514 nm laser. A total of 2,500 images were acquired with an exposure time of 30 ms.

The number of analysed cells and RecD2-mVenus tracks for each condition are shown in the **Table 20**. The number of cells presenting RecD2-mVenus tracks was around 30-40% in all the conditions tested. It was previously observed that ~30% of the *recD2-mVenus* cells showed fluorescence during exponential growth in epifluorescence microscopy. However, most of them presented a faint and diffuse pattern with no clear RecD2-mVenus foci (Romero, 2018), which is in concordance to the low abundancy of RecD2 (see section 4.4.2, Chapter 4) and the reduced number of RecD2-mVenus tracks obtained per cell (~2-8 tracks/cell) (**Table 20**). It should be noted that the number of tracks per cell is probably underestimated due to the photobleaching of the fluorescence during tracking acquisition.

Single-molecule experiments were performed during the stay of three months at the Dr. Peter Graumann's laboratory (Chemistry Department, University of Marburg, Germany), which is specialist in the study of the dynamics and the diffusion patterns of bacterial proteins at single-molecule level. Once the tracking of a fluorescent protein is acquired by single-molecule microscopy, the output data are processed and finally analysed by the SMTracker software that allows the quantitative and qualitative study of protein trajectories (Rösch *et al*., 2018) (see section 3.2.22., Methods). Gaussian mixture model was followed to fit the probability of the density distribution of the protein molecules. Two major populations were normally distinguished depending on the apparent diffusion coefficient (*D*): a static population with a slow diffusion (i.e. protein molecules interacting with or bound to the DNA) and a mobile population with a higher diffusion.

Previous authors explored the dynamics of several replisome proteins by single-molecule microscopy, such as PolC, DnaE, DnaG, DnaC or DnaX. During unperturbed exponential growth, PolC is highly dynamic and 55% of molecules had a slow or static behaviour (D_{static} = 0.120 ± 0.021 μm^2/s), whereas 45% showed a mobile diffusion (D_{mobile} = 0.930 ± 0.160 μm^2/s) (Hernández-Tamayo *et al*., 2019). Other authors observed similar PolC dynamics, although the diffusion values were different: D_{static} = 0.026 ± 0.005 μm^2/s and D_{mobile} = 0.5 ± 0.2 μm^2/s (Li *et al*., 2019). Comparable patterns were observed for the DnaE polymerase and the DnaG primase, although a slight reduction in the diffusion coefficients was noticed: D_{static} = 0.053 ± 0.005 μm^2/s and D_{mobile} = 0.750 ± 0.014 μm^2/s for DnaE, and D_{static} = 0.100 ± 0.005 μm^2/s and D_{mobile} = 0.880 ± 0.020 μm^2/s for DnaG (Hernández-Tamayo *et al*., 2021). In contrast, the replicative helicase DnaC showed a great increase in the static population (81%), indicating a more stable association with the replication machinery (Hernández-Tamayo *et al*., 2021). DnaX, which is frequently used as a marker of the position in the cell of the replisome, showed similar dynamics to DnaE or PolC, but its diffusion coefficients were substantially lower (D_{mobile} = 0.230 ± 0.008 μm^2/s and D_{static} = 0.029 ± 0.002 μm^2/s) (Hernández-Tamayo *et al*., 2019; Li *et al*., 2019), consistent with the previous observation that the DnaX movement is limited to a reduced domain of ~100 nm (Liao *et al*., 2015). The results obtained for RecD2-mVenus showed that 57% of the protein molecules had a slow diffusion (D_{static} = 0.033 ± 0.0002 μm^2/s), whereas 43% showed a mobile behaviour (D_{mobile} = 0.3 ± 0.0025 μm^2/s) (**Figure 42**, *green bubbles*). It should be noted that the diffusion coefficients obtained for RecD2 were considerably lower than the observed for several replication proteins and similar to DnaX, implying that RecD2 appears to be a low diffusive protein.

The dynamics of replication proteins had been analysed in the presence of DNA damage by other authors. Whereas the treatment for 1 h with 50 ng/ml MMC (crosslinks the DNA and leads to the production of one-ended DSBs) did not promote substantial effects in the diffusion pattern of the PolC and DnaE polymerases, DnaG and DnaC molecules became significantly more mobile (Hernández-Tamayo *et al*., 2019; Hernández-Tamayo *et al*., 2021). The interpretation of these data was that DNA replication is not blocked in the presence of this type of DNA damage, but the DNA synthesis is reduced to giving time for the DNA repair machinery. Consequently, DnaG and DnaC molecules may be more frequently exchanged from the replication fork than the polymerases (Hernández-Tamayo *et al*., 2021). Similar experiments were done with the *recD2-mVenus* cells using the same concentration of MMC. As observed for DnaE and PolC, the addition of 50 ng/ml MMC did not greatly change the dynamics of RecD2-mVenus and a slight increase in the mobile population was observed (48.3%) (**Figure 42**, *yellow bubbles*), as previously shown for PolC (Hernández-Tamayo *et al*., 2019). At higher concentration of MMC (100 ng/ml), RecD2 molecules were substantially more static than in the absence of DNA damage (66.3%). *recD2-mVenus* cells were also treated for 1 h with H_2O_2, a DNA damaging agent that produces oxidant

radicals and induces different types of DNA damage, like DNA breaks and crosslinks. After the treatment with 0.5 mM H_2O_2, the diffusion pattern of the RecD2 molecules was not considerably altered, and only a marginal raise in the static population was noticed (58.6%) (**Figure 42**, *orange bubbles*).

The diffusion pattern of RecD2-mVenus was studied after the treatment with chemical agents that induce replicative stress, like HPUra, which inhibits PolC (Brown, 1970). Previous authors showed that the treatment for 1 h with 50 µg/ml HPUra affected differently the dynamics of DnaE, DnaG and DnaC. A little increase in the mobile population of DnaE was noticed respect to the distribution observed during unperturbed growth, whereas the fraction of highly diffusive DnaC molecules strongly grew. In contrast, DnaG molecules became greatly static, suggesting that the blockage of PolC slows down the priming activity of DnaG or blocks it bound to the DNA (Hernández-Tamayo *et al*., 2021). Similar experiments were carried out with the *recD2-mVenus* strain at the same concentration of HPUra, showing a little increase in the mobile fraction of molecules (45.8%) respect to the absence of treatment, (**Figure 42**, *dark blue bubbles*), as previously observed with DnaE (Hernández-Tamayo *et al*., 2021).

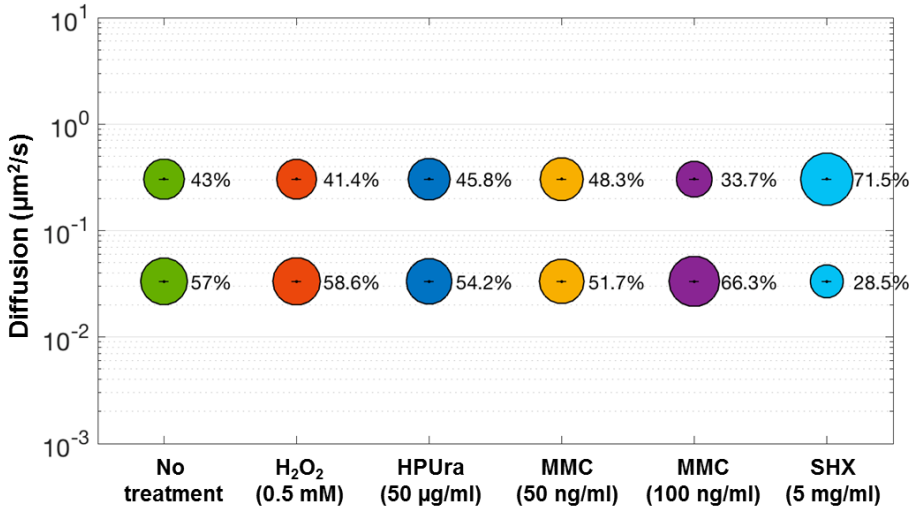

Figure 42. Diffusion patterns of RecD2-mVenus.
RecD2-mVenus tracking was acquired by single-molecule microscopy by excitation with a 514 nm laser after the treatment with 0.5 mM H_2O_2, 50 µg/ml HPUra, 50 or 100 ng/ml MMC or 5 mg/ml SHX. RecD2 molecules were classified in two populations depending on the diffusion (µm²/s) after the Gaussian mixture model analysis: mobile population (upper circles) and static population (lower circles). Bubble plots show a comparison of the population size (%) between the untreated and the treated cells.

SHX is an amino acid analogue that promotes the accumulation of uncharged tRNAs and induces the stringent response, leading to the (p)ppGpp production which inhibits the priming activity of DnaG (Wang *et al*., 2007). The effect of nutritional control of DNA replication by (p)ppGpp synthesised after the treatment for 15 min with SHX promoted severe changes in the dynamics of replication proteins. More than 85% of DnaE, DnaC and DnaG molecules were highly mobile, revealing an intense replisome disassembly (Hernández-Tamayo *et al*., 2021) that

leads to a stop in the cell growth (Wang *et al*., 2007). Likewise, 71.5% of RecD2-mVenus molecules showed a high diffusive pattern (**Figure 42**, *clear blue bubbles*). This result suggests that the majority of the RecD2 molecules may disengage from the DNA when the replisome disassembles probably because the protein may be associated to the replication fork machinery.

Table 21. Dwell times (τ_2) of RecD2-mVenus.

Condition	τ_2 dwell time (s)	Fraction τ_2 (%)
No treatment	0.40 ± 0.022	35 ± 3.7
50 ng/ml MMC	0.42 ± 0.027	32 ± 6.1
100 ng/ml MMC	0.57 ± 0.075	13.4 ± 1.9
0.5 mM H_2O_2	0.46 ± 0.035	34 ± 3.9
50 µg/ml HPUra	0.29 ± 0.016	51 ± 1.7
5 mg/ml SHX	0.84 ± 0.47	5.4 ± 2.7

Dwell times τ_2 (s) of RecD2-mVenus during normal exponential growth or after the treatment with 50 or 100 ng/ml MMC, 0.5 mM H_2O_2, 50 µg/ml HPUra or 5 mg/ml SHX, shown as mean ± SEM for at least 400 tracks with 5 steps for each condition in a defined confinement radius of 100 nm.

To further investigate the effect of perturbing DNA replication on the molecular dynamics of RecD2-mVenus, the dwell times, defined as the time that molecules remain in a specific area, were calculated for each condition by SMTracker. The dwell time of the RecD2 molecules was analysed within a radius of 100 nm for at least 5 steps in the tracks and estimated using a two-population decay function that distinguished two fraction of molecules: τ_1 and τ_2. Fraction τ_1 normally corresponds to free-mobile molecules that remain shorter times in that defined radius, whereas fraction τ_2 shows longer dwell times because the molecules are interacting with a particular subcellular structure or a molecular partner. Previous authors observed that the τ_2 dwell time of several replication proteins, like PolC, DnaE, DnaX or DnaC, decreased after the treatment with DNA damaging agents or the induction of replicative stress, implying a higher turnover or the disengagement of these proteins from the replication fork (Liao *et al*., 2016; Hernández-Tamayo *et al*., 2019; Hernández-Tamayo *et al*., 2021). The results for RecD2 showed the contrary effect. During unperturbed growth, ~35% of RecD2 tracks were included in the fraction τ_2, with a dwell time of 0.4 ± 0.022 s (**Table 21**). A slight increase in τ_2 dwell time was observed after the treatment for 1 h with 50 ng/ml MMC (~32% of tracks) or 0.5 mM H_2O_2 (~34%). The addition of 100 ng/ml MMC raised the dwell time ~1.4-fold respect to that obtained during normal growth (**Table 21**), consistent with the more static pattern visualised in the **Figure 42**. However, the treatment for 15 min with SHX produced a great increment in the τ_2 dwell time (~2-fold) (**Table 21**), but only ~5% of tracks showed a confined motion, in accordance to the high diffusive pattern observed in the **Figure 42**. In contrast, similar as observed in PolC, DnaE or

DnaC, the treatment with HPUra reduced the τ_2 dwell time (~1.4-fold) (**Table 21**), but the fraction of confined RecD2 tracks inside the 100 nm radius was higher than in the absence of any treatment (~51% of tracks). These data suggest that at 100 ng/ml MMC, RecD2 molecules became more static maybe due to their association with the DNA, as observed with the raised of the τ_2 dwell time. On the other hand, after the SHX treatment, the majority of the molecules were non-confined, in agreement with the high level of replisome disassembly after the induction of stringent response, and a few population of molecules showed a confined behaviour, probably because these confined molecules could be engaged in a process of replication restart.

4.4.6. Analysis of the subcellular localisation of RecD2

Due to the similarities in the diffusion pattern observed between RecD2 and some replication proteins, in addition to the dwell times obtained in the presence of perturbed DNA replication, the subcellular localisation of RecD2-mVenus was analysed during normal exponential growth or after the treatment with the drugs with the aim to elucidate if the protein remains close to replication forks or it is recruited during stress conditions. Epifluorescence microscopy determined that PolC-GFP foci localised in discrete intracellular positions, predominantly at the midcell, instead of their random distribution along the nucleoid region (Lemon and Grossman, 1998). On the other hand, single-molecule microscopy revealed some accumulation of PolC, DnaE, DnaG and DnaC molecules in the entire nucleoid, implying that these replication proteins are in fact very dynamic and are mainly distributed in this region (Hernández-Tamayo *et al*., 2019; Hernández-Tamayo *et al*., 2021). After the addition of MMC or HPUra, the subcellular distribution of these proteins did not substantially change. However, the treatment with SHX promoted a more peripheral position of DnaE, DnaG and DnaC molecules, maybe due to replisome disassembly. In addition, nucleoids appeared more decondensed after the induction of the stringent response (Hernández-Tamayo *et al*., 2021).

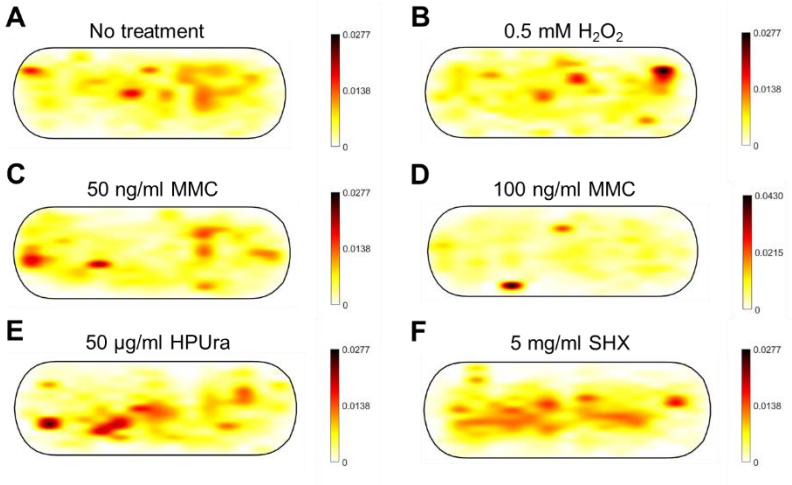

Figure 43. Spatial distribution of RecD2-mVenus in the *B. subtilis* cell.
2D heat maps summarising the localisation of the total number of RecD2-mVenus trajectories during (**A**) normal growth, or after the treatment with (**B**) 0.5 mM H_2O_2, (**C**) 50 ng/ml MMC, (**D**) 100 ng/ml MMC, (**E**) 50 µg/ml HPUra or (**F**) 5 mg/ml SHX.

The heat maps showed that during unperturbed growth, RecD2-mVenus was mainly localised in the nucleoid region, but with a diffuse distribution (**Figure 43 A**). After the treatment with the DNA damaging agents MMC or H_2O_2, the position of the molecules was not considerably altered, although a more disperse localisation was observed at 100 ng/ml MMC, maybe because RecD2 could contribute to DNA repair in regions outside the replication fork (**Figure 43 B-D**). On the other hand, the induction of replicative stress after the addition of HPUra or SHX resulted in a distribution closer to the centre, whereas lesser accumulation of RecD2 was visible in the periphery (**Figure 43 E** and **F**).

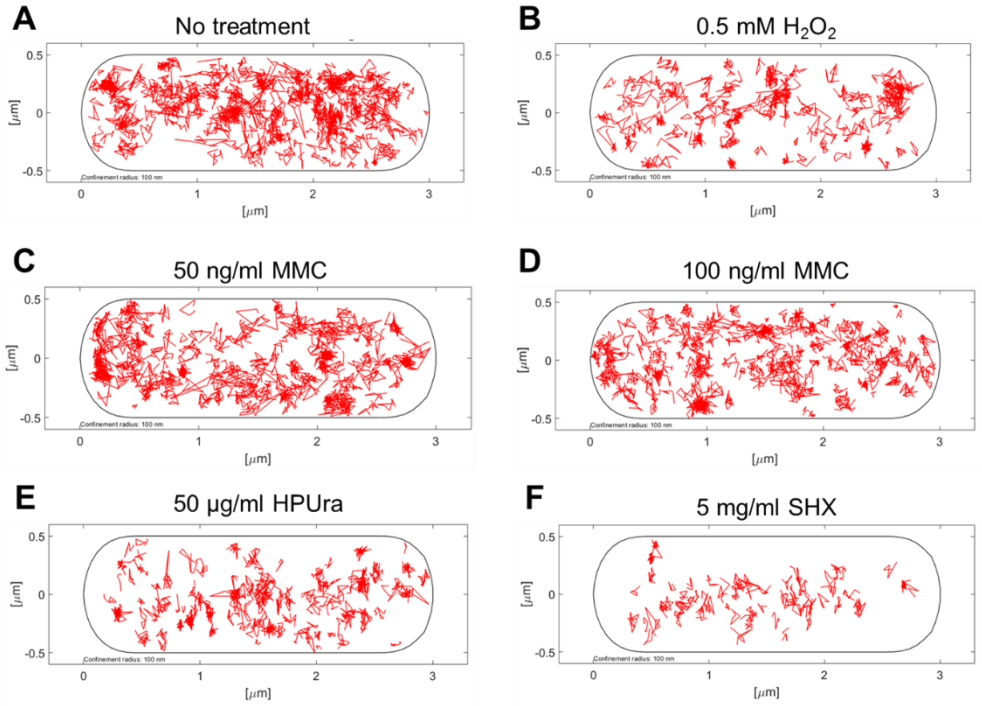

Figure 44. Subcellular localisation of confined RecD2-mVenus tracks.
Confinement maps showing the intracellular location of confined motion (tracks stayed inside a radius of 100 nm) of the RecD2-mVenus projected into a standard *B. subtilis* cell size (3 x 1 µm) during (**A**) normal growth, or after the treatment with (**B**) 0.5 mM H_2O_2, (**C**) 50 ng/ml MMC, (**D**) 100 ng/ml MMC, (**E**) 50 µg/ml HPUra or (**F**) 5 mg/ml SHX.

To obtain more information about the molecular distribution of the RecD2-mVenus molecules, RecD2 tracks were classified based on their dwell times within a radius of 100 nm. Confined motion was considered as molecules staying inside this radius and may occur when a protein has a restricted movement for an extended amount of time, which may be due to its interaction with the DNA or other proteins. Tracks that move outside this defined area were interpreted as free diffusive (non-confined) (Hernández-Tamayo *et al*., 2021). The confined RecD2-mVenus tracks obtained are shown in **Figure 44**. During unperturbed growth, 45% of the RecD2-mVenus trajectories showed a confined pattern with non-specific localisation in the cell, although some accumulations were observed in the centre and at 1/4 and 3/4, where the replisome machinery is supposed to be located (**Figure 44 A**). The treatment with 50 ng/ml MMC and 0.5 mM H_2O_2 reduced the confined fraction to 40% and 42%, respectively, whereas a slight increase

was noticed with 100 ng/ml MMC (47%). Similar proportion was acquired after the treatment with HPUra (46%), but SHX leaded to a great decrease in the confined tracks (25%), which is in agreement with the high dynamics observed with this chemical as shown in the **Figure 42**. In addition, the distribution of the confined tracks did not considerably change in the presence of DNA damage (**Figure 44 B-D**). In contrast, the induction of replicative stress with HPUra or SHX produced an accumulation of confined RecD2-mVenus tracks in the central region, more estimable after the treatment with SHX (**Figure 44 E** and **F**). These data support the hypothesis that RecD2 may accumulate in the nucleoid region probably associated to a stalled replication fork after the induction of a replicative stress by indirect inhibition of the replisome.

4.4.7. Study of the distance between RecD2 and the replisome

The results described in the section above suggested that RecD2-mVenus molecules were distributed mostly in the nucleoid with a non-specific position and accumulated in discrete subcellular regions when the replication process is compromised. To determine if RecD2 is associated to the replication fork or if there is a recruitment after the induction of replicative stress, the distance between the RecD2-mVenus tracks and the replisome was measured by using single-molecule microscopy. For that purpose, the *dnaX-cfp recD2-mVenus* strain was constructed. DnaX is part of the clamp loader complex ($\tau_3\delta\delta'$) and the DnaX-CFP fusion had been used in previous works as a marker of the replisome (Hernández-Tamayo *et al*., 2019; Hernández-Tamayo *et al*., 2021). In this work, the DnaX-CFP fusion was expressed ectopically from the *amyE* site of the *B. subtilis* chromosome and regulated with a xylose promoter. The ectopic expression of the fusion protein did not affect the viability (Hernández-Tamayo *et al*., 2019; Hernández-Tamayo *et al*., 2021).

Single-molecule microscopy was carried out as described in sections above during unperturbed growth or after the treatment with DNA damaging agents (MMC and H_2O_2) or the induction of replicative stress (HPUra and SHX). The position of the DnaX-CFP foci was first acquired by excitation with a 418 nm laser, which revealed the localisation of the replisomes. Then, RecD2-mVenus molecules were tracked by exciting with a 514 nm laser. The distances between the RecD2 trajectories and the DnaX-CFP foci were measured with SMTracker, which allows visualising the tracks of a protein molecule relative to a defined position in the cell, in this case the replisome. The number of analysed cells is shown in the **Table 20** (see section 4.4.5). 82.5% of the non-treated cells showed DnaX-CFP foci, but this percentage decreased after the treatments: 73.9% (50 ng/ml MMC), 51.8% (0.5 mM H_2O_2), 37.1% (100 ng/ml MMC) and 26.4% (50 µg/ml HPUra). After the incubation with SHX, less than 5% of cells showed DnaX-CFP foci, which indicated that the replisomes were mostly disassembled. For that reason, the distances could not be measured in that condition.

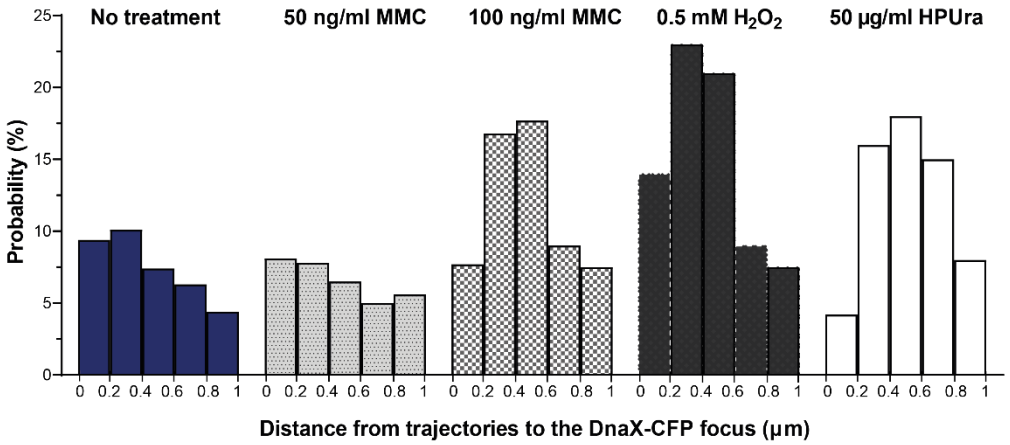

Figure 45. Localisation of RecD2 relative to the DnaX-CFP focus.
B. subtilis cells expressing DnaX-CFP, as a marker of the replisome, and RecD2-mVenus were grown at 30ºC until exponential phase. Then, MMC (50 or 100 ng/ml), H_2O_2 (0.5 mM) or HPUra (50 µg/ml) were added for 1 h. The DnaX-CFP foci were first detected exciting with a 418 nm laser and, then, the tracking of RecD2-mVenus molecules was acquired with a 514 nm laser. The histograms show the probability (%) respect to the distances from the RecD2-mVenus trajectories to the DnaX-CFP focus (µm) in a range between 0-1 µm.

The **Figure 45** shows the histograms that represent the probability of the distances of RecD2-mVenus trajectories to the location of DnaX-CFP in a range of 1 µm. The first bar, which represents the percentage of tracks that are in a distance between 0-0.2 µm, was assumed as the ones in which RecD2 and DnaX colocalised. In non-treated cells, ~9% of RecD2-mVenus trajectories colocalised with the DnaX-CFP foci, suggesting that RecD2 is not normally associated to the replication or its association occurs during short intervals of time. Similar distances were visualised after the treatment for 1 h with 50 ng/ml MMC and 100 ng/ml MMC, in which ~8% and ~7.5% of RecD2-mVenus colocalised with the replisome, respectively. However, at 100 ng/ml MMC, the tracks may get closer to the replication fork machinery than in the absence of DNA damage, because ~17% of the trajectories were distributed in a distance between 0.2-0.4 µm from DnaX-CFP compared to the ~10% observed in the absence of DNA damage. Interestingly, a recruitment of RecD2 was noticed after the treatment for 1 h with H_2O_2 and ~14% of the trajectories colocalised with DnaX-CFP. Moreover, more than 20% of RecD2 tracks localised closer to the DnaX-CFP foci (between 0.2-0.4 µm). In contrast, less colocalisation was observed with HPUra (~4%), although, similar as observed with 100 ng/ml MMC and H_2O_2, an approach to the replication machinery or to the site where forks had stalled was visualised (~16%). Taking into account all these data, most of the RecD2 molecules did not colocalise with the replisome, suggesting that its association with the replication machinery is very dynamic and transitory. The presence of certain types of DNA damage could promote a recruitment of this helicase or its approach to regions around stalled replication forks, maybe because RecD2 could participate in the repair of DNA lesions in these zones.

4.4.8. RecD2 dynamics is affected by defects in the replisome assembly

The dynamics of the RecD2 molecules was also analysed by single-molecule microscopy when the replisome assembly was defective. For that purpose, the RecD2-mVenus fusion was introduced in *dnaB37* or *dnaD23* thermosensitive backgrounds. DnaB and DnaD are involved in the initiation of DNA replication in *B. subtilis* at *oriC*, promoting the activation of DnaA and mediating the assembly of the replicative helicase DnaC to the origin of replication. DnaB and DnaD are also essential for PriA-dependent replication restart. Together with DnaI, DnaB and DnaD form the DnaC helicase loading system (Sanders *et al*., 2010; Jameson and Wilkinson, 2017; Beattie and Reyes-Lamothe, 2015). Because both proteins are essential, temperature sensitive mutants were used, as described in Alonso *et al*., 1988. The experiments at non-permissive temperature (42ºC) showed that the *dnaB37* Δ*recD2* and *dnaD23* Δ*recD2* double mutant strains were as sensitive as *dnaB37 rec*$^{+}$ and *dnaD23 rec*$^{+}$, suggesting that RecD2 cannot bypass the helicase activity of DnaC, probably because it is not processive enough. To gain insight into the contribution of RecD2 in this context, single-molecule microscopy was carried out with the *recD2-mVenus dnaB37* and *recD2-mVenus dnaD23* strains. The cells were grown at 30ºC (permissive temperature) until reach exponential phase. Then, the cells were grown for 1 h at 30ºC or at 42ºC (non-permissive temperature). The tracking of RecD2-mVenus molecules was acquired by a 514 nm laser using a temperature controller in the microscope to guarantee a stable temperature, 30 or 42ºC, during track acquisition. The total number of analysed cells and RecD2-mVenus tracks for each condition is shown in the **Table 22**.

Table 22. Summary of the total number of cells and RecD2-mVenus tracks analysed by single-molecule microscopy in thermosensitive backgrounds.

	Background	Number of cells	Number of cells with RecD2-mVenus tracks	Number of RecD2-mVenus tracks
30ºC	***wt***	230	94	419
	dnaB37	423	151	485
	dnaD23	277	129	559
42 ºC	***wt***	264	73	321
	dnaB37	181	67	343
	dnaD23	280	91	447

recD2-mVenus cells with no thermosensitive (*wt*) or with thermosensitive backgrounds (*dnaB37* or *dnaD23*) were grown until reach exponential phase and then incubated for 1 h at permissive (30ºC) and non-permissive (42ºC) temperatures. Single-molecule microscopy was carried out for the detection of RecD2-mVenus tracks by excitation with a 514 nm laser. A total of 2,500 images were acquired with an exposure time of 30 ms.

Similar as observed in the section 4.4.5, two populations of molecules were distinguished in terms of the diffusion: a static fraction (D_{static} = 0.031 ± 0.0004 µm²/s) or a mobile population (D_{mobile} = 0.33 ± 0.0003 µm²/s). As expected, the distribution of the RecD2 molecules in the two populations did not substantially change in *dnaB37* or *dnaD23* at permissive temperature respect to the *wt* background, and ~50% of molecules showed a static or a mobile behaviour (**Figure 46 A**). In contrast, the pattern changed at non-permissive temperature, in which ~60-70% of RecD2 molecules became mobile in the thermosensitive strains, whereas the mobile fraction remained essentially constant in the *wt* background, with only a slight decrease compared to 30ºC (**Figure 46 B**). At non-permissive temperature, the process of DNA replication restart was impaired. Similar as observed after the treatment with SHX (see section 4.4.5), RecD2 molecules were more mobile when the replisome assembly was compromised, suggesting a dissociation of RecD2 from the DNA or a rapid exchange or turnover of the molecules.

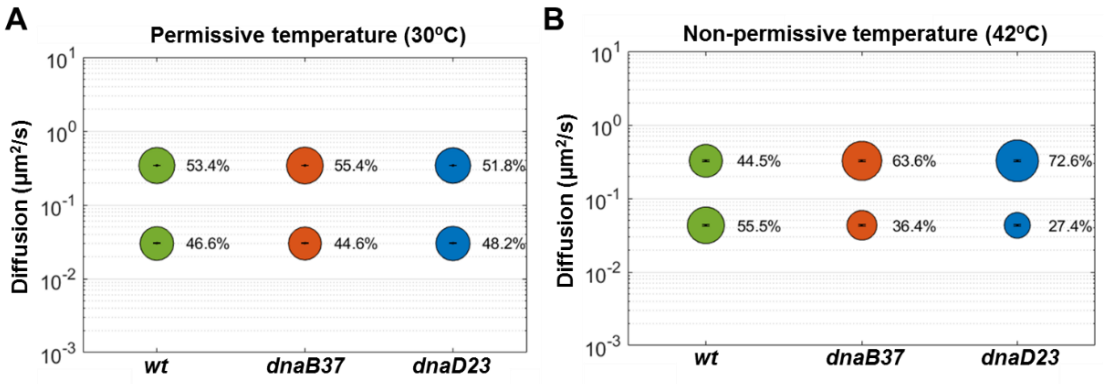

Figure 46. Diffusion patterns of RecD2-mVenus in *dnaB37* or *dnaD23* thermosensitive backgrounds.
The dynamics of RecD2-mVenus without (*wt*) or with a thermosensitive background (*dnaB37* or *dnaD23)* was analysed by single-molecule microscopy after the growth at (**A**) permissive or at (**B**) non-permissive temperatures. The molecules were distributed in two populations depending on their diffusion (µm²/s) after a Gaussian mixture model analysis: mobile population (upper circles) and static population (lower circles). Bubble plots show the population size (%) for each condition.

The dwell times of the fraction τ_2 (confined fraction) for RecD2-mVenus were also calculated in the *dnaB37* and *dnaD23* mutations at permissive and non-permissive temperatures setting a confinement radius of 100 nm and at least 5 steps in the RecD2 trajectories (**Table 23**). As expected, no significant differences in the dwell times were observed between *wt*, *dnaB37* and *dnaD23* backgrounds at permissive temperature. In contrast, the dwell times considerably increased with the inactivation of DnaB or DnaD at 42ºC, similarly as obtained with SHX, implying that RecD2 molecules could remain more time associated to the DNA, probably because RecD2 could be engaged in some event of replication restart either at *oriC* or other chromosomal regions.

Table 23. Dwell times (τ_2) of RecD2-mVenus in *dnaB37* and *dnaD23* backgrounds.

	Background	τ_2 dwell time (s)
30ºC	***wt***	0.36 ± 0.012
	dnaB37	0.33 ± 0.009
	dnaD23	0.35 ± 0.022
42 ºC	***wt***	0.38 ± 0.013
	dnaB37	0.47 ± 0.039
	dnaD23	0.56 ± 0.055

Dwell times τ_2 (s) of RecD2-mVenus in *wt*, *dnaB37* or *dnaD23* backgrounds after the growth at permissive (30ºC) or non-permissive (42ºC) temperatures. The data are shown as mean ± SEM for at least 300 tracks with 5 steps for each condition in a defined confinement radius of 100 nm.

Due to the similarities observed between the treatment with SHX, which indirectly inhibits DnaG, and when there are defects in the replisome assembly, the subcellular localisation of RecD2-mVenus was explored in *dnaB37* and *dnaD23* backgrounds after the growth at 42ºC to see if the RecD2 molecules distributed similarly as after the induction of stringent response. In the *wt* background, some accumulation of RecD2 appeared in the midcell region, maybe because of more replication events at 42ºC than at 30ºC (**Figure 47 A**). After the inactivation of DnaB or DnaD, mainly a hotspot of RecD2 was visualised. In *dnaB37* background, this hotspot of RecD2 was close to the centre of the cell, whereas in *dnaD23* background, it was a bit displaced from the centre (**Figure 47 B** and **C**). This indicated that the helicase might accumulate in the nucleoid region close to the collapsed replication forks when DNA replication restart is needed.

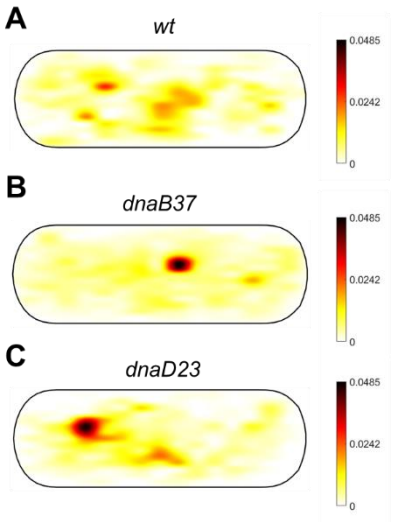

Figure 47. Spatial distribution of RecD2-mVenus after the inactivation of DnaB or DnaD.
2D heat maps summarising the localisation of the total number of RecD2-mVenus trajectories in (**A**) *wt*, (**B**) *dnaB37* or (**C**) *dnaD23* backgrounds after 1 h of incubation at 42ºC as non-permissive temperature.

4.5. Chapter 5: *B. subtilis* RecD2 balances RecA activities

4.5.1. RecD2 interacts with RecA

Because the deletion of the *recD2* gene in *B. subtilis* was lethal in combination with the absence of the branch migration translocases RuvAB or RecG, a function of RecD2 during the postsynaptic step of HR was suggested (Torres *et al*., 2017). Moreover, this work has revealed a crucial role of RecD2 in natural transformation processes, which are dependent on the HR machinery, in particular during interspecies chromosomal transformation and viral transfection (Serrano *et al*., 2020; Serrano *et al*., 2021; see Chapter 1). To gain insight into the possible contribution of RecD2 in HR, first, the interaction between this helicase and the RecA recombinase, which is the central player in this process, was explored by immuno dot-blot. Previous work had shown that the human HELB colocalised *in vivo* with Rad51 (the eukaryotic RecA), suggesting that both proteins might interact (Liu *et al*., 2015). The results showed that RecD2 interacts with RecA and, as observed with SsbA, this interaction may be independent of the presence of DNA (**Figure 48**) (Ramos *et al*., 2022).

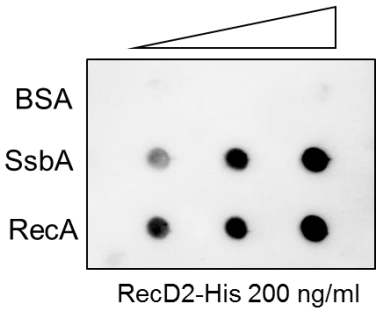

Figure 48. Interaction between RecD2 and RecA by immuno dot-blot.
Increasing amounts of BSA, SsbA and RecA (100 to 400 ng) were applied to a nitrocellulose membrane. RecD2-His (200 ng/ml) was added into the binding solution. The membrane was first treated with the primary antibody anti-6xHis (1:6,000) to detect bound RecD2-His protein and then with the second antibody anti-IgG mouse conjugated with peroxidase (1:5,000). The experiment was performed three times to validate the result.

4.5.2. RecD2 modulates DNA strand exchange

During HR, the RecA nucleoprotein filament formed on the ssDNA catalyses the DNA strand exchange reaction between two homologous sequences for the repair of a DSB or the integration of a homologous or homeologous sequence during chromosomal transformation. This process needs RecO and SsbA proteins for the proper polymerization of RecA onto the ssDNA, and is dependent of ATP hydrolysis (Carrasco *et al*., 2015). The putative effect of RecD2 in DNA strand exchange was analysed performing *in vitro* three-stranded exchange reactions in the presence of RecA, RecO, SsbA and an ATP regeneration system. The KpnI-linearised pGEM-3Zf (+) dsDNA (*lds*) and its homologous circular pGEM-3Zf (+) ssDNA (*css*) were used as DNA substrates for the strand exchange reactions. RecA, in the presence of RecO and SsbA, binds and filaments onto the circular ssDNA, and catalyses first the formation of three-stranded DNA structures (joint molecules, *jm*), which are DNA molecules with different degree of strand displacement. As final products of the strand exchange, the nicked circular DNA (*nc*) and the linear ssDNA (*lss*) are obtained. The effect of RecD2 in strand exchange reactions was tested at

two different moments: (i) at the beginning (added together with RecA, RecO and SsbA proteins), to analyse if RecD2 could modulate the formation of the RecA nucleoprotein filament on the ssDNA; (ii) after 20 min of reaction, to examine if RecD2 could branch migrate recombination intermediates and/or affect the nucleoprotein filament of RecA once is formed and strand invasion is catalysed (**Figure 49**).

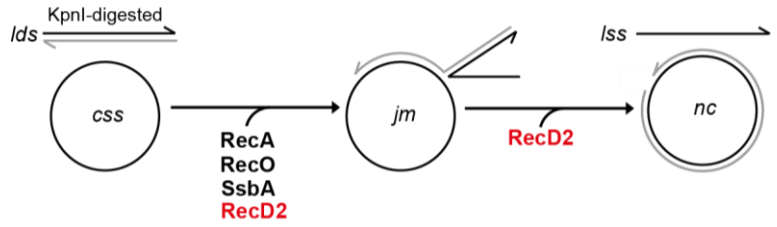

Figure 49. Schematic representation of the *in vitro* DNA strand exchange reaction.
The KpnI-linearised pGEM-3Zf (+) dsDNA (*lds*) and its homologous circular pGEM-3Zf (+) ssDNA (*css*) are incubated at 37ºC with RecA, RecO and SsbA. After the addition of ATP, joint molecules intermediates (*jm*) are initially formed. At longer times of incubation, the final products, which are the nicked circular (*nc*) and the linear pGEM-3Zf (+) ssDNA (*lss*), are obtained. RecD2 was added at two conditions: at the same time than RecA, RecO and SsbA (before starting the reaction with ATP) or after 20 min of reaction, in which the amount of *jm* accumulated.

Strand exchange reactions were started by the addition of ATP and incubated for 20 or 40 min at 37ºC. After 20 min of reaction, RecA catalysed the DNA strand exchange invasion and promoted mostly the accumulation of *jm* (~30%), which do not run as unique band, but at different positions in the agarose gel because they may have different degree of strand invasion and displacement. At this time of the reaction, *nc* and *lss* products were also obtained, but in a lesser extent (~15% of *nc*), (**Figure 50 A**, *lane 3*, and **B**). When increasing concentrations of RecD2 (1.5 to 50 nM) were added at time = 0 (at the same time than RecA, RecO and SsbA) and the reactions were incubated for 20 min, the fraction of *jm* decreased as the amount of RecD2 was higher. Moreover, a slight increase in the *nc* product formation was observed in the presence of 1.5 nM (~1.3-fold), 3 nM (~2-fold), 6 nM (~1.4-fold) and 12.5 nM (~1.3-fold) RecD2 (**Figure 50 A**, *lanes 7, 9, 11 and 13*, and **B**). Particularly, the amount of *nc* product was significantly higher at 3 nM (ratio RecD2:DNA of 1) (*p-value* = 0.023). At 25 nM RecD2 (ratio RecD2:DNA of 8.3), the production of both *jm* and *nc* products was reduced, (~20-fold and ~1.5-fold, respectively) and practically undetectable at 50 nM RecD2 (ratio RecD2:DNA of 16.7) (**Figure 50 A**, *lanes 15 and 17*, and **B**).

On the other hand, after 40 min of reaction, in reactions where only RecA, RecO and SsbA were present, the fraction of *nc* product increased ~2.7-fold respect to that observed after 20 min of reaction, whereas the amount of *jm* was reduced ~2-fold (**Figure 50 A**, *lane 4*, and **C**), implying that most of the substrate present was converted to final products of the strand exchange reaction after this time of incubation. When RecD2 was added together with RecA, RecO and SsbA at time = 0, no significant differences were observed after 40 min at 1.5 to 12.5 nM RecD2

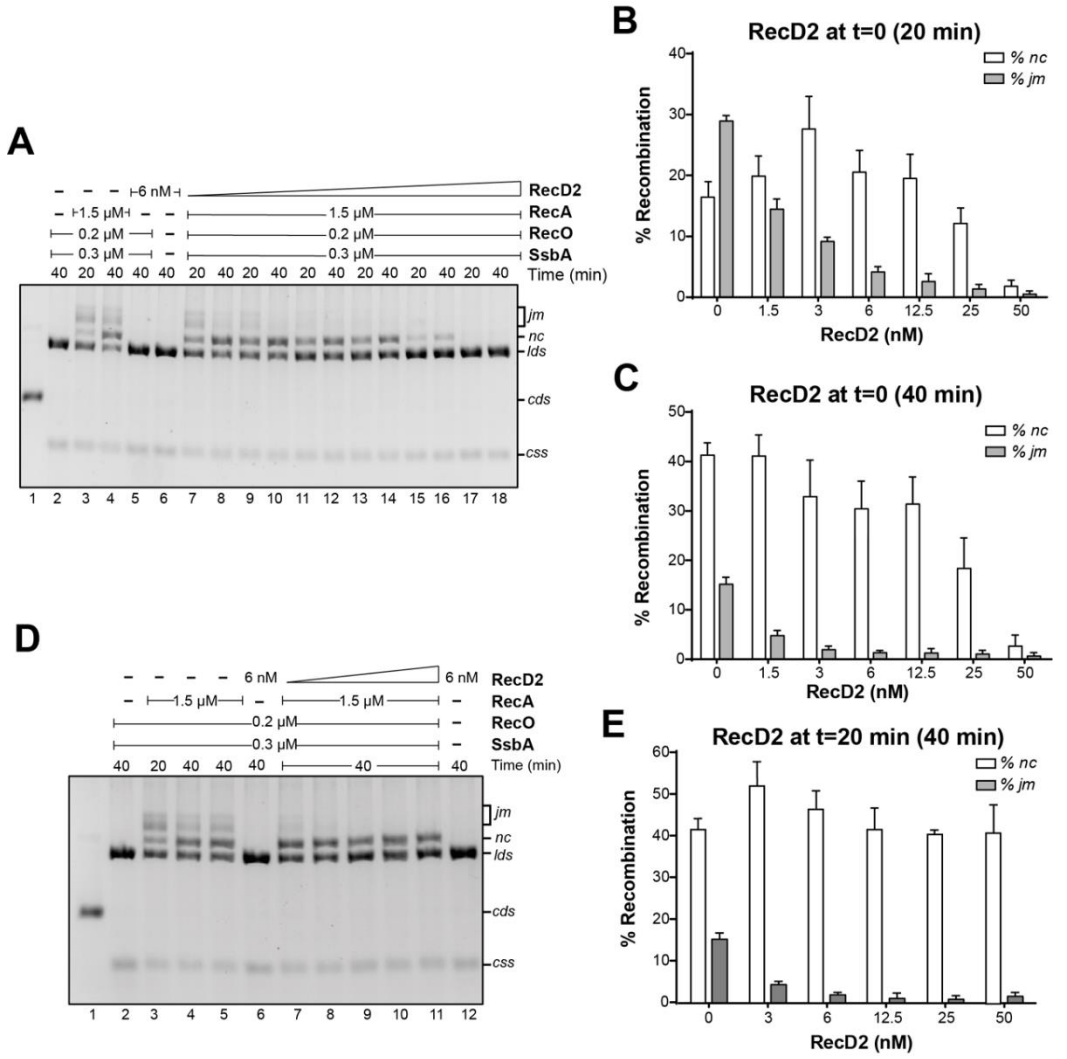

Figure 50. RecD2 modulates DNA strand exchange.
The KpnI-linearised pGEM-3Zf (+) dsDNA (*lds*) and its homologous circular pGEM-3Zf (+) ssDNA (*css*) (3 nM in molecules) were incubated at 37ºC in the presence of RecA (1.5 µM), RecO (200 nM as dimer) and SsbA (300 nM as tetramer). Reactions were started by the addition of 2 mM ATP and stopped after 20 or 40 min. (**A**) Strand exchange reactions in the absence (*lanes 3 and 4*) or in the presence of RecD2 at time = 0: 1.5 nM (*lanes 7 and 8*), 3 nM (*lanes 9 and 10*), 6 nM (*lanes 11 and 12*), 12.5 nM (*lanes 13 and 14*), 25 nM (*lanes 15 and 16*) and 50 nM (*lanes 17 and 18). Lane 1* shows a control with the running position of supercoiled and nicked DNA. *Lane 2* shows a control reaction with RecO and SsbA, but without RecA. *Lane 5* represents a control reaction with RecO, SsbA and RecD2, but without RecA. *Lane 6* is a control reaction with only 6 nM RecD2 added. (**B**) Quantification of the percentage of joint molecules intermediates (*jm, grey bars*) and nicked circular products (*nc, white bars*) after 20 min of reaction when RecD2 was added at time = 0. Results are plotted as the mean ± SD of three independent experiments. (**C**) Quantification of the percentage of *jm* and *nc* after 40 min of reaction when RecD2 was added at time = 0. Results are plotted as the mean ± SD of three independent experiments. (**D**) Strand exchange reactions in the absence (*lanes 4 and 5*) or in the presence of RecD2 added after 20 min of reaction (time = 20 min): 3 nM (*lane 7*), 6 nM (*lane 8*), 12.5 nM (*lane 9*), 25 nM (*lane 10*) and 50 nM (*lane 11*). *). Lane 1* shows a control with the running position of supercoiled and nicked DNA. *Lane 2* represents a control reaction with RecO and SsbA, but without RecA. *Lane 3* shows a strand exchange reaction after 20 min of incubation, time in which RecD2 was added. *Lane 6* represents a control reaction with RecO, SsbA and RecD2, but without RecA. *Lane 12* is a control reaction with only 6 nM RecD2 added. (**E**) Quantification of the percentage of *jm* and *nc* after 40 min of reaction when RecD2 was added at time = 20 min. Results are plotted as the mean ± SD of three independent experiments.

in the formation of *nc* products (*p-values* > 0.05), but the fraction of *nc* decreased ~2-fold at 25 nM RecD2 (*p-value* = 0.029) (**Figure 50 A**, *lanes 8, 10, 12, 14 and 16*, and **C**). Similarly as observed after 20 min of incubation, after 40 min of reaction, the RecA activity was strongly inhibited at 50 nM RecD2 and the fraction of *jm* was reduced and practically undetectable (*p-value* = 0.017) (**Figure 50 A**, *lane 18*, and **C**).

To examine a possible role in the late steps of the strand exchange reaction, the effect of RecD2 was analysed 20 min after the reactions had started and *jm* had been formed. In these experiments, RecA, RecO and SsbA were incubated with the DNA substrates (*lds* and *css*) and the strand exchange reaction was started by the addition of ATP. After 20 min, increasing amounts of RecD2 were added and the reactions continued for another 20 min, so the total reaction time was 40 min. In this case, the amount of *jm* intermediates was practically undetectable in the presence of RecD2, especially at 50 nM RecD2 (*p-values < 0.05*) (**Figure 50 D**, *lanes 7 to 11*, and **E**). Moreover, an increase in *nc* products was obtained at 3 nM RecD2 (*p-value* = 0.033), whereas no significant differences were observed at higher concentrations respect to the absence of RecD2 (*p-values > 0.05*) (**Figure 50 D**, *lanes 4, 5, 7 to 11*, and **E**). In contrast to when RecD2 was added at time = 0, the strand exchange reactions were not blocked at 50 nM RecD2, because *nc* products were produced with a similar yield than in the absence of RecD2.

In summary, the results showed that the effect of RecD2 in RecA-mediated strand exchange reaction was different depending on the moment in which the helicase was added and the protein concentration used. At the early step of the strand exchange reaction, low concentrations of RecD2 (RecD2:DNA ratios lower than 4) slightly facilitated the RecA activity, as observed in the amount of *nc* product formed, probably via branch migrating some recombination intermediates. In contrast, higher RecD2 concentrations inhibited the reaction, suggesting that RecD2 may negatively modulate the formation of the RecA nucleoprotein filament on the ssDNA. At a later step of the strand exchange reaction, the presence of RecD2 reduced the amount of the *jm* intermediates, so this helicase might branch migrate these structures facilitating their resolution. Furthermore, the reaction was not blocked even at high protein concentrations, implying that once RecA is engaged onto the strand exchange reaction, RecD2 cannot displace RecA and the strand exchange reaction is not inhibited (Ramos *et al*., 2022).

4.5.3. RecD2 reverses the inhibition of RecA on replication restart

Previous work showed that RecA, in concert with RecO, inhibits replication restart in an *in vitro* model of a blocked replication fork. The presence of RecA and RecO reduce both leading and lagging strand synthesis. Moreover, when *in vitro* replication reactions are performed without SsbA, RecA alone was sufficient to block DNA replication (Vlašić *et al*., 2013). Due to the observation of the physical interaction between RecD2 and RecA by immuno dot-blot, and the

modulatory action of RecD2 on the RecA nucleoprotein filament in the strand exchange reaction, the effect of RecD2 was tested on replication restart in the presence of RecA, to examine if this helicase was able to modulate the inhibitory effect of RecA.

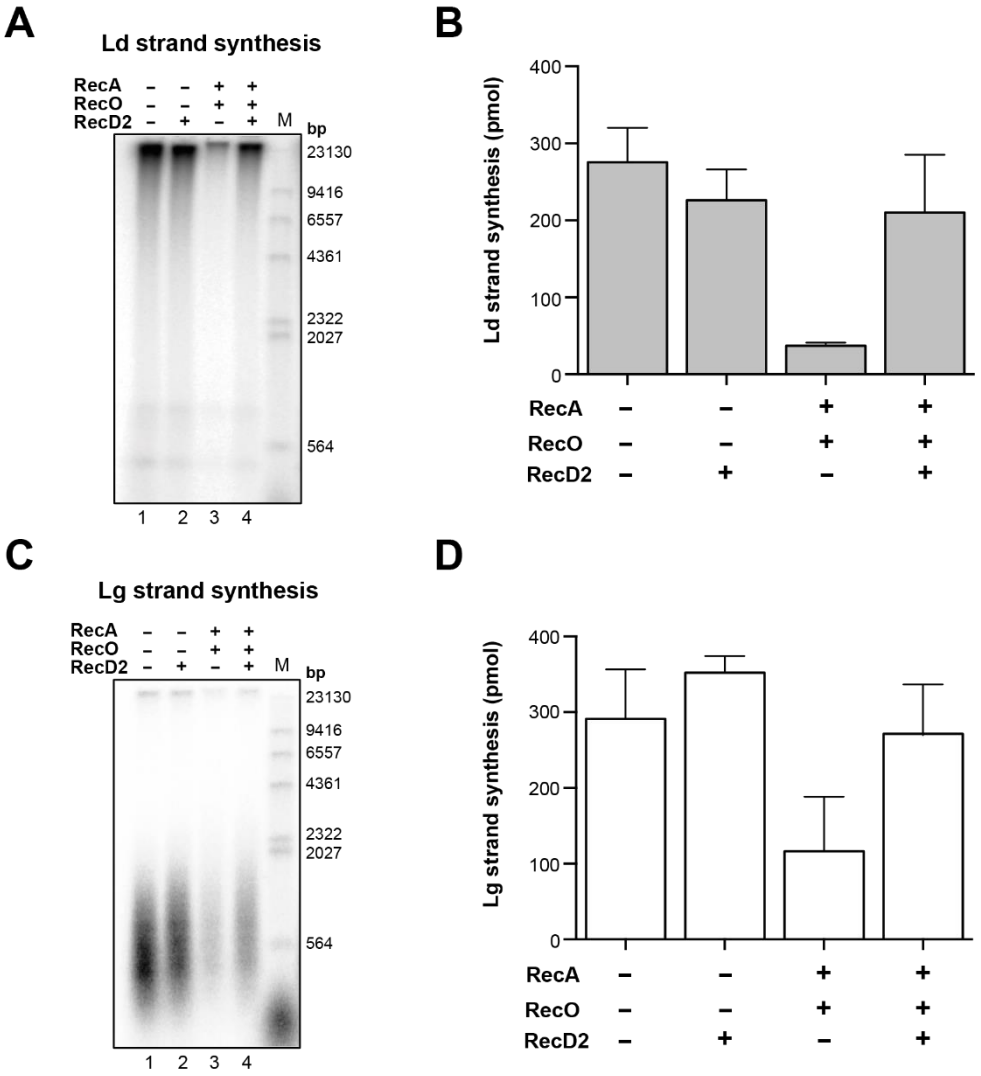

Figure 51. RecD2 overcomes the inhibitory effect of RecA on replication restart.
The minicircular DNA template (5 nM) was incubated with SsbA (90 nM as tetramer) in the absence or in the presence of RecD2 (5 nM), RecA (500 nM) and RecO (50 nM as dimer). Then, the replisome proteins were added and reactions were initiated by the addition of dNTPs and 1 mM ATP at 37ºC and stopped after 2 min. (**A**) and (**C**) Leading and lagging strand synthesis without (*lanes 1*) or with RecD2 (*lanes 2 and 4*) or with RecA and RecO (*lanes 3 and 4*). (**B**) and (**D**) Quantification of the leading and lagging strand synthesis (pmol) for each condition. Results are plotted as a mean ± SD of three independent experiments. Ld: leading strand. Lg: lagging strand. M: radiolabeled λ-HindIII digested as molecular weight marker (bp).

In vitro replication assays were carried out as previously described in section 4.4.3, but in the presence of RecA and RecO. The minicircular DNA template was first incubated 5 min with SsbA, RecD2, RecA and RecO and, then, the replisome was preassembled in the presence of ATPγS. Then, reactions started with the addition of dNTPs and ATP. After 2 min, the reactions were stopped and leading and lagging strand synthesis was analysed. As reported previously, the

presence of RecA and RecO significantly reduced DNA synthesis in both leading (*p-value* = 0.028) and lagging strands (*p-value* = 0.016) (**Figure 51 A** and **C**, *lanes 3*, **B** and **D**). 5 nM RecD2 (ratios RecA:RecD2 of 100 and RecD2:DNA of 1) was sufficient to bypass the inhibitory effect observed on DNA replication, with no significant differences respect to the reactions without RecA and RecO (*p-values* > 0.05) (**Figure 51 A** and **C**, *lanes 4*, **B** and **D**). This result suggested that RecD2 could promote the disassembly of RecA molecules from the ssDNA and thus, RecD2 may act as a negative modulator of the RecA nucleoprotein filament (Ramos *et al*., 2022). When similar experiments where done in the presence of the Walker A motif mutant, RecD2 K373A, the inhibition on replication restart by RecA and RecO was still observed (**Figure 52**, *lanes 6 and 12*). Hence, the ATP hydrolysis activity of RecD2 seems to be crucial for the clearance of RecA molecules bound to the ssDNA (Ramos *et al*., 2022).

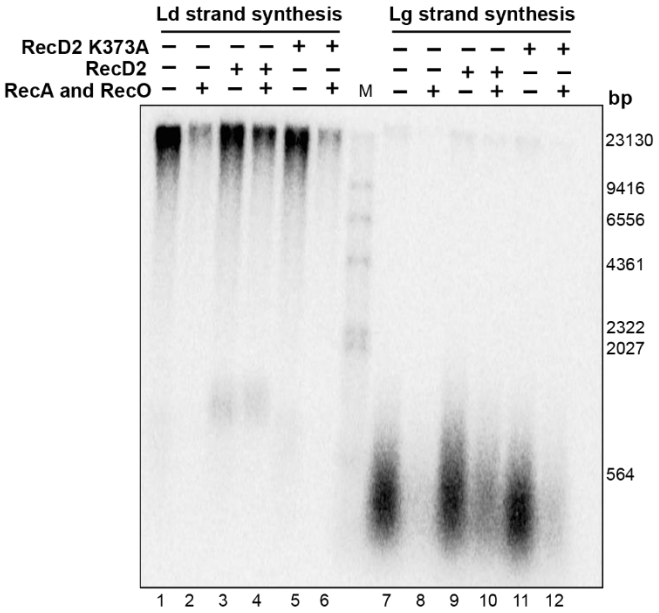

Figure 52. RecD2 K373A does not bypass the inhibitory effect of RecA on replication restart.
The minicircular DNA template (5 nM) was incubated with SsbA (90 nM as tetramer) in the absence (*lanes 1 and 7*) or in the presence of RecD2 (5 nM) (*lanes 3, 4, 9 and 10*), RecD2 K373A (5 nM) (*lanes 5, 6, 11 and 12*), RecA (500 nM) and RecO (50 nM as dimer) (*lanes 2, 4, 6, 8, 10 and 12*). Then, the replisome proteins were added and reactions were initiated by the addition of dNTPs and 1 mM ATP at 37ºC and stopped after 2 min. Ld: leading strand. Lg: lagging strand. M: radiolabeled λ-HindIII digested as molecular weight marker (bp).

In vitro replication reactions were also performed with RecA and RecD2, but in the absence of SsbA. In this context, RecA does not need RecO for the efficient loading onto the ssDNA (Carrasco *et al*., 2015). Without SsbA, RecA efficiently blocked the replication restart (**Figure 53 A** and **C**, *lanes 3*, **B** and **D**), as previously described in Vlašić *et al*., 2013. In this case, the presence of 5 nM RecD2 reversed the inhibitory effect of RecA in lagging strand synthesis. However, this recovery was lower in the leading strand synthesis when reactions contained RecD2 respect to the results obtained with RecA alone (**Figure 53 A** and **C**, *lanes 4*, **B** and **D**). This observation could be consistent with the fact that, due its translocation polarity (5' to 3'), RecD2,

as the replicative helicase DnaC, may translocate naturally along the lagging strand. For that reason, the clearance of RecA molecules by RecD2 might be more efficient during its translocation along the lagging strand (Ramos *et al*., 2022).

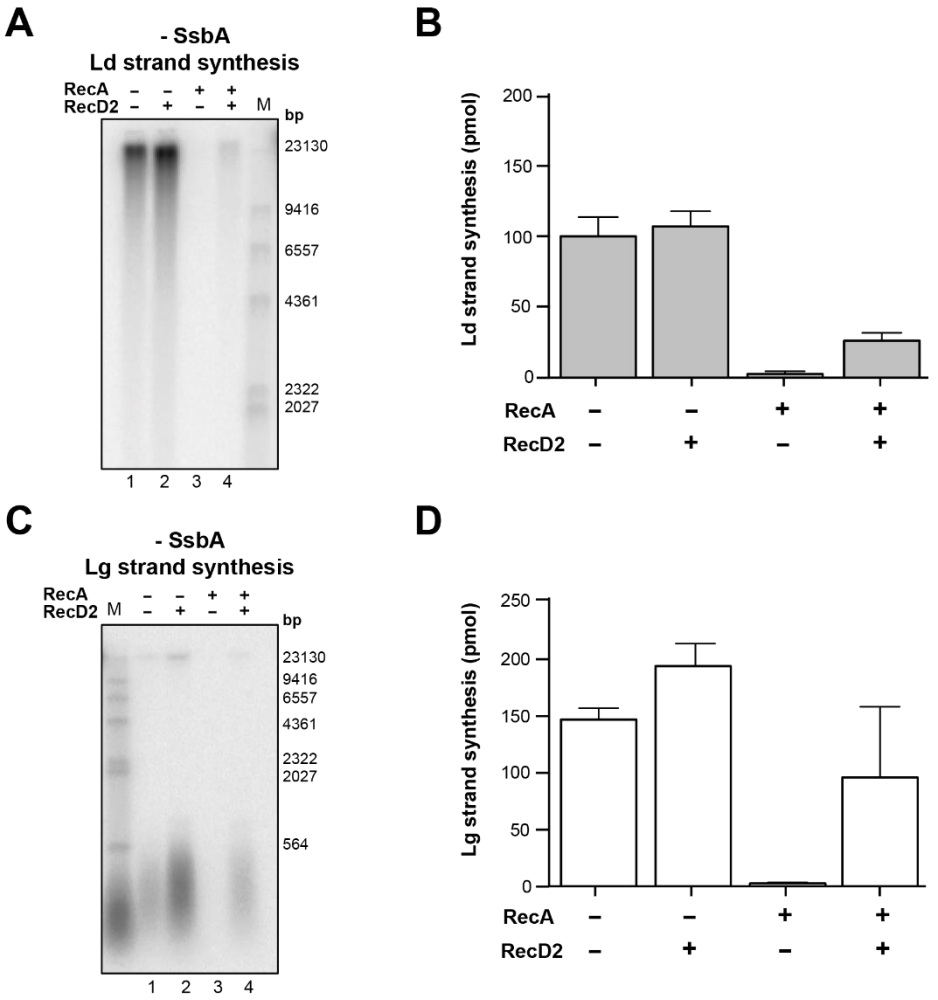

Figure 53. RecD2 still counteracts the inhibition of RecA on replication restart without SsbA at the lagging strand.

The minicircular DNA template (5 nM) was incubated without SsbA in the absence or in the presence of RecD2 (5 nM), RecA (500 nM) and RecO (50 nM as dimer). Then, the replisome proteins were added and reactions were initiated by the addition of dNTPs and 1 mM ATP at 37ºC and stopped after 2 min. (**A**) and (**C**) Leading and lagging strand synthesis without (*lanes 1*) or with RecD2 (*lanes 2 and 4*) or with RecA (*lanes 3 and 4*). (**B**) and (**D**) Quantification of the leading and lagging strand synthesis (pmol) for each condition. Results are plotted as a mean ± SD of three independent experiments. Ld: leading strand. Lg: lagging strand. M: radiolabeled λ-HindIII digested as molecular weight marker (bp).

4.5.4. RecD2 slightly displaces streptavidin blocks from the ssDNA

The results that are shown in the section above suggest that RecD2 might act displacing RecA molecules from the ssDNA, reverting the inhibition on DNA replication and, thus, promoting the replication fork progression. The ATP hydrolysis activity of RecD2 may be required, because the ATPase defective mutant, RecD2 K373A, did not revert the inhibitory effect of RecA. These observations are consistent with the results obtained in strand exchange reactions,

where RecD2, added at the same time than RecA, inhibited the reactions probably negatively modulating the RecA nucleoprotein filament formation. Similar hypothesis has been postulated in this work for the action of RecD2 on SsbA during replication restart, because, as observed in the section 4.4.3, increasing amounts of RecD2 reduced DNA replication when SsbA was present, but this inhibitory effect was not observed in reactions performed with the full replisome and SsbA. Therefore, RecD2 could promote the clearance of SsbA molecules from the ssDNA in an ATP hydrolysis-dependent manner, because the presence of RecD2 K373A had no effect on DNA replication. Taking into account all these data, RecD2 would translocate along the ssDNA and may displace proteins that are bound.

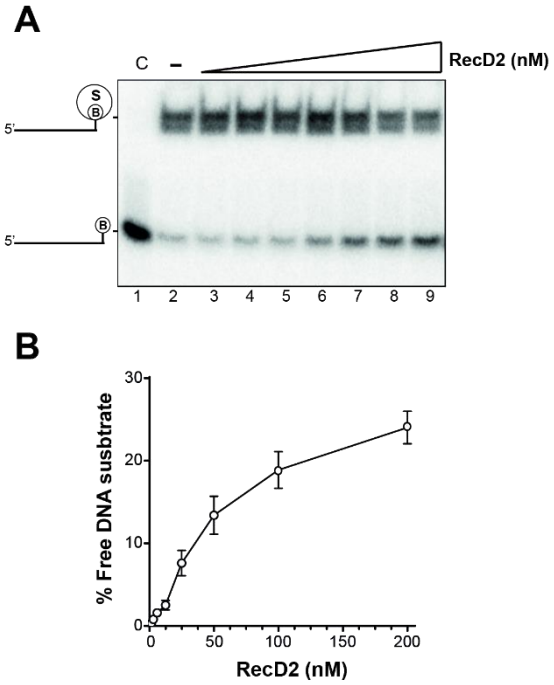

Figure 54. Streptavidin displacement from the ssDNA in the presence of RecD2.
(**A**) The biotinylated BioT-45 (0.25 nM) was radiolabeled and incubated with streptavidin (2.5 nM) for 5 min at room temperature. Then, increasing amounts of RecD2 were added: 3 nM (*lane 3*), 6 nM (*lane 4*), 12.5 nM (*lane 5*), 25 nM (*lane 6*), 50 nM (*lane 7*), 100 nM (*lane 8*) and 200 nM (*lane 9*). Biotin (50 nM) was also applied as a trap for the displaced streptavidin molecules. Reactions were incubated for 20 min at 37ºC and separated on 10% PAGE run in 1 X TBE. *Lane 1* represents the free biotinylated DNA without streptavidin bound. *Lane 2* shows the control reaction without RecD2. (**B**) Quantification of the percentage of free biotinylated DNA as a function of the concentration of RecD2 (nM). Results are plotted as the mean ± SD of three independent experiments.

The ability of RecD2 to displace protein blocks from the ssDNA was measured by biotin-streptavidin assays. The BioT-45 DNA, biotinylated at 3' end was used in the reaction due to the 5' to 3' translocation polarity of RecD2. The results showed that the amount of free biotinylated DNA (not bound to streptavidin) was practically undetectable at 3 to 12.5 nM RecD2 (**Figure 54 A**, *lanes 3, 4 and 5*, and **B**). Less than the 10% and 15% free biotinylated DNA was obtained at 25 nM and 50 nM RecD2, respectively (**Figure 54 A**, *lanes 6 and 7*, and **B**). At 100 and 200 nM RecD2 (ratios RecD2:streptavidin of 40 and 80, respectively), a marginal increase in the displacement of streptavidin molecules was observed, although the maximum percentage of free DNA obtained was only ~25% (**Figure 54 A**, *lanes 8 and 9*, and **B**). Given these data, RecD2 appears to have a reduced activity removing proteins that are bound to the ssDNA. Perhaps, the interaction between RecD2 and the bound proteins is crucial for an efficient displacement (Ramos *et al*., 2022).

4.5.5. RecA does not affect the helicase activity of RecD2

In both *in vitro* DNA replication and strand exchange assays, the effect of RecD2 on the activity of RecA was explored. To analyse the action of RecA on the activity of RecD2, helicase assays were carried out in the presence of RecA. RecA had not any effect on the unwinding activity of RecD2 with the fork 30-30 (not shown). Therefore, the pGEM-Hind24 structure was used as DNA substrate to allow the simultaneous binding of both proteins, as performed in helicase experiments with SsbA (section 4.3.3.2). RecA was added at non-saturating concentrations to avoid the competition of both proteins to the ssDNA, as done in strand exchange reactions and *in vitro* replication assays, being 200 nM the maximum concentration used in helicase assays. One molecule of RecA binds 3 nt, and the pGEM-Hind24 substrate contains 3,173 nt, so the amount of RecA required to saturate the ssDNA would be ~1 μM. Helicase experiments were performed at 2 and 10 mM $MgCl_2$ to test if the conformation of the ssDNA could have any effect. At 2 mM $MgCl_2$, helicase activity of RecD2 alone (6 and 12 nM) was more than 2-fold higher respect to the unwinding observed at 10 mM $MgCl_2$, similar to previous observations (see section 4.3.3.2) (**Figure 55**, *lanes 2 and 6*, compared to *lanes 11 and 15*). The addition of increasing concentrations of RecA (50 to 200 nM) did not significantly affect the helicase activity of RecD2, neither at 2 or 10 mM $MgCl_2$ (**Figure 55**, *lanes 3 to 5*, *7 to 9*, *12 to 14* and *16 to 18*). These results suggest that RecA might not affect the helicase activity of RecD2.

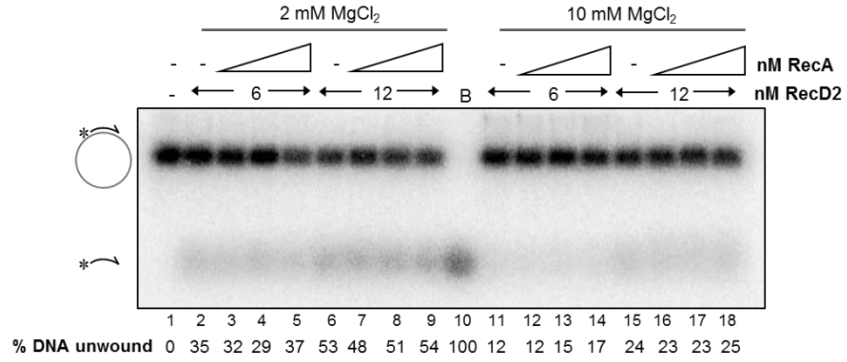

Figure 55. RecA does not alter the helicase activity of RecD2.
RecD2 was incubated for 5 min at 37ºC with RecA in a reaction buffer containing 50 mM Tris-HCl pH 7.5, 2 mM DTT, 0.05 mg/ml BSA and 0.25 nM of radiolabeled pGEM-Hind24. ATP (2 mM) was added and reactions were incubated for 10 min at 37ºC. After stopping the reactions (20 mM EDTA pH 8, 0.5% (v/v) SDS and 0.5 mg/ml proteinase K), DNA structures were separated on 1.2% (w/v) agarose gel electrophoresis run in 1 X TAE. Helicase activity of RecD2 at 6 nM (*lanes 2 to 5, and 11 to 14*) or 12 nM (*lanes 6 to 9, and 15 to 18*) in the presence of increasing concentrations of RecA: 50 nM (*lanes 3, 7, 12 and 16*), 100 nM (*lanes 4, 8, 13 and 17*) and 200 nM RecA (*lanes 5, 9, 14 and 18*). *Lanes 2 to 9*: activity at 2 mM $MgCl_2$. *Lanes 11 to 18*: activity at 10 mM $MgCl_2$. *Lane 1* is the control reaction without RecD2. The percentage (%) of DNA unwound in each reaction was shown as a mean of three independent experiments. B: boiled DNA at 100ºC, which represents the unwound product of the reaction. *: radiolabeled 5' end.

Because RecD2 interacts with SsbA and RecA, helicase experiments were performed in the presence of the three proteins to gain insight into the interplay of SsbA and RecA in the unwinding activity of RecD2. In these assays, two conditions were assayed: (i) the simultaneous incubation of the RecD2, SsbA and RecA with the radiolabeled pGEM-Hind24 for 5 min at 37ºC prior to start the reactions with ATP; (ii) the incubation of RecD2 and SsbA, together with the DNA, for 5 min at 37ºC before the addition of RecA and the initiation of the reactions. The experiments were also carried out at 2 and 10 mM $MgCl_2$ to examine the influence of the DNA conformation in the reactions.

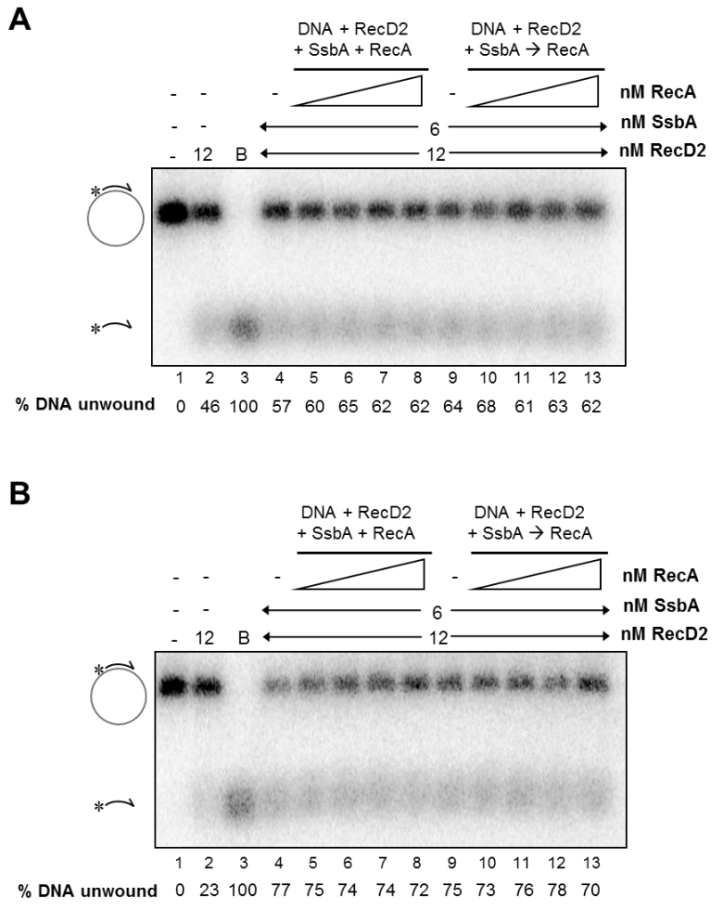

Figure 56. Helicase activity of RecD2 in the presence of RecA and SsbA.
RecD2 (12 nM) was incubated in the absence (*lanes 2*) or in the presence of 6 nM SsbA (*lanes 4 to 13*) or increasing concentrations of RecA: 25 nM (*lanes 5 and 10*), 50 nM (*lanes 6 and 11*), 100 nM (*lanes 7 and 12*) and 200 nM (*lanes 8 and 13*), in a reaction buffer containing 50 mM Tris-HCl pH 7.5, 2 mM DTT, 0.05 mg/ml BSA and 0.25 nM of radiolabeled pGEM-Hind24. ATP (2 mM) was added and reactions were incubated for 10 min at 37ºC. After stopping the reactions (20 mM EDTA pH 8, 0.5% (v/v) SDS and 0.5 mg/ml proteinase K), DNA structures were separated on 1.2% (w/v) agarose gel electrophoresis run in 1 X TAE. Two conditions were tested: incubation of RecD2, SsbA, RecA and the DNA for 5 min at 37ºC prior to initiate the reactions with ATP (*lanes 5 to 8*), or incubation of RecD2, SsbA and the DNA for 5 min at 37ºC before adding RecA and starting the reactions (*lanes 10 to 13*). *Lanes 1* are the control reaction without proteins. Reactions at (**A**) 2 mM and (**B**) 10 mM $MgCl_2$. The percentage (%) of DNA unwound in each reaction was shown as a mean of three independent experiments. B: boiled DNA at 100ºC, which represents the unwound product of the reaction. *: radiolabeled 5' end.

As reported in the section 4.3.3.2, SsbA enhanced the helicase activity of RecD2 with the pGEM-Hind24 substrate, especially at 10 mM $MgCl_2$, probably because SsbA may contribute in

the removal of secondary structures (**Figure 56 A** and **B**, *lanes 4 to 13*, compared to *lanes 2*). However, the presence of RecA did not significantly affect the unwinding action of RecD2, neither with or without SsbA at both $MgCl_2$ concentrations. In addition, no differences were observed between the two conditions of incubation (RecD2, SsbA and RecA together with the pGEM-Hind24 DNA, *lanes 5 to 8*; or RecD2 with SsbA and the DNA before adding RecA, *lanes 10 to 13*). A slight decrease in the unwound product was noticed at 10 mM $MgCl_2$ in the presence of 200 nM RecA, but the differences were not significant (**Figure 56 B**, *lanes 8 and 13*). These results conclude that RecA may not alter the unwinding activity of RecD2, suggesting that RecD2 might efficiently remove RecA molecules bound to ssDNA regions.

4.5.6. RecD2 interacts with RarA

As demonstrated in this work, RecD2 may act as an accessory helicase that modulates replication restart and regulates the RecA nucleoprotein formation. Another protein that has been reported as an accessory factor in these processes in *B. subtilis* is RarA, which, as RecD2, was identified as part of the SsbA interactome (Costes *et al*., 2010). RarA is an ATPase protein that may modulate replication restart in *B. subtilis* by preventing the initiation of DNA replication on blocked forks. Similar as observed with RecD2, increasing amounts of RarA inhibited DNA replication *in vitro* and this effect was not detected in the absence of SsbA (Carrasco *et al*., 2018). Moreover, RarA and RecD2 may regulate the filamentation of RecA onto the ssDNA, but with opposite functions. Whereas RarA acts as a positive modulator of RecA, promoting the formation of the nucleoprotein filament (Romero *et al*., 2020), RecD2 may contribute to the disassembly of the RecA molecules bound to the ssDNA (Ramos *et al*., 2020). For that reason, the interplay between RecD2 and RarA in the context of DNA replication and RecA regulation would be of interest. The interaction between both proteins was tested by immuno dot-blot, showing that RecD2 and RarA interact (**Figure 57**). Future experiments are needed to elucidate the possible joint of these two proteins in the context of DNA replication and HR.

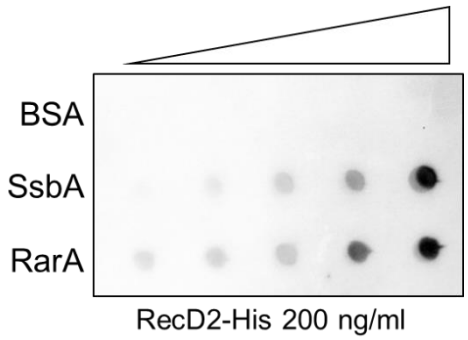

Figure 57. Interaction between RecD2 and RarA.
Increasing amounts of RarA (25 to 400 ng) were applied to a nitrocellulose membrane. The same amounts of BSA and SsbA were added as negative and positive controls. RecD2-His (200 ng/ml) was included into the binding solution. The membrane was first treated with the primary antibody anti-6xHis (1:6,000) to detect the RecD2-His protein retained in the membrane and then with the second antibody anti-IgG mouse conjugated with peroxidase (1:5,000). The experiments were performed three times to validate the results.

Discussion

5. Discussion

5.1. Translocation and unwinding requirements for *B. subtilis* RecD2

RecD2 helicases are proteins widely conserved in bacteria that lack the RecBCD complex. In spite of the structural similarities that RecD and RecD2 proteins share, their biological roles are different. Both RecD and RecD2 are SF1B helicases, which show 5' to 3' unwinding polarity (Saikrishnan *et al*., 2008; Montague *et al*., 2009; Saikrishnan *et al*., 2009). However, RecD2 proteins contain an N-terminal extension with unknown function (Saikrishnan *et al*., 2008). In addition, structural data support that RecD2 appears to act as a monomeric protein, whereas RecD is necessarily associated to RecB and RecC enzymes to be active (Masterson *et al*., 1992). In contrast to RecD, the study of RecD2 helicases had been practically unexplored, except for some works in *D. radiodurans*, and part of these works was done with an N-terminal truncated protein. In this work, the biochemical activities of *B. subtilis* RecD2 (simply named RecD2 here) have been thoroughly analysed (see Chapter 2).

DNA binding and translocation activities of RecD2 were characterised by measuring the ATPase rate of this protein in the presence of diverse DNAs as effectors. The presence of ssDNA substantially increased the ATPase activity of RecD2, as already observed in $RecD_{Eco}$ and $RecD2_{Dra}$ (Chen *et al*., 1997; Wang and Julin, 2004). The maximal activity was obtained especially with $polydT_{80}$, which does not contain secondary structures (**Figure 13** and **Table 16**). It supports that RecD2 prefers the binding and/or translocation along ssDNA without secondary structures. Likewise, human HELB, which shares similarities in sequence and function to bacterial RecD2, shows a higher ATP hydrolysis rate with $polydT_{70}$ than with ΦX174 ssDNA (5,386 nt), which contains secondary structures (Hormeño *et al*., 2022). On the other hand, this work found that RecD2 shows nucleobase bias with a preference for polydT (pyrimidine) rather than polydA (purine) for DNA binding and/ or translocation (**Figure 13** and **Table 16**). This tendency was also observed in helicase assays, in which the unwinding efficiency of RecD2 was considerably better with the fork 30-dT_{30} rather than the fork 30-dA_{30}, especially at low protein concentrations (below 12.5 nM) (**Figure 18**). There are diverse examples of helicases whose activity is affected for the sequence of nucleotides, such as human UPF1 (SF1), whose binding affinity to polydA appears to be lower than to polydT or polydU (Dehghani-Tafti and Sanders, 2017), or the viral NPH-II enzyme (SF2), with a strong purine sequence bias (Taylor *et al*., 2010).

In terms of ATPase rates, no considerable differences were observed between $polydT_{20}$, $polydT_{30}$, $polydT_{40}$ or $polydT_{60}$, with a global k_{cat} ~100 s^{-1} (**Figure 13 B** and **Table 16**). This result is in concordance to previous data from N-terminal truncated Δ150-$RecD2_{Dra}$ that determined a

k_{cat} = 98 ± 12 s^{-1} with polydTs of 20, 30, 40, 50 and 60 nt (Saikrishnan *et al*., 2009) and a k_{cat} = 86.9 ± 1.5 s^{-1} with polydT$_{20}$ (Toseland and Webb, 2013). This implies that the N-terminal extension of the RecD2 proteins may not be involved in ATP hydrolysis activity. However, at higher polydT lengths (70 and 80 nt), the ATPase rates increased more than 1.5-fold, whereas a slower rate was observed in the presence of polydT$_{15}$, with a reduction of ~1.8-fold respect to that global k_{cat} value (**Figure 13 B** and **Table 16**). Previous authors have also shown that the ATPase activity of RecD$_{Eco}$ is stimulated with a polydT of 221 nt and the hydrolysis decays more than 50-fold at shorter lengths (polydT$_{12}$) (Chen *et al*., 1997). The observed reduction in the k_{cat} can be explained because RecD2 may require a minimum site size for proper DNA binding. As observed in EMSA assays in this work, only one RecD2-ssDNA complex was visualised with polydT$_{20}$ because of the binding of just one RecD2 molecule (**Figure 24 D**). Similar result was obtained with polydT$_{30}$, but two RecD2-ssDNA complexes were formed in the presence of the ssDNA of 30 nt with random sequence at the same protein concentration, suggesting that the DNA structure also affects the binding of the protein (**Figure 24 A** and **D**). Moreover, at least three RecD2-ssDNA complexes were noticed with longer polydTs and ssDNAs with random sequence (**Figure 24 B**, **C** and **E**). These entire results suggest that one monomer of RecD2 may bind a site size between 15-30 nt. Larger ssDNA regions promote the binding of several RecD2 monomers and both translocation and unwinding are consequently enhanced. For that reason, ATPase and helicase activities were reduced with polydT$_{15}$ and the fork 30-16 (**Figures 13 B** and **18**), respectively. The crystal structure of the N-terminal truncated Δ150-RecD2$_{Dra}$ revealed that the protein is able to contact 8 nt (Saikrishnan *et al*., 2009), as described for SF1 helicases (Gilhooly *et al*., 2013). This work found that more site size is required for a stable interaction. Likewise, it was observed that human HELB requires a site size of ~20 nt for the binding, and an additional DNA binding site was assumed (Hormeño *et al*., 2022). RecD2, as HELB, could harbour a secondary DNA binding site that would explain the site size larger than 8 nt needed for the binding. Another possibility is that RecD2 could dimerise on the ssDNA and thus, protein-DNA complexes observed could be dimeric forms of the protein bound to the ssDNA instead of individual monomers.

The presence of secondary structures in the ssDNA also alters the activity of RecD2, and for that reason, the concentration of Mg^{2+} is crucial for its biochemical action. Both, ATP hydrolysis and helicase activities were reduced at high $MgCl_2$ concentrations (15 and 20 mM), and RecD2 showed the maximum activity at lower amounts of this cation (1 and 2 mM) (**Figures 14** and **17**). Similarly, RecD$_{Eco}$ exhibits more ATPase activity at 2 mM $MgCl_2$ than in the presence of greater concentrations (Chen *et al*., 1997). Whereas no substantial differences were observed between 2 or 10 mM $MgCl_2$ in the ATPase rates with polydT$_{80}$, the activity of RecD2 increased ~5-fold at 2 mM $MgCl_2$ respect to 10 mM with sspGEM-3Zf (+), which contains regions of

secondary structures (**Figure 14**). At 2 mM $MgCl_2$, sspGEM-3Zf (+) has a less condensed conformation and dsDNA regions diminish. This situation may favour the translocation of RecD2 along the ssDNA. Similar conclusion was obtained from helicase assays with the pGEM-Hind24 substrate, in which the unwinding activity at 6 nM RecD2 was ~3-fold higher at 2 mM than at 10 mM $MgCl_2$ (**Figure 35**). Furthermore, RecD2 binding to ssDNAs with random sequence showed also differences between 2 and 10 mM $MgCl_2$, obtaining ~3-fold greater affinities at lower magnesium concentration with ssDNAs of 60 and 80 nt (**Table 17**). The influence of Mg^{2+} on the activity of RecD2 helicases had not been examined in previous works, so these results contribute to understanding the optimal conditions for DNA binding, translocation and helicase activities of this protein.

The affinity of RecD2 to ATP was also characterised in this work. ATP hydrolysis experiments showed that RecD2 preferentially hydrolyses ATP rather than dATP (**Figure 13 A**). The affinity to ATP was not substantially dependent to the presence of ssDNA secondary structures and the Mg^{2+} concentration used. The assays carried out with polydT$_{80}$ and sspGEM-3Zf (+) at 2 and 10 mM $MgCl_2$ revealed comparable affinities to ATP (K_m between 100-120 µM ATP), although a marginal reduction in the affinity was obtained in the presence of sspGEM-3Zf (+) at 10 mM $MgCl_2$ (**Figure 15**). These results were different to previous data from the N-terminal truncated Δ150-RecD2$_{Dra}$ that found a K_m = 30.3 ± 1.5 µM ATP with a polydT$_{20}$ (Toseland and Webb, 2013). The discrepancies observed can be explained because of the experimental conditions, such as the temperature or the concentration of NaCl or the DNA used as effector in the reactions, or biological differences between both proteins. On the other hand, as visualised in EMSA assays, ATP binding was found to be important for DNA binding, because the presence of the non-hydrolysable ATP analogue, ATPγS, improved the RecD2-ssDNA interaction (**Figure 23**). Similar conclusion was obtained from the EMSA assays with the RecD2 K373A variant, whose ATP binding activity was defective (**Figure 26 B**).

Interestingly, this work found that RecD2 has a high preference for a non-replicated fork structure (fork 30-30), as determined in EMSA experiments, with a K_{app} = 2.1 ± 0.7 nM RecD2 (**Figure 26** and **Table 18**), close to the affinity values obtained for polydT$_{60}$, polydT$_{70}$ and polydT$_{80}$ (**Table 17**). On the other hand, the affinity to partially replicated forks (5' and 3'-forked substrates) decreased more than 5-fold compared to the non-replicated fork (**Figure 27** and **Table 18**), probably because these structures contain only one ssDNA region of 30 nt, whereas the fork 30-30 harbours two. Nevertheless, the helicase activity of RecD2 appears to be increased with the 5'-forked structure, in which the parental leading and lagging strands were entirely unwound at very low protein concentration, below 3 nM (**Figure 20**). In contrast, only ~40% of the fork 30-30 was unwound at 3 nM RecD2 (**Figures 18** and **19**). Furthermore, 3 nM RecD2 was sufficient to completely unwind the parental strands in the 5'-regressed fork, which contains a ssDNA gap

in the lagging strand, as the 5'-forked structure (**Figure 21 A**). Helicase activity of RecD2 in the presence of non-replicated forks containing dsDNA regions longer than 30 bp (40, 50 and 70 bp) was reduced as the length of the dsDNA increased, similar as previous observations in $RecD2_{Dra}$ (Wang and Julin, 2004). However, the presence of polydTs enhanced the unwinding activity, probably because the binding of RecD2 was better (**Figure 19**). Additionally, RecD2 efficiently bound 3' and 5'-invading D-loop structures, but with a reduction of ~2-2.5-fold respect to the non-replicated fork (**Figure 28**). RecD2 also showed an efficient helicase activity with the D-loops, promoting, from one side, the unwinding of the duplex region and, from other side, the removal of the invading strand (**Figure 22**). These entire results obtained in this work suggest that, in addition to non-replicated forks, as previously determined for $RecD2_{Dra}$ (Wang and Julin, 2004; Shadrick and Julin, 2010), partially replicated forks containing a gap in the parental lagging strand, as well as D-loops, may be potential targets for the RecD2 unwinding action *in vivo*.

5.2. SsbA interacts with and contributes to RecD2 activity

Previous authors had already determined that RecD2 interacts with SsbA (Costes *et al.,* 2010; Walsh *et al*., 2014). The results obtained in this work confirmed that purified RecD2 and SsbA interact *in vitro* with independence to the presence of DNA or any other factor (see Chapter 3, **Figure 29**). Furthermore, the absence of interaction between RecD2 and SsbB, which lacks the C-terminal extension present in SsbA, verified that this region of SsbA is probably crucial for the association. However, no ternary RecD2-SsbA-ssDNA complex was observed in the presence of ssDNA even after the addition of glutaraldehyde (**Figure 30 B**). This result was unexpected because the RecD2-SsbA association may occur mostly on the ssDNA, where SsbA is naturally bound. In fact, several proteins that interact with the single-stranded binding proteins require the presence of ssDNA for the association. For instance, the interaction between human HELB and RPA only was visualised when RPA was bound on the ssDNA (Hormeño *et al*., 2022). In spite of the interaction observed, the functional significance of the RecD2-SsbA interplay had not been explored so far. For that reason, the effect of SsbB and SsbA on the biochemical activities of RecD2 has been extensively analysed in this work (see Chapter 3).

The data obtained from ATP hydrolysis experiments showed that SsbB competes with RecD2 for the binding to ssDNA, regardless of the presence or the absence of secondary structures and the Mg^{2+} concentration (**Figures 31 B** and **32**). SsbA also reduced the ATPase activity of RecD2 when the ssDNA used as effector did not contain secondary structures, such as $polydT_{80}$, or these secondary structures are few abundant, like in sspGEM-3Zf (+) at 2 mM $MgCl_2$ (**Figures 31 A** and **33 A**). This observation was also unexpected because the interaction with SsbA normally enhances biochemical activities, as observed for PriA or RarA, whose ATP hydrolysis with ssDNAs harbouring secondary structures are stimulated in the presence of SsbA (Lecointe

et al., 2007; Carrasco *et al*., 2018). However, the Mg^{2+} concentration used in these experiments should be noted, because reactions were done at 5 mM Mg^{2+} for PriA and 10 mM Mg^{2+} for RarA (Lecointe *et al*., 2007; Carrasco *et al*., 2018), concentrations in which DNA secondary structures accumulate. Likewise, SsbA was found to stimulate the ATP hydrolysis activity of RecD2 in sspGEM-3Zf (+) at 10 mM $MgCl_2$ (**Figure 33 B**). The effect of SsbA was in a dose-dependent manner, suggesting that this protein contributes to the dissociation of secondary structures from the ssDNA and consequently facilitates the binding and translocation of RecD2. Moreover, the RecD2-SsbA interaction may be fundamental, because no stimulation in the ATPase activity of RecD2 was shown in the presence of SsbB at similar experimental conditions. In contrast to these observations, RPA was found to enhance the ATP hydrolysis activity of human HELB in the presence of ΦX174 ssDNA or a polydT$_{70}$ at 1 mM $MgCl_2$ (Hormeño *et al*., 2022), implying that, although RecD2 and HELB show functional similarities, some differences appear perhaps because of the evolutionary distance between both proteins.

On the other hand, helicase experiments with the addition of SsbA revealed that this protein inhibits the unwinding activity of RecD2 on very short substrates, containing ssDNAs of 30 nt, because of competition (**Figure 34**). The contrary effect was noticed with the long pGEM-Hind24 structure, obtaining a stimulation of the helicase action, mainly at 10 mM $MgCl_2$ and when the ratio was one monomer of RecD2:one tetramer of SsbA (**Figure 35**). This result supports that both the removal of ssDNA secondary structures by SsbA and the interaction with SsbA are crucial for the biochemical activities of RecD2. Taking into account all the data, SsbA may facilitate the association of RecD2 to the ssDNA *in vivo*, probably to the replication fork or other DNA structures containing ssDNA regions (i.e. D-loops). Single-molecule approaches like optical and magnetic tweezers would be interesting to analyse in more detail the biochemical interplay between both proteins.

5.3. The potential role of RecD2 in replication restart

RecD2 has been postulated as an accessory helicase in DNA replication because several observations. First, the interaction between RecD2 and SsbA during unperturbed growth suggests that RecD2 is regularly associated to the replication fork machinery (Costes *et al*., 2010). Second, the absence of RecD2 *in vivo* promoted an increase of replication fork collapse (Walsh *et al*., 2014) and the accumulation of unsegregated chromosomes (Torres *et al*., 2017). Third, RecD2$_{Dra}$ inactivated paused but not elongating replisomes in a heterologous model of replication fork (*E. coli*) *in vitro* (Gupta *et al*., 2013). Fourth, human HELB has been proposed to participate in the initiation of DNA replication due to its interaction with TOPBP1 and Cdc45 initiation proteins (Gerhardt *et al*., 2015). Hence, a role of RecD2 on replication restart was suggested. In this work, the study of RecD2 in the context of DNA replication was comprehensively examined.

It has been previously reported that the replisome stalls when a lesion is encountered, but it could remain engaged to the replication fork. This situation allows the continuity of DNA replication beyond the lesion in both leading and lagging strand templates, a mechanism known as lesion skipping, due to the action of the replicative helicase DnaC or another helicase in the 5' to 3' unwinding of the parental duplex, promoting the cycling of the polymerases (Yeeles and Marians, 2011; Marians, 2018). First observations in helicase assays determined that RecD2 might contribute in the processing of some stalled forks (see Chapter 2). The activity of RecD2 observed with the 5'-forked, that contains a gap in the parental lagging strand, showed that RecD2 may bind to the ssDNA gap present in the lagging strand template and translocate in a 5' to 3' direction unwinding the parental strands and thus, extending the ssDNA gap (**Figure 20**). Therefore, RecD2 may be acting as an accessory helicase supporting the unwinding activity of the replicative helicase. A gap in the lagging strand can be repaired with the annealing of the nascent leading and lagging strands by RecA-mediated template switching or with the remodeling of the stalled fork by fork reversal or regression, leading to replication restart (Marians, 2018).

A stalled replication fork can be remodeled to a HJ-like structure by the action of branch migration translocases as RecG and RuvAB (Atkinson and McGlynn, 2009; Gupta *et al*., 2014; Torres *et al*., 2021). Depending on the length of the nascent strands, several intermediates could be formed. If a gap is present in the lagging strand template and a longer nascent leading strand is produced, regression yields a partially 5'-regressed fork. In this structure, RecD2 could unwind the parental duplex, similarly as observed with the 5'-forked substrate (**Figure 21 A** and **D**). As concluded with the 5'-forked, the action of RecD2 here may be to support the unwinding action of the DnaC helicase and thus promote the re-initiation of DNA replication surpassing the lesion. On the other hand, if a gap is located in the leading strand template and a longer nascent lagging strand is formed, a partially 3'-regressed fork structure is created. In this situation, depending on the length of the ssDNA formed, RecD2 could bind to this 5'-ssDNA flap and unwind it, facilitating the processing of the regressed fork (**Figure 21 A** and **D**). Likewise, when a regressed fork contains an extended nascent lagging strand with a tail of 30 nt, RecD2 unwound the structure, although increased amounts of protein were needed, probably due to the length of the dsDNA regions (80 bp instead of 42 or 18 bp present in the partially regressed forks) (**Figure 21 C** and **D**). In contrast, RecD2 was not able to process HJ-like structures containing blunt ends, as expected because of the requirement of a 5' ssDNA for the binding to initiate unwinding (**Figure 21 B**). All these results provide different possible roles of RecD2 in replication restart. From one side, RecD2 may support the DnaC unwinding contributing to the initiation of DNA replication by lesion skipping when a gap in the lagging strand is present. From other side, RecD2 may contribute in the processing of regressed forks. Like RecD2, *B. subtilis* RadA/Sms unwinds regressed forks through its binding to the 5'-ssDNA flap of the longer nascent lagging strand

because of its 5' to 3' polarity. Interestingly, this helicase is also able to process regressed forks having a longer nascent leading strand that contains a 3'-ssDNA flap only in concert with RecA (Torres and Alonso, 2021). It may not be the case of RecD2, because its helicase activity was not affected in the presence of RecA, probably due to the clearance of RecA molecules during RecD2 translocation (see Chapter 5, **Figures 55** and **56**).

The study of RecD2 on replication restart was approached in this work with the use of an *in vitro* model of a blocked replication fork harbouring a gap in the lagging strand template (see Chapter 4). This model mimics a PriA-dependent replication restart (Sanders *et al*., 2010). The results showed that RecD2 inhibited replication restart when an excess of protein was added, but at concentration of one RecD2 molecule per DNA molecule, no effect was observed (**Figure 38**). $RecD2_{Dra}$ inhibited the resumption of DNA replication in a heterologous model of a stalled replication fork, but a ratio $RecD2_{Dra}$:DNA of ~50 was used in the assays (Gupta *et al*., 2013). Moreover, RecD2 did not alter the progression of an unperturbed replication (**Figure 41**), implying that this helicase might act during the initiation step of DNA replication. Similarly, RarA protein, which was found in this work to interact with RecD2 (see Chapter 5, **Figure 57**), inhibits replication restart *in vitro*, but does not alter replication progression (Carrasco *et al*., 2018). The low abundancy of RecD2 in the cell, as determined in this work by Western blot analysis (~25 monomers/cell) (**Figure 37**) and single-molecule microscopy (~2-8 RecD2 tracks/cell) (**Table 20**), suggests that the role of RecD2 *in vivo* may not be the inhibition of replication restart, but its modulation (Ramos *et al*., 2022). This work also showed that the inhibition observed in replication restart might be done over SsbA, because DNA synthesis was not affected in the absence of SsbA even at great amounts of RecD2 (**Figure 39**). Hence, RecD2 may catalyse the clearance of SsbA molecules bound to the ssDNA during its translocation along the lagging strand gap (Ramos *et al*., 2022). Likewise, human HELB catalyses the clearance of RPA molecules from the ssDNA (Hormeño *et al*., 2022). This hypothesis was demonstrated with the ATP-defective RecD2 mutant (RecD2 K373A), which did not inhibit replication restart in the presence of SsbA (**Figure 40**). The absence of SsbA promotes a less efficient DNA synthesis because it is required for the properly activity of several replisome proteins, such as the PolC and DnaE polymerases (Seco and Ayora, 2017), with which RecD2 interacts as detected by immuno dot-blot assays (**Figure 36**). Furthermore, in addition to SsbA, PolC and DnaE replisome partners, RecD2 can also interact with DnaD (**Figure 36**), a protein that, together with DnaB and DnaI, promotes the loading of the replicative helicase to the paused replication fork. Interestingly, human HELB interacts with the pol-prim complex (Taneja *et al*., 2002), equivalent to DnaE and DnaG, and with TOPBP1 and Cdc45, involved in replication initiation like DnaD (Gerhardt *et al*., 2015). Although it has been assumed that the interaction with SsbA is crucial for the association of RecD2 to the replication fork, the interaction with DnaD, PolC or DnaE could also facilitate its recruitment. A direct effect

of RecD2 on these replisome proteins could not be discarded, because RecD2 promoted a slight increase in the length of Okazaki fragments during replication elongation (Ramos *et al*., 2022) (**Figure 41**), a process that needs DnaG, PolC, DnaE and the replicative helicase activities. This effect had been observed before in reconstituted replisomes lowering the concentration of the DnaG primase (Sanders *et al*., 2010; Seco and Ayora, 2017). The importance of the interactions between RecD2 and PolC, DnaE and DnaD should be explored in future works to elucidate the interplay of these proteins during DNA replication.

Single-molecule analysis was used in this work to explore the dynamics of RecD2 molecules at real-time in the context of DNA replication and DNA repair *in vivo* (see Chapter 4). DnaX shows a slow diffusion, implying that it stays in a confined area and is used as a marker of the replication fork (Liao *et al*., 2015; Hernández-Tamayo *et al*., 2019). PolC, DnaE and DnaG are very diffusive proteins whose association to the replisome may be dynamic (Hernández-Tamayo *et al*., 2019; Li *et al*., 2019; Hernández-Tamayo *et al*., 2021). On the other hand, the replicative helicase DnaC appears to be a very static protein, maybe due to its stable binding to the replication fork structure (Hernández-Tamayo *et al*., 2021). PolA and ExoR, which are involved in the Okazaki fragment maturation (Duigou *et al*., 2005; Randall *et al*., 2019), are highly dynamic proteins, because more than 80% of the molecules show a mobile pattern (Hernández-Tamayo *et al*., 2019). This work found that, under unperturbed replication, RecD2 is a dynamic protein with a similar diffusion pattern to PolC, DnaE, DnaG, DnaX and RarA (Hernández-Tamayo *et al*., 2019; Hernández-Tamayo *et al*., 2021; Romero *et al*., 2019) (**Figure 42**), suggesting that it is recruited to and released from the replisome. Consistent with this result, less than 10% of RecD2 molecules trajectories were assumed to colocalise with DnaX-CFP foci (distance below 0.2 μm) (**Figure 45**). This was also observed for PolA and ExoR (Hernández-Tamayo *et al*., 2019). The analysis of the subcellular localisation of RecD2 showed that it was distributed in non-specific positions of the nucleoid region (**Figure 43 A**), as also occurs with PolA and ExoR (Hernández-Tamayo *et al*., 2019). However, some confined RecD2 molecules seemed to accumulate mostly in the centre of the cell and in the quarters (**Figure 43 A**), which represent the regions where the replication fork machinery is mainly positioned, as previously observed with PolC-GFP (Lemon and Grossman, 1998).

Single-molecule fluorescence microscopy analysis was performed also after DNA damage induction by the treatment with MMC and H_2O_2. The dynamics of RecD2 molecules only appears to be affected depending on the type of DNA damage that is produced, because just a noticeable increase in the static fraction was observed with 100 ng/ml MMC (**Figure 42**). In addition, the τ_2 dwell time was higher after the treatment with this chemical (**Table 21**), indicating that in the presence of 100 ng/ml MMC, RecD2 molecules could be mostly bound to the DNA contributing in the repair of the damage. In agreement with this, previous authors have shown that

recD2 mutants are more sensitive to MMC than to H_2O_2 (Walsh *et al*., 2014; Torres *et al*., 2017). Moreover, the subcellular localisation of the RecD2 molecules after the treatment with 100 ng/ml MMC appeared more diffuse than in the absence of DNA damage (**Figure 43 D**), suggesting that RecD2 could be in charge of some DNA repair events outside the replication fork machinery. The analysis of the distance between RecD2 and DnaX-CFP foci after the treatment with 100 ng/ml MMC showed that RecD2 trajectories significantly accumulated in vicinity regions of the replisome, probably contributing in the repair of lesions produced in these areas (**Figure 45**). Interestingly, the single-molecule analysis of the RarA dynamics also revealed changes after the induction of DNA damage. RarA molecules appear to be further from the replication fork machinery upon the treatment with MMC or H_2O_2, suggesting that, although RarA might be normally associated to the replisomes, also is recruited to other damaged regions (Romero *et al*., 2019).

The blockage of the PolC polymerase with HPUra may limit the formation of new replisome complexes (Liao *et al*., 2016). This work showed that the inhibition of PolC by the treatment with HPUra did not greatly affect the diffusion pattern of RecD2 compared to the absence of any treatment, and just a slight increase in the mobile fraction was noticed (**Figure 42**), similar as occurs with DnaE after HPUra addition (Hernández-Tamayo *et al*., 2021). However, a substantial decrease in the τ_2 dwell time was noticed (**Table 21**). This could be consequence of the interaction between PolC and RecD2, so the blockage of PolC could be related to less association of RecD2 to the replication fork. This observation could be in agreement with the ~2-fold reduction in the number of RecD2 trajectories that colocalised with the DnaX-CFP after the treatment with HPUra (**Figure 45**).

The most notable changes in the dynamics of RecD2 molecules were obtained after the induction of the stringent response by SHX, which promotes the production of (p)ppGpp that inhibits the DnaG primase (Wang *et al*., 2007). Replisome disassembly by SHX treatment is in accordance to the high fraction of DnaG, DnaE and DnaC molecules that became fast mobile (Hernández-Tamayo *et al*., 2021). In agreement with that, less than 5% of DnaX-CFP foci were observed in this work after the treatment with SHX, indicating that the replisome was mostly disassembled. This work observed similar behaviour of the RecD2 molecules to DnaG, DnaE and DnaC after the induction of stringent response (**Figure 42**), implying that this protein might be associated to the DNA, probably the replication fork machinery, despite its transitory interaction or its rapid exchange. However, whereas the confined DnaE, DnaG and DnaC molecules localise mostly in the periphery of the nucleoid region after SHX treatment (Hernández-Tamayo *et al*., 2021), the confined molecules of RecD2 appeared to stay closer to the midcell and 1/4 and 3/4 of the cell length (**Figures 43 F** and **44 F**), suggesting that they may be associated to certain nucleoid regions. In spite of the τ_2 fraction was much reduced (only ~5% of the RecD2 tracks), the τ_2 dwell

time was greatly elevated, even higher than after the treatment with 100 ng/ml MMC (**Table 21**). These results suggest that RecD2 molecules could be involved in some replication restart events after the induction of stringent response.

Because a role of RecD2 was thought in replication initiation and replication restart, single-molecule dynamics of this helicase was examined in *dnaB37* and *dnaD23* thermosensitive backgrounds. Both DnaB and DnaD are essential proteins in *B. subtilis* that mediate the initiation of DNA replication at *oriC* together with DnaA (Smits *et al*., 2011), or replication restart in concert with the PriA helicase (Polard *et al.,* 2002; Gabbai and Marians, 2010). The pre-primosomal DnaA-DnaB-DnaD or PriA-DnaB-DnaD complexes, together with DnaI, promote the binding of the replicative helicase DnaC to a ssDNA region and this allows the recruitment of the rest of replisome components to constitute the replisome (Sanders *et al*., 2010; Jameson and Wilkinson, 2017; Beattie and Reyes-Lamothe, 2015). The switch to non-permissive temperature (42ºC) leads to the inactivation of DnaB and DnaD. Consequently, replication initiation at *oriC* and outside *oriC* are impaired because of the defect in DnaC loading. Interestingly, after the incubation for 1 h at non-permissive temperature (42ºC), RecD2 molecules were considerably more mobile especially in the *dnaD23* background (**Figure 46 B**), similarly as occurred after the treatment with SHX. This suggest that RecD2 could be disassembled from the replication fork machinery or that there could be a rapid protein turnover. Furthermore, the τ_2 dwell time at non-permissive temperature was almost 2-fold higher in *dnaD23* background (**Table 23**). These results suggest that RecD2 could remain associated to a stalled replication fork, maybe contributing to attempt replication restart. However, RecD2 appears to not be able to bypass the helicase action of DnaC when the loading of the replicative helicase is impaired, because Δ*recD2 dnaD23* mutants are as sensitive as *rec*$^+$ *dnaD23* at non-permissive temperature. These results reveal that RecD2 may act as an accessory helicase in DNA replication rather than as a potential replicative helicase.

In summary, the *in vitro* experiments suggested that RecD2 may contribute to DNA replication via modulating replication restart. As determined by single-molecule microscopy, the association of RecD2 to the replisome is transitory. Moreover, this helicase might contribute in the repair of DNA damages outside the region where the replisome is located. The recruitment of RecD2 to the replication fork should not be only attributed to its interaction with SsbA, because other interacting partners were discovered in this work, PolC, DnaE and DnaD, which could also mediate the association of RecD2 to the replisome machinery. The results from the biochemical data infer that once RecD2 is associated to the replication fork structure, this helicase might participate in the unwinding of stalled and regressed forks facilitating the processing of these structures and contributing to the replisome assembly. Finally, because RecD2 can displace SsbA molecules that are bound to the ssDNA, protein blocks that hinder the advance of a normal

replisome or impede the replication restart could be removed by the translocation activity of RecD2. The last hypothesis was tested in *in vitro* DNA replication assays in the presence of RecA and it will be discussed in the next section.

5.4. The potential role of RecD2 in homologous recombination

A function of RecD2 as a recombination protein has been proposed because the absence of *recD2* confers sensitivity to a wide variety of DNA damaging agents that arrest or collapse replication forks. The combination of Δ*recD2* with the absence of several recombination enzymes (i.e. AddAB, RecQ, RecS) showed a non-epistatic phenotype after the induction of DNA damage (Torres *et al*., 2017). Due to the absence of viability of the Δ*recD2* Δ*recG* and Δ*recD2* Δ*ruvAB* double mutants, a role as a branch migration helicase has been suggested (Torres *et al*., 2017). In this work, the possible function of RecD2 in the context of HR was approached by different strategies: (i) natural transformation frequencies in the absence of RecD2; (ii) helicase activity with D-loops structures; (iii) and the analysis of the possible interplay between RecD2 and the RecA recombinase in strand exchange reactions and *in vitro* DNA replication assays.

Natural transformation mechanisms are dependent on the HR machinery. The central protein is RecA, which filaments on the incorporated ssDNA, searches for homology and catalyses the integration of this exogenous ssDNA into the *B. subtilis* chromosome if there is homology (chromosomal transformation). However, if no homology to the chromosome is detected, the RecA nucleoprotein filament disassembles and the DNA can remain as an extrachromosomal element if it contains an independent origin of replication (plasmid transformation). RecA needs the presence of RecO and DprA-SsbA mediators that contribute to the loading and polymerisation of the recombinase on the incoming ssDNA. Whereas RecA is not needed for plasmid transformation, DprA and RecO are required, because both participate in the intramolecular recombination for the circularisation of the plasmid DNA (Yadav *et al*., 2012; Serrano *et al*., 2018; Serrano *et al*., 2021). RecX and RecU proteins are negative RecA modulators that promote the disassembly of the recombinase from the ssDNA. Hence, both proteins are required in plasmid transformation, although RecX and RecU (in the absence of RecX) become also needed in chromosomal transformation (Le *et al*., 2017; Serrano *et al*., 2018). On the other hand, the activity of branch migration translocases is important for the displacement of the three-stranded recombination intermediate (D-loop) formed during the RecA-mediated strand exchange reaction. In the context of natural transformation processes, RecG and RuvAB are not crucial, because only a marginal decrease in chromosomal and plasmid transformation is noticed in the absence of any of both translocases (Torres *et al*., 2019). RadA/Sms plays a central role during chromosomal transformation, implying that this helicase contributes to the integration of genetic material to the *B. subtilis* chromosome (Torres *et al*., 2019b).

In this work, the possible role of RecD2 in natural transformation was examined (see Chapter 1). The results showed that the absence of *recD2* did not considerably affect the chromosomal transformation efficiency, and just a marginal decrease was obtained in plasmid transformation (**Table 10**) (Serrano *et al*., 2020). This phenotype was similar to the obtained in the absence of RecG or RuvAB activities (Torres *et al*., 2019). Furthermore, the combination of *recD2* and *radA/sms* mutations leaded to a defect in chromosomal transformation, similar than in the absence of *radA/sms* alone (**Table 11**) (Serrano *et al*., 2020). Likewise, Δ*radA/sms* Δ*recG* and Δ*radA/sms* Δ*ruvAB* double mutants, which are viable in contrast to Δ*recD2* Δ*recG*, Δ*recD2* Δ*ruvAB* and Δ*recG* ΔruvAB, show similar defects in chromosomal transformation than Δ*radA/sms* (Torres *et al*., 2017; Sanchez *et al*., 2007). These results confirm that RadA/Sms is the prominent translocase in chromosomal transformation (Torres *et al*., 2019; Serrano *et al*., 2020), but could be added by other helicases since chromosomal transformation is blocked in the absence of RadA/Sms and RecG activities (Torres *et al*., 2019). Remarkably, a markedly reduction in the plasmid transformation efficiency was obtained in Δ*radA/sms* Δ*recD2* mutant (**Table 11**) (Serrano *et al*., 2020), similar as occurred in Δ*radA/sms* Δ*recG* (Torres *et al*., 2019). It suggests an interplay between RadA/Sms and RecD2 or RecG during plasmid transformation, but the precise action of these helicase remains unclear.

The acquisition of external ssDNA harbouring partially homeologous sequences contributes to bacterial adaptation and evolution. Interspecies chromosomal transformation was assayed in this work using donors DNAs containing the *rpoB*482 variant gene (C482T that confers Rif^R) from other *Bacilli* species, so with different degree of sequence divergence respect to the *rpoB*482 variant from *B. subtilis* 168 (*wt* strain). It was previously observed that two different recombination mechanisms may occur: (i) up to 15% sequence divergence, homology-directed HR participates in the integration of divergent sequences (longer than 130 nt); (ii) beyond 15% sequence divergence, integration of just few nucleotides (3-10 nt) at micro-homologous regions is observed probably by homology-facilitated recombination (Carrasco *et al*., 2019). Because the acquisition of highly divergent sequences supposes a markedly reduction in the efficiency of chromosomal transformation, the *rok* gene was inactivated to increase the number of cells with induced competence and bypass the barrier for the detection of transformants (Carrasco *et al*., 2016). Interestingly, Δ*recD2* Δ*rok* mutants showed a substantial reduction in the chromosomal transformation efficiency in comparison to Δ*recD2* rok^+ when the homologous donor DNA was used (**Table 12**). This has been also observed when Δ*rok* is combined with the mutation of *recJ,* Δ*recX,* Δ*dprA* or Δ*radA/sms*, but was not observed in other backgrounds (Serrano *et al*., 2021). In the absence of Rok, the macro-domain structure of the nucleoid is predicted to be altered and this change in the nucleoid conformation may affect the action of some recombination factors during chromosomal transformation (Serrano *et al*., 2021b). As with other recombination

mutants, a decrease in chromosomal transformation frequencies were observed as the percentage of sequence divergence increased, reaching a plateau over 8% sequence divergence in Δ*recD2* *rok*$^{+}$ and Δ*recD2* Δ*rok* (**Figures 9** and **11**). In terms of the integration length, no significant differences to the *rec*$^{+}$ were observed below 15% sequence divergence in Δ*recD2*. However, the absence of RecD2 limited the integration of sequences beyond ~15% sequence divergence in Δ*rok* background, and beyond ~10% in *rok*$^{+}$, revealing a crucial role of RecD2 in the acquisition of homeologous sequences (**Figure 10** and **Table 13**).

Although the contribution of RecD2 during interspecies chromosomal transformation is not still well understood, the results suggest a role during homology-facilitated micro-homologous recombination (Serrano *et al*., 2021). During homology-directed HR (up to 15% sequence divergence), RecA forms the nucleoprotein filament on the incoming ssDNA. In the search for homology, RecA identifies in the recipient genome an identical or almost identical sequence (MEPS, ~25-30 nt, or a MEPS with 1 mismatch). RecA, in concert with SsbA, DprA and RecX promotes DNA strand invasion and pairing to produce a metastable heteroduplex DNA (Yadav *et al*., 2014; Le *et al*., 2017). Then, RecA interacts with and loads the branch migration translocase RadA/Sms to stabilise the heteroduplex (Marie *et al*., 2017; Torres *et al*., 2019b). At the heteroduplex, RecA, in concert with RadA/Sms, promotes the expansion of the D-loop until a region with higher local sequence divergence (≥ 20%) is encountered. This is consistent with the *in vitro* observation that RecA-mediated strand exchange is halted at more than 16% sequence divergence (Carrasco *et al*., 2019). Then, the heteroduplex is resolved by an unknown enzyme. Finally, the ends are sealed, leading to the acquisition of homeologous DNA longer than 130 nt (Serrano *et al*., 2021). On the other hand, it has been proposed that during homology-facilitated micro-homologous recombination, RecA, with the help of the mediators/modulators DprA, RecX, RadA/Sms (and perhaps RecD2), forms the nucleoprotein filament and identifies a MEPS on the *rpoB*482 sequence, which is used as an anchor region in this case. Once the chromosomal DNA is anchored at MEPS, DprA could mediate the annealing of short stretches of homeologous DNA (~3-8 nt) (Yadav *et al*., 2014). Then, the donor ssDNA loop between the anchored region and the micro-homologous paired segment has to be removed perhaps by the action of RecJ in concert with RecD2 (Serrano *et al*., 2020). RecD2 could also act as a branch migration helicase on three-stranded recombination intermediates helping to bypass short heterologous regions that become integrated. Finally, the ends of the integrated segment are sealed and rapidly expressed (Dalia and Dalia, 2019; Serrano *et al*., 2021).

Host-encoded recombination proteins are also required to reconstitute a complete viral genome from fragmented linear viral ssDNA acquired by natutal transformation (viral transfection). In the absence of *recD2*, great reduction in the SPP1 transfection efficiency was observed (**Table 14**), implying a crucial role of this helicase in the intermolecular recombination

required between the exogenous ssDNA fragments for the reconstitution of the SPP1 genome (Serrano *et al*., 2020). Other recombination factors that were found to be required in viral transfection are RecA, DprA and RecO (RecA mediators), and RecX and RecU (negative RecA modulators) (Serrano *et al*., 2020). The action of the branch migration translocases RecG, RuvAB or RadA/Sms is not crucial, because the SPP1 transfection efficiency is not significantly altered in the absence of any of them. In addition, the combination with the Δ*recD2* mutant with the absence of *radA/sms* showed a similar decrease in the viral transfection efficiency than in the absence of RecD2 alone (**Table 15**), suggesting that RecD2 performs a central function in the branch migration of the recombination intermediates resulted during the reformation of the SPP1 genome (Serrano *et al*., 2020). In viral transfection processes, RecA nucleates onto SPP1 ssDNA in concert with RecO and DprA-SsbA. Because no homology on the chromosome is found, RecX, RecU and/or RecD2 may promote RecA filament disassembly. Once RecA releases from the ssDNA, it is rapidly coated by SsbA/SsbB that recruit DprA or RecO. DprA or RecO bound to the ssDNA perform the single strand annealing between complementary strands from the fragmented SPP1 ssDNA. As a result, several tailed dsDNA fragments are formed. Then, RecA nucleates onto the ssDNA ends of the tailed dsDNAs and performs the strand exchange invasion between complementary strands with the help of the branch migration activity of RecD2 to regenerate a complete linear viral genome. Finally, the genome is circularised after intramolecular annealing by DprA and RecO in concert with SsbA/SsbB. A summary of the different RecD2 activities required in viral transfection, plasmid transformation and chromosomal transformation is shown in the **Figure 58.**

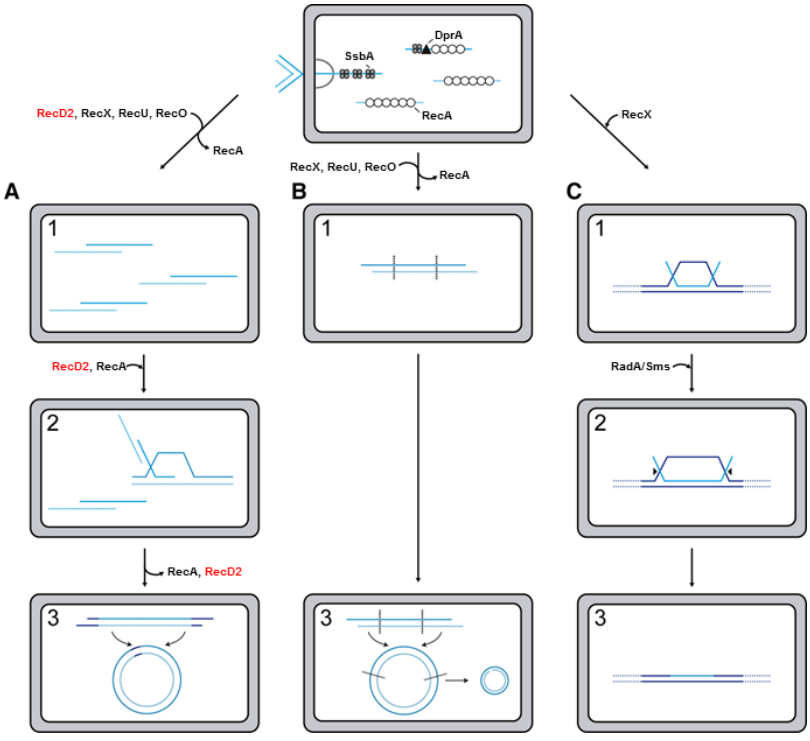

Figure 58. Model depicting the role of RecD2 during natural transformation in *B. subtilis*.

Figure 58. Model depicting the role of RecD2 during natural transformation in *B. subtilis* (continued).
During natural transformation, the uptake apparatus, localised at the *B. subtilis* cell pole, internalises ssDNA fragments that rapidly are coated by SsbA (and SsbB). RecA with the help of the RecO and DprA-SsbA mediators forms the nucleoprotein filament onto the ssDNAs and searches for homology on the bacterial chromosome. (**A**) In viral transfection, RecA is disassembled from the viral ssDNA fragments by the RecX, RecU and RecD2 negative modulators. (1) Then, the SsbA/SsbB-coated ssDNA recruits DprA or RecO to perform the intermolecular single strand annealing between complementary fragments. As a result of ssDNA annealing, tailed dsDNAs are formed and coated by SsbA/SsbB/DprA. (2) RecA is consequently recruited and nucleates onto the tails. In the presence of ATP, RecA catalyses the strand exchange reaction between complementary sequences in concert with the branch migration activity of RecD2. (3) Finally, the complete linear SPP1 genome is reconstituted and then circularised by DprA or RecO through intramolecular single strand annealing activity. (**B**) In plasmid transformation, an oligomeric ssDNA plasmid is incorporated. (1) RecA disassembles from the ssDNA with the help of RecX, RecU and perhaps RecD2, and this facilitates the synthesis of the complementary strand by DNA replication or the annealing with the other internalised complementary strand by DprA or RecO. (3) The intramolecular recombination reaction carried out by DprA or RecO is predicted to circularise the oligomeric plasmid molecule that after DNA replication is established as a monomeric plasmid. (**C**) In chromosomal transformation with homologous donor DNA, the RecA-nucleoprotein filament efficiently searches for homology. (1) In the presence of ATP, RecA catalyses the strand exchange invasion into the bacterial chromosome. (2) RadA/Sms branch migrates the heteroduplex and helps to the integration of the ssDNA into a homologous region of the chromosome. (3) Then, the heteroduplex is resolved by the action of an unknown nuclease. RecD2 has a minor role in chromosomal transformation with homologous DNA, but it is involved in homology-facilitated micro-homologous recombination contributing to the integration of homeologous sequences up 15% sequence divergence. Figure adapted from Serrano *et al*., 2020.

Natural transformation assays revealed that RecD2 might act as a branch migration translocase in viral transfection processes. However, its action in the heteroduplex migration during chromosomal transformation seems to be limited. This could be because the linear SPP1 fragments and the bacterial circular chromosome have different topologies and it could affect the action of RecD2. The activity of RecD2 as a branch migration helicase was assayed *in vitro* (see Chapter 2). RecD2 is able to unwind D-loop structures, but depending on where the protein is loaded, the outcome is different. The 3'-invading D-loop structure mimics a plectonemic heteroduplex structure that resulted because of the invasion of a 3' ssDNA end. Here, an anti-recombinogenic activity of RecD2 was observed, because the invading strand was efficiently separated of the duplex at very low protein concentrations (**Figure 22 A** and **C**). This anti-recombinogenic activity visualised for RecD2 with this type of structure was also observed for RadA/Sms (Torres *et al*., 2019). On the other hand, the 5'-invading D-loop mimics a plectonemic heteroduplex structure in which a 5' ssDNA end invades a homologous duplex. In this structure, RecD2 was able to bind to the displaced ssDNA strand and unwind in a 5' to 3' separating the duplex, therefore favouring the branch migration of a heteroduplex (**Figure 22 B** and **C**).

The RecA-mediated three-stranded exchange was analysed *in vitro* in the presence of RecD2 (see Chapter 5). The results revealed a dual activity of the helicase during the HR reaction (**Figure 50**). At the early steps of the recombination reaction, RecD2 slightly enhanced strand exchange via branch migrating recombination intermediates in a stoichiometry ~1 helicase/DNA substrate and thus promoting the appearance of the final strand exchange products. However, increasing amounts of RecD2 inhibited the strand exchange reaction, suggesting that the helicase impaired the RecA nucleation onto the ssDNA. The inhibitory effect of RecD2 was not observed

at later steps of the strand exchange reaction, in which recombination intermediates accumulate and RecA molecules are bound to the ssDNA. These results imply that RecD2 may have two roles. From one side, the helicase interacts with (**Figure 48**) and can contribute as a negative RecA modulator either promoting the RecA disassembly from the ssDNA, similar as RecX or RecU, or preventing the nucleoprotein filament formation (**Figure 59 A1**). From other side, RecD2 can facilitate the RecA activity with the 5' to 3' branch migration of the recombination intermediates (Ramos *et al*., 2022) (**Figure 59 A2** and **3**). The first role of RecD2 was supported by the observation of the dynamics of RecA-mVenus filaments *in vivo*, which persist longer time upon the induction of DNA damage in the absence of *recD2*, and with the accumulation of RecA-ssDNA at lower concentrations of MMC in Δ*recD2* background (Ramos *et al*., 2022). The second role of RecD2 was confirmed in branch migration assays, in which the helicase was incubated alone in the presence of ATP with recombination intermediates, resulted from a previous strand exchange reaction by RecA and the two-component mediator RecO-SsbA. In these assays, RecD2 catalysed branch migration and enhanced the formation of the final strand exchange product (Ramos *et al*., 2022). Human HELB was found to stimulate *in vitro* the Rad51-mediated heteroduplex extension in 5' to 3' direction in the presence of a dsDNA containing a 3' ssDNA end, but the strand exchange reaction was inhibited in the presence of a dsDNA with blunt ends or having a 5' ssDNA end (Liu *et al*., 2015). Another human helicase, BLM, involved in genome maintenance and recombination repair, appears to disrupt the Rad51-ssDNA filament by promoting the Rad51 disassembly and inhibits the DNA strand activity. However, BLM stimulates the D-loop extension at later steps of the recombination reaction (Bugreev *et al*., 2007; Bugreev *et al*., 2009). These findings uncover the importance of the regulation of the RecA nucleoprotein filament in the HR reaction and the contribution of RecD2 as a regulator of RecA.

In addition to recombination repair and natural transformation processes, the HR machinery acts on collapsed replication forks and several recombination factors modulate replication restart. RecA, alone or in the presence of the two-component mediator RecO and SsbA, inhibits the initiation of DNA replication in an *in vitro* model of blocked replication fork (Vlašić *et al*., 2013). This inhibition might prevent potentially dangerous forms of DNA repair that can occur upon several stress conditions. Alternatively, RecA participates on replication restart by a template switching mechanism (Marians, 2018). This work revealed an interplay between RecD2 and RecA on blocked replication forks *in vitro* (see Chapter 5). At concentrations of 1 helicase/DNA molecule, RecD2 efficiently overcame the inhibition of initiation of DNA replication conferred by RecA and RecO (**Figure 51**). In the absence of SsbA and RecO, the presence of RecD2 was also capable to bypass the blockage on DNA synthesis by RecA, especially at the lagging strand (**Figure 53**). These results confirm the action of RecD2 as a negative RecA modulator and suggest a role in the removal of protein blocks that halt the initiation

of DNA replication (**Figure 59 B**). RecD2 may perform the clearance of RecA molecules during translocation along the ssDNA, because RecD2 K373A was not able to revert the inhibitory effect of RecA on DNA replication (**Figure 52**) (Ramos *et al*., 2022). This was consistent with the no effect observed in the helicase activity of RecD2 by the presence of RecA, implying that RecD2 could efficiently displace RecA molecules during its translocation (**Figures 55** and **56**). Additional data may be needed to confirm this activity of RecD2 on RecA, perhaps from optical and magnetic-tweezers, to gain insight into the interplay between the two proteins on ssDNA at single-molecule resolution.

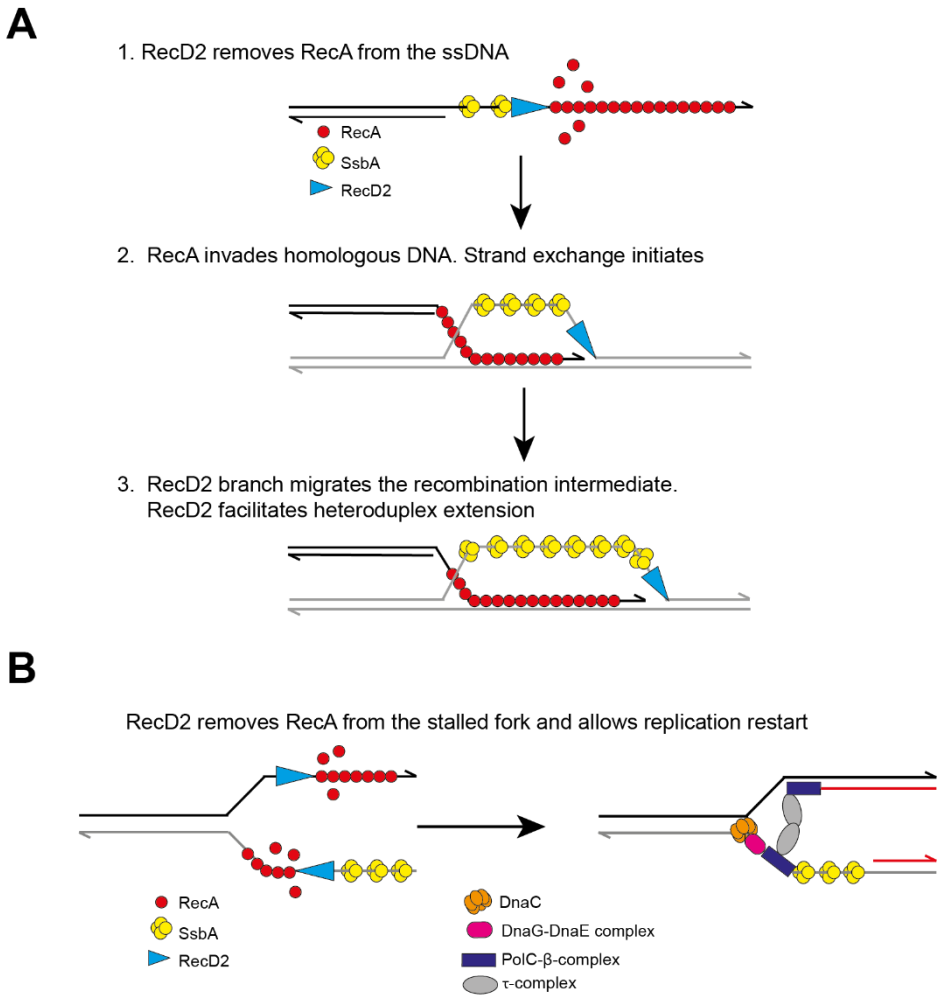

Figure 59. Model of the action of RecD2 in the modulation of RecA activities.
(**A**) (1) During homologous recombination reaction, RecA nucleates onto a SsbA-coated ssDNA in the presence of RecO and ATP. RecD2 binds to the ssDNA and translocates in a 5' to 3' direction promoting the disassembly of the RecA molecules and thus inhibiting the RecA-nucleoprotein filament formation. (2) RecA-nucleoprotein filament invades a homologous DNA and catalyses the strand exchange reaction forming a heteroduplex structure (D-loop). (3) At later steps of the strand exchange reaction, RecD2 can bind to the displaced ssDNA strand and branch migrates the heteroduplex in a 5' to 3' direction facilitating the recombination process. (**B**) RecA binds to ssDNA regions of a blocked replication fork and inhibits replication restart. RecD2 removes RecA from the stalled fork and thereby, facilitates replisome loading and replication restart. Figure from Ramos *et al*., 2022.

Conclusions

6. Conclusions

1. RecD2 preferentially binds and translocates along ssDNA with no secondary structures in the presence of ATP. In addition, RecD2 shows a nucleotide bias with a preference for polydTs rather than polydAs. A minimum site size between 15-30 nt is needed for the stable binding of one monomer of RecD2.

2. RecD2 requires a 5' ssDNA end to perform the unwinding of a dsDNA region in a 5' to 3' direction. The preferred structures that RecD2 binds are non-replicated forks and D-loops, and that RecD2 unwinds are partially replicated forks containing a gap in the parental lagging strand and D-loops.

3. SsbA enhances ATPase and helicase activities of RecD2 with the reduction of ssDNA secondary structures. Physical interaction between SsbA and RecD2 is also crucial for the stimulation, because the presence of SsbB, which does not interact with RecD2, inhibits the ATPase activity of this helicase.

4. In addition to SsbA, RecD2 interacts with the replisome proteins DnaE and PolC polymerases and DnaD. RecD2 also interacts with RarA.

5. RecD2 is a low abundant protein (~25 monomers/CFU) that shows a high dynamics *in vivo* and distributes mostly in the nucleoid region with a non-specific localisation. Both RecD2 dynamics and its subcellular localisation are affected by the presence of certain perturbations in DNA replication.

6. The association of RecD2 to the replisome is transient. The presence of certain types of DNA lesions can promote a recruitment of RecD2 or its approach to regions around the replication fork machinery where RecD2 can be involved in DNA repair.

7. RecD2 may contribute to replication restart via the unwinding of stalled forks, containing a gap in the parental lagging strand, or regressed forks. RecD2 may act as an accessory helicase supporting the unwinding activity of the replicative helicase DnaC. RecD2 may also modulate replication restart via the removal of protein blocks, as RecA, which can inhibit the assembly and/or the advance of the replisome. RecD2 does not affect the progression of an unperturbed replication process.

8. RecD2 interacts with RecA and negatively regulates the RecA nucleoprotein filament formation on the ssDNA. Nevertheless, once the RecA nucleoprotein filament is formed and strand exchange reaction is catalysed, RecD2 facilitates the homologous recombination reaction via the branch migration of three-stranded recombination intermediates.

9. In the absence of Rok, RecD2 is crucial for intra- and interspecies natural chromosomal transformation. RecD2 is required in homology-facilitated recombination for the integration of micro-homologous sequences beyond ~15% sequence divergence. RecD2 is also important during natural plasmid transformation in concert with RadA/Sms.

10. RecD2 is required for SPP1 transfection, either via the branch migration of the three-stranded recombination intermediates resulted during the reconstitution of the SPP1 genome inside the *B. subtilis* cell and/or the negative modulation of the RecA nucleoprotein filament.

Conclusiones

7. Conclusiones

1. RecD2 se une y transloca preferentemente a lo largo de ADN de cadena sencilla sin estructuras secundarias en presencia de ATP. Además, RecD2 muestra un sesgo de nucleótidos con preferencia por polidTs que polidAs. Un sitio mínimo de entre 15-30 nt es necesario para la unión estable de un monómero de RecD2.

2. RecD2 requiere un extremo 5' de cadena sencilla para realizar el desenrollamiento de una región de ADN de cadena doble en dirección 5' a 3'. Las estructuras preferidas que RecD2 une son horquillas no replicadas y *D-loops*, y que RecD2 desenrolla son horquillas replicadas parcialmente con un hueco en la cadena retardada parental y *D-loops*.

3. SsbA mejora la actividad ATPasa y helicasa de RecD2 con la reducción de estructuras secundarias en el ADN de cadena sencilla. La interacción física entre SsbA y RecD2 es también crucial para la estimulación, ya que la presencia de SsbB, la cual no interacciona con RecD2, inhibe la actividad ATPasa de esta helicasa.

4. Además de SsbA, RecD2 interacciona con las proteínas del replisoma DnaE y PolC, polimerasas, y DnaD. RecD2 también interacciona con RarA.

5. RecD2 es una proteína poco abundante (~25 monómeros/CFU) que muestra una dinámica elevada *in vivo* y se distribuye mayormente en la región del nucleoide sin una localización específica. Tanto la dinámica de RecD2 como su localización subcelular se ven afectadas por la presencia de ciertas perturbaciones en la replicación del ADN.

6. La asociación de RecD2 al replisoma es transitoria. La presencia de ciertos tipos de lesiones en el ADN puede promover un reclutamiento de RecD2 o su acercamiento a regiones alrededor de la maquinaria de la horquilla de replicación donde RecD2 puede estar involucrada en la reparación del ADN.

7. RecD2 puede contribuir al reinicio de la replicación desenrollando horquillas bloqueadas que contienen un hueco en la hebra retardada parental u horquillas regresadas. RecD2 puede actuar como helicasa accesoria contribuyendo a la actividad de desenrollamiento de la helicasa replicativa DnaC. RecD2 también puede modular el reinicio de la replicación eliminado proteínas bloqueantes, como RecA, que pueden inhibir el ensamblaje y/o el avance del replisoma. RecD2 no afecta el progreso de un proceso de replicación sin perturbaciones.

8. RecD2 interacciona con RecA y regula negativamente la formación del filamento nucleoproteico de RecA sobre el ADN de cadena sencilla. Sin embargo, una vez el filamento nucleoproteico de RecA se forma y la reacción de intercambio de cadenas es catalizada, RecD2 facilita la recombinación homóloga migrando intermediarios de recombinación de tres cadenas.

9. En ausencia de Rok, RecD2 es crucial en transformación cromosómica con ADN donadores de la misma (intraespecie) o de distintas especies (interespecie) de *Bacillus*. RecD2 se requiere en recombinación facilitada por homología para la integración de secuencias micro-homólogas por encima del ~15% de divergencia de secuencia. RecD2 es también importante en transformación plasmídica en conjunto con RadA/Sms.

10. RecD2 se require en transfección de SPP1 mediante la migración de los intermediarios de recombinación de tres cadenas que resultan durante la reconstitución del genoma de SPP1 en el interior de la célula de *B. subtilis* y/o la modulación negativa del filamento nucleoproteico de RecA.

References

Alonso, J.C., Tailor, R.H., Lüder, G. (1988). Characterization of recombination-deficient mutants of *Bacillus subtilis*. *J. Bacteriol*. 170: 3001–3007.

Antony E., Weiland E., Yuan Q., Manhart C.M., Nguyen B., Kozlov A.G., McHenry C.S., Lohman T.M. (2013). Multiple C-terminal tails within a single *E. coli* SSB homotetramer coordinate DNA replication and repair. *J. Mol. Biol.* 425(23): 4802-4819.

Atkinson J., McGlynn P. (2009). Replication fork reversal and the maintenance of genome stability. *Nucleic Acid Res*. 37(11): 3475-3492.

Ayora S., Carrasco B., Cárdenas P.P., César C.E., Cañas C., Yadav T., Marchisone C., Alonso J.C. (2011). Double-strand break repair in bacteria: a view from *Bacillus subtilis*. *FEMS Microbiol. Rev*. 35(6): 1055-1081.

Ayora S., Missich R., Mesa P., Lurz R., Yang S., Egelman E.H., Alonso J.C. (2002). Homologous-pairing activity of the *Bacillus subtilis* bacteriophage SPP1 replication protein G35P. *J. Biol. Chem*. 277: 35969-35979.

Beattie T.R., Reyes-Lamothe R. (2015). A replisome's journey through the bacterial chromosome. *Front. Microbiol.* 6: 562.

Briggs G.S., Smits W.K., Soultanas P. (2012). Chromosomal replication initiation machinery of low-G+C-content *Firmicutes*. *J. Bacteriol*. 194(19): 5162-5170.

Brown N.C. (1970). 6-(p-hydroxyphenylazo)-uracil: a selective inhibitor of host DNA replication in phage-infected *Bacillus subtilis*. *Proc. Natl. Acad. Sci. U S A*. 67(3): 1454-1461.

Brüning J.G., Howard J.A.L., McGlynn P. (2016). Use of streptavidin bound to biotinylated DNA structures as model substrates for analysis of nucleoprotein complex disruption by helicases. *Methods*. 108: 48-55.

Bugreev D.V, Mazina O.M., Mazin A.V. (2009). Bloom syndrome helicase stimulates RAD51 DNA strand exchange activity through a novel mechanism. *J. Biol. Chem*. 284(39): 26349-26359.

Bugreev D.V., Yu X., Egelman E.H., Mazin A.V. (2007). Novel pro- and anti-recombination activities of the Bloom's syndrome helicase. *Genes Dev*. 21(23): 3085-3094.

Canosi U., Morelli G., Trautner T.A. (1978). The relationship between molecular structure and transformation efficiency of some *S. aureus* plasmids isolated from *B. subtilis*. *Mol. Gen. Genet*. 166(3): 259-267.

Cañas C., Suzuki Y., Marchisone C., Carrasco B., Freire-Benéitez V., Takeyasu K., Alonso J.C., Ayora S. (2014). Interaction of branch migration translocases with the Holliday junction-resolving enzyme and their implications in Holliday junction resolution. *J. Biol. Chem*. 289(25): 17634-17646.

Cardenas P.P., Carrasco B., Sanchez H., Deikus G., Bechhofer D.H., Alonso J.C. (2009). *Bacillus subtilis* polynucleotide phosphorylase 3' to 5' DNase activity is involved in DNA repair. *Nucleic Acids Res*. 37(12): 4157-4169.

Carrasco B., Ayora S., Lurz R., Alonso J.C. (2005). *Bacillus subtilis* RecU Holliday-junction resolvase modulates RecA activities. *Nucleic Acids Res*. 33(12): 3942-3952.

Carrasco B., Seco E.M., López-Sanz M., Alonso J.C., Ayora S. (2018). *Bacillus subtilis* RarA modulates replication restart. *Nucleic Acids Res*. 46(14): 7206-7220.

Carrasco B., Serrano E., Martín-González A., Moreno-Herrero F., Alonso J.C. (2019). *Bacillus subtilis* MutS modulates RecA-mediated DNA strand exchange between divergent DNA sequences. *Front. Microbiol*. 10: 237.

Carrasco B., Serrano E., Sánchez H., Wyman C., Alonso J.C. (2016). Chromosomal transformation in *Bacillus subtilis* is a non-polar recombination reaction. *Nucleic Acids Res*. 44(6): 2754-2768.

Carrasco B., Yadav T., Serrano E., Alonso J.C. (2015). *Bacillus subtilis* RecO and SsbA are crucial for RecA-mediated recombinational DNA repair. *Nucleic Acids Res*. 43(12): 5984-5997.

Ceglowski P., Lüder G., Alonso J.C. (1990). Genetic analysis of *rec*E activities in *Bacillus subtilis*. *Mol. Gen. Genet*. 222: 441-445.

Chatterjee N., Walker G.C. (2017). Mechanisms of DNA damage, repair and mutagenesis. *Environ. Mol. Mutagen*. 58(5): 235-263.

Chédin F., Handa N., Dillingham M.S., Kowalczykowski. (2006). The AddAB helicase/nuclease forms a stable complex with its cognate χ sequence during translocation. *J. Biol. Chem*. 281(27): 18610-18617.

Chédin F., Kowalczykowski S.C. (2002). A novel family of regulated helicases/nucleases from Gram-positive bacteria: insights into the initiation of DNA recombination. *Mol. Microbiol*. 43(4): 823-834.

Chen H.W., Ruan B., Yu M., Wang J.d., Julin D.A. (1997). The RecD subunit of the RecBCD enzyme from *Escherichia coli* is a single-stranded DNA-dependent ATPase. *J. Biol. Chem*. 272(15): 10072-10079.

Costes A., Lecointe F., McGovern S., Quevillon-Cheruel S., Polard P. (2010). The C-terminal domain of the bacterial SSB protein acts as a DNA maintenance hub at active chromosome replication forks. *PLos Genet*. 6(12): e1001238.

Dalhus B., Laerdahl J.K., Backe P.H., Bjoras M. (2009). DNA base repair-recognition and initiation of catalysis. *FEMS Microbiol. Rev*. 33(6): 1044-1078.

Dalia A.B., Dalia T.N. (2019). Spatiotemporal analysis of DNA integration during natural transformation reveals a mode of nongenetic inheritance in bacteria. *Cell*. 179: e1410.

de Vries J., Wackernagel W. (2002). Integration of foreign DNA during natural transformation of *Acinetobacter* sp. by homology-facilitated illegitimate recombination. *Proc. Natl. Acad. Sci. U S A*. 99: 2094-2099.

Dehghani-Tafti S., Sanders C.M. (2017). DNA substrate recognition and processing by the full-length human UPF1 helicase. *Nucleic Acids Res*. 45(12): 7354-7366.

Dillingham M.S., Spies M., Kowalczykowski S.C. (2003). RecBCD enzyme is a bipolar DNA helicase. *Nature*. 423(6942): 893-897.

Dubnau D., Cirigliano C. (1972). Fate of transforming DNA following uptake by competent *Bacillus subtilis*. Formation and properties of products isolated from transformed cells, which are derived entirely from donor DNA. *J. Mol. Biol*. 64: 9-29.

Dugar G., Hofmann A., Heermann D.W., Hamoen L.W. (2022). A chromosomal loop anchor mediates bacterial genome organization. *Nat. Genet*. 54(2): 194-201.

Duigou S., Ehrlich S.D., Noirot P., Noirot-Gros M.F. (2005). DNA polymerase I acts in translesion synthesis mediated by the Y-polymerases in *Bacillus subtilis*. *Mol. Microbiol*. 57(3): 678-690.

Epshtein V., Kamarthapu V., McGary K., Svetlov V., Ueberheide B., Proshkin S., Mironov A., Nudler E. (2014). UvrD facilitates DNA repair by pulling RNA polymerase backwards. *Nature*. 505(7483): 372-377.

Fornili S.L., Fox M.S. (1977). Electron microscope visualization of the products of *Bacillus subtilis* transformation. *J. Mol. Biol*. 113: 181-191.

Fraser C., Hanage W.P., Spratt B.G. (2007). Recombination and the nature of bacterial speciation. *Science*. 315: 476-480.

Gabbai C.B., Marians K.J. (2010). Recruitment to stalled replication forks of the PriA DNA helicase and replisome-loading activities is essential for survival. *DNA repair (Amst)*. 9(3): 202-209.

Gerhardt J., Guler G.D., Fanning E. (2015). Human DNA helicase B interacts with the replication initiation protein Cdc45 and facilitates Cdc45 binding onto chromatin. *Exp. Cell. Res*. 334(2): 283-293.

Gilhooly N.S., Gwynn E.J., Dillingham M.S. (2013). Superfamily 1 helicases. *Front. Biosci. (Schol. Ed.)*. 5(1): 206-216.

Gu J., Xia X., Yan P., Liu H., Podust V.N., Reynolds A.B., Fanning E. (2004). Cell cycle-dependent regulation of a human DNA helicase that localizes in DNA damage foci. *Mol. Biol. Cell*. 15(7): 3320-3332.

Guler G.D., Liu H., Vaithiyalingam S., Arnett D.R., Kremmer E., Chazin W.J., Fanning E. (2012). Human DNA helicase B (HDHB) binds to replication protein A and facilitates cellular recovery from replication stress. *J. Biol. Chem*. 287(9): 6469-6481.

Guler G.D., Rosenwaks Z., Gerhardt J. (2018). Human DNA helicase B as a candidate for unwinding secondary CGG repeat structures at the fragile X mental retardation gene. *Front. Mol. Neurosci*. 11: 138.

Gupta M.K., Guy C.P., Yeeles J.T.P., Atkinson A., Bell H., Lloyd R.G., Marians K.J., McGlynn P. (2013). Protein-DNA complexes are the primary sources of replication fork pausing in *Escherichia coli*. *Proc. Natl. Acad. Sci. U S A*. 110(18): 7252-7257.

Gupta S., Yeeles J.T.P., Marians K.J. (2014). Regression of replication forks stalled by leading-strand template damage. *J. Biol. Chem*. 289(41): 28376-28387.

Guy C.P., Atkinson J., Gupta M.K., Mahdi A.A., Gwynn E.J., Rudolph C.J., Moon P.B., van Knippenberg I.C., Cadman C.J., Dillingham M.S., Lloyd R.G., McGlynn P. (2009). Rep provides a second motor at the replisome to promote duplication of protein-bound DNA. *Mol. Cell*. 36(4): 654-666.

Hazeslip L., Zafar M.K., Chauhan M.Z., Byrd A.K. (2020). Genome maintenance by DNA helicase B. *Genes (Basel)*. 11(5): 578.

Heller R.C., Marians K.J. (2007). Non-replicative helicases at the replication fork. *DNA repair (Amst)*. 6(7): 945-952.

Heller R.C., Marians K.J. (2005). Unwinding of the nascent lagging strand by Rep and PriA enables the direct restart of stalled replication forks. *J. Biol. Chem*. 280(40): 34143-34151.

Hernández-Tamayo R., Oviedo-Bocanegra L.M., Fritz G., Graumann P.L. (2019). Symmetric activity of DNA polymerases at and recruitment of exonuclease ExoR and of PolA to the *Bacillus subtilis* replication forks. *Nucleic Acids Res*. 47(16): 8521-8536.

Hernández-Tamayo R., Schmitz H., Graumann P.L. (2021). Single-Molecule dynamics at a bacterial replication fork after nutritional downshift or chemically induced block in replication. *mSphere*. 6(1): e00948-20.

Hishida T., Han Y.W., Shibata T., Kubota Y., Ishino Y., Iwasaki H., Shinagawa H. (2004). Role of the *Escherichia coli* RecQ DNA helicase in SOS signaling and genome stabilization at stalled replication forks. *Genes Dev*. 18(15): 1886-1897.

Hormeño S., Wilkinson O.J., Aicart-Ramos C., Kuppa S., Antony E., Dillingham M.S., Moreno-Herrero F. (2022). Human HELB is a processive motor protein which catalyses RPA clearance from single-stranded DNA. *Proc. Natl. Acad. Sci. U S A*. 119(15): e2112376119.

Humphreys G.O., Trautner T.A. (1981). Structure of *Bacillus subtilis* bacteriophage SPP1 DNA in relation to its transfection activity. *J. Virol*. 37: 574-579.

Jameson K.H., Wilkinson A.J. (2017). Control of initiation of DNA replication in *Bacillus subtilis* and *Escherichia coli*. *Genes (Basel).* 8(1): 22.

Kidane D., Ayora S., Sweasy J.B., Graumann P.L., Alonso J.C. (2012). The cell pole: the site of cross talk between the DNA uptake and genetic recombination machinery. *Crit. Rev. Biochem. Mol. Biol*. 47(6): 531-555.

Kramer N., Hahn J., Dubnau D. (2007). Multiple interactions among the competence proteins of *Bacillus subtilis*. *Mol. Microbiol*. 65(2): 454-464.

Le S., Serrano E., Kawamura R., Carrasco B., Yan J., Alonso, J.C. (2017). *Bacillus subtilis* RecA with DprA-SsbA antagonizes RecX function during natural transformation. *Nucleic Acids Res*. 45: 8873–8885.

Lecointe F., Sérèna C., Velten M., Costes A., McGovern S., Meile J.C., Errington J., Ehrlich S.D., Noirot P., Polard P. (2007). Anticipating chromosomal replication fork arrest: SSB targets repair DNA helicases to active forks. *EMBO J*. 26(19): 4239-4251.

Lemon K.P., Grossman A.D. (1998). Localization of bacterial DNA polymerase: evidence for a factory model of replication. *Science*. 282(5393): 1516-1519.

Lenhart J.S., Brandes E.R., Schroeder J.W., Sorenson R.J., Showalter H.D., Simmons L.A. (2014). RecO and RecR are necessary for RecA loading in response to DNA damage and replication fork stress. *J. Bacteriol*. 196(15): 2851-2860.

Lenhart J.S., Schroeder J.W., Walsh B.W., Simmons L.A. (2012). DNA repair and genome maintenance in *Bacillus subtilis*. *Microbiol. Mol. Biol. Rev*. 76(3): 530-564.

Li Y., Chen Z., Matthews L.A., Simmons L.A., Biteen J.S. (2019). Dynamic exchange of two essential DNA polymerases during replication and after fork arrest. *Biophys. J*. 116(4): 684-693.

Li Y., Schroeder J.W., Simmons L.A., Biteen J.S. (2018). Visualizing bacterial DNA replication and repair with molecular resolution. *Curr. Opin. Microbiol*. 43: 38-45.

Liao Y., Schroeder J.W., Gao B., Simmons L.A., Biteen J.S. (2015). Single-molecule motions and interactions in live cells reveal target search dynamics in mismatch repair. *Proc. Natl. Acad. Sci. U S A*. 112(50): E6898-E6906.

Liao Y., Li Y., Schroeder J.W., Simmons L.A., Biteen J.S. (2016). Single-Molecule DNA polymerase dynamics at a bacterial replisome in live cells. *Biophys. J*. 111(12): 2562-2569.

Liu H., Yan P., Fanning E. (2015). Human DNA helicase B functions in cellular homologous recombination and stimulates Rad51-mediated 5'-3' heteroduplex extension *in vitro*. *PLoS One*. 10(1): e0116852.

Lo Piano A., Martinez-Jimenez M.I., Zecchi L., Ayora S. (2011). Recombination-dependent concatemeric viral DNA replication. *Virus Res*. 160: 1-14.

Maaβ S., Wachlin G., Bernhardt J., Eymann C., Fromion V., Riedel K., Becher D., Hecker M. (2014). Highly precise quantification of protein molecules per cell during stress and starvation responses in *Bacillus subtilis. Mol. Cell. Proteomics*. 13(9): 2260-2276.

Maamar H., Dubnau D. (2005). Bistability in the *Bacillus subtilis* K-state (competence) system requires a positive feedback loop. *Mol. Microbiol*. 56: 615-624.

Majewski J., Cohan F.M. (1999). DNA sequence similarity requirements for interspecific recombination in *Bacillus. Genetics*. 153: 1525-1533.

Manfredi C., Carrasco B., Ayora S., Alonso J.C. (2008). *Bacillus subtilis* RecO nucleates RecA onto SsbA-coated single-stranded DNA. *J. Biol. Chem*. 283(36): 24837-24847.

Marians K.J. (2018). Lesion bypass and the reactivation of stalled replication forks. *Annu. Rev. Biochem*. 87: 217-238.

Marie L., Rapisarda C., Morales V., Bergé M., Perry T., Soulet A.L., Gruget C., Remaut H., Fronzes R., Polard P. (2017). Bacterial RadA is a DnaB-type helicase interacting with RecA to promote bidirectional D-loop extension. *Nat. Commun*. 8: 15638.

Masterson C., Boehmer P.E., McDonald F., Chaudhuri S., Hickson I.D., Emmerson P.T. (1992). Reconstitution of the activities of the RecBCD holoenzyme of *Escherichia coli* from the purified subunits. *J. Biol. Chem*. 267(19): 13564-13572.

McIlwraith M.J., West S.C. (2001). The efficiency of strand invasion by *Escherichia coli* RecA is dependent upon the length and polarity of ssDNA tails. *J. Mol. Biol*. 305(1): 23-31.

McKie S.J., Neuman K.C., Maxwell A. (2021). DNA topoisomerases: advances in understanding of cellular roles and multi-protein complexes via structure-function analysis. *Bioessays*. 43(4): e2000286.

Montague M., Barnes C., Smith H.O., Chuang R.Y., Vashee S. (2009). The evolution of RecD outside of the RecBCD complex. *J. Mol. Evol*. 69: 360-371.

Moreno-del Álamo M., Carrasco B., Torres R., Alonso J.C. (2021). *Bacillus subtilis* PcrA helicase removes trafficking barriers. *Cells*. 10(4): 935.

Muntel J., Fromion V., Goelzer A., Maaβ S., Mäder U., Büttner K., Hecker M., Becher D. (2014). Comprehensive absolute quantification of the cytosolic proteome of *Bacillus subtilis* by data independent, parallel fragmentation in liquid chromatography/mass spectrometry (LC/MS(E)). *Mol. Cell. Proteomics*. 13(4): 1008-1019.

Newing T.P., Oakley A.J., Miller M., Dawson C.J., Brown S.H.J., Bouwer J.C., Tolun G., Lewis P.J. (2020). Molecular basis for RNA polymerase-dependent transcription complex recycling by the helicase-like motor protein HelD. *Nat. Commun*. 11(1): 6420.

Nguyen B., Shinn M.K., Weiland E., Lohman T.M. (2021). Regulation of *E. coli* Rep helicase activity by PriC. *J. Mol. Biol*. 433(15): 167072.

Nicolas P., Mäder U., Dervyn E., Rochat T., Leduc A., Pigeonneau N., Bidnenko E., Marchadier E., Hoebeke M., Aymerich S., Becher D., Bisicchia P., Botella E., Delumeau O., Doherty G., Denham E.L., Fogg M.J., Fromion V., Goelzer A., Hansen A., Härtig E., Harwood C.R., Homuth G., Jarmer H., Jules M., Klipp E., Le Chat L., Lecointe F., Lewis P., Liebermeister W., March A., Mars R.A., Nannapaneni P., Noone D., Pohl S., Rinn B., Rügheimer F., Sappa P.K., Samson F., Schaffer M., Schwikowski B., Steil L., Stülke J., Wiegert T., Devine K.M., Wilkinson A.J., van Dijl J.M., Hecker M., Völker U., Bessières P., Noirot P. (2012). Condition-dependent transcriptome reveals high-level regulatory architecture in *Bacillus subtilis. Science*. 335(6072): 1103-1106.

Paschalis V., Le Chatelier E., Green M., Képès F., Soultanas P., Janniere L. (2017). Interactions of the *Bacillus subtilis* DnaE polymerase with replisomal proteins modulate its activity and fidelity. *Open Biol*. 7(9): 170146.

Petit M.A., Dervyn E., Rose M., Entian K.D., McGovern S., Ehrlich S.D., Bruand C. (1998). PcrA is an essential DNA helicase of *Bacillus subtilis* fulfilling functions both in repair and rolling-circle replication. *Mol. Microbiol*. 29(1): 261-273.

Polard P., Marsin S., McGovern S., Velten M., Wigley D.B., Ehrlich S.D., Bruand C. (2002). Restart of DNA replication in Gram-positive bacteria: functional characterisation of the *Bacillus subtilis* PriA initiator. *Nucleic Acids Res*. 30(7): 1593-1605.

Prudhomme M., Libante V., Claverys J.P. (2002). Homologous recombination at the border: insertion-deletions and the trapping of foreign DNA in *Streptococcus pneumoniae*. *Proc. Natl. Acad. Sci. U S A*. 99: 2100-2105.

Qin W., Liu N.N., Wang L., Zhou M., Ren H., Bugnard E., Liu J.L., Zhang L.H., Vendôme J., Hu J.S., Xi X.G. (2014). Characterization of biochemical properties of *Bacillus subtilis* RecQ helicase. *J. Bacteriol*. 196(24): 4216-4228.

Ramos C., Hernández-Tamayo R., López-Sanz M., Carrasco B., Serrano E., Alonso J.C., Graumann P.L., Ayora S. (2022) The RecD2 helicase balances RecA activities. *Nucleic Acids Res*. 50(6): 3432-3444.

Randall J.R., Nye T.M., Wozniak K.J., Simmons L.A. (2019). RNase HIII is important for Okazaki fragment processing in *Bacillus subtilis*. *J. Bacteriol*. 201(7): e00686-18.

Rannou O., Le Chatelier E., Larson M.A., Nouri H., Dalmais B., Laughton C., Jannière L., Soultanas P. (2013). Functional interplay of DnaE polymerase, DnaG primase and DnaC helicase within a ternary complex, and primase to polymerase hand-off during lagging strand DNA replication in *Bacillus subtilis*. *Nucleic Acids Res*. 41(10): 5303-5320.

Reuß D.R., Faßhauer P., Mroch P.J., Ul-Haq I., Koo B.M., Pöhlein A., Gross C.A., Daniel R., Brantl S., Stülke J. (2019). Topoisomerase IV can functionally replace all type 1A topoisomerases in *Bacillus subtilis. Nucleic Acids Res*. 47(10): 5231-5242.

Riva S., Polsinelli M. (1968). Relationship between competence for transfection and for transformation. *J. Virol*. 2: 587-593.

Robinson A., Causer R.J., Dixon N.E. (2012). Architecture and conservation of the bacterial DNA replication machinery, an underexploited drug target. *Curr. Drug Targets*. 13: 352-372.

Romero H. (2018). Single-molecule dynamics in protein interactions: Characterization of RarA and RecD2 of *Bacillus subtilis*. (Promotion dissertation). Fachbereich Chemie, Philipps Universität Marburg.

Romero H., Rösch T.C., Hernández-Tamayo R., Lucena D., Ayora S., Alonso J.C., Graumann P.L. (2019). Single molecule tracking reveals functions for RarA at replication forks but also independently from replication during DNA repair in *Bacillus subtilis*. *Sci. Rep*. 9(1): 1997.

Romero H., Serrano E., Hernández-Tamayo R., Carrasco B., Cárdenas P.P., Ayora S., Graumann P.L., Alonso J.C. (2020). *Bacillus subtilis* RarA acts as a positive RecA accessory protein. *Front. Microbiol*. 11:92.

Rösch T.C., Oviedo-Bocanegra L.M., Fritz G., Graumann P.L. (2018). SMTracker: a tool for quantitative analysis, exploration and visualization of single-molecule tracking data reveals highly dynamic binding of *B. subtilis* global repressor AbrB throughout the genome. *Sci. Rep*. 8: 15747.

Rottländer E., Trautner T.A. (1970). Genetic and transfection studies with *B. subtilis* phage SP 50. I. Phage mutants with restricted growth on *B. subtilis* strain 168. *Mol. Gen. Genet*. 108(1): 47-60.

Roy R., Kozlov A.G., Lohman T.M., Ha T. (2007). Dynamic structural rearrangements between DNA binding modes of *E. coli* SSB protein. *J. Mol. Biol*. 369(5): 1244-1257.

Saikrishnan K., Griffiths S.P., Cook N., Court R., Wigley D.B. (2008). DNA binding to RecD: role of the 1B domain in SF1B helicase activity. *EMBO J*. 27(16): 2222-2229.

Saikrishnan K., Powell B., Cook N.J., Webb M.R., Wigley D.B. (2009). Mechanistic basis of 5'-3' translocation in SF1B helicases. *Cell*. 137(5): 849-859.

Samadpour A.N., Merrikh H. (2018). DNA gyrase activity regulates DnaA-dependent replication initiation in *Bacillus subtilis*. *Mol. Microbiol*. 108(2): 115-127.

Sanchez H., Carrasco B., Cozar M.C., Alonso J.C. (2007). *Bacillus subtilis* RecG branch migration translocase is required for DNA repair and chromosomal segregation. *Mol. Microbiol*. 65(4): 920-935.

Sanders G.M., Dallmann H.G., McHenry C.S. (2010). Reconstitution of the *B. subtilis* replisome with 13 proteins including two distinct replicases. *Mol. Cell.* 37(2): 273-281.

Seco E.M., Ayora S. (2017). *Bacillus subtilis* DNA polymerases, PolC and DnaE, are required for both leading and lagging strand synthesis in SPP1 origin-dependent DNA replication. *Nucleic Acids Res*. 45(14): 8302-8313.

Serrano E., Carrasco B. (2019). Measurement of the length of the integrated donor DNA during *Bacillus subtilis* natural chromosomal transformation. *Bio Protoc*. 9(16): e3338.

Serrano E., Carrasco B., Gilmore J.L., Takeyasu K., Alonso J.C. (2018). RecA regulation by RecU and DprA during *Bacillus subtilis* natural plasmid transformation. *Front Microbiol*. 9: 1514.

Serrano E., Ramos C., Alonso J.C., Ayora S. (2021). Recombination proteins differently control the acquisition of homeologous DNA during *Bacillus subtilis* natural chromosomal transformation. *Environ. Microbiol*. 23(1): 512-524.

Serrano E., Ramos C., Ayora S., Alonso J.C. (2020). Viral SPP1 DNA is infectious in naturally competent *Bacillus subtilis* cells: inter- and intramolecular recombination pathways. *Environ. Microbiol*. 22(2): 714-725.

Serrano E., Torres R., Alonso J.C. (2021b). Nucleoid-associated Rok differentially affects chromosomal transformation on *Bacillus subtilis* recombination-deficient cells. *Environ. Microbiol*. 23(6): 3318-3331.

Servinsky M.D., Julin D.A. (2007). Effect of a *recD* mutation on DNA damage resistance and transformation in *Deinococcus radiodurans*. *J. Bacteriol*. 189(14): 5101-5107.

Shadrick W.R., Julin D.A. (2010). Kinetics of DNA unwinding by the RecD2 helicase from *Deinococcus radiodurans*. *J. Biol. Chem*. 285(23): 17292-17300.

Shereda R.D., Kozlov A.G., Lohman T.M., Cox M.M., Keck J.L. (2008). SSB as an organizer/mobilizer of genome maintenance complexes. *Crit. Rev. Biochem. Mol. Biol*. 43(5): 289-318.

Singleton M.R., Dillingham M.S., Wigley D.B. (2007). Structure and mechanism of helicases and nucleic acid translocases. *Annu. Rev. Biochem*. 76: 23-50.

Smits W.K., Merrikh H., Bonilla C.Y., Grossman A.D. (2011). Primosomal proteins DnaD and DnaB are recruited to chromosomal regions bound by DnaA in *Bacillus subtilis*. *J. Bacteriol*. 193(3): 640-648.

Spatz H.C., Trautner T.A. (1971). The role of recombination in transfection of *B. subtilis. Mol. Gen. Genet*. 113: 174-190.

Tada S., Kobayashi T., Omori A., Kusa Y., Okumura N., Kodaira H., Ishimi Y., Seki M., Enomoto T. (2001). Molecular cloning of a cDNA encoding mouse DNA helicase B, which has homology to *Escherichia coli* RecD protein, and identification of a mutation in the DNA helicase B from tsFT848 temperature-sensitive DNA replication mutant cells. *Nucleic Acids Res.* 29(18): 3835-3840.

Taneja P., Gu J., Peng R., Carrick R., Uchiumi F., Ott R.D., Gustafson E., Podust V.N., Fanning E. (2002). A dominant-negative mutant of human DNA helicase B blocks the onset of chromosomal DNA replication. *J Biol Chem*. 277(43): 40853-40861.

Tasaki E., Mitaka Y., Nozaki T., Kobayashi K., Matsuura K., Iuchi Y. (2018). High expression of the breast cancer susceptibility gene BRCA1 in long-lived termite kings. *Aging (Albany NY)*. 10(10): 2668-2683.

Taylor S.D., Solem A., Kawaoka J., Pyle A.M. (2010). The NPH-II helicase displays efficient DNA-RNA helicase activity and a pronounced purine sequence bias. *J. Biol. Chem*. 285(15): 11692-11703.

Tkáč J., Xu G., Adhikary H., Young J.T.F., Gallo D., Escribano-Díaz C., Krietsch J., Orthwein A., Munro M., Sol W., Al-Hakim A., Lin Z.Y., Jonkers J., Borst P., Brown G.W., Gingras A.C., Rottenberg S., Masson J.Y., Durocher D. (2016). HELB is a feedback inhibitor of DNA end resection. *Mol. Cell*. 61(3): 405-418.

Torres R., Alonso J.C. (2021). *Bacillus subtilis* RecA, DisA, and RadA/Sms interplay prevents replication stress by regulating fork remodeling. *Front. Microbiol*. 12: 766897.

Torres R., Gándara C., Carrasco B., Baquedano I., Ayora S., Alonso J.C. (2021). DisA limits RecG activities at stalled or reversed replication forks. *Cells*. 10(6): 1357.

Torres R., Romero H., Rodríguez-Cerrato V., Alonso J.C. (2017). Interplay between *Bacillus subtilis* RecD2 and the RecG or RuvAB helicase in recombinational repair. *DNA repair (Amst)*. 55: 40-46.

Torres R., Serrano E., Alonso J.C. (2019). *Bacillus subtilis* RecA interacts with and loads RadA/Sms to unwind recombination intermediates during natural chromosomal transformation. *Nucleic Acids Res*. 47(17): 9198-9215.

Torres R., Serrano E., Tramm K., Alonso J.C. (2019b). *Bacillus subtilis* RadA/Sms contributes to chromosomal transformation and DNA repair in concert with RecA and circumvents replicative stress in concert with DisA. *DNA Repair (Amst)*. 77:45-57.

Toseland C.P., Webb M.R. (2013). ATPase mechanism of the 5'-3' DNA helicase, RecD2. *J. Biol. Chem*. 288(35): 25183-25193.

Trautner T.A., Spatz H.C. (1973). Transfection in *B. subtilis*. *Curr. Top Microbiol. Immunol*. 62: 61-88.

Truglio J.J., Croteau D.L., Van Houten B., Kisker C. (2006). Prokaryotic nucleotide excision repair: the UvrABC system. *Chem. Rev*. 106(2): 233-252.

Valero-Rello A., López-Sanz M., Quevedo-Olmos A., Sorokin A., Ayora S. (2017). Molecular mechanisms that contribute to horizontal transfer of plasmids by the bacteriophage SPP1. *Front. Microbiol*. 8: 1816.

Veaute X., Delmas S., Selva M., Jeusset J., Le Cam E., Matic I., Fabre F., Petit M.A. (2005). UvrD helicase, unlike Rep helicase, dismantles RecA nucleoprotein filaments in *Escherichia coli. EMBO J*. 24(1): 180-189.

Vlašić I., Mertens R., Seco E.M., Carrasco B., Ayora S., Reitz G., Commichau F.M., Alonso J.C., Moeller R. (2013). *Bacillus subtilis* RecA and its accessory factors, RecF, RecO, RecR and RecX, are required for spore resistance to DNA double-strand break. *Nucleic Acids Res*. 42(4): 2295-2307.

Walsh B.W., Bolz S.A., Wessel S.R., Schroeder J.W., Keck J.L., Simmons L.A. (2014). RecD2 helicase limits replication fork stress in *Bacillus subtilis*. *J. Bacteriol*. 196(7): 1359-1368.

Walsh B.W., Lenhart J.S., Schroeder J.W., Simmons L.A. (2012). Far western blotting as a rapid and efficient method for detecting interactions between DNA replication and DNA repair proteins. *Methods Mol. Biol.* 922: 161-168.

Wang J.D., Sanders G.M., Grossman A.D. (2007). Nutritional control of elongation of DNA replication by (p)ppGpp. *Cell*. 128(5): 865-875.

Wang J., Julin D.A. (2004). DNA helicase activity of the RecD protein from *Deinococcus radiodurans*. *J. Biol. Chem*. 279(50): 52024-52032.

Weller G.R., Kysela B., Roy R., Tonkin L.M., Scanlan E., Della M., Devine S.K., Day J.P., Wilkinson A., d'Adda di Fagagna F., Devine K.M., Bowater R.P., Jeggo P.A., Jackson S.P., Doherty A.J. (2002). Identification of a DNA nonhomologous end-joining complex in bacteria. *Science*. 297(5587): 1686-1689.

Wright W.D., Shah S.S., Heyer W.D. (2018). Homologous recombination and the repair of DNA double-strand breaks. *J. Biol. Chem*. 293(27): 10524-10535.

Wu L., Hickson I.D. (2006). DNA helicases required for homologous recombination and repair of damaged replication forks. *Annu. Rev. Genet*. 40: 279-306.

Xue Z.Y., Wu W.Q., Zhao X.C., Kumar A., Ran X., Zhang X.H., Zhang Y., Guo L.J. (2020) Single-molecule probing the duplex and G4 unwinding patterns of a RecD family helicase. *Int. J. Biol. Macromol*. 164: 902-910.

Yadav T., Carrasco B., Myers A.R., George N.P., Keck J.L., Alonso J.C. (2012). Genetic recombination in *Bacillus subtilis*: a division of labor between two single-strand DNA-binding proteins. *Nucleic Acids Res.* 40(12): 5546-5559.

Yadav T., Carrasco B., Serrano E., Alonso J.C. (2014). Roles of *Bacillus subtilis* DprA and SsbA in RecA-mediated genetic recombination. *J. Biol. Chem*. 289: 27640-27652.

Yang H., Yung M., Sikavi C., Miller J.H. (2011). The role of *Bacillus anthracis* RecD2 helicase in DNA mismatch repair. *DNA repair (Amst)*. 10(11): 1121-1130.

Yeeles J.T.P., Marians K.J. (2011). The *Escherichia coli* replisome is inherently DNA damage tolerant. *Science*. 334(6053): 235-238.

Annex: Publications

1. Serrano E., Ramos C., Ayora S., Alonso J.C. (2020). Viral SPP1 DNA is infectious in naturally competent *Bacillus subtilis* cells: inter- and intramolecular recombination pathways. *Environ. Microbiol*. 22(2): 714-725. doi: 10.1111/1462-2920.14908.

2. Serrano E., Ramos C., Alonso J.C., Ayora S. (2021). Recombination proteins differently control the acquisition of homeologous DNA during *Bacillus subtilis* natural chromosomal transformation. *Environ. Microbiol*. 23(1): 512-524. doi: 10.1111/1462-2920.15342.

3. Ramos C., Hernández-Tamayo R., López-Sanz M., Carrasco B., Serrano E., Alonso J.C., Graumann P.L., Ayora S. (2022) The RecD2 helicase balances RecA activities. *Nucleic Acids Res*. 50(6): 3432-3444. doi: 10.1093/nar/gkac131.